Investigation of the emergence of thermodynamic behavior in closed quantum systems and its relation to standard stochastic descriptions

Dissertation (kumulativ)

zur Erlangung des Grades eines
Doktors der Naturwissenschaften (Dr. rer. nat.)

dem Fachbereich Physik der Universität Osnabrück
vorgelegt von

M. Sc. Daniel Schmidtke

Osnabrück, im März 2018

Constituent parts:

Investigation of the emergence of thermodynamic behavior in closed quantum systems and its relation to standard stochastic descriptions

Dissertation (Cumulative)

Daniel Schmidtke[1,*]

[1] *Fachbereich Physik, Universität Osnabrück, Barbarastrasse 7, D-49069 Osnabrück, Germany*

(Dated: May 28, 2018)

Our everyday experiences teach us that any imbalance like temperature gradients, non-uniform particle-densities etc. will approach some equilibrium state if not subjected to any external force. Phenomenological descriptions of these empirical findings reach back to the 19th century where Fourier and Fick presented descriptions of relaxation for macroscopic systems by stochastic approaches. However, one of the main goals of thermodynamics remained the derivation of these phenomenological description from basic microscopic principles. This task has gained much attraction since the foundation of quantum mechanics about 100 years ago. However, up to now no such conclusive derivation is presented.

In this dissertation we will investigate whether closed quantum systems may show equilibration, and if so, to what extend such dynamics are in accordance with standard thermodynamic behavior as described by stochastic approaches. To this end we consider i.a. Markovian dynamics, Fokker-Planck and diffusion equations. Furthermore, we consider fluctuation theorems as given e.g. by the Jarzynski relation beyond strict Gibbsian initial states. After all we find indeed good agreement for selected quantum systems.

PACS numbers: 05.60.Gg, 05.70.Ln, 05.30.-d, 72.15.Rn

CONTENTS

I. INTRODUCTION

From everyday experience we know that e.g. some hot (macroscopic) system, respective to its environment, cools down by exchanging energy with the environment until both system and environment feature the same temperature. This experience can be extended to all kinds of imbalances, i.e., non-equilibrium situations as e.g. for particle or charge densities etc. where the system relaxes toward equilibrium densities. However, we never encounter processes where e.g. heat flows from some cold regime towards a hotter one. This phenomenon, i.e., the obvious (temporal) direction of processes, and thus irreversibility, is connected with the

* danischm@uos.de

so called entropy via the second law of thermodynamics [8, 9]. It reads in its basic form for closed (isolated) systems: $\delta S \geqslant 0$ where δS is the change in entropy. Thus, entropy can only increase during processes and never decrease if no external protocols force it to.
The physical and mathematical description of such equilbration phenomena has therefore always been a major goal of classical thermodynamics and transport theories (see e.g. [8, 10, 11]). For example, about 200 years ago, Fourier proposed the still valid phenomenological laws of heat conduction based on macroscopic observations [8, 12, 13] or a couple of years later Fick introduced his law for (diffusive) particle transport [14]. However, as said above, all these macroscopic phenomena present irreversible processes while on the underlying microscopic level the physical laws, i.e., Newton and Schrödinger equations, are time-symmetric and thus describe reversible processes.

Boltzmann equation

One of the first attempts to resolve this inconstistency goes back to Boltzmann's work in 1855 [15] in which he explained and quantified the observation of the irreversible process of expanding gas molecules. Rather than describing the system in real space Boltzmann introduced the μ-space, i.e., a six-dimensional space spanned by the positions $\vec{r}$ and velocities $\vec{v}$ of each particle. Furthermore, he treated the multitude of particles not as individual points in the μ-space but used a continuous function $f(\vec{r}, \vec{v}, t)$ to describe their dynamics. This function can be seen as kind of particle density in μ-space. In order to define such a function properly he divided the μ-space into equal-sized cells that are large enough to contain many particles but small compared to length scales onto which the number of particles would drastically change for adjacent cells. Thus, this description disregards the individual microscopic features of each particle, which is an essential part of this approach, and already excludes system states that can not be described by a smooth function $f(\vec{r}, \vec{v}, t)$. Boltzmann showed that a dynamical change of $f(\vec{r}, \vec{v}, t)$ arises basically from two different processes [16, 17]: non-interacting particles and particle-particle interactions like e.g. two-particle scattering. Such particle interactions are micro-reversible according to the fundamental laws of mechanics. However, Boltzmann proposed his renowned *Stosszahl ansatz* which promotes the idea of non-existing correlations between particles before direct interactions. This later assumption, though often criticized, allows indeed for a more or less correct description of irreversible relaxation behavior. At last we emphasize that the above mention graining of the underlying phase space is artificial and bears no deeper physical reasoning. As we will see, this shortcoming is also present in most of the other concepts discussed below.

Ergodic hypothesis

The ergodic hypothesis, also pursued by Boltzmann, is based on the assumption that timescales of actual measurements are quasi-infinite long compared to the the timescales of molecular motion; see e.g. [18]. In consequence the result of a measurement can be seen as the time-averaged outcome w.r.t. many hypothetical instantaneous measurements. Assuming now that a trajectory ventures eventually through all points in the (accessible) phase space, irrespective of its actual starting point, one might treat the system (during measurements) as occupying each accessible phase point at the same time. Following these lines one can show that the amount of time spend by the trajectory in some volume is proportional to the size of this volume [19]. This renders time average and the ensemble average, i.e., the average over all accesible states, equal. Furthermore, one may introduce entropy as a measure that is connected to the volume the trajectory ventures through w.r.t. the time passed. However, how exactly this measure should be defined is not obvious (see e.g. [8]). Note that the approach as stated so far must be false since a trajectory can never venture through all accessible points in phase space in finite time [19]. In order to get rid of this shortcoming one introduces the quasi-ergodic hypothesis that states that the trajectory ventures arbitrarily close to any point in the accessible regime. As demonstrated in Refs. [20, 21] there are indeed systems that behave quasi-ergodic but a generalization of the underlying proof towards a larger class of systems cannot be given.

Ensemble approach

In 1902, Gibbs introduced his ensemble approach [22] where the basic idea is that, in general, a macroscopic observation is consistent with a multitude of microscopic configurations. The points in phase space corresponding to these configurations form the ensemble, i.e., the ensemble is in general represented by a density distribution on phase space. In order to describe the evolution of the system one considers no longer the evolution of a single trajectory but rather the dynamics of the density distribution. To do so, one employs the Liouville theorem [22, 23] which basically states that the phase space volume cannot change under Hamiltonian mechanincs, though it may change its shape drastically. Thus, if the system is initially described by a density function that is uniformly distributed over the entire accessible regime then it is in a stationary state since the volume cannot change. This state is also associated as equilibrium state. One might connect entropy again with the occupied volume here but doing so would mean that any state that starts not in an equilibrium state would also never

reach it. This is because the volume cannot increase. In order to resolve this problem Ehrenfest introduced a *coarse graining* of the phase space so that entropy is connected to the number of cells (grains) in which the density function features non-zero contributions. The size of the cells, however, must be defined artificially. Nevertheless, entropy can in this interpretation increase by deforming the volume into a complex structure with non-zero contribution in many cells. Due to its resemblance with mixing of ink (fix volume) in a glass of water this process is sometimes also denoted as *mixing* [22]. Mixing has been demonstrated for a range of systems but a generalization cannot be given here, also.

Macroscopic cell approach

The macroscopic cell approach goes also back to Ehrenfest who, however, called such cells *stars* [19]. A star is a regime in phase space that features configurations that are consistent with one macroscopic description of the system e.g. the volume V and internal energy U of a gas. Due to this approach a graining arises *naturally*. The cells, however, are not equal-sized but form complex shaped structures which may differ drastically in size. Now, one makes the plausible assumption (law of large numbers) that the *equilibrium cell* is by far the largest, i.e., has the largest volume w.r.t. phase space (see e.g. [8]). Thus, a trajectory wandering about the phase space will most likely spend the entire time in this equilibrium cell even if it started off in a much smaller cell corresponding to some possibly far-off equilibrium state. Furthermore, one has no longer need of the ergodic hypothesis or mixing. As will turn out below this approach is conceptually closely related to the typicality which we will discuss in more details in Sec. II B. Similar as in the prior approaches entropy can again be connected with the volume of the cell the trajectory is momentarily wandering through. Determining, however, the exact volume in this approach follows no deeper physical reasoning either. One has, as done above, to introduce again some subjective measure (cf. e.g. [8]). There are still some other approaches but since they are in general not as much acknowledged as the presented ones or involve open system scenarios [24] we will not review them here.

However, we emphasize that so far all concepts originated from a classical point of view although on the microscopic level one rather has to consider quantum mechanics. Numerous investigations reveal that also for closed quantum systems equilibration is observed in both, theoretic studies [1, 3, 4, 25–32] and experiments, enabled by recent progress in probing quasi-isolated systems e.g. with ultra cold atoms [33–38] or trapped ions [39, 40]. On the theoretical side some approaches have similar classical counterparts (e.g. typicality) whereas other approaches originate solely from quantum mechanic viewpoints.

In this dissertation, however, we rather focus on the actually description of the way from non-equilibrium towards equilibrium which the above approaches are not apt to provide (except the Boltzmann equation which, however, is not generic). To be precise, we will consider the description of thermodynamic behavior by means of standard stochastic processes, i.e., by considering probability distributions whose evolutions can be calculated by transition probabilities. Focusing on closed quantum systems we begin by reviewing central concepts of equilibration in such systems, i.e., Fermi's Golden Rule, typicality and the eigenstate thermalization hypothesis in Sec. II. These concepts will allow for first insights as to when quantum systems may possibly be described by stochastic processes. In Sec. III, we will then introduce the general notion of stochastic trajectories before discussing the special case of Markovian processes. We also provide evidence that for closed quantum systems such behavior can indeed be observed. The description of dynamics of probability distributions by means of master equations is discussed in Sec. IV. We will furthermore derive from such master equations the renowned Fokker-Planck equation that is applied in many investigations to describe irreversible behavior in classical mechanics. Introducing projection operator methods (i.e. the time-convolutionless projection operator method) we demonstrate analytically and numerically that Fokker-Planck dynamics can also be found in closed quantum systems.
Diffusive processes, as essential in transport theory, can be described by the Fokker-Planck equation as well where certain simplifications lead directly to the diffusion equation (Sec. V). We furthermore exploit the relationship between the diffusion coefficient, spatial variance and conductivity of some appropriate current (Kubo formula, Einstein relation). The analytic results are again backed by numerical results. At last, in Sec. VI, we investigate whether the validity of the Jarzynski relation can be extended to a much wider class of initial states than the commonly used strict Gibbsian states. We introduce thereby a property called *stiffness of distribution functions* that immediately ensures the validity of the Jarzynski relation. In Sec. VII, we will summarize our findings and discuss conclusions.

II. APPROACHES TO EQUILIBRATION IN CLOSED QUANTUM SYSTEMS

In this section we will discuss several essential approaches describing equilibration in closed systems. We will start by introducing Fermi's Golden Rule (FGR) which basically states that quantum dynamics may be described in terms of transition rates between energy eigenstates and thus hints already to the

applicability of stochastic approaches. However, as will turn out below, such an description is rather restricted to specific systems.
Thereafter, we will explain in more details the concepts of typicality and the eigenstate thermalization hypothesis (ETH) since both are especially important in the here discussed context of closed quantum systems. Furthermore, the typicality concept not only offers a direct conceptional approach but also gives rise to computational simplifications (at least for some specific systems as described below). In most articles constituting this dissertation we made use of this fact.
Though both aforementioned concepts are apt to describe equilibrium properties and also the possible dynamical approach towards an equilibrium state when started from a (strongly) non-equilibrium state they cannot per se describe the exact way such relaxation proceeds. Nevertheless, these approaches can be employed to decide whether dynamics may possibly be in accordance with (macroscopic) stochastic descriptions as e.g. Markov processes. This point becomes apparent in particular in Sec. II C.

A. Fermi's Golden Rule

In this section we introduce a concept, namely Fermi's Golden Rule (FGR), that allows for a description of quantum dynamics in terms of transition rates γ_{ij} though the Schrödinger equation per se does not allow for (exponential) relaxation towards a unique fix point. On one hand, such kind of description of quantum dynamics in closed systems is one ultimate goal of this dissertation as will be pointed out in Sec. III. On the other hand, the applicability of this concept is rather restricted, as we will see below. Thus, it may serve in most cases just as a first approximation towards the actual dynamics.

Here we only repeat the essential aspects of this approach and refer to Refs. [8, 41] for more details. In general one divides the full Hamiltonian $\hat{H}$ into a time-independent part $\hat{H}_0$ and a so-called time-dependent interaction part $\hat{V}(t)$, i.e., $\hat{H} = \hat{H}_0 + \kappa\hat{V}(t)$ where κ denotes the interaction strength. The above mentioned transition rates γ_{ij} from one energy eigenstate $|i\rangle$ to another one $|j\rangle$ (w.r.t. $\hat{H}_0$) are then essentially gained by first order (time-dependent) perturbation theory [41], i.e., dynamics are iteratively described in time steps of amount dt. Note that one usually also assumes that the the system is initially in an energy eigenstate w.r.t. $\hat{H}_0$, since only then one will eventually obtain transition rates that do not depend on the time t. This aspect is crucial for the application of standard master equations (see Sec. III). However, in most scenarios, after each iteration stepthe system is already in a superposition of several energy eigenstates according to the above scheme although it may have been initially in a single eigenstate (see for details [8]). Finally, though the FGR is clearly not universal applicable, it already reveals essential connections of quantum mechanics with stochastic processes.

B. Concept of typicality

Although basically already present in the works of Boltzmann and Ehrenfest (see above) the later called *typicality approach* has until recently not gained as much attraction as the *standard approaches* mentioned above. However, in the last decades the concept received more and more attention after e.g. Lebowitz et al. had done pioneering work involving classical mechanics [42–44] as well as quantum dynamics [45–47].
Here we are going to review the main points of the typicality approach without going too deep into details since, as mentioned above, the scope of this dissertation is to study the ways relaxation proceeds rather than its sheer existence (for a detailed review of the typicality concept see Refs. [8, 48]).
The concept of typicality neither involves time averaging as in the ergodicity approach nor will an initial microstate evolve into some ensemble as is the case for the *mixing approach*. It, however, has great similarity with the macroscopic cell approach by Ehrenfest (see above). The basic idea is that a huge amount of microstates from a specific region in phase space, Hilbert space etc. gives already rise for very similar results with respect to functions of an observable like e.g. expectation values. Thus, by drawing states from such a region at random the vast majority of results will be close to each other and one may view this fact as an analogue to the idea that (nearly) all states of the region are "occupied at the same time". This renders the microstates indistinguishable from the *ensemble*.

Typicality of expectation values

To introduce the concept in a more formal wise we first of all consider a system that can occupy a set of microstates $\mathbf{X}$ and represent each as e.g. a point in phase space (classical system) or point in Hilbert space (pure quantum state). Now we consider a special set of states formed by such states that feature a common property (e.g. the expectation value of some observable like energy) that is conserved under the dynamics of the system. Note that this restriction is not mandatory but makes the argumentation below easier to follow [8]. Since the system can occupy any state from this region but not leave the region we call the corresponding set of states the *accessible region* $\mathcal{X}_{\mathrm{AR}}$. Next we define some function $f[\mathbf{X}]$ on the set of states which can be any appropriate observable (classical system) or expectation

values, or anything alike, in the quantum case. The average w.r.t. the accessible region is then defined as

$$\mathbb{E}_{\mathrm{AC}}[f] := \int_{\mathrm{AR}} f[\mathbf{X}]\, dV_{\mathbf{X}} \quad . \tag{1}$$

($dV_{\mathbf{X}}$ implies that an appropriate metric has to be defined on $\mathcal{X}_{\mathrm{AR}}$). Accordingly the variance is defined as

$$\mathbb{V}_{\mathrm{AC}}[f] := \mathbb{E}_{\mathrm{AC}}[(f - \mathbb{E}_{\mathrm{AC}}[f])^2] = \mathbb{E}_{\mathrm{AC}}[f^2] - \mathbb{E}^2_{\mathrm{AC}}[f] \quad . \tag{2}$$

Now typicality w.r.t. f is said to hold if and only if

$$\sqrt{\mathbb{V}_{\mathrm{AC}}[f]} \ll f_{\max} - f_{\min} \quad , \tag{3}$$

where $f_{\min}, f_{\max}$ denote the smallest and largest possible value of $\mathbb{E}_{\mathrm{AC}}[f]$, respectively. Thus $\mathbb{E}_{\mathrm{AC}}[f]$ is the typical value of $f[\mathbf{X}]$ on $\mathcal{X}_{\mathrm{AC}}$.

Dynamical aspects of typicality

So far the considerations based on static microstates only which we now extend towards actual dynamics. To do so, we consider now dynamics that preserve the microstate volume (what can be achieved by an appropriate representation of the microstate space). Formally expressed this reads:

$$\frac{d\mathbf{X}}{dt} = g[\mathbf{X}] \quad , \quad \mathrm{div}_{\mathbf{X}}\, g[\mathbf{X}] = 0 \quad . \tag{4}$$

Furthermore, we divide $\mathcal{X}_{\mathrm{AC}}$ into two distinct subsets $\mathcal{A}, \mathcal{B}$, i.e.,

$$\mathcal{A} = \left\{ \mathbf{X} \in \mathcal{X}_{\mathrm{AC}} \middle| \, \epsilon \geqslant \, |f[\mathbf{X}] - \mathbb{E}_{\mathrm{AC}}[f]| \right\} \tag{5}$$

and

$$\mathcal{B} = \left\{ \mathbf{X} \in \mathcal{X}_{\mathrm{AC}} \middle| \, \epsilon < \, |f[\mathbf{X}] - \mathbb{E}_{\mathrm{AC}}[f]| \right\} \quad . \tag{6}$$

We define the volume of a set $\mathcal{C}$ as

$$\Omega(\mathcal{C}) := \int_{\mathcal{C}} dV_{\mathbf{X}} \quad . \tag{7}$$

If we choose $\epsilon \ll f_{\max} - f_{\min}$ and assume that typicality holds for almost all $\mathbf{X}$'s in the accessible region we eventually find $\Omega(\mathcal{A}) \gg \Omega(\mathcal{B})$, i.e., there any many more states featuring an value $f[\mathbf{X}]$ close to the averaged value $\mathbb{E}_{\mathrm{AC}}[f]$ than other states. Thus, it is reasonable to call $\mathcal{A}$ the *equilibrium set* and $\mathcal{B}$ the *non-equilibrium set*. Additionally to these sets let us define the sets that contain states that initially are located in either the equilibrium set or the non-equilibrium set and venture eventually into the other one. Hence, states that start in the equilibrium set (and venture to the other set) belong to $\Omega_t(\mathcal{A} \to \mathcal{B})$ whereas in turn the states starting in the non-equilibrium set belong to $\Omega_t(\mathcal{B} \to \mathcal{A})$. Under preservation of the microstate volume both sets are necessarily equal in size, i.e., $\Omega_t(\mathcal{A} \to \mathcal{B}) = \Omega_t(\mathcal{B} \to \mathcal{A})$. But weighted by the respected starting volume we find

$$\frac{\Omega_t(\mathcal{A} \to \mathcal{B})}{\Omega(\mathcal{A})} \ll \frac{\Omega_t(\mathcal{B} \to \mathcal{A})}{\Omega(\mathcal{B})} \quad , \tag{8}$$

i.e., relatively much more states actually venture from the non-equilibrium set into the equilibrium set than otherwise. This result can be seen as explanation why systems initially in a (single) non-equilibrium state will nevertheless exhibit relaxation towards an unique equlibrium state that behaves like the system occupies all accessible states at the same time. Note that there may still be states in the non-equilibrium set that will never leave $\mathcal{B}$ or even intial states that eventually evolve from equilibrium to non-equilibrium. However, these states are few and their relative ratio with respect to the whole volume decreases as the later increases (for details see e.g. [8]).

The above statement does only state that a system initially in a non-equilibrium state may eventually reach equilibrium but does not give any insight into the concrete way such relaxation proceeds, especially whether the relaxation behavior does depend on the actual initial state. While typicality is indeed not able to describe the actual relaxation dynamics it can, however, give insight into the dependency on the intial state. To see this we repeat some main results from [27] (though we note that similar non-analytical results were already presented in e.g. [49]). To this end we consider now several different intial states $|\phi\rangle$ that belong to the same accessible region and furthermore feature at some point in time (often chosen to be $t_0 = 0$) the same expecatation value with respect to an observable $\hat{B}$, i.e., $b(t_0) = \langle\phi|\hat{B}(t = t_0)|\phi\rangle$. The studies in [27] reveal that the vast majority of such pure quantum states yield also similar expectation values at any other time for high dimensional Hilbert spaces. Thus, the dynamics are typically well described by the ensemble average upon the underlying set of states.

Hilbert space average method

We demonstrate here the connection of the typicality approach with the Hilbert space average method (HAM) [8] for closed quantum systems. To do so, we consider at first pure states $|\psi\rangle$ that are drawn at random according to a distribution that is invariant under any unitary transformation in Hilbert space (cf. the Haar measure). Note that the choice of such a specific distribution is crucial for the following results. According to the HAM the average of expectation values of some observable $\hat{A}$ on the underlying accessible Hilbert

space w.r.t. such states $|\psi\rangle$ reads

$$\mathrm{HA}[\langle\psi|\hat{A}|\psi\rangle] = \frac{\mathrm{tr}\left[\hat{A}\right]}{d} \tag{9}$$

and the corresponding variance

$$\mathrm{HV}[\langle\psi|\hat{A}|\psi\rangle] = \frac{1}{d-1}\left[\frac{\mathrm{tr}\left[\hat{A}^2\right]}{d} - \left(\frac{\mathrm{tr}\left[\hat{A}\right]}{d}\right)^2\right] \quad , \tag{10}$$

where d denotes the Hilbert space dimension (cf. [8, 27]). Thus, if the underlying system features a large Hilbert space dimension and observable-bound spectra the HV vanishes and typicality applies. The typical expectation value is then given by $\mathrm{HA}[\langle\psi|A|\psi\rangle]$. As said above, in [27] it is demonstrated that typicality may also hold for any time point if it already applies at some other time point t_0, i.e., $\mathrm{HV}[\langle\psi|\hat{A}(t)|\psi\rangle] \to 0 \;\forall\, t$.

Numerical tool

The above results can be employed to significantly reduce numerical efforts for investigations of large systems (as was done in most projects contributing to this dissertation). To see this, we start by considering the time evolution of the expectation value of some oberservable $\hat{B}$ w.r.t. the initial state ρ, i.e.,

$$\langle\hat{B}(t)\rangle = \mathrm{tr}\left[\hat{B}(t)\,\rho\right] \quad . \tag{11}$$

In order to calculate $\mathrm{tr}\left[\hat{B}(t)\,\rho\right]$ directly one has to employ advanced methods such as exact diagonalization that are in general only feasible for rather small systems. The reason among others is that ρ is in general not a pure quantum state.
Using the cyclic invariance of the trace operation we can rearrange Eq. (11) and find by virtue of Eq. (9)

$$\mathrm{tr}\left[\sqrt{\rho}\,\hat{B}(t)\,\sqrt{\rho}\right] \approx d\,\langle\phi|\sqrt{\rho}\hat{B}(t)\sqrt{\rho}|\phi\rangle \quad , \tag{12}$$

i.e., $|\phi\rangle$ are drawn at random according to the Haar measure and we assume that $\sqrt{\rho}\,\hat{B}(t)\,\sqrt{\rho}$ fulfills the typicality approach where the Hilbert space dimension is d. Note that we can express the constant d by virtue of Eq. (9) as $d = \langle\phi|\rho|\phi\rangle^{-1}$ since the trace of ρ equals 1. Thus, after some rearranging we eventually find

$$\langle\hat{B}(t)\rangle \approx \langle\psi|\hat{B}(t)|\psi\rangle = \langle\psi(t)|\hat{B}|\psi(t)\rangle \quad , \tag{13}$$

where

$$|\psi\rangle = \langle\phi|\rho|\phi\rangle^{-1/2}\,\sqrt{\rho}\,|\phi\rangle \quad . \tag{14}$$

The time evolution of $|\psi(t)\rangle$ is much easier to calculate than that of $\rho(t)$ or $\hat{B}(t)$ e.g. by some iterative time propagation method like a fourth-order Runge-Kutta or Chebyshev scheme (for details on the concrete numeric handling see e.g. [7, 50, 51]).

C. Eigenstate thermalization hypothesis and initial state independent equilibration

The eigenstate thermalization hypothesis (ETH) is closely related to initial state independent (ISI) equilibration. The later is one of the main aspects in stochastic approaches (cf. Sec. III) and will be investigated intensively in the second part of this section. In order to see this we write the initial state (possible far-from equilibrium) in the eigenbasis of the underlying Hamiltonian as

$$|\psi(t_0)\rangle = \sum_n c_n\,|E_n\rangle \quad , \tag{15}$$

where $|E_n\rangle$ is eigenstate to the n-th eigenvalue E_n and $c_n = \langle E_n|\psi(t_0)\rangle$. Assume that the E_n's are sorted in ascending order.
Now the expectation value of any observable $\hat{A}$ at time t reads

$$\langle\psi(t)|\hat{A}|\psi(t)\rangle = \sum_{m,n} c_m\,c_n^*\,A_{mn}\,e^{-i\frac{t}{\hbar}(E_m-E_n)} \quad , \tag{16}$$

where $A_{mn} = \langle E_m|\hat{A}|E_n\rangle$. A physical reasonable assumption is that the E_n's are indeed incommensurable [25]. Thus for large times one finds

$$\lim_{t\to\infty}\langle\psi(t)|\hat{A}|\psi(t)\rangle \approx \sum_n |c_n|^2\;A_{nn} \quad . \tag{17}$$

This expression states that the longtime expectation value may be approximated by a diagonal ensemble. However, this is definitely different from the microcanonical ensemble average since the later would yield results independent of the actual initial state whereas Eq. (17) may explicit depend on $|\psi(t_0)\rangle$ as encoded in the coefficients $|c_n|^2$.

ETH ansatz for operators

The basic idea of the ETH ansatz is to assume that the diagonal elements A_{nn} vary smoothly with energy and the differences between adjacent diagonal matrix elements, i.e., $A_{nn} - A_{n+1,n+1}$ become exponentially small in system size. In order to express the later formally we define

$$\bar{A} = \sum_n p_n(\bar{E})\,A_{nn} \quad , \quad \Sigma^2 = \sum_n p_n(\bar{E})\,A_{nn}^2 - \bar{A}^2 \quad , \tag{18}$$

where $p_n(\bar{E})$ describes a probability distribution centered at $\bar{E}$. Σ^2 denotes the variance of matrix elements along the diagonal. Note that the ETH is said to be fulfilled iff $\Sigma = 0$ [52]. In finite closed systems one finds that Σ is in general not equal to zero. However, numerous investigations on translational invariant, solid-state-type observables and models indicate that

Σ scales approximately as $\Sigma \propto d^{-\gamma}$ where d is the effective Hilbert space dimension, i.e., the number of states within the respective energy shell, and γ is some constant [53–55]. Note that the scaling will in general depend on whether the observable scales extensively, intensively or else wise. Nevertheless, since d generally increases (exponentially) with system size, Σ tends towards zero whenever $\gamma > 0$.
In literature one finds $0 \leqslant \gamma \leqslant 1/2$ for few body observables. $\gamma = 0$ is associated to integrable systems while $\gamma = 1/2$ corresponds to fully chaotic systems. We emphasize that the definitions may vary depending on the respective author.
There are also examples for $\gamma < 0$ for extensive observables. E.g. in Ref. [54] this occurs for spin and energy currents in the integrable Heisenberg chain at a certain parameter regime. However, for the same model but another extensive observable one finds $\gamma = 0$ [30].

The ETH ansatz also makes statements about the off-diagonal elements. They must (i) be much smaller than the diagonal elements and (ii) also become exponentially small in system size. Hence, the ETH is fulfilled if the corresponding operator in energy eigenbasis has the follwing structure (see e.g. Ref. [32]):

$$A_{mn} \approx \bar{A}(\bar{E})\,\delta_{m,n} + N(\bar{E})^{-1/2}\, f_A(\bar{E},\omega)\, R_{mn} \quad , \quad (19)$$

where $\bar{E} = (E_m + E_n)/2$, $\omega = E_n - E_m$ and $N(\bar{E})$ is the partition function at energy $\bar{E}$. The matrix elements R_{mn} are randomly distributed where their mean is zero ($\overline{R_{mn}} = 0$) and their variance equals one ($\overline{R_{mn}^2} = 1$). Note that in turn any operator that has the above representation fulfills the ETH. We will take a closer look at this matrix representation in Sec. VI.
Plugging the above ansatz into Eq. (17) reveals

$$\lim_{t\to\infty} \langle\psi(t)|A|\psi(t)\rangle \approx \bar{A}(\bar{E}) \sum_n |c_n|^2 = \bar{A}(\bar{E}) \quad . \quad (20)$$

Thus, if the ETH is fulfilled the long-time expectation value depends only on the energy of the initial state not on specific details. Moreover, this expectation value coincides with the microcanonical average value of $\hat{A}$.

Predicting and determining ISI equilibration

As pointed out above, if the ETH is fulfilled ISI equilibration is inevitable. Whether the fulfillment of the ETH is indeed a necessary condition for ISI equilibration was e.g. investigated in Refs. [4, 56, 57].
In order to "predict" ISI equilibration, in particular when the ETH breaks down, we consider not the "bare" ETH quantity Σ but a closely related expression, following suggestions in [30]. This "new" quantity reads:

$$\nu = \frac{\Sigma^2}{\delta_A^2} \quad , \quad (21)$$

where $\delta_A^2 = \sum_n p_n(\bar{E})\,(A^2)_{nn} - \bar{A}^2$ defines the spectral variance of $\hat{A}$. Note that, in contrast to Σ, ν is dimensionless. Thus, the scaling of Σ, i.e., extensive, intensive, or else, is not relevant for the behavior of ν. As proposed in Ref. [30], ISI equilibration is said to hold iff $\nu \to 0$ in the thermodynamic limit.
Note that ν may approach zero even so Σ does not. This is e.g. the case if ν increases much faster than Σ.

In the following we consider expectation values of some observable $\hat{A}$ that are calculated by means of states ρ that are operator functions of the corresponding Hamiltonian and the investigated observable itself, i.e., $\rho = \rho(\hat{H}, \hat{A})$ (see below). Thus, these states allow for energy selective probabilities p_n as introduced above.
In case the ETH applies we expect the time evolution of the expectation value, denoted as $\langle\hat{A}(t)\rangle$, to converge against a microcanonical equilibrium value A_{eq}. The later can be calculated directly. We emphasize that into its calculation no details other than the initial energy of the initial state enter, i.e., the value is universal. This may allow to check directly whether ISI equilibration applies by comparing the long-time value of $\langle\hat{A}(t)\rangle$ with A_{eq}. However, we use here a slightly different scheme since for small (closed) systems there is numerical evidence that the long time expectation value may not exactly match with the microcanonical equilibrium value but rather "remembers" details from the specific initial state, i.e., the final value "sticks" at some value different from the microcanonical equilibrium value ("stick effect"). Nevertheless, there is also numerical evidence that the stick effects (affecting the long time expectation value) decrease under certain conditions with increasing system size N; cf. [30]. Therefore, we investigate the following quantity:

$$r := \lim_{t\to\infty} \frac{\langle\hat{A}(t)\rangle}{\langle\hat{A}(t_0)\rangle} = \frac{a_\infty}{a_0} \quad (22)$$

This quantity compares the initial expectation value a_0 to the longtime value a_∞. In the following we assume that $|a_0|$ is close to the outmost possible eigenvalue of $\hat{A}$. By doing so, we circumvent trivial relaxation processes and can investigate stick effects most clearly since these effects are expected to be the strongest the larger the initial deviation from the equilibrium value.
If the stick effect vanishes for large systems we expect r to tend towards zero, i.e., ISI equilibration emerges. Otherwise we expect r to converge against a finite value or even to increase for large systems. In these cases ISI equilibration does not emerge. Hence, by

investigating r we can easily decide whether for the current parameter sets ISI equilibration emerges while by means of Eq. (18) we can simultaneously determine whether the ETH holds or not. Moreover, if there is no agreement between these both quantities w.r.t. indicating the emergence of ISI equilibration, we can check whether at least the above quantity ν predicts it correctly.

Analytic and numerical investigations in closed quantum systems

In Ref. [4], we investigate systems that allow for tuning the scaling parameter γ from $\gamma > 0$ to $\gamma < 0$. Thus, we are able to determine whether (i) ν indeed is a good quantifier to predict ISI equilibration and (ii) ISI equilibration emerges even so the ETH is strongly violated. To this end we consider the following asymmetric Heisenberg spin–1/2 ladder model described by $\hat{H} = \hat{H}_L + \hat{H}_R + \hat{H}_{\text{int}}$. The partial Hamiltonian read for the left/right beam

$$\hat{H}_{L,R} = \sum_{i=1}^{N_{L/R}-1} \left[\hat{S}_i^x \hat{S}_{i+1}^x + \hat{S}_i^y \hat{S}_{i+1}^y + \Delta \hat{S}_i^z \hat{S}_{i+1}^z \right] \tag{23}$$

and the interaction between the beams

$$\hat{H}_{\text{int}} = \kappa \sum_{i=1}^{N_L} \left[\hat{S}_i^{x,L} \hat{S}_i^{x,R} + \hat{S}_i^{y,L} \hat{S}_i^{y,R} + \Delta \hat{S}_i^{z,L} \hat{S}_i^{z,R} \right] \quad , \tag{24}$$

where $\hat{S}^{x,y,z}$ are spin–1/2 operators and κ is an exchange coupling constants (for details see e.g. [4, 57]). $\Delta = 0.1$ accounts for an anisotropy along the z axis. The asymmetry within this model arises from $N_L < N_R$ which denote the number of sites along the left and right beam, respectively. By varying the coupling strength κ we are able to tune the scaling of Σ (see below).
We investigate in the following the energy difference between the left and right part of the system, i.e., $\hat{D} = \hat{H}_L - \hat{H}_R$.

As suggested in [30], we construct the initial states as follows

$$\rho(t_0) \propto \exp\left(-\frac{\hat{H}^2}{2\,\sigma^2} - \frac{(\hat{D} - D_0)^2}{2\sigma_D^2} \right) \quad , \tag{25}$$

where σ, σ_D^2 are parameters by which we can adjust the variances of the initially peaked distributions w.r.t. the spectra of H and D, respectively. Note that the parameters σ, σ_D^2 do not coincide with the the "true" variances since Hamiltonian and observable $\hat{D}$ do not commute. By carefully tuning σ, σ_D^2 and D_0 we ensure that our initial state is peaked w.r.t. energy around zero with a standard deviation ≈ 0.6. Hence, these states are basically microcanonical states at energy $E = 0$ that also yield a sharp initial expectation value of $\hat{D}$ around D_0, i.e., these states provide the above used energy selective probabilities.
Next we will simply display and briefly discuss the main results of Ref. [4]. In Fig. 1(a) a finite-size scaling (w.r.t. system size $N = N_L + N_R$) of the ETH quantifier Σ for different κ is shown. One can distinguish mainly two regimes: Σ converges against a non-zero value in the thermodynamic limit and $\Sigma \to 0$ for increasing system size. The threshold seems to be close to $\kappa = 3.7$. For the same parameters, Fig. 1(b) displays the behavior of ν. Apparently there are also the two regimes regarding the behavior in the thermodynamic limit, but the threshold seems to be a little larger ($\kappa \approx 4$) than for Σ. This may hint towards ISI equilibration even though the ETH is violated. In Fig. 2 dynamics of the system ($N = 26$) are exemplary shown for intermediate coupling ($\kappa = 3.0$) and strong coupling ($\kappa = 4.5$), i.e., for cases below and above the predicted thresholds, respectively. Apparently for intermediate coupling the expectation values tends towards a universal long-time value. Note, however, that there are still residues of the initial states visible ("stick effect"). For strong coupling the "stick effects" are rather strong, i.e., the residues of the initial state are large and will most likely not vanish in the thermodynamic limit. The results are consistent with the idea of the ETH. In order to quantify this directly we display in Fig. 3 for different values of κ around the predicted thresholds the results for $r = d_\infty/d_0$. Indeed, ISI equilibration seems to appear for $\kappa = 3.7$ though the ETH is for this case violated. ISI equilibration seems to break down at $\kappa = 4$ what coincides with the predicted threshold by ν.
Conclusively, we demonstrated that ISI equilibration may emerge even so the ETH is violated and the quantifier ν predicts the threshold w.r.t. κ above which ISI equilibration breaks down correctly while the "bare" ETH quantity Σ does not.

In the followup work [57] the authors investigate another class of initial states:

$$\rho(t_0) \propto e^{-\beta\,\hat{H} + \delta \hat{D}} \quad , \tag{26}$$

where β corresponds to an inverse temperature and $\hat{D}$ is again the observable of interest. δ regulates the displacement from equilibrium w.r.t. the equilibrium expectation value $\langle \hat{D} \rangle_{eq}$. Such states are physical reasonable assumptions, see e.g. [56].
For small δ, i.e., small displacement, ISI equilibration was analytically investigated revealing a linear dependence of the initial expectation value $d_0 := \langle \hat{D}(t_0) \rangle$ as well as the longtime expectation value $d_\infty := \langle \hat{D}(t \to \infty) \rangle$ on δ if the ETH is violated. Moreover, if the expectation value of $\hat{D}$ in thermal equilibrium vanishes (which can always be achieved by properly constructing the observable) one finds that $r = d_\infty/d_0$ is (i) inde-

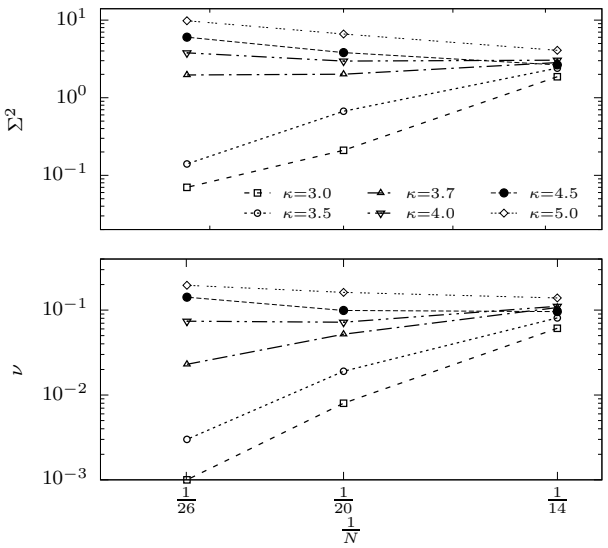

FIG. 1. In (a) the scaling of the ETH quantifier Σ^2 w.r.t. coupling strength κ and system size N is displayed. One can distinguish mainly two regimes: (i) Σ^2 tends towards zero for $N \to \infty$ (ETH is valid) and (ii) Σ^2 tends towards non-zero values (or even diverges) for large systems (ETH is violated). The threshold is roughly at $\kappa \approx 3.7$. In contrast the scaling of ν as shown in (b) suggests a slightly larger threshold at $\kappa \approx 4.0$. This hints toward ISI equilibration even when the ETH is violated.

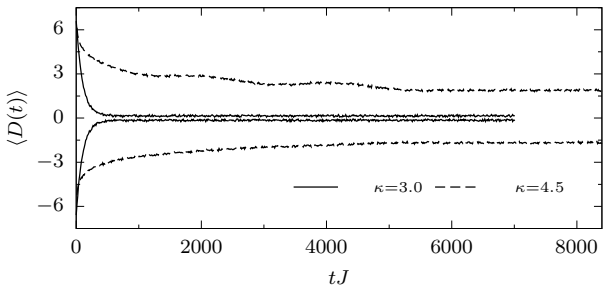

FIG. 2. Relaxation behavior of the energy difference $\hat{D}$ for $\kappa = 3.0$ (solid lines) and $\kappa = 4.5$ (dashed lines). For weak coupling the system seems to relax toward a unique value (the visible gap will vanish in the thermodynamic limit) whereas for strong coupling there remain large residues of the initial state (stick effects). The behavior is consistent with the ETH and the thresholds derived from Fig. 1(a).

pendent of δ for small displacements and (ii) describes a linear scaling of d_∞ with d_0. In particular $r \equiv \nu$ holds, i.e., this supports the above findings that $\nu \to 0$ indicates ISI equilibration.

Numerical studies (for the same model as above) show that depending on the specific observable $\hat{D}$ the linear dependency of d_∞ on d_0 may remain true also for large displacements from equilibrium.

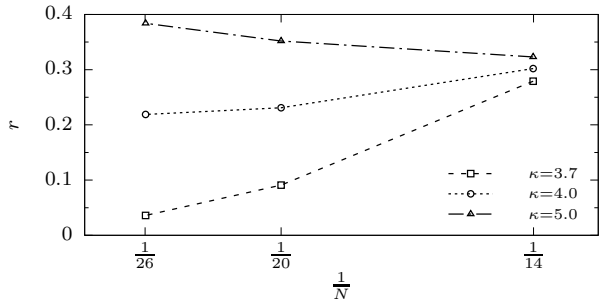

FIG. 3. Finite-size scaling of the ISI quantifier r for three distinct coupling strength near the thresholds predicted in Fig. 1. The data suggest that ISI equilibration is still possible for $\kappa = 3.7$. This is consistent with the threshold of ν but in contrast to the threshold for Σ^2.

III. STOCHASTIC PROCESSES AND MARKOVIANITY IN CLOSED QUANTUM SYSTEMS

As pointed out above the emergence of equilibration in certain closed quantum systems is backed by both experiments and theory (as e.g. eigenstate thermalization hypothesis and typicality). While these concepts allow to make statements about equilibrium properties they do not embed any description of the way into equilibrium when started from some non-equilibrium state. As a first step towards investigating relaxation behavior we are going to introduce stochastic processes in this section. This will set the foundation on which we can built several special stochastic approaches in order to describe equilibration in the consecutive sections.

A stochastic process is described by a sequence of consecutive stochastic variables $\{x_n\}_{n\leqslant N}$, ordered according to some parameter n [58]. In physics these stochastic variables are commonly associated with outcomes of measurements (*events*) on the underlying system that may be subjected to some random interaction giving rise to non-deterministic dynamics. The ordering parameter is then in general the time point at which the measurement was performed. Furthermore, to each sequence consisting of N events one assigns a N-parameter trajectory probability function on phase space, i.e.,

$$p_N[\{x_i(t_m)\}_{m\leqslant N};\rho] \quad , \tag{27}$$

where $x_i(t_m)$ means that the event x_i is measured at time t_m and $t_1 \leqslant \cdots \leqslant t_{N-1} \leqslant t_N$. The parameter ρ expresses that the value of the trajectory probability function may depend on the initial state ρ. Note that fully deterministic dynamics are also included in this framework where only one specific trajectory yields a non-zero probability, i.e., $p_N[\{x_i(t_m)\}_{m\leqslant N};\rho] = 1$. We mention already here that in order to actually obtain such probability functions for quantum systems we will

introduce in Sec. III A a measurement scheme that is based on the concept of consistent histories, but until then we take the probability functions as already given.

According to the above definition a stochastic process is completely characterized by a sequence of probability functions, i.e.,

$$p_1[x_i(t_1);\rho] \to p_2[x_i(t_1), x_j(t_2);\rho] \to ... \quad , \tag{28}$$

where p_1 is a one-parameter function, p_2 a two-parameter function and so on. Hence, to describe some stochastic process properly one may need information about infinitely many probability functions and events $x_i(t_m)$. In Sec. III B we will introduce a special kind of processes that reduces the amount of needed information drastically.

In general, one assumes that the events form a complete set, i.e.,

$$\sum_{x_i} p[x_i(t)] = 1 \quad . \tag{29}$$

In plain words Eq. (29) states: Each measurement performed at any time t must result in one single event or a linear combination of events of the corresponding set. By virtue of Eq. (29) we can introduce the notion of sub-trajectories that are defined as

$$p_{N-1}[x_i(t_1) \; ... \; x_j(t_{N-1});\rho] = \sum_{x_k} p_N[x_i(t_1) \; ... \; x_j(t_{N-1}), x_k(t_N);\rho] \quad , \tag{30}$$

where the sum runs over all possible events measured at the time point t_N. Thus, one can reduce each trajectory probability function to any probability function with less events by succesively applying Eq. (30). Note that such reductions can be applied also on any other time point in between, not only the last one. However, in these cases one has to make sure that the third Kolmogorov axiom is satisfied [59, 60]. We will discuss this issue in the next section.

A. Measurement scheme and decoherence functional

Measurements in quantum systems can be described in various ways e.g. as an external compound acting on the system which is usually the case in open system scenarios. Here we are going to discuss a von Neuman measurement scheme along the lines of the *consistent history approach* [61] (sometimes also called *decoherent history approach* [62, 63]), i.e., measurements are mathematically encoded in a set of projection operators π_i. Thus, trajectories (in this context often referred to as *histories*) are "generated" by alternating actions of such measuring operators and time-propagating the resulting state according to the Schrödinger equation. Note that the more philosophic aspects of these approaches exceeding the above measurement scheme are not relevant here. For critical reviews on consistent histories see e.g. Refs. [64, 65].

The mentioned measurement operators form a complete set [cf. Eq. (29)], i.e.,

$$\sum_i \hat{\pi}_i = \mathbb{1} \quad , \tag{31}$$

where $\mathbb{1}$ denotes the unity operator and each projector $\hat{\pi}_i$ corresponds to a distinct event x_i while the whole set of projectors corresponds to a certain property of the system like magnetization or energy.
When we denote $\rho(t)$ as the density operator describing the system at time t then the probability to measure the event x_i at time t reads

$$p_1[x_i(t)] := \mathrm{tr}\left[\hat{\pi}_i \, \rho(t)\right] \quad . \tag{32}$$

Introducing $U(\tau)$ as time-translation operator which propagates the a state in amounts of τ, and following the above described concept, we define trajectory probabilities as

$$p_N[x_i(0), x_j(\tau_1), \cdots, x_N(\tau')] := \mathrm{tr}\left[\hat{\Pi}_N \, \mathcal{U}(\tau') \; \cdots \; \hat{\Pi}_j \, \mathcal{U}(\tau_1) \, \hat{\Pi}_i \, \rho\right] \quad , \tag{33}$$

where we used the following abbreviations:

(i) $\hat{\Pi}_i \, \rho := \hat{\pi}_i \, \rho \, \hat{\pi}_i$,

(ii) $\mathcal{U}(\tau_i) \, \rho := U(\tau_i) \, \rho \, U(\tau_i)^\dagger$ and

Without loss of generality, we assume hereafter that all time steps τ_i are equal and therefore omit the explicit time parameters unless necessary.

Next, we are going to discuss the decoherence functional (or consistency condition) which provides statements about the validity of the third Kolmogorov axiom of probability theory [59]. In order to explain this properly let us exemplary consider a 3-step trajectory probability function where only the first and last event are actually known (measured), i.e., in the time in between there was no measurement performed. In this case the probability function reads

$$\begin{aligned} p_3[x_n, —, x_m;\rho] &= \mathrm{tr}\left[\hat{\Pi}_m \, \mathcal{U}^2 \, \hat{\Pi}_n \, \rho\right] \\ &= \sum_{x_k} p_3[x_n, x_k, x_m] + \\ &\quad \sum_{i \neq j} \mathrm{tr}\left[\hat{\Pi}_m \, \mathcal{U}\left(\hat{\pi}_i(\, \mathcal{U} \, \hat{\Pi}_n \, \rho) \, \hat{\pi}_j\right)\right] \quad , \end{aligned} \tag{34}$$

where "—" should indicate that at the corresponding time point no measurement was performed. Note that the first sum is basically described by Eq. (30) whereas the second sum accounts for possible interference phenomena. Thus, the second sum is defined as decoherence functional

$$D(n,m) := \sum_{i\neq j} \mathrm{tr}\left[\hat{\Pi}_m\, U\, \hat{\pi}_i\, U\, (\hat{\Pi}_n\, \rho)\, U^\dagger\, \hat{\pi}_j\, U^\dagger\right] \quad . \tag{35}$$

Now the third Kolmogorov axiom (KA3) demands that $D(n,m) = 0$, or to put it plain: If some main event may be obtained as the result of many different independent *sub-events*, then the probability for the main event to occur is given by the sum of the probabilities of the *sub-events* (given here by the first sum term). Although it seems reasonable to assume $D(n,m) = 0$ to hold for classical processes (absence of interference) in the quantum regime we have indeed to deal with interference (cf. e.g. the famous double-slit experiment where KA3 is obviously violated). Thus, in general one finds for finite quantum systems $D(n,m) \neq 0$. Nevertheless, there may be quantum systems for which $D(n,m)$ will indeed vanish in the thermodynamic limit; cf. Sec. III C and especially the analysis in Sec. III of Ref. [3].
Thus, for the discussions in the next section we are going to assume that KA3 is always fulfilled.

B. Markov processes and Markovianity

Now we introduce Markov processes that are a special sort of stochastic processes and allow to reduce the information needed to fully describe a stochastic process enormously. These processes are indicated by the fact that the probability to measure an event x_n does only depend on the last measured events $\{x_i \cdots x_{n-1}\}$ instead of the whole prior event sequence (history) [24, 66, 67]. This is formally best expressed by means of conditional probabilities

$$\omega(x_n|x_1\ ...\ x_{n-1};\rho) = \frac{p[x_1\ ...\ x_n;\rho]}{p[x_1\ ...\ x_{n-1};\rho]} \quad . \tag{36}$$

For convenience we omitted the subscripts of the probability functions that indicate the lengths of each trajectory and will do so unless confusions may arise otherwise. We emphasize here again that Eq. (36) can only be an accurate definition of a Markov process if the trajectory probability functions also fulfill KA3.

Now, according to Eq. (36) we call a process one-step Markovian if

$$\omega(x_n|x_1\ ...\ x_{n-1};\rho) = \omega(x_n|x_{n-1};\rho) \tag{37}$$

holds true, two-step Markovian if only

$$\omega(x_n|x_1\ ...\ x_{n-1};\rho) = \omega(x_n|x_{n-2},\ x_{n-1};\rho) \tag{38}$$

holds true, and so on. Note that Markovian behavior (*Markovianity*) is an ambigious term especially w.r.t. open (quantum) systems, see e.g. [24]. Thus, the above definition of Markovianity is just one possibility which we made use of also in [3].

Let us now assume one-step Markovianity applies to some process. Then one can characterize each possible trajectory just by the initial measurement and the corresponding transition probabilities ω, i.e.,

$$p[x_1 ... x_n;\rho] = \omega(x_n|x_{n-1};\rho)\ ...\ \omega(x_2|x_1;\rho)\, p[x_1;\rho] \quad . \tag{39}$$

Note that due to the possible dependence of the transistion probabilities and especially the first measurement result on the initial state ρ one still may need for each destinct ρ a corresponding set of the aforementioned quantities. In the next section we are going to discuss the results of Ref. [3] where we explicitly used a class of initial states that renders the transition probabilities independent of the specific initial state. But before doing so we will use one-step Markovianity and the consistency condition to derive the renowned Chapman-Kolmogorov equation. To this end we firstly write $p[x_1, —, x_3]$ as $\omega(x_3|x_1)\ p[x_1;\rho]$, i.e., as a conditional transition probability weighted by the initial occurrence probability of x_1. Recalling Eq. (34) where we already used $D(n,m) = 0$ and write again explicit time arguments yields

$$\omega[x_3(t_3)|x_1(t_1)]\ p[x_1(t_1);\rho] = \sum_{x_2} p[x_1(t_1), x_2(t_2), x3(t_3)] \quad . \tag{40}$$

According to Eq. (39) we can further expand the addend and obtain finally

$$\omega[x_3(t_3)|x_1(t_1)] = \sum_{x_2} \omega[x_3(t_3)|x_2(t_2)]\ \omega[x_2(t_2)|x_1(t_1)] \quad , \tag{41}$$

where we already divided by the initial probability $p[x_1(t_1);\rho]$. This is the renowned Chapman-Kolmogorov equation that will allow us to derive master equations in Sec. IV most elegantly.

C. Occurrence of Markovianity and consistency in closed spin models

In Ref. [3] we investigate a spin–1/2 lattice model (consisting of two spin ladders) described by $\hat{H} = \hat{H}_L + \hat{H}_R + \hat{H}_{\mathrm{int}}$. The uncoupled ladder parts are described

by

$$\hat{H}_{L,R} = \sum_{r=1}^{2} \sum_{i=1}^{N/2-1} \Big[\hat{S}^x_{i,r} \hat{S}^x_{i+1,r} + \hat{S}^y_{i,r} \hat{S}^y_{i+1,r} + 0.6\, \hat{S}^z_{i,r} \hat{S}^z_{i+1,r} \Big] \tag{42}$$

and the interaction between these parts by

$$\hat{H}_{\rm int} = 0.5 \sum_{i=1}^{N/2} \left[\hat{S}^{x,L}_{i,2} \hat{S}^{x,R}_{i,1} + \hat{S}^{y,L}_{i,2} \hat{S}^{y,R}_{i,1} + 0.6\, \hat{S}^{z,L}_{i,2} \hat{S}^{z,R}_{i,1} \right] . \tag{43}$$

The parameter r accounts for the left ($r = 1$) and right beam ($r = 2$) of the respective spin ladder and N is the number of sites per ladder. The observable of interest is the magnetization difference between left and right ladder, i.e.,

$$\hat{X} = \sum_{r=1}^{2} \sum_{i=1}^{N/2} \hat{S}^{z,L}_{i,r} - \hat{S}^{z,R}_{i,r} \quad , \tag{44}$$

where we use a measuring scheme as described in Sec. III A; for more details see the corresponding article below.

The main focus of this work is to test (i) whether the consistency condition, Eq. (35), is satisfied for the studied model and (ii) whether we can (at least) observe λ-step Markovian behavior (λ being a possibly large number). Both consistency condition and Markovianity are also studied w.r.t. their behavior when the time interval τ between consecutive measurements is varied. First analytic studies based on typicality arguments give rise to the assumption that at least for systems featuring large Hilbert spaces and few symmetries, i.e., systems for which the concept of typical behavior may be applied, the dynamics are indeed consistent in the sense of $D(n, m) \to 0$ for arbitrarily events x_n and x_m. Furthermore, one-step Markovian behavior should hold also. However, we should emphasize that the analytical studied is not exhaustive since it focus on a 3-step trajectory only; see for further details Sec. III in [3].

Nevertheless, motivated by these first results (and the behavior of the relaxation dynamics as displayed in Fig. 2 in [3]) we also numerically studied the consistency condition and one-step Markovianity for one specific 3-step trajectory ($x_1 \to x_2 \to x_3$) (see below). We furthermore resticted the investigation to narrow energy regime. Thus, in order to discuss the findings of [3] some preliminary remarks are necessary.

According to the measurement scheme introduced in Sec. III A the events corresponding to the magnetization difference are associated to projectors $\hat{\pi}_x$. These projectors $\hat{\pi}_x$ are spanned by all eigenstates of the corresponding magnetization difference operator that feature the same eigenvalue x. However, because of the restriction to a certain energy shell ΔE w.r.t. the uncoupled system $\hat{H}_0 = \hat{H}_L + \hat{H}_R$ the "true" projectors read

$$\hat{\pi}_{x,E} = \hat{\pi}_{\Delta E}\, \hat{\pi}_x\, \hat{\pi}_{\Delta E} \quad , \tag{45}$$

where $\hat{\pi}_{\Delta E}$ accounts for the energy restriction. Since the set of $\hat{\pi}_{x,E}$'s does not form a complete set we have to introduce the pseudo event

$$\tilde{\hat{\pi}}_{x,E} = \mathbb{1} - \sum_{x \in \Delta E} \hat{\pi}_{x,E} \quad . \tag{46}$$

This pseudo event can be interpreted as measuring the probability loss arising by dynamics that "venture" beyond the boundaries of the respected energy shell. However, as indicated in [3], almost no loss of probability is detected on our observation time scales.

One other remark involves the class of initial states that are simply linear combinations of the measuring projectors itself, i.e.,

$$\rho = \sum_n c_n\, \hat{\pi}_n \quad c_n \geq 0 \quad . \tag{47}$$

It is straightforward to show that such initial states indeed produce initial-state-independent transition probabilities ω. (See the corresponding article for further motivations for this specific class of states.)

Quantifying consistency and Markovianity

In order to decide whether the studied dynamics fulfill the consistency condition we calculate the following quantity:

$$C(x_1, ..., —, ..., x_n) := \left| 1 - \frac{p(x_1,\ ...\ , —,\ ...\ , x_{n-1})}{\sum_\gamma\ p(x_1,\ ...\ , x_{n-1})} \right| \quad , \tag{48}$$

where $\sum_\gamma \cdots$ denotes a sum over all possible intermediate event sequences according to the discussion above. Thus, if the dynamics indeed fulfill the consistency condition then both the numerator and denominator yield the same value and $C(x_k,\ ...\ , —,\ ...\ , x_n) = 0$.

In a very similar fashion we define the quantifier w.r.t. Markovian behavior:

$$M(x_k,\ ...\ , x_n) := \left| 1 - \frac{\omega(x_n | x_k\ ...\ x_{n-1})}{\omega(x_n | x_{k+1}\ ...\ x_{n-1})} \right| \tag{49}$$

Hence, $M(x_k\ ...\ x_n) = 0$ implies perfect Markovianity. Note, however, that this quantity just tests whether the transistion probability changes if one includes one more event into the sequence but it may be possible (though unlikely) that just the inclusion of two or more events actually changes the value. Therefore, one is possibly forced to perform further checks. For the present model we found that $M(x_k\ ...\ x_n)$ is sufficient to ensure Markovian behavior (though not explicit

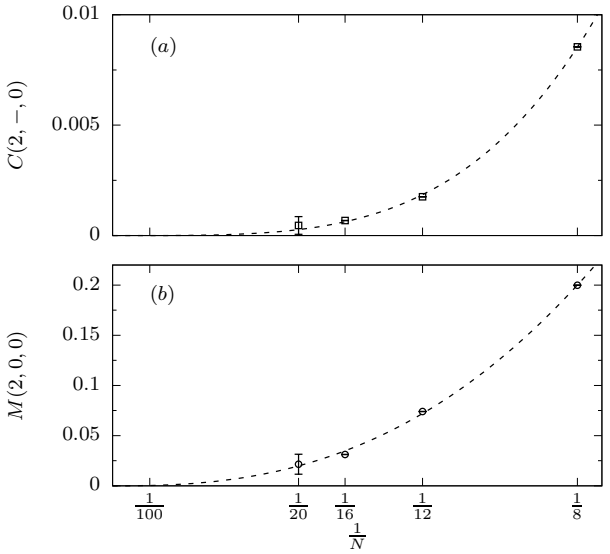

FIG. 4. In (a) the results on the consistency condition for a spin lattice model and various system sizes are shown where the dashed line indicates a power-law fit. The data suggest that in the thermodynamics limit, i.e., $1/N \to 0$, the system is perfectly consistent with the third Kolmogorov axiom. Similarly, in (b) results for Markovianity are shown for the same parameters. The data suggest that Markovianity holds in the thermodynamic limit, also.

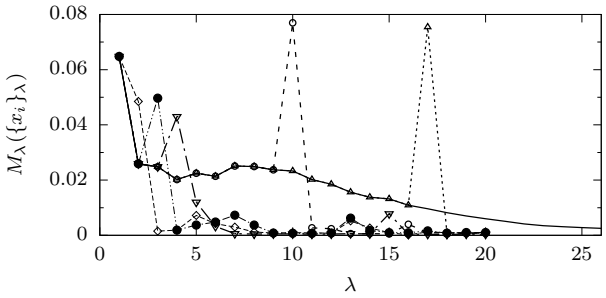

FIG. 5. Display of the behavior of λ-step Markovianity as λ increases for $N = 16$. The solid line corresponds to a history arising from repeatedly measuring the same property while the symbols show results for quasi-random histories that are, however, weighted with transition probabilities ω (see text). Though the random histories feature high peaks at the first occurrence of a event different from the uniform history the data suggests that many-step Markovianity is always valid for sufficient large λ.

discussed in [3]).

The results on the consistency condition by means of Eq. (48) are shown in Fig. 4(a) for several system sizes N and the sequence $(x_1, x_2, x_3) = (2, 0, 0)$. The data suggests that at least in the thermodynamic limit the trajectory probability functions obey indeed the consistency condition. Hence, it is reasonable to investigate the Markovianity condition, i.e., Eq. (49). The corresponding results are summarized in Fig. 4(b) which also suggest that at least in the thermodynamic limit one-step Markovianity is fulfilled. As said above, we also investigated the behavior of $C(x_1, —, x_3)$ and $M(x_1, x_2, x_3)$ in case one varies the duration of time steps τ between consecutive measurements. We found that both consistency condition and one-step Markovianity are well fulfilled if the time steps are larger than 1/10-th of the relaxation time of the underlying system (see Fig. 3 in [3]). Below this threshold the violation of both increases rather strongly.

So far only the emergence of one-step Markovianity in the thermodynamic limit was studied. As remarked above, this, however, does not neccessarily ensure that two-step, three-step, etc. Markovianity also holds. For repeatedly measuring the same property one can analytic show (consistency is taken for granted here) that λ-step Markovianity always emerges for a sufficient large sequence length λ (see [3]). Note that this result is correct for any system and is not restricted to the so far studied spin models. Since such analytic investigation is not present for sequences that feature various possible events we study now λ-step Markovianity, M_λ, for "quasi-random" sequences. All studied sequences start with the measurement of the same property ($x = 0$). Consecutive measurements are randomly selected (weighted by a corresponding transition probability) to either remain at the current property ($x \to x$) or jump to a neighboring one ($x \to x \pm 1$). In Fig. 5 we summarize the results for some of these sequences. Note that the solid line represents the sequence of repeatedly measuring $x = 0$, which tends towards zero just as the analytic investigation predicts. Symbols (connected by dashed lines) correspond to the quasi random sequences. Interesting is the fact that the first measurement of a property $x \neq 0$ results in a significant increase of the respective value of the quantity M_λ while M_λ decreases thereafter drastically (in comparison to the corresponding value for the uniform sequence) irrespective of the actual measured property, $x = 0$ or $x \neq 0$. Though we cannot provide any reasoning for this behavior, it at least strongly suggests that even if one allows for random sequences Markovianity will emerge for sufficient large sequence lengths λ.

IV. MASTER EQUATIONS AND FOKKER-PLANCK EQUATIONS IN CLOSED QUANTUM SYSTEMS

In this section we are going to introduce standard stochastic approaches, i.e., master and Fokker-Planck equations, that successfully describe the time evolution of many (classical) relaxation processes; see e.g. [66]. As will be demonstrated below, the later can be de-

rived from fundamental master equations and involves already the notion of *diffusion* which will be the main topic of Sec. V.

In order to derive the (discretized) master equation we start with the Chapman-Kolmogorov equation, Eq. (41), and consider the case $t = t_3 = t_2 = t_1$:

$$\omega[x_3(t_3)|x_1(t)] = \sum_{x_2} \omega[x_3(t_3)|x_2(t)]\, \omega[x_2(t)|x_1(t)] \quad , \tag{50}$$

where we immediately see that $\omega[x_2(t)|x_1(t)] = \delta_{x_2,x_1}$ must hold. With this result the short-time transition probability reads:

$$\begin{aligned}\omega[x_2(t+\Delta t)|x_1(t)] = \delta_{x_2,x_1}\,[1-\Gamma[x_1(t)]\,\Delta t] + \\ W_t(x_2|x_1)\,\Delta t + \mathcal{O}(\Delta t^2) \quad ,\end{aligned} \tag{51}$$

where $W_t(x_2|x_1)$ denotes the transition probability (per unit of time) from x_1 to x_2 at time t. Since $\omega[x_2(t+\Delta t)|x_1(t)]$ must be normalized for any Δt the expression $1-\Gamma[x_1(t)]\,\Delta t$ is interpreted as the probability that no transition takes place during $[t; t+\Delta t]$. Thus, we get

$$\Gamma[x_1(t)] = \sum_{x_2} W_t(x_2|x_1) \quad . \tag{52}$$

Now, considering the short-time expression for Eq. (41) yields

$$\begin{aligned}\omega[x_3(t_2+\Delta t)|x_1(t_1)] \backsimeq \sum_{x_2}[\delta_{x_2,x_3}[1-\Gamma(x_2(t_2))\Delta t] + \\ W_{t_2}(x_3|x_2)\,\Delta t]\,\omega[x_2(t)|x_1(t)] \quad .\end{aligned} \tag{53}$$

Taking into account the Kronecker delta δ_{x_2,x_3} and substituting $\Gamma[x_2(t_2)]$ we eventually obtain

$$\begin{aligned}\frac{\partial}{\partial t}\,\omega[x_3(t)|x_1(t')] = \sum_{x_2} W_t(x_3|x_2)\,\omega[x_2(t)|x_1(t')] - \\ W_t(x_2|x_3)\,\omega[x_3(t)|x_1(t')] \quad ,\end{aligned} \tag{54}$$

where we changed the discrete time points to continuous variables, i.e., $t_1 \to t'$, $t_2 \to t$ and performed the the limit $\Delta t \to 0$. This equation is a differential form of the (discretized) Chapman-Kolmogorov equation and sometimes already called master equation. However, here, we want to obtain a differential equation for the actual occurrence probabilities of certain event rather than for transition probabilities. Therefore, by multiply Eq. (54) on both sides with $p[x_1(t_1)]$ and using the history generation according to Eq. (39), we find:

$$\begin{aligned}\frac{\partial}{\partial t}\,p[x_3(t)] = \sum_{x_2} W_t(x_3|x_2)\,p[x_2(t)] - \\ W_t(x_2|x_3)\,p[x_3(t)]\end{aligned} \tag{55}$$

This equation is commonly denoted as discretized master equation. For the further proceeding it is convenient to turn over to a continuous version of Eq. (55):

$$\begin{aligned}\frac{\partial}{\partial t}\,p[x,t] = \int dx'\, W_t(x|x')\,p[x',t] - \\ W_t(x'|x)\,p[x,t] \quad ,\end{aligned} \tag{56}$$

where we adjusted the notation a little.

Next we may perform a Kramers-Moyal expansion that transforms the above integro-differential equation into a ordinary differential equation of infinite order. To do so, we first of all define $W(x'; r) := W(x|x')$ with $r := x - x'$, i.e., r describes the "distance" between to events. Note that we omit unnecessary indices. Then Eq. (56) reads:

$$\frac{\partial}{\partial t}\,p[x,t] = \int dr\, W(x-r; r)\,p[x-r,t] - W(x; -r)\,p[x,t] \tag{57}$$

If we now assume that $W(x; r)$ is sharply peaked for variation in r but smooth for variations in x, and furthermore that $p[x,t]$ is also a smooth function with respect to x than we can perform a Taylor expansion. This results after some straightforward calculus and rearranging in

$$\frac{\partial}{\partial t}\,p[x,t] = \sum_{n=0}^{\infty} \frac{(-1)^n}{n!}\,\frac{\partial^n}{\partial x^n}\left\{\left[\int dr\, r^n\, W(x; r)\right]\,p[x,t]\right\} \tag{58}$$

We may also define *jump moments*

$$a^{(n)}(x,t) := \int dr\; r^n\; W(x; r) \tag{59}$$

and write Eq. (58) in the compact form

$$\frac{\partial}{\partial t}\,p[x,t] = \sum_{n=0}^{\infty} \frac{(-1)^n}{n!}\,\frac{\partial^n}{\partial x^n}\left\{a^{(n)}(x,t)\,p[x,t]\right\} \tag{60}$$

Note that this equation is basically identical to Eq. (56), and thus may also be difficult to solve. However, there may exist situations where one can truncate the sum after a few terms.
Here we will consider the case where the expansion breaks off after the second term, i.e.,

$$\begin{aligned}\frac{\partial}{\partial t}\,p[x,t] = -\frac{\partial}{\partial x}\left\{a^{(1)}(x,t)\,p[x,t]\right\} + \\ \frac{1}{2}\frac{\partial^2}{\partial x^2}\left\{a^{(2)}(x,t)\,p[x,t]\right\} \quad ,\end{aligned} \tag{61}$$

which is the renowned Fokker-Planck equation. $a^{(1)}$ is usually referred to as drift coefficient whereas $a^{(2)}$ is known as diffusion coefficient. We mention already here that Eq. (61) already contains the diffusion equation

that we are going to investigation w.r.t. the accordance with quantum dynamics below in Sec. V.
But prior, we will again discuss (analytic and numerical) results on the accordance of quantum dynamics with Fokker-Planck dynamics.

A. Projection operator method

A prominent scheme to describe relaxation behavior (Markovian as well as non-Markovian) in quantum systems is provided by so called projection operator methods. These schemes allow to describe the relaxation dynamics based on an effective set of relevant variables rather than a detailed microscopic description [8]. Although developed orginally in the context of open quantum systems [68, 69] and well-established in this field (see e.g. Ref. [24]) there are also studies demonstrating the applicability for closed quantum systems [1, 26, 70]. In literature there are mainly two different approaches, the Nakajima-Zwanzig approach [68, 69] and the time-convolutionless (TCL) method [71–74]. We will focus here only on the later.

The full quantum dynamic of some quantum system can be described by the Liouville-von Neumann equation [8, 24]:

$$\frac{d\rho(t)}{dt} = -\frac{i}{\hbar}[\hat{H}, \rho(t)] \quad , \tag{62}$$

where H denotes the Hamilton operator of the underlying system featuring the general form $\hat{H} = \hat{H}_0 + \hat{V}$. $\hat{V}$ is in this context in general denoted as perturbation operator. For the further proceeding we turn over to the Dirac picture which leads to the "new" Liouville-von Neumann equation

$$\frac{d\rho_D(t)}{dt} = -i[\hat{V}_D(t), \rho_D(t)] \equiv \mathcal{L}(t)\,\rho_D(t) \quad . \tag{63}$$

The superoperator $\mathcal{L}$ is commonly known as Liouvillian. In order to map the dynamics onto a closed system of effective dynamic equations for a set of relevant variables one has to choose an appropriate projection superoperator $\mathcal{P}$. Formally a projection superoperator is a linear map that operates on system states ρ and can be defined as a linear combination of relevant observables $\hat{B}_n$, i.e.,

$$\mathcal{P}\rho = \sum_n \mathrm{tr}\left[\hat{B}_n\,\rho\right]\,\hat{B}_n = \sum_n b_n\,\hat{B}_n \quad , \tag{64}$$

where $\hat{B}_n = \hat{B}_n^\dagger$ holds. Hereafter, we assume that the $\hat{B}_n$'s form themselves a complete set of orthogonal projection operators which in particular means that $\mathcal{P}^2 = \mathcal{P}$ holds. Analog to Eq. (64) we define a superoperator projecting onto the "irrelevant" part of the system as

$$\mathcal{Q}\rho = \sum_n \mathrm{tr}\left[\hat{\tilde{B}}_n\,\rho\right]\,\hat{\tilde{B}}_n \quad , \quad \mathcal{Q} = \mathbb{1} - \mathcal{P} \quad . \tag{65}$$

Employing Eq. (63) to describe the time-evolution of $\mathcal{P}\rho$ we find after straightforward calculations (for a detailed derivation see e.g. see [24, 75]):

$$\frac{d}{dt}\mathcal{P}\rho(t) = \mathcal{K}(t)\,\mathcal{P}\rho(t) + \mathcal{I}(t)\,\mathcal{Q}\,\rho(t) \quad , \tag{66}$$

where both TCL generator $\mathcal{K}(t)$ and inhomogeneity $\mathcal{I}(t)$ are explicit time-dependent superoperators. One can show that, if $\mathcal{P}\,\rho(0) = \rho(0)$ holds, the much shorter equation

$$\frac{d}{dt}\mathcal{P}\,\rho(t) = \mathcal{K}(t)\,\mathcal{P}\,\rho(t) \tag{67}$$

is valid, i.e., the irrelevant parts of the system do no longer play a role for the dynamics. In general Eq. (66) and also Eq. (67) are as difficult to solve as the Liouville-von Neumann equation itself. Therefore, focusing on Eq. (67), we will discuss a perturbation expansion with respect to the strength of the interaction $V_D(t)$. This leads to:

$$\mathcal{K}(t) = \sum_{n=1}^{\infty} \mathcal{K}^{(n)}(t) \tag{68}$$

For many physical applications one finds that all odd-numbered $\mathcal{K}^{(n)}(t)$'s vanish [24, 76]. Employing $b_n(t) = \mathrm{tr}\left[\hat{B}_n\,\rho(t)\right]$ we find

$$\frac{d}{dt}b_n(t) = \sum_m K_{nm}(t)\,b_m(t) \quad , \tag{69}$$

with

$$K_{nm}(t) = \mathrm{tr}\left[\hat{B}_n\,\mathcal{K}(t)\,\hat{B}_m\right] = K_{nm}^{(2)}(t) + K_{nm}^{(4)}(t) + \cdots \quad . \tag{70}$$

In many cases already the second-order expansion term $\mathcal{K}^{(2)}(t)$ is sufficient to yield reasonable results. One finds for $K_{nm}^{(2)}(t)$ (see [24, 75, 76]):

$$K_{nm}^{(2)}(t) = \int_0^t dt'\,\mathrm{tr}\left[\hat{B}_n\,\mathcal{L}(t)\mathcal{L}(t')\,\hat{B}_m\right] \tag{71}$$

or by directly writing out the Liouvillian:

$$K_{nm}^{(2)}(t) = -\int_0^t dt'\,\mathrm{tr}\left[\hat{B}_n[\hat{V}_D(t), [\hat{V}_D(t'), \hat{B}_m]]\right] \tag{72}$$

Comparing Eq. (69) and Eq. (55) reveals that the TCL method ultimately leads to a (quantum) master equation with rates given by $K_{nm}(t)$. We emphasize, however, that the explicit time-dependence of the $K_{nm}(t)$'s may encode memory effects w.r.t. the former history of the dynamics. Nevertheless, as demonstrated in [1], under certain conditions a second-order TCL generator yields constant transition rates (w.r.t. time). Thus, we are able to compare such rates with such ones obtained by a simple statistic model in the next section.

B. Emergence of Fokker-Planck dynamics within spin-based models

In Ref. [1], we study again a (symmetric) spin–1/2 ladder model (i.e. in comparison to the Hamiltonian in Sec. II C this means $N = N_L = N_R$). The observable is again the magnetization difference between left and right beam, i.e.,

$$\hat{X} = \sum_{i=1}^{N} \hat{S}_i^{z,L} - \hat{S}_i^{z,R} \quad . \tag{73}$$

We repeat here the main results. To this end, we firstly consider a classical statistic model whose dynamics is describable by a master equation as discussed above. The general assumptions made are: (i) there are non-zero transition rates for simultaneously spin flips of adjacent spins only if both spins are anti-parallel, (ii) these transition rates are proportional to the square of the coupling strength between the corresponding spins, i.e., J, κ. For $J \gg \kappa$ the dynamics along the beams is approximately in an instantaneous equilibrium on time scales of relevant dynamics along the rungs. This leads to (iii) equal probabilities to find the spin "pointing up (down)" for each site along each individual beam. Following these basic assumptions we obtain transition rates of the form

$$W(X \pm 1|X) = \frac{\gamma\,\kappa^2\,N}{2}\,\left(\frac{1}{2} \mp \frac{2X}{N}\right)^2 \quad , \tag{74}$$

where X is a eigenvalue of observable $\hat{X}$. The parameter γ cannot be determined from the simple statistic model but must be determined by more sophisticated methods. Below we will demonstrate that this can be done e.g. by projection operator methods like the second-order TCL generator (see above).

Note that restricting the investigation to the magnetization subspace featuring a total magnetization zero we find $|X| \leqslant N/4$. Now, assuming that the probability for both $X = -N/4$ and $X = N/4$ are zero (or at least negligible) we can derive that the first and second moment of X will relax mono-exponentially, i.e.,

$$\langle X(t)\rangle \propto \exp(-R_1\,t) \quad \text{with} \quad R_1 = 2\gamma\kappa^2 \tag{75}$$

and

$$\langle X^2(t)\rangle \propto \exp(-R_2\,t) \quad \text{with} \quad R_2 = 4\left(1 - \frac{1}{N}\right)\gamma\kappa^2 \quad . \tag{76}$$

This is very similar to the results arising from the Fokker-Planck equation for an over-damped particle in a quadratic potential. In this case we would find $2\,R_1 = R_2$. The Fokker-Planck equation for our model reads

$$\frac{\partial}{\partial t}\,p(x,t) = \frac{\partial}{\partial x}\left\{\frac{\partial\,U(x)}{\partial x}\,p(x,t)\right\} + \frac{1}{2}\,\frac{\partial^2}{\partial x^2}\left\{D(x)\,p(x,t)\right\} \quad , \tag{77}$$

with $U(x) = \gamma\,\kappa^2 x^2$ and $D(x) = \gamma\kappa^2\left(1/4 + 4x^2\right)/N$. Note that we used the magnetization difference density $x = X/N$ here. It becomes in the limit of large N quasi-continuous. Eq. (77) emphasizes again the similarity to the particle in a quadratic potential. (Note that the dependency on the position in $D(x)$ becomes negligible if x is close to equilibrium, i.e., $x = 0$ here.)

In order to investigate now whether the quantum dynamics are similar to a description based on Eq. (77) we have to ensure that the occupation probabilities for $X = \pm 4/N$ remain negligible small for all times. This can be achieved by introducing an appropriate energy restriction on the initial state. (Since we consider only closed systems this restriction remains for all times.) Moreover, as found numerically in [1], quantum dynamics are only describable by the above approach if we also demand that the initial expectation value w.r.t. $\hat{X}$ is close to the equilibrium value (here close to zero). Both requirements can formally be captured by the following initial states $\rho_X(t_0)$:

$$\rho_X(t_0) = \frac{1}{Z}\,\hat{\pi}_{\Delta E}\,\hat{\pi}_X\,\hat{\pi}_{\Delta E} \quad , \quad Z = \mathrm{tr}\left[\hat{\pi}_{\Delta E}\,\hat{\pi}_X\,\hat{\pi}_{\Delta E}\right] \quad , \tag{78}$$

where $\hat{\pi}_X$ denotes a projection operator onto the eigenspace of $\hat{X}$ corresponding to the eigenvalue X and $\hat{\pi}_{\Delta E}$ accounts for an energy projection onto an energy interval ΔE. Here we choose $\Delta E = [-1; 1]$.

The parameter γ in Eq. (74) is determined by a comparison of the rates according to Eq. (74) and data obtained by applying a second-order TCL generator (see Sec. IV A). As a reminder, the TCL rates are defined as

$$K^{(2)}_{X,X\pm1}(t) = -\int_0^t dt'\,C_{X,X\pm1}(t') \tag{79}$$

with

$$C_{X,X\pm1}(t') = \mathrm{tr}\left[\hat{\pi}_{X,\Delta E}[\hat{V}_D(t),[\hat{V}_D(t'),\tilde{\hat{\pi}}_{X\pm1,\Delta E}]]\right] \quad , \tag{80}$$

where $\hat{V}$ is here given by $\hat{H}_{\mathrm{int}}$ and $\hat{\pi}_{X,\Delta E} = \hat{\pi}_{\Delta E}\,\hat{\pi}_X\,\hat{\pi}_{\Delta E}$. We find

$$C_{X,X\pm1}(0) \propto \frac{W(X \pm 1|X)}{4\gamma} \quad . \tag{81}$$

In order to grant that this proportionality remains also for all rates after the time integration in Eq. (79) several conditions must be fulfilled: (i) The "true" quantum dynamics can be well approximated by a second-order TCl generator and (ii) the correlation functions $C_{X,X\pm1}(t)$ must decay for all subspaces X in a similar fashion and on similar timescales. Moreover, the decay must be faster than the relaxation time in order to allow for constant TCL-rates in the sense discussed above; cf. [1].

Regarding the first condition, there are numeruos studies suggesting that second-order TCL generators yield

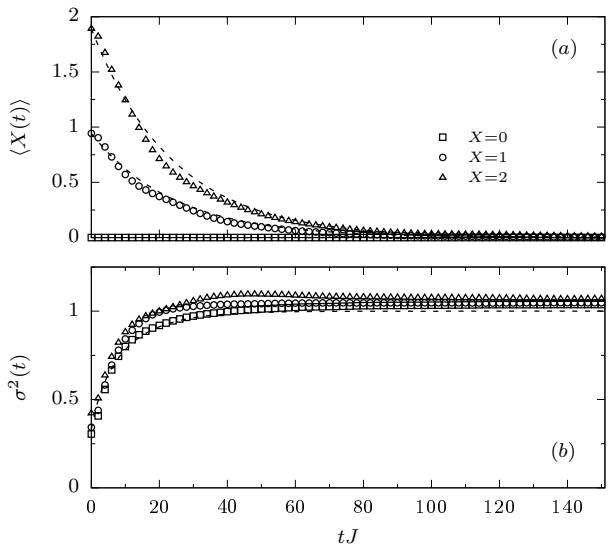

FIG. 6. In (a) the dynamics of $\langle \hat{X}(t) \rangle$ are displayed as calculated from the Schrödinger equation (symbols) and the master equation, Eq. (74), (dashed lines). In (b) the dynamics of $\sigma^2(t) = \langle \hat{X}^2(t) \rangle - \langle \hat{X}(t) \rangle^2$ are displayed. The data suggest good agreement of both dynamics.

good results if the interaction operator $\hat{V}$ features a certain matrix structure when transformed into the eigenbasis of the unperturbed Hamitlonian $\hat{H}_0$. The formal description of these features is quite complex and exceeds the scope of this review section. For details see e.g. [26, 77]. However, matrices whose elements are drawn at random (according to some distribution with zero mean) belong to this class of operators (see e.g. [26]). In the present case our "perturbation" operator does feature such structures (see Fig. 4,5 and their discussion in [1]).

In respect to the second requirement we find that it holds only for a rather restrict parameter regime, i.e., $\kappa \in [0.15; 0.2]$. The fact that there is a lower and upper bound is in accordance with literature [8, 26].

Eventually we find that the $K^{(2)}_{X,X\pm1}$'s indeed remain proportional to the simple statistic rates (the outmost rates, however, yield some deviations). Chosen an appropriate value for γ, we compare in Fig. 6 the actual quantum dynamics (symbols) with Fokker-Planck dynamics (dashed lines) where 6(a) displays the dynamics of $\langle \hat{X}(t) \rangle$ and 6(b) the corresponding dynamics of the variance $\sigma^2(t) = \langle \hat{X}^2(t) \rangle - \langle \hat{X}(t) \rangle^2$. As discussed in Ref. [1], the agreement between both types of dynamics is very well for X being small compared to the largest possible $|X| = N/4$. A detailed investigation of the deviations in the dynamic behavior for initial values closer to the outmost possible values is given in [28]. Therein the authors introduce quantum transition rates that lead to much more accurate results for such initial states.

V. DIFFUSION EQUATION IN CLOSED QUANTUM SYSTEMS

A special (renowned) case of the Fokker-Planck equation arises if one assumes that (i) there is no (external) potential Φ applied to the system that may influence the observable of interest and (ii) the diffusion coefficient does not depend on x and t, i.e., $D(x,t) \equiv D$. The first assumption can also be written as

$$0 = \frac{\partial V(x,t)}{\partial x} = -a^{(1)}(x,t) \quad . \tag{82}$$

Hence, the drift coefficient equals zero. Plugging these assumptions into Eq. (61) and rearranging the resulting expression a bit yields

$$\frac{\partial p(x,t)}{\partial t} - 2\,D\,\frac{\partial^2 p(x,t)}{\partial x^2} = 0 \quad . \tag{83}$$

Eq. (83) is commonly known as the (homogeneous) diffusion equation. It was already proposed by Fourier in 1822 [78, 79] as heat equation in order to describe heat conduction in several materials (without the notion of diffusion). Furthermore, the diffusion equation may also be derived from the (linearized) Boltzmann equation under certain assumptions (see e.g. [80–82]). The general solution of Eq. (83) is rather subtle. Therefore we begin by introducing the fundamental solution, i.e., for an initial distribution function $p(x,0) = \delta(x)$ and $p(x,t) \to 0$ for $|x| \to \infty$. The correpsonding solution reads (see e.g. [83]):

$$\tilde{p}(x,t) = \frac{1}{\sqrt{2\pi\,Dt}}\,\exp\left(-\frac{x^2}{2Dt}\right) \tag{84}$$

For general initial distributions $p(x,0) = f(x)$ one can obtain the solutions by calculating the convolution integral

$$p(x,t) = \int_{\mathbb{R}^n} dy\,\tilde{p}(x-y,t)\,f(y) \quad . \tag{85}$$

Hence, if for $f(x)$ mean expectation value μ and variance a^2 exist the corresponding variance of $p(x,t)$ reads $\sigma^2(t) = D\,t + a^2$, i.e., the variance is linearly connected to the diffusion coefficient. Moreover, we find

$$D = \frac{1}{2}\frac{d}{dt}\langle \sigma^2(t) \rangle \quad . \tag{86}$$

A. Scaling behavior of the diffusion coefficient and Einstein relation

As explained above diffusive processes lead to an linear increase of the variance with respect to time. However, in order to derive Eq. (86) we had to make several assumptions. First of all we assumed that D does not depend on the time. However this might not be entirely

true for some special cases. Consider e.g. any kind of lattice on which a particles can experience scattering only at few sites. The particles may have initially a constant velocity $\vec{v}_i$ each. Now, as long as the particles experience no scattering (which may be a long time) they evolve as free particles. Thus, we may describe the trajectory of each particle as:

$$\vec{x}_i(t) = \vec{x}_i(0) + \vec{v}_i\, t \tag{87}$$

The variance eventually reads then

$$\sigma^2(t) = \langle \vec{x}^2(t) \rangle - \langle \vec{x}(t) \rangle^2 = (\langle \vec{v}^2 \rangle - \langle \vec{v} \rangle^2)\, t^2 \quad , \tag{88}$$

i.e., the variance scales quadratic in time. This is inconsistent with the findings above. Consequently, one divides the transport behavior into several regimes depending on the scaling behavior of the variance with respect to time, i.e., $\sigma^2 \propto t^\alpha$. For $0 < \alpha < 1$ we call the regime subdiffusive, for $\alpha = 1$ we have diffusive transport and for $1 < \alpha \leqslant 2$ there is the superdiffusive regime. The special case at $\alpha = 2$ is also known as describing ballistic transport. For $\alpha = 0$ the system is in a localized phase.

The Einstein relation of transport coefficients connects the diffusion coefficient D with some *conductivity* σ_{con} of charge, energy, etc., i.e., a force driven quantity. In its most elementary form it reads

$$D(t) = \frac{k_B\, T}{\epsilon^2} \sigma_{\text{con}}(t) \quad , \tag{89}$$

where T denotes temperature, k_B is the Boltzmann constant and ϵ^2 is associated with the uncertainty of the transport quantity per site at equilibrium [84]. There are numerous studies that demonstrate the validity of the Einstein relation in the classical context (see e.g. [85]) and quantum context [84, 86].

In the framework of linear response theory the conductance $\sigma_{\text{con}}(t)$ can be calcualted by the Kubo formula. In the limit of high temperature and low particle densities n it reads (cf. [85, 87, 88])

$$\sigma_{\text{con}}(t) = \frac{n}{k_B\, T} \int_0^t \langle \hat{\jmath}(t') \hat{\jmath}(0) \rangle \, dt' \quad , \tag{90}$$

where $\langle \hat{\jmath}(t') \hat{\jmath}(0) \rangle = \text{tr}\,[\hat{\jmath}(t') \hat{\jmath}(0)]$ is the autocorrelation function of the current density operator corrsponding to the transported quantity. The study of the decay behavior of $\langle \hat{\jmath}(t') \hat{\jmath}(0) \rangle$ may already yield essential informations. We find e.g. that mono-exponential decay corresponds to transport behavior as described by a linearized Boltzmann equation or as expected for a simple heuristic Drude model. In the later the general assumption is that the conductivity is proportional to the squared mean velocity and the relaxation time τ, i.e., $\sigma_{\text{con}} \propto v^2 \tau$ [88–90].
Note that for low densities we find $\epsilon^2 \approx n$. Thus, in this case we may define

$$D_{\text{Kubo}}(t) = \int_0^t \langle \hat{\jmath}(t') \hat{\jmath}(0) \rangle \, dt' \quad , \tag{91}$$

i.e., we can calculate the diffusion coefficient also from transport properties. The Einstein relation can then rephrased as $D_{\text{Kubo}}(t) = D_{\text{var}}(t)$ where D_{var} denotes the diffusion coefficient as calculated from the variance. However, if this equality indeed holds has to be tested individual for each model. In the next section we will among others provide evidence that the equality holds at least for a specific quantum model in the thermodynamic limit.

B. Investigation of diffusive behavior in closed quantum systems

In this section we will discuss briefly several numerical investigation on different closed quantum systems w.r.t. the emergence of diffusive behavior. In [2] we focus on normal diffusive behavior and the validity of the Einstein relation while in [5] and [6] we consider the temporal behavior of the diffusion parameter D and the spatial variance. In the later studies we find cases that are inconsistent with normal diffusion.

Validity of the Einstein relation for a tight-binding model

In Ref. [2] we investigate three-dimensional tight-binding bond percolation models w.r.t. finite conductivity and diffusive transport behavior. The systems are described by

$$\hat{H} = \sum_{\langle ij \rangle} t_{ij}\, \hat{a}_i^\dagger\, \hat{a}_j \quad , \tag{92}$$

where $\langle ij \rangle$ denotes that the sum runs only over neighboring sites on the lattice. t_{ij} are *hoping amplitudes* and $\hat{a}_i^\dagger, \hat{a}_i$ are creation and annihilation operators on site i, respectively.
Percolation emerges by succecively removing either bonds (bond percolation) or sites (site percolation) from an otherwise ideal crystal, lattice or anything alike. In this way *impurities* are introduced that may lead (in addition to possible particle-particle collisions) to diffusive transport behavior or localization similar to Anderson localization (see below). Percolation models were vastly studied (i.a. due to the increase interest in microscopic structures) in the framework of classical

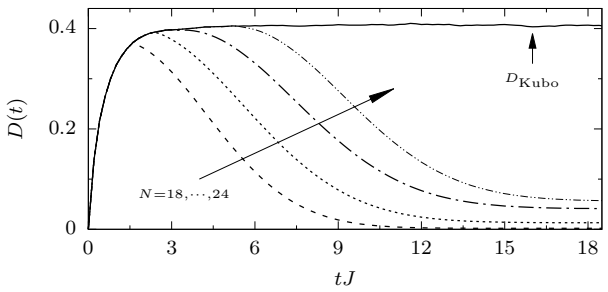

FIG. 7. Time-evolution of the diffusion coefficient $D(t)$ as calculated by means of the Kubo formula for $N = 26$ (solid line) and the spatial variance (dashed lines). Obviously the curves coincide for longer times the larger the system size N becomes. The behavior of the diffusion coefficient for large times in case of $D_{\rm var}$ arises from finite-size effets (see [2] for details).

mechnics [91–93] as well as in the quantum context [94–97]. Furthermore, percolation has also been addressed in other contexts such as quantum hall effects [98], Fermi-Bose mixtures [99] and (anti)ferromagnetic systems [100]. However, most investigations focus on the determination of the thresholds (e.g. number of defects relative to the total number of sites) below which transport is no longer possible, i.e., $\sigma_{\rm con} = 0$. One finds that the classical thresholds for both bond and site percolation are in general larger than their quantum counterparts.

In the quantum context one usually calculates the portion of energy eigenstates that are still expanded over the entire system e.g. with the inverse participation number method [101–103]. Such states belong to the delocalized eigenstate regime and it is obvious that transport may be possible as long as there exist a non-trivial delocalized regime. Furthermore, we investigated among other things $\sigma_{\rm con}(t)$ close to the bond percolation threshold via the Kubo formula, cf. Eq. (90). Finding exponential decay of the autocorrelation function, we furthermore compared the diffusion coefficients $D(t)$ that we either calculated by Eq. (86) ($D_{\rm var}$) or Eq. (89) ($D_{\rm Kubo}$). The results are displayed in Fig. 7 for intermediate deviation from the percolation threshold. Since the variance $\sigma(t)$ is strongly influenced by finite-size effects (see [2] for details) we display several $D_{\rm var}$'s for different system sizes N in order to demonstrate that with increasing N both diffusion coefficients coincide for longer times. Thus, in the thermodynamic limit we expect the Einstein relation to hold in the present case. Fig. 7 also demonstrates that the diffusion coefficient is indeed time-dependent for small times. In fact, in the very beginning we find $D(t) \propto t$, i.e., the spatial variance scales ballistic $\sigma^2(t) \propto t^2$. For $t \to \infty$, however, the diffusion coefficient becomes constant and we find indeed normal diffusive behavior, i.e., $\sigma^2(t) \propto t$.

Emergence of sub-diffusive behavior in Anderson localized systems

Apart from scattering induced by defects we investigate in Ref. [5] an Anderson localized spin chain. In Anderson models scattering centers are induced by random on-site potentials. In case of one-dimensional systems and non-interacting particles the particles are always localized [104–107], i.e., there is no finite conductivity for all disorder strengths and temperatures. Recently, the investigation of localization for interacting particles has seen a huge attraction. Even for weak interaction a localized phase seems to persists [108, 109]. Moreover, such localization phase may also exist beyond the weak interaction limit and at infinite temperature [110–112]. This phenomenon is commonly called many-body localization; see [113, 114] for recent reviews.
Most studies focus on the localization phase transition in dependence of the disorder strength [115–117]. Much less is know for the transition at fixed disorder strength while varing the number of interacting particles [118, 119]. For the half-filling sector one finds a delocalized phase at intermediate interaction and disorder strength (see e.g. [120]). Thus, the question arises whether and when the phase transition actually occurs in dependence of the particle number. Furthermore, it stands to question how (if there is a delocalized phase) transport behavior may be described. These questions were studied in [5] for a disordered spin chain and pure initial states of densely packed particles. The model is described by

$$\hat{H} = J \sum_{r=1}^{L} \left[\hat{S}_r^x \hat{S}_{r+1}^x + \hat{S}_r^y \hat{S}_{r+1}^y + \Delta \hat{S}_r^z \hat{S}_{r+1}^z \right] + \sum_{r=1}^{L} h_r \hat{S}_r^z \ , \tag{93}$$

where h_r are for each site drawn at random sampling the disorder potential. L is the length of the chain. Note that Δ is a direct measure for the interaction strengths. The main observable is the expansion of the particle density distribution $p_r(t) = \mathrm{tr}\left[\hat{n}_r(t)\rho\right]$ ($\hat{n}_r$: particle number operator at site r), i.e., the behavior of the standard deviation

$$\sigma(t) = \sqrt{\sum_{r=1}^{L} r^2 \, p_r(t) - \left(\sum_{r=1}^{L} r \, p_r(t) \right)^2} \tag{94}$$

Results are displayed in Fig. 8 for 1 up to 4 particles and intermediate interaction and disorder strengths (corresponding results at half-filling suggest a delocalized phase for these parameters). While the one-particle case shows a constant variance for large times consistent with Anderson localization for non-interacting particles there seems to occur saturation also for the two-particle

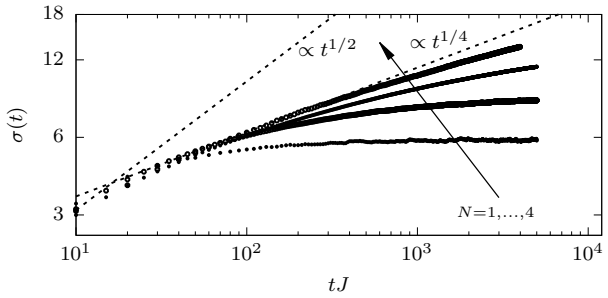

FIG. 8. Time-evolution of the variance for $N = 1, \cdots, 4$ particles. For the one and two-particle case the curves eventually stagnate for large times consistent with literature (see text). For $N = 3, 4$ the increase of the standard deviation does not stagnate but rather hints towards (sub)-diffusive behavior with $\sigma(t) \propto t^{1/4}$.

case. The latter may also be consistent with similar studies for bosons [121–125]. For three and four particles we found no saturation on the depicted time-scales hinting toward a delocalized phase. Power-law fits suggest that the standard deviation scales as $\sigma(t) \propto t^{1/4}$, i.e., subdiffusively, which becomes more pronounced as the particle number increases.

Role of internal correlations for the emergence of diffusive behavior

The study in Ref. [6] focuses, in contrast to the aforementioned works, on the impact of randomness embedded in the initial states on the behavior of the variance. The model investigated is again a spin chain of length L but without any disorder or scattering centers, i.e., $h_r = 0$ for all sites [cf. Eq. (93)]. The investigation also involves the particle density $p_r(t) = \mathrm{tr}\,[\hat{n}_r(t)\rho]$ (see above). The essential point in this work is the initial state defined as

$$|\psi\rangle \propto \hat{n}_{L/2}|\varphi\rangle \quad , \quad |\varphi\rangle = \sum_k c_k\,|\phi_k\rangle \quad , \tag{95}$$

where $n_{L/2}$ is a projection operator ensuring the concentration of the initial particle density around the center at site $L/2$ and $|phi_k\rangle$ is the eigenstate corresponding to site k. It turns out to be crucial in which way one chooses the coefficients c_k. Choosing the c_k's at random according to the Haar measure may render the typicality approach (see Sec. II B) valid while choosing the coefficients as being equal, i.e., $c_k = c\;\forall\, k$, does not per se allow for a similar approach.

In case of random c_k's one can derive by virtue of typicality arguments that the expectation value of $p_r(t)$ can be connected to an equilibrium correlation function, i.e.,

$$p_r(t) - p_{\mathrm{eq}} = 2\langle(\hat{n}_{L/2} - p_{\mathrm{eq}})(\hat{n}_r(t) - p_{\mathrm{eq}})\rangle \quad , \tag{96}$$

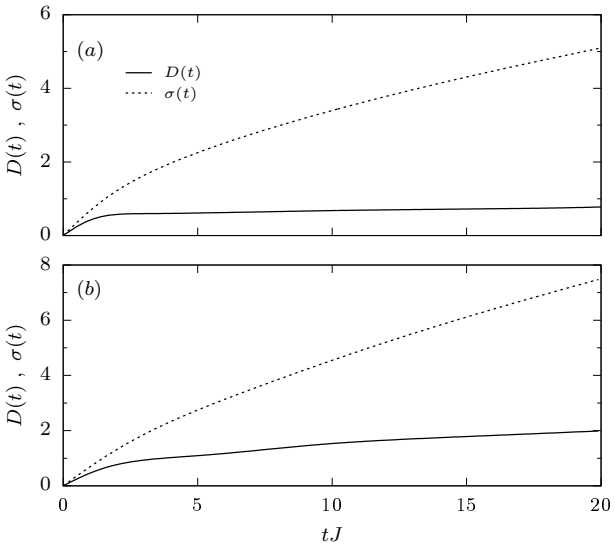

FIG. 9. Time-evolutions of the spatial standard deviation $\sigma(t)$ and diffusion coefficient $D(t)$. In (a) the results are shown for $\Delta = 1.5$ and typical states. $D(t)$ eventually becomes constant and the $\sigma(t) \propto \sqrt{t}$. In (b) the results are shown for $\Delta = 1.0$ and "untypical" states (equal c_k's). $D(t)$ does not reach a finite constant value on the depicted time scales suggesting that there is superdiffusive scaling behavior.

where p_{eq} is its equilibrium expectation value (see [6] for further details). Thus, an approach by linear response theory (Kubo formula) is possible where the current operator in the present case is the well known spin current density operator $\hat{\jmath} = \sum_r \hat{s}^x_r \hat{s}^y_{r+1} - \hat{s}^y_r \hat{s}^x_{r+1}$ (cf. e.g. [126]). Eventually, following the argumentations in [84], we derive for the diffusion coefficient

$$D(t) = \frac{4}{L}\int_0^t \langle\hat{\jmath}(t')\hat{\jmath}(0)\rangle\, dt' \quad . \tag{97}$$

For $\Delta = 0$ one finds $[\hat{\jmath}, \hat{H}] = 0$, i.e., $D(t) \propto t$. Thus, in this case there is ballistic transport behavior. Numerous investigations demonstrate that for $\Delta < 1$ there seems to occur partial conservation of the current $\hat{\jmath}$ which excludes normal diffusive behavior [126–138]. There are, however, indications that in the regime of large Δ and high temperatures normal diffusive expansion of the variance can indeed be observed. In Fig. 9(a), we display the time evolutions of $\sigma(t)$ as actually calculated from Eq. (94) and $D(t)$ as calculated by Eq. (97) for $\Delta = 1.5$. Indeed after some time the diffusion coefficient becomes constant and $\sigma(t) \propto \sqrt{t}$, supporting the above statement. (Actually we also computed other cases, i.e., $\Delta = 0.5, 1$, finding agreement with literature, too.) In case of equal c_k's the relation in Eq. (96) cannot be derived. Thus, the transport behavior may be completely different here. Performing the same investigations as for the typical states we display

in Fig. 9(b) again the time evolutions of $\sigma(t)$ and $D(t)$ for $\Delta = 1$. Obviously $D(t)$ does not reach a constant value on the depicted time scales. Consequently, the behavior of $\sigma(t)$ is inconsistent with normal diffusion. The results suggest that internal randomness in the initial condition has an essential impact on the transport behavior, i.e., nonequilibrium dynamics.

VI. INVESTIGATION OF THE JARZYNSKI RELATION FOR CLOSED QUANTUM SYSTEMS

Apart from investigations on the relaxation behavior of closed systems, recently renewed interest in the emergence of universal non-equilibrium behavior involving driven systems arose (see e.g. [139]). Such non-equilibrium behavior can be captured by fluctuation theorems [140]. One prominent example apart from the Einstein relation (see above) is the Jarzynski relation (JR). It provides a general statement on work that has to be invested to drive processes [141, 142]. It especially holds also for drivings far from equilibrium.

The JR has been tested in various settings such as classical Hamiltonian mechanics, stochastic dynamics (as described by Langevin or master equations) and quantum mechanics [140, 142–147]. But in almost all of these investigations it is assumed that the system (which is subjected to some external force) is initially in a Gibbsian state whereas in the field of thermalization the general starting point is entirely different. As a reminder, we demonstrated that thermalization emerges from properties of the system itself (cf. Sec. II C) rather than invoking external baths or specifying initial states. Thus, it is questionable whether the JR holds also for other initial states.

In this section we are going to present results indicating that the JR may be valid also for microcanonical initial states (although the following arguments also hold in a similar fashion for certain other initial states [7]) in the thermodynamic limit for driven closed quantum systems. In order to keep the consideration simple we imply the following features of the work inducing driving protocol $\boldsymbol{\lambda}$. (i) Forward and backward protocols are symmetric w.r.t. time, i.e., the action of forward protocol ($\boldsymbol{\lambda}$) and backward protocol ($\tilde{\boldsymbol{\lambda}}$) is the same, and (ii) the protocols are cyclic, i.e., the initial and final Hamiltonian are also the same ($H_i = H_f$). Hence, the JR reads in this special case:

$$\langle \exp(-\beta\, \hat{H}) \rangle_E = 1 \quad , \tag{98}$$

where $\langle \cdots \rangle_E$ denotes the microcanonical expectation value w.r.t. energy E and β is related to the corresponding inverse temperature.

Below we will demonstrate that the validity of the JR (at least in the above set-up) is basically founded on the fact that probability distribution functions (pdf's) of work are found to remain stiff for varying the initial energy E of the initial microcanonical state within a certain energy regime. These energy regimes are distinguished by the exponential growth behavior of the density of states (DOS) of the underlying closed system.

In order to compute the work pdf's we again employ a projection measurement scheme (cf. III A):

$$p_{\boldsymbol{\lambda},\mathrm{work}}(W;E) = \frac{1}{\delta}\,\mathrm{tr}\left[\hat{\pi}^f_{E+W,\delta}\,\mathbf{U}_{\boldsymbol{\lambda}}\,\rho(E)\,\mathbf{U}^\dagger_{\boldsymbol{\lambda}}\right] \quad , \tag{99}$$

where $\hat{\pi}^f_{E',\delta}$ denotes a projector on all energy eigenstates (w.r.t. H_f) within a energy shell of width δ around energy E'. The initial state of the system is denoted as $\rho(E)$ and associated to the mean energy E. The time-propagation operator $\mathbf{U}_{\boldsymbol{\lambda}}$ comprises the full action of the protocol $\boldsymbol{\lambda}$. Note that we may interpreted $p_{\boldsymbol{\lambda},\mathrm{work}}(W;E)$ as transition probabilities from energy E to $E+W$ that may depend on the very initial energy E. For simplicity, we omit hereafter unnecessary indices unless confusion may arise otherwise.

Microcanonical fluctuation theorems provide connenctions of such work pdf's and the density of states (DOS) of the correpsonding Hamiltonians [148, 149], i.e.,

$$\frac{p_{\boldsymbol{\lambda}}(W;E)}{\tilde{p}_{\tilde{\boldsymbol{\lambda}}}(-W;W+E)} = \frac{\Omega_f(E+W)}{\Omega_i(E)} \quad , \tag{100}$$

where $\tilde{p}_{\tilde{\boldsymbol{\lambda}}}$ denotes the work pdf for reverse protocol $\tilde{\boldsymbol{\lambda}}$. Ω_i, Ω_f are the DOS for the initial and final Hamiltonian, respectively. (Note that Eq. (100) holds in general only if the protocols are indeed microreversible.) Due to the above assumptions regarding the work protocols $\boldsymbol{\lambda}$ one finds $p_{\boldsymbol{\lambda}} \equiv \tilde{p}_{\tilde{\boldsymbol{\lambda}}}$. Thus, we can also write it in the compact form

$$\frac{p(E+W;E)}{p(E;E+W)} = \frac{\Omega(E+W)}{\Omega(E)} \quad , \tag{101}$$

where we used that the initial and final Hamiltonians are the same (they feature also the same DOS).

"Stiffness" assumption and validity of the Jarzynski relation

We assume now that the work pdf's do not change in shape if varying the initial energy within a certain energy regime. In particular, this means that they depend only on the energy differences, i.e., $p(E+W;E) = p(W)$. With this assumption we may write Eq. (101) as

$$\frac{p(W)}{p(-W)} = \frac{\Omega(E+W)}{\Omega(E)} \quad . \tag{102}$$

Note that the l.h.s. of this equality depends solely on W whereas the r.h.s. may also depend on E. Thus, for this

equality to hold the DOS must feature a exponential scaling behavior w.r.t. energy, i.e., $\Omega(E) \propto \exp(\beta E)$ with β being some constant factor. Finally, we obtain the following equality:

$$\frac{p(W)}{p(-W)} = \exp(\beta W) \quad . \tag{103}$$

In plain words: Stiffness of work pdf's can only occur if the DOS of the underlying system scales exponentially with energy. For some systems this may be the case only on certain energy regimes (see below).
Consider now the following integral:

$$\int \tilde{p}_{\tilde{\boldsymbol{\lambda}}}(E; E+W)\, dW = \int p(-W)\, dW = 1 \quad , \tag{104}$$

where we used stiffness in the second step and finally that the $p(W)$'s are normalized. Employing now Eq. (103), we can rewrite the above equation as

$$\int p(W)\, \exp(-\beta W)\, dW = 1 \quad , \tag{105}$$

which is basically the JR for microcanonical initial states if β can be interpreted as inverse temperature (see above). In [7] we demonstrate that this is indeed the case via considerations of basic thermodynamic relations. Thus, the property of stiffness suffices to ensure the validity of the JR for microcanonical initial states. For completeness, we remark that in case stiffness holds only for a certain energy regime which will be the case in most finite-sized systems (see below) we may find

$$\int_{E'-\Delta/2}^{E'+\Delta/2} p(-W)\, dW \approx 1 \quad , \tag{106}$$

where we integrate over the energy interval of width Δ around the mean energy E'. Note that Eq. (106) holds as long as the contributions of $p(W)$ vanish beyond the outlined energy regime.

Numerical investigation of stiffness for closed spin systems

We numerically investigate again closed spin systems since there is evidence that the DOS of such systems scales approximately exponentially with energy on certain intermediate energy ranges; see e.g. [150]. We "divide" our systems into a "system part" (here simply a single spin) onto which our work inducing protocol acts directly and into a "bath part" coupled to the single system spin. Note that we do not actually investigate open system-bath scenarios but just use this terminology for simplicity here.
We will consider two different bath models: (i) a spin ladder, as already investigate above, where the system spin couples to the leading spins of each leg and (ii) a spin chain where the system spin enlarges the system simply by one additional site. Note that the spin ladder is non-integrable (in the sense of the Bethe ansatz [151]) while the spin chain is integrable. Thus, we will be able to study the influence of integrability on the stiffness of work pdf's.

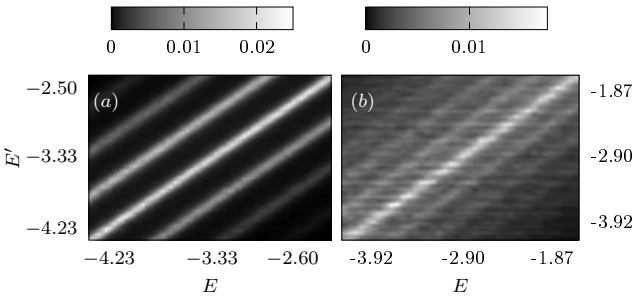

FIG. 10. Grayscale map of the energy dependence of $p(E'; E)$ for different initial energies E. (a) displays results for the weakly coupled and weakly driven ladder model and (b) for the strongly driven chain model. In both cases the work pdf's suggest independence on E as indicated by constant values along the counter diagonals.

For the ladder model the Hamiltonian of the bath reads

$$\begin{aligned}\hat{H}'_{\text{ladder}} = &\sum_{r=1}^{2}\sum_{i=1}^{L-1}(\hat{S}^x_{i,r}\hat{S}^x_{i+1,r} + \hat{S}^y_{i,r}\hat{S}^y_{i+1,r} + \hat{S}^z_{i,r}\hat{S}^z_{i+1,r}) \\ &+ \sum_{i=1}^{L}(\hat{S}^x_{i,1}\hat{S}^x_{i,2} + \hat{S}^y_{i,1}\hat{S}^y_{i,2} + \hat{S}^z_{i,1}\hat{S}^z_{i,2}) \quad ,\end{aligned} \tag{107}$$

where $\hat{S}^{x,y,z}_{i,r}$ are spin–1/2 operators at site (i,r). Likewise, for the chain model the Hamiltonian of the bath reads

$$\hat{H}'_{\text{chain}} = \sum_{i=1}^{L-1}(\hat{S}^x_i\hat{S}^x_{i+1} + \hat{S}^y_i\hat{S}^y_{i+1} + \hat{S}^z_i\hat{S}^z_{i+1}) \quad . \tag{108}$$

As for the system-bath coupling, it is given for the ladder model by

$$\begin{aligned}\hat{H}''_{\text{ladder}} = &(\hat{S}^x_{L,1} + \hat{S}^x_{L,2})\,\hat{S}^x_{sys} + (\hat{S}^y_{L,1} + \hat{S}^y_{L,2})\,\hat{S}^y_{sys} \\ &+ (\hat{S}^z_{L,1} + \hat{S}^z_{L,2})\,\hat{S}^z_{sys}\end{aligned} \tag{109}$$

and for the chain model by

$$\hat{H}''_{\text{chain}} = \hat{S}^x_L\,\hat{S}^x_{sys} + \hat{S}^y_L\,\hat{S}^y_{sys} + \hat{S}^z_L\,\hat{S}^z_{sys} \quad . \tag{110}$$

Note that the total number of spins is for the ladder model $N = 2L+1$ and for the chain model $N = L+1$.
Since we want to employ a work protocol in resemblance of a spin resonant experiment we apply a static

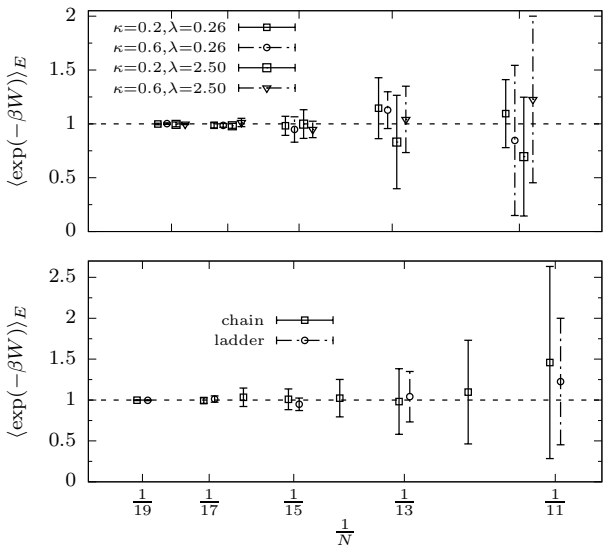

FIG. 11. Results for the direct calculation of the JR for microcanonical states with mean energies E from intervals as specified in the text. (a) summarizes the results for various parameter sets for the ladder model and (b) shows a comparison of results from the chain model and strongly driven ladder model. In all cases the finite-size scaling suggests that the JR becomes true in the thermodynamic limit. Thus, integrability and non-resonant driving seem to have not effect here.

magnetic field $B = 0.5$ (in z direction) to the system spin in the ladder model, i.e.,

$$\hat{H}_{\mathrm{mag}} = 0.5\,\hat{S}^z_{sys} \quad . \tag{111}$$

We do not apply any magnetic field for the chain model and thus are also able to investigate the influence of non-resonant driving (see below).
Finally, the full time-independent Hamiltonian for the ladder model reads

$$\hat{H}^0_{\mathrm{ladder}} = \hat{H}'_{\mathrm{ladder}} + \kappa\,\hat{H}''_{\mathrm{ladder}} + \hat{H}_{\mathrm{mag}} \tag{112}$$

and for the chain model

$$\hat{H}^0_{\mathrm{chain}} = \hat{H}'_{\mathrm{chain}} + \hat{H}''_{\mathrm{chain}} \quad . \tag{113}$$

Note that we allow for the ladder model for a variable system-bath coupling strength κ while for the chain model all coupling strengths are set to 1.
The time-dependent work protocol (driving) is described by

$$\hat{H}_D(t,\nu) = \lambda\,\sin(\nu\,t)\,\hat{S}^x_{sys} \quad , \tag{114}$$

i.e., we apply a time-dependent (sine-wave-modulated) magnetic field in x direction on the system spin with frequency ν and strength λ. This whole set-up is close to spin resonance experiments [152, 153] where for the ladder model we set $\nu = 0.5$ and for the chain model $\nu = 0.75$ (for details see [7]). We emphasize that although this kind of protocol is not per se microreversible we discussed in the appendix of [7] that for our specific models Eq. (100) still holds true.
At last, we introduce our initial states that are (due to limitations in numerics [7]) microcanonical states with a finite but sufficiently small energy range σ, i.e.,

$$\rho(E) = \frac{\hat{\pi}_{E,\sigma}}{\mathrm{tr}\,[\hat{\pi}_{E,\sigma}]} \quad . \tag{115}$$

Investigating the DOS of either model we find that on some intermediate energy ranges the DOS is indeed well described by exponential growth. The width of these regimes as well as the overall agreement increases with enlarging the systems; see [7]. Since, however, the scaling is not perfectly exponential (especially for small systems) work pdf's may slightly dependent on the initial energy (see [7] for details where we investigated explicit the "similarity" between different work pdf's). In Fig. 10, we display exemplary for $N = 19$ a colormap of work pdf's corresponding to adjacent initial energies (horizontal axis) from the energy regime where $\Omega(E) \propto \exp(\beta\,E)$ holds (see [7] for details). Fig. 10(a) corresponds to the ladder model ($\kappa = 0.6, \lambda = 2.5$) and Fig. 10(b) to the chain model ($\lambda = 3.9$). In both cases we immediately see that the general structure of the work pdf's does not change (apart from minor fluctuations). Thus, stiffness is well fulfilled for both models, i.e., integrability and non-resonant driving seem not to be relevant here. Note that we quantified the fluctuations in [7] directly (also for different parameters and system sizes).

Furthermore, we computed the JR directly for various parameter sets and display the results in Fig. 11. For all considered scenarios the JR seems to be fulfilled in the thermodynamic limit ($N \to \infty$) which proves the relevance of the emergence of stiffness for the validity of the JR for microcanonical initial states.

Relation of stiffness towards FGR and ETH

The emergence of stiffness in the limit of large systems gives rise to the question whether this can be understood by more general concepts. Here we will demonstrate that at least in the weak driving regime stiffness can be connected to the validity of FGR and ETH.
To this end we consider at first the matrix representation of the perturbation operator $\hat{V}$ (cf. Sec. II A) in the eigenbasis of $\hat{H}^0$ of the respective model. This operator is given for both models by $\hat{V} = \hat{S}^x_{sys}$.
Since the work pdf's can be interpreted as transition probabilities we may calculate the transition rates in the weak driving regime (i.e. weak perturbation) by FGR from this matrix representation. We denote these rates from E to E' by $\gamma_{E\to E'}$.

This ultimately yields

$$\gamma_{E\to E'} \approx \frac{2\pi}{N(E)} \sum_{\substack{i\,\in\,E\\ f\,\in\,E'}} |V_{ij}|^2 \quad , \tag{116}$$

where $N(E)$ the total number of states contributing to the initial state (for details see [7]).
For the emergence of stiffness we have to demand that $\gamma_{E\to E+W} \equiv \gamma(W)$ holds. Thus, the matrix representation of V_{ij} must feature a corresponding structure which may be numerically investigated via exact diagonalization. One could therefore calculate the transition rates directly. However, here we will proceed by relating the emergence of stiffness to the validity of the ETH. To this end, we recall that any operator featuring the following structure (cf. Sec. II C)

$$V_{ij} \approx \bar{V}(\bar{E})\,\delta_{ij} + N(\bar{E})^{-1/2}\, f_V(\bar{E},\omega)\, R_{ij} \quad , \tag{117}$$

fulfills the ETH ansatz. As a reminder, $\bar{E} = (E_i + E_j)/2, \omega = E_j - E_i$ and $\bar{V}(\bar{E}), f_V(\bar{E},\omega)$ are smooth functions of their arguments. R_{ij} are randomly distributed (complex) numbers with zero mean and variance 1. Note that we consider here energy intervals E, E'. Thus, we may also write $\bar{E} = (E + E')/2$ and $\omega = E' - E$. Inserting this into Eq. (116) yields

$$\gamma_{E\to E'} \approx \frac{2\pi}{N(E)} \sum_{\substack{i\,\in\,E\\ f\,\in\,E'}} \frac{f_V^2(\bar{E},\omega)\, R_{ij}^2}{N(\bar{E})} \quad . \tag{118}$$

Since only the factor R_{ij}^2 is actually affected by the summation we find

$$\sum_{\substack{i\,\in\,E\\ f\,\in\,E'}} R_{ij}^2 \approx N(E)\, N(E') \quad . \tag{119}$$

Thus, the rates are eventually given by

$$\gamma_{E\to E'} \approx \frac{2\pi\, f_V^2(\bar{E},\omega)\, N(E')}{N(\bar{E})} \quad . \tag{120}$$

Recalling that stiffness can only emerge if the corresponding DOS scales exponentially with energy we finally find

$$\gamma_{E\to E'} \approx 2\pi\, f_V^2(\bar{E},\omega)\, \exp(-\beta\,\omega/2) \quad , \tag{121}$$

which plainly demonstrates that the stiffness of the rates ultimately depends on the function $f_V^2(\bar{E},\omega)$. Only if this function varies only slightly with $\bar{E}$, stiffness may emerge (the above expression depends only on the energy difference ω).
In Fig. 12, we display a colormap of $f_V^2(\bar{E},\omega)$ (in arbitrary units) which clearly shows that for both models the structure is smooth, i.e., $f_V^2(\bar{E},\omega)$ varies only slightly with $\bar{E}$. This indicates stiffness. Although these results are in agreement with the results discussed in detail above, we point out that the validity of results here is only ensured for the weak driving regime.

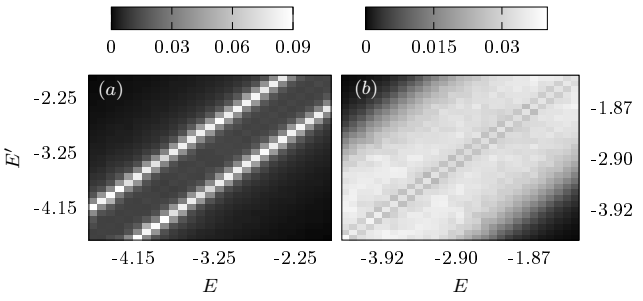

FIG. 12. Grayscale map of the perturbation operator $\hat{V}$ in energy eigenbasis of $\hat{H}^0$ of the respective model. (a) displays results for the ladder model and (b) correspondingly for the chain model. In both cases the matrix structure is consistent with the ETH ansatz.

VII. SUMMARY AND CONCLUSION

In this dissertation we investigated whether quantum dynamics of closed systems may behave like described by standard thermodynamic approaches, i.e., whether there is equilibration/thermalization for explicit non-equilibrium scenarios, and if so, can the corresponding dynamics be mapped e.g. onto stochastic processes.
As a first step towards the answer of the first question we introduced well-established approaches for equilibration in closed quantum systems, namely Fermi's Golden Rule, the typicality approach and the eigenstate thermalization hypothesis (ETH). While we found that Fermi's Golden Rule is applicable only for rather restricted scenarios (weak perturbation, initial energy eigenstates etc.) we found that the typicality approaches as well as the ETH may be valid for a much wider class of systems, initial states and observables. These discussions unveil that though the system might be initially in far-from-equilibrium state its time-evolved state may feature unique equilibrium properties consistent with thermodynamic equilibrium states. One major shortcoming of these approaches, however, is that they do not give any insight into the actual relaxation behavior.
In order to analyze such relaxation behavior in relation to standard stochastic processes, that are usually expected to emerge for thermodynamic behavior, we introduced thereafter the notion of stochastic trajectories. Since in the most general case each trajectory requires knowledge of the entire history of the system which is clearly not the case in usual thermodynamic consideration we discussed the special case of Markovian dynamics. Markovian dynamics can be constructed by knowledge of the most recent history of the system only. Such dynamics are indeed in accordance with standard thermodynamics and we could show that quantum dynamics can in some cases actually give rise to such description schemes.

Based on Markovian dynamics we derived so called master equations that basically involve transition rates from one system state to another describing dynamics of density functions. Solutions of such master equations feature in particular fix points in some underlying phase space, Hilbert space etc. in contrast to the unitary dynamics described by the Schrödinger equation (and Newton equation for classical scenarios). Thus, equilibration towards unique equilibrium states is obvious.
The renowned Fokker-Planck equation, often used to describe classical stochastic processes as e.g. Brownian motions, can be directly derived from master equations. We presented numerical and analytic evidence that in closed quantum system (to be specific: spin systems) Fokker-Planck-like dynamics can be found. We furthermore discussed projection operator techniques that result in a master-equation-like description of quantum dynamics coinciding with the Fokker-Planck related results.
A further specification of the Fokker-Planck equation lead directly to the famous diffusion equation that in its essential form was already introduced about 200 years ago, though not acknowledged for its universal impact. The diffusion coefficient (appearing in the diffusion equation) bears a direct correlation with the (spatial) variance of the underlying density function.
Employing the Einstein relation that connects the diffusion coefficient with a conductivity of some current we showed that diffusion coefficient can also be calculated via linear response theory (Kubo formula). In order to demonstrate that diffusive processes can indeed be observe in quantum systems we provided several numerical results on disordered systems (percolation and Anderson models) and the role of randomness embedded in the initial condition of the system.
At last we studied under what conditions we may find that the actual initial condition (to be specific: the initial energy of a microcanonical state) does have no influence on the resulting distribution functions of work under the action of some work-inducing protocol. To be more precise, we investigated if the shape of work distribution functions remain stiff if the initial energy of the initial state is shifted. A direct consequence of stiff distributions is the validity of the famous Jarzynski relation beyond Gibbsian initial conditions. It turned out that the exponential scaling of the underlying density of states is crucial for the observation of stiff distributions (where we restricted the investigation on cyclic and microreversible driving protocols). Finally we explored a connection of our findings with the applicability of Fermi's Golden Rule and the eigenstate thermalization hypothesis.

After all we presented evidence that standard thermodynamics behavior as described by stochastic approaches emerges in various applications of closed quantum systems.

ACKNOWLEDGMENTS

At last it is my pleasure to thank all the persons who advised and supported me in the last years especially during my PhD studies.

First of all, I sincerely thank my supervisor Prof. Dr. Gemmer for his constant support and interest in the progress of my studies reaching back to my bachelor and master theses. He encouraged me to look into a multitude of interesting topics and provided a very pleasant working atmosphere.
I would also like to thank Prof. Dr. Maass for being second supervisor of my PhD thesis.

Special thanks also to my present and former colleagues. Most of all, Hendrik Niemeyer and Abdellah Khodja with whom I shared an office and worked on many articles together. It was always a pleasure to talk about private matters apart from work.

Furthermore, thanks to the members of the Physik Didaktik who were always happy to help in all kinds of things.

Finally, I am very much indebted to my family since they showed great endurance and support during the last years though it may have been not always easy. Moreover, they were always very interested in my works where I was glad to explain to them the complex topics. I will never be able to repay all your kindness and efforts.

[1] H. Niemeyer, D. Schmidtke, and J. Gemmer, EPL **101**, 10010 (2013).
[2] D. Schmidtke, A. Khodja, and J. Gemmer, Phys. Rev. E **90**, 032127 (2014).
[3] D. Schmidtke and J. Gemmer, Phys. Rev. E **93**, 012125 (2016).
[4] A. Khodja, D. Schmidtke, and J. Gemmer, Phys. Rev. E **93**, 042101 (2016).
[5] D. Schmidtke, R. Steinigeweg, J. Herbrych, and J. Gemmer, Phys. Rev. B **95**, 134201 (2017).
[6] R. Steinigeweg, F. Jin, D. Schmidtke, H. De Raedt, K. Michielsen, and J. Gemmer, Phys. Rev. B **95**, 035155 (2017).
[7] D. Schmidtke, L. Knipschild, M. Campisi,

R. Steinigeweg, and J. Gemmer, arXiv preprint arXiv:1710.10871 (2017).
[8] G. Jochen, M. Michel, and G. Mahler, *Quantum thermodynamics. Emergence of thermodynamic behavior within composite quantum systems*, 2nd ed. (Springer, 2009).
[9] H. D. Baehr and S. Kabelac, Springer, Berlin, Heidelberg, New York (2009).
[10] G. Beretta, A. Ghoniem, and G. Hatsopoulos, in *AIP Conference Proceedings*, Vol. 1033 (2008).
[11] K. Stierstadt, *Thermodynamik: von der Mikrophysik zur Makrophysik* (Springer-Verlag, 2010).
[12] S. R. de Groot, P. Mazur, and A. L. King, American Journal of Physics **31**, 558 (1963).
[13] T. Sobota, in *Encyclopedia of Thermal Stresses* (Springer, 2014) pp. 1769–1778.
[14] A. Fick, Annalen der Physik **170**, 59 (1855).
[15] L. Boltzmann, *Vorlesungen über Gastheorie* (University of California Press, 1964).
[16] C. Cercignani, in *The Boltzmann Equation and Its Applications* (Springer, 1988) pp. 40–103.
[17] G. Adam and O. Hittmair, *Wärmetheorie* (Springer-Verlag, 2013).
[18] C. R. d. Oliveira and T. Werlang, Revista Brasileira de Ensino de Física **29**, 189 (2007).
[19] P. C. W. Davies, *The physics of time asymmetry* (Univ of California Press, 1977).
[20] G. D. Birkhoff, Proceedings of the National Academy of Sciences **17**, 656 (1931).
[21] J. von Neumann, *Mathematische Grundlagen der Quantenmechanik.*, 2nd ed. (Berlin: Springer, 1996) p. 262.
[22] J. W. Gibbs, *Elementary principles in statistical mechanics* (Courier Corporation, 2014).
[23] J. W. Gibbs, The Collected Works of J. Willard Gibbs, Ph. D., LL. D , 16 (1957).
[24] H.-P. Breuer and F. Petruccione, *The theory of open quantum systems* (Oxford University Press on Demand, 2002).
[25] M. Srednicki, Journal of Physics A: Mathematical and General **32**, 1163 (1999).
[26] C. Bartsch, R. Steinigeweg, and J. Gemmer, Phys. Rev. E **77**, 011119 (2008).
[27] C. Bartsch and J. Gemmer, Phys. Rev. Lett. **102**, 110403 (2009).
[28] H. Niemeyer, K. Michielsen, H. De Raedt, and J. Gemmer, Phys. Rev. E **89**, 012131 (2014).
[29] H. Niemeyer, *The approach to Equilibration in Closed Quantum Systems*, Ph.D. thesis, Universität Osnabrück (2014).
[30] A. Khodja, R. Steinigeweg, and J. Gemmer, Phys. Rev. E **91**, 012120 (2015).
[31] C. Gogolin and J. Eisert, Reports on Progress in Physics **79**, 056001 (2016).
[32] L. D'Alessio, Y. Kafri, A. Polkovnikov, and M. Rigol, Advances in Physics **65**, 239 (2016).
[33] M. Greiner, O. Mandel, T. W. Hänsch, and I. Bloch, Nature **419**, 51 (2002).
[34] M. Greiner, O. Mandel, T. Esslinger, T. W. Hänsch, and I. Bloch, nature **415**, 39 (2002).
[35] A. Tuchman, C. Orzel, A. Polkovnikov, and M. Kasevich, Physical Review A **74**, 051601 (2006).
[36] M. Aidelsburger, M. Atala, S. Nascimbène, S. Trotzky, Y.-A. Chen, and I. Bloch, Physical review letters **107**, 255301 (2011).
[37] I. Bloch, Nature Physics **1**, 23 (2005).
[38] T. Langen, R. Geiger, and J. Schmiedmayer, Annual Review of Condensed Matter Physics **6**, 201 (2015).
[39] D. Porras and J. I. Cirac, Physical review letters **92**, 207901 (2004).
[40] A. Friedenauer, H. Schmitz, J. T. Glueckert, D. Porras, and T. Schätz, Nature Physics **4**, 757 (2008).
[41] J. J. Sakurai and J. J. Napolitano, *Modern quantum mechanics* (Pearson Higher Ed, 2014).
[42] J. L. Lebowitz, Physics today **46**, 32 (1993).
[43] J. L. Lebowitz, in *25 Years of Non-Equilibrium Statistical Mechanics* (Springer, 1995) pp. 1–20.
[44] J. L. Lebowitz, Boltzmann's Legacy , 63 (2007).
[45] S. Goldstein, J. L. Lebowitz, R. Tumulka, and N. Zanghì, Phys. Rev. Lett. **96**, 050403 (2006).
[46] S. Popescu, A. J. Short, and A. Winter, Nature Physics **2**, 754 (2006).
[47] P. Reimann, Phys. Rev. Lett. **99**, 160404 (2007).
[48] S. Goldstein, in *Probability in physics* (Springer, 2012) pp. 59–71.
[49] G. A. Álvarez, E. P. Danieli, P. R. Levstein, and H. M. Pastawski, Phys. Rev. Lett. **101**, 120503 (2008).
[50] H. De Raedt and K. Michielsen, arXiv preprint quant-ph/0406210 (2004).
[51] T. A. Elsayed and B. V. Fine, Phys. Rev. Lett. **110**, 070404 (2013).
[52] M. Rigol, Phys. Rev. Lett. **103**, 100403 (2009).
[53] S. Dubey, L. Silvestri, J. Finn, S. Vinjanampathy, and K. Jacobs, Phys. Rev. E **85**, 011141 (2012).
[54] R. Steinigeweg, J. Herbrych, and P. Prelovšek, Phys. Rev. E **87**, 012118 (2013).
[55] W. Beugeling, R. Moessner, and M. Haque, Phys. Rev. E **89**, 042112 (2014).
[56] G. De Palma, A. Serafini, V. Giovannetti, and M. Cramer, Phys. Rev. Lett. **115**, 220401 (2015).
[57] C. Bartsch and J. Gemmer, EPL (Europhysics Letters) **118**, 10006 (2017).
[58] J. L. Speyer and W. H. Chung, *Stochastic processes, estimation, and control* (SIAM, 2008).
[59] Y. Ohkuwa, Phys. Rev. D **48**, 1781 (1993).
[60] H.-P. Breuer, E.-M. Laine, J. Piilo, and B. Vacchini, Rev. Mod. Phys. **88**, 021002 (2016).
[61] R. B. Griffiths, Journal of Statistical Physics **36**, 219 (1984).
[62] M. Gell-Mann and J. B. Hartle, Addison-Wesley **8**, 425 (1991).
[63] J. J. Halliwell, Phys. Rev. D **80**, 124032 (2009).
[64] A. E. Allahverdyan, R. Balian, and T. M. Nieuwenhuizen, Physics Reports **525**, 1 (2013).
[65] E. Okon and D. Sudarsky, Foundations of Physics **44**, 19 (2014).
[66] N. G. Van Kampen, *Stochastic processes in physics and chemistry*, Vol. 1 (Elsevier, 1992).
[67] A. Eberle, "Introduction to stochastic analysis," (2011).
[68] S. Nakajima, Progress of Theoretical Physics **20**, 948 (1958).
[69] R. Zwanzig, The Journal of Chemical Physics **33**, 1338 (1960).
[70] R. Steinigeweg, *Application of Projection Operator Techniques to Transport Investigations in Closed*

Quantum Systems, Ph.D. thesis, Universität Osnabrück (2008).
[71] F. Shibata, Y. Takahashi, and N. Hashitsume, Journal of Statistical Physics **17**, 171 (1977).
[72] S. Chaturvedi and F. Shibata, Zeitschrift für Physik B Condensed Matter **35**, 297 (1979).
[73] F. Shibata and T. Arimitsu, Journal of the Physical Society of Japan **49**, 891 (1980).
[74] C. Uchiyama and F. Shibata, Physical Review E **60**, 2636 (1999).
[75] H.-P. Breuer, J. Gemmer, and M. Michel, Phys. Rev. E **73**, 016139 (2006).
[76] J. Gemmer and H.-P. Breuer, The European Physical Journal Special Topics **151**, 1 (2007).
[77] L. Van Hove, Physica **21**, 517 (1954).
[78] J. B. J. Fourier, *The Analytical Theory of Heat*, edited by A. Freeman (Cambridge University Press, 1872).
[79] M. Michel, *Nonequilibrium Aspects of Quantum Thermodynamics*, Ph.D. thesis, Universität Stuttgart (2006).
[80] R. Balescu, *Equilibrium and nonequilibrium statistical mechanics.* (New York, NY Wiley, 1975).
[81] W. Brenig, *Statistical Theory of Heat: Nonequilibrium Phenomena* (Springer, New York, 1989).
[82] M. Kadiroglu, *Transport und Relaxation in Quantenmodellen*, Ph.D. thesis, Universität Osnabrück (2009).
[83] L. C. Evans, *Partial differential equations.* (Providence, RI: American Mathematical Society, 1998).
[84] R. Steinigeweg, H. Wichterich, and J. Gemmer, EPL (Europhysics Letters) **88**, 10004 (2009).
[85] R. Kubo, Reports on Progress in Physics **29**, 255 (1966).
[86] Y. Roichman and N. Tessler, Applied Physics Letters **80**, 1948 (2002).
[87] R. Kubo, Journal of the Physical Society of Japan **12**, 570 (1957).
[88] J. Jäckle, *Einführung in die Transporttheorie* (Springer-Verlag, 2013).
[89] N. W. Ashcroft and N. D. Mermin, *Solid State Physics* (Saunders College, Philadelphia, 1976).
[90] G. D. Mahan, *Many-particle physics*, 3rd ed. (Springer, Berlin, 2000).
[91] S. Kirkpatrick, Rev. Mod. Phys. **45**, 574 (1973).
[92] A. W. Sandvik, Phys. Rev. B **66**, 024418 (2002).
[93] D. Stauffer, "Classical percolation," in *Quantum and Semi-classical Percolation and Breakdown in Disordered Solids*, edited by B. K. Chakrabarti, K. K. Bardhan, and A. K. Sen (Springer Berlin Heidelberg, Berlin, Heidelberg, 2009) pp. 1–19.
[94] C. M. Soukoulis, Q. Li, and G. S. Grest, Phys. Rev. B **45**, 7724 (1992).
[95] R. Berkovits and Y. Avishai, Phys. Rev. B **53**, R16125 (1996).
[96] A. Kaneko and T. Ohtsuki, Journal of the Physical Society of Japan **68**, 1488 (1999).
[97] G. Schubert, A. Weiße, and H. Fehske, Phys. Rev. B **71**, 045126 (2005).
[98] D.-H. Lee, Phys. Rev. B **50**, 10788 (1994).
[99] A. Sanpera, A. Kantian, L. Sanchez-Palencia, J. Zakrzewski, and M. Lewenstein, Phys. Rev. Lett. **93**, 040401 (2004).
[100] R. Yu, T. Roscilde, and S. Haas, Phys. Rev. Lett. **94**, 197204 (2005).
[101] R. J. Bell and P. Dean, Discuss. Faraday Soc. **50**, 55 (1970).
[102] R. Bell, Reports on Progress in Physics **35**, 1315 (1972).
[103] D. Thouless, Physics Reports **13**, 93 (1974).
[104] P. W. Anderson, Phys. Rev. **109**, 1492 (1958).
[105] N. F. Mott, The Philosophical Magazine: A Journal of Theoretical Experimental and Applied Physics **17**, 1259 (1968).
[106] B. Kramerf and A. MacKinnonj, Rep, Prog, Phys **56**, 1469 (1993).
[107] F. Evers and A. D. Mirlin, Reviews of Modern Physics **80**, 1355 (2008).
[108] L. Fleishman and P. W. Anderson, Phys. Rev. B **21**, 2366 (1980).
[109] D. Basko, I. Aleiner, and B. Altshuler, Annals of physics **321**, 1126 (2006).
[110] V. Oganesyan and D. A. Huse, Phys. Rev. B **75**, 155111 (2007).
[111] A. Pal and D. A. Huse, Phys. Rev. B **82**, 174411 (2010).
[112] D. J. Luitz, N. Laflorencie, and F. Alet, Phys. Rev. B **91**, 081103 (2015).
[113] R. Nandkishore and D. A. Huse, Annual Review of Condensed Matter Physics **6**, 15 (2015).
[114] D. A. Abanin and Z. Papić, Annalen der Physik **529**, 1700169 (2017).
[115] J. A. Kjäll, J. H. Bardarson, and F. Pollmann, Phys. Rev. Lett. **113**, 107204 (2014).
[116] S. Gopalakrishnan, M. Müller, V. Khemani, M. Knap, E. Demler, and D. A. Huse, Phys. Rev. B **92**, 104202 (2015).
[117] M. Filippone, P. W. Brouwer, J. Eisert, and F. von Oppen, Phys. Rev. B **94**, 201112 (2016).
[118] G. Roux, T. Barthel, I. McCulloch, C. Kollath, U. Schollwöck, and T. Giamarchi, Physical Review A **78**, 023628 (2008).
[119] R. Mondaini and M. Rigol, Physical Review A **92**, 041601 (2015).
[120] C. Monthus and T. Garel, Phys. Rev. B **81**, 134202 (2010).
[121] D. Shepelyansky, Physical review letters **73**, 2607 (1994).
[122] K. M. Frahm, The European Physical Journal B-Condensed Matter and Complex Systems **10**, 371 (1999).
[123] D. O. Krimer, R. Khomeriki, and S. Flach, JETP letters **94**, 406 (2011).
[124] M. Ivanchenko, T. Laptyeva, and S. Flach, Physical Review B **89**, 060301 (2014).
[125] M. Aizenman and S. Warzel, Communications in Mathematical Physics **290**, 903 (2009).
[126] R. Steinigeweg, J. Gemmer, and W. Brenig, Phys. Rev. Lett. **112**, 120601 (2014).
[127] B. S. Shastry and B. Sutherland, Phys. Rev. Lett. **65**, 243 (1990).
[128] B. N. Narozhny, A. J. Millis, and N. Andrei, Phys. Rev. B **58**, R2921 (1998).
[129] X. Zotos, Phys. Rev. Lett. **82**, 1764 (1999).
[130] F. Heidrich-Meisner, A. Honecker, D. C. Cabra, and W. Brenig, Phys. Rev. B **68**, 134436 (2003).
[131] S. Fujimoto and N. Kawakami, Phys. Rev. Lett. **90**, 197202 (2003).

[132] J. Benz, T. Fukui, A. Klümper, and C. Scheeren, Journal of the Physical Society of Japan **74**, 181 (2005).
[133] T. Prosen, Phys. Rev. Lett. **106**, 217206 (2011).
[134] J. Herbrych, P. Prelovšek, and X. Zotos, Phys. Rev. B **84**, 155125 (2011).
[135] C. Karrasch, J. H. Bardarson, and J. E. Moore, Phys. Rev. Lett. **108**, 227206 (2012).
[136] T. Prosen and E. Ilievski, Phys. Rev. Lett. **111**, 057203 (2013).
[137] C. Karrasch, J. Hauschild, S. Langer, and F. Heidrich-Meisner, Phys. Rev. B **87**, 245128 (2013).
[138] R. Steinigeweg, J. Gemmer, and W. Brenig, Phys. Rev. B **91**, 104404 (2015).
[139] H. J. D. Miller and J. Anders, New Journal of Physics **19**, 062001 (2017).
[140] U. Seifert, Eur. Phys. J. B **64**, 423 (2008).
[141] C. Jarzynski, Phys. Rev. Lett. **78**, 2690 (1997).
[142] C. Jarzynski, Annu. Rev. Condens. Matter Phys. **2**, 329 (2011).
[143] M. A. Cuendet, Phys. Rev. Lett. **96**, 120602 (2006).
[144] M. Esposito, U. Harbola, and S. Mukamel, Rev. Mod. Phys. **81**, 1665 (2009).
[145] A. J. Roncaglia, F. Cerisola, and J. P. Paz, Phys. Rev. Lett. **113**, 250601 (2014).
[146] P. Hänggi and P. Talkner, Nat. Phys. **11**, 108 (2015).
[147] B. Cleuren, C. Van den Broeck, and R. Kawai, Phys. Rev. Lett. **96**, 050601 (2006).
[148] P. Talkner and P. Hänggi, J. Phys. A **40**, F569 (2007).
[149] P. Talkner, P. Hänggi, and M. Morillo, Phys. Rev. E **77**, 051131 (2008).
[150] D. Forster, *Hydrodynamic fluctuations, broken symmetry, and correlation functions* (Perseus Books, 1975).
[151] H. Bethe, Zeitschrift für Physik **71**, 205 (1931).
[152] C. P. Poole, *Electron spin resonance* (Courier Corporation, 1996).
[153] A. C. Melissinos and J. Napolitano, *Experiments in modern physics* (Gulf Professional Publishing, 2003).

Preprint version

Original publication: EPL 101, 10010 (2013)
doi: 10.1209/0295-5075/101/10010

Onset of Fokker-Planck dynamics within a Closed Finite Spin System

Hendrik Niemeyer,[1,*] Daniel Schmidke,[1,†] and Jochen Gemmer[1,‡]

[1] *Fachbereich Physik, Universität Osnabrück, Barbarastrasse 7, D-49069 Osnabrück, Germany*

(Dated: May 28, 2018)

Relaxation according to Fokker-Planck equations is a standard scenario in classical statistical mechanics. It is however not obvious how such an equilibration may emerge within a closed, finite quantum system. We present an analytical and numerical analysis of a system comprising sixteen spins in which spatial inhomogeneities of the magnetization relax approximately in accord with a standard Fokker-Planck equation for a Brownian particle in a parabolic potential.

PACS numbers: 05.70.Ln, 05.30.-d, 05.10.Gg

Do closed quantum systems show thermal equilibration and if so how does this equilibration proceed? Since the Schroedinger equation does not feature any attractive fixed point and many systems may ultimately be viewed as closed quantum systems, this question has been debated from the early days of quantum mechanics [1–5]. Recently this question has regained considerable attention, partially due to experimental progress in the field of ultra-cold atomic gases, which may provide the possibility of observing isolated quantum equilibration experimentally in a well controlled way [6, 7]. On the other hand theoretical concepts have been and are being developed. Some of these approaches focus on the existence of an equilibrium for generic quantum systems and analyze properties of pure states concluding that an overwhelming majority of them features certain "typical" properties which are then identified as equilibrium properties [2, 8–12]. The idea that energy eigenstates are likely to belong to this typical majority as well is now known as the eigenstate thermalization hypothesis (ETH) [2, 13–16]. Existence of equilibrium in specific models, such as interacting spin or interacting bosonic/fermionic model is also a subject of current research, cf., e.g., [17–22].
Other approaches focus primarily on the thermalization process and aim at mapping the dynamics of crucial quantities such as certain expectation values, reduced density matrices , etc. onto (quantum) master equations, sometimes taking the form of Fokker-Planck equations (e.g., for the Caldeira Legett model, etc.). This concept has been developed in great detail for open quantum systems [23], i.e., the scenario of a comparatively small system in contact with a much larger system which is usually called a bath. However, concrete examples which are not of this "system + bath" structure but can nevertheless be reliably shown to exhibit features of standard phenomenological equilibration seem to be rare. Or as stated in [24] "It is an intriguing question whether such a Fokker-Planck equation can actually also be found for a thermalizing and closed many-body quantum system". This recent publication addresses a system of coupled spins in which the z-component of the magnetization is reported to follow a Fokker-Planck equation (FPE), close to equilibrium and with a non-linear rescaling of the magnetization. Furthermore the FPE-generator is found to grow linear in time rather than being constant. The work at hand is aimed in a similar direction. However, we intend to present a finite spin model in which the (unrescaled) magnetization difference between to equal parts of the system relaxes according to a FPE with an time independent generator and a diffusion term that is almost constant w.r.t. the magnetization difference.
Our spin model may be described as a finite, anisotropic Heisenberg spin-ladder of length $N/2 = 8$. The Hamiltonian reads

$$\begin{aligned}\hat{H} &= \hat{H}_0 + \kappa\hat{V}\\ \hat{H}_0 &= \sum_{i,\alpha}^{7} J(\hat{\sigma}_x^{\alpha,i}\hat{\sigma}_x^{\alpha,i+1} + \hat{\sigma}_y^{\alpha,i}\hat{\sigma}_y^{\alpha,i+1} + 0.6\,\hat{\sigma}_z^{\alpha,i}\hat{\sigma}_z^{\alpha,i+1})\\ \hat{V}_0 &= \sum_{i} \kappa(\hat{\sigma}_x^{L,i}\hat{\sigma}_x^{R,i} + \hat{\sigma}_y^{L,i}\hat{\sigma}_y^{R,i} + 0.6\,\hat{\sigma}_z^{L,i}\hat{\sigma}_z^{R,i}) \qquad (1)\end{aligned}$$

where $J = 1$ is the coupling strength along the beams (labeled by $\alpha = L, R$) and κ the coupling strength along the rungs. Specifically we investigate $\kappa = 0.2$ and $\kappa = 0.15$. (This model has been suggested in the context of relaxation dynamics in [25], it is non-integrable at least in the sense of not being accessible by a Bethe ansatz). The observable of which we intend to analyze the dynamics

* hniemeye@uos.de
† dschmid@uos.de
‡ jgemmer@uos.de

is the magnetization difference between the beams, $\hat{x}$:

$$\hat{x} = \frac{1}{2}\left(\sum_i \hat{\sigma}_z^{L,i} - \hat{\sigma}_z^{R,i}\right) \quad (2)$$

Since the z-component of the total magnetization of the entire system $\hat{S}_z$ is conserved we may restrict our analysis to a corresponding subspace. Here we choose S_z=0, which means, loosely speaking, half of the spins point up, half down. In the following we are going to compare the true quantum dynamics of the magnetization difference to the dynamics as generated by a naive, stochastic model formulated on the level of a master equation. The stochastic model is constructed as follows: Assume there is a rate at which mutual spin-flips, i.e., simultaneous, contrariwise flips of adjacent spins occur. Let these rates be proportional to i.) the probability with which the adjacent spins actually point in opposite directions, ii.) the square of the coupling constant between the adjacent spins. Since the rates for spin-flips within the beams are much larger than for spin-flips across the beams, one may assume that the spin-flip dynamics within the chains is at an approximate local and instantaneous equilibrium during the ongoing much slower spin-exchange dynamics between the beams. This implies that the probability for an, say, up-pointing spin on the, say right beam, is the same for every site on the beam, namely just the total number of up-pointing spins on the right beam divided by the number of beam sites. Of course the respective applies to the left beam and down-spins. Furthermore due to the above time scale separation the probabilities factorize. Following these principles the rates for transitions between the magnetization difference subspaces X are found to be:

$$R_{(X\to X\pm 1)} = \frac{\gamma\kappa^2 N}{2}\left(\frac{1}{2} \mp \frac{2X}{N}\right)^2 \quad (3)$$

The corresponding master equation exhibits already in its finite, discrete form strong similarities with a FPE for an over-damped particle in a parabolic potential: As long as the respective probabilities P_X are negligible for the extreme magnetization differences $X = \pm N/4$, the first and second moments $\overline{X} := \sum_X X P_X, \overline{X^2} := \sum_X X^2 P_X$ both relax mono-exponentially with corresponding relaxation rates, $R_1 = 2\gamma\kappa^2$, $R_2 = 4(1-1/N)\gamma\kappa^2$. (The FPE would yield corresponding rates with $R_2^{FP} = 2R_1^{FP}$). Regarding large N and X it is adequate to change to a "magnetization difference density" $z = X/N$ which becomes effectively continuous in the limit of large N. Performing a truncated Kramer-Moyal expansion w.r.t. z yields

$$\partial_t p(t,z) = -\partial_z((-\partial_z U(z)p) + \frac{1}{2}\partial_z^2(D(z)p) + \mathcal{O}(\partial_z^3) \quad (4)$$

with $U(z) = \gamma\kappa^2 z^2$ and $D(z) = \gamma\kappa^2(1/4 + 4z^2)/N$. Up to second order in the spatial derivative (i.e., in the large length scale limit) this is very similar to the standard FPE for a Brownian particle in a quadratic potential $U(z)$. The only difference is an additional quadratic dependence of the diffusion coefficient $D(z)$ on the position. This, however, becomes irrelevant for positions sufficiently close to the equilibrium position.

Above the emergence of standard FPE type dynamics from the analogous stochastic model has been established. But do the quantum dynamics as generated by the Schroedinger equation (setting $\hbar = 1$) indeed follow the stochastic model? This will be analyzed in the following. But before embarking upon a theoretical argument let us simply illustrate the existence of this similarity by some numerical data.

The first class of initial states of which we are going to display the dynamics is constructed as follows: Let $\hat{P}_X$ be the projector comprising all states that span a subspace with a given magnetization difference X. Let $\hat{P}_{(E,\Delta E)}$ be a projector comprising all energy eigenstates from the interval $[E - \Delta E/2, E + \Delta E/2]$. Then we chose our initial states as

$$\hat{\rho}_X(0) = \frac{1}{Z}\hat{P}_{(0,2)}\hat{P}_X\hat{P}_{(0,2)}, \quad Z = \mathrm{Tr}\{\hat{P}_{(0,2)}\hat{P}_X\hat{P}_{(0,2)}\} \quad (5)$$

We consider initial magnetization differences $X = 0, 1, 2$, and compute the corresponding evolutions of mean and variance, i.e., $a(t) = \langle\hat{x}(t)\rangle$ and $\sigma^2(t) = \langle\hat{x}^2(t)\rangle - \langle\hat{x}(t)\rangle^2$. This is simply done by numerically exact diagonalization. Fig. 1 shows the evolutions of the probabilities for the various magnetization differences, i.e., $P_X(t) = \langle\hat{P}_X(t)\rangle$ for the above initial state with $X = 1$. The solid lines represent the evolutions as obtained from (3). In order to analyze more initial states and see the relation to the FPE dynamics in more detail we plot more data. In Fig. 2 the $a(t)$'s are displayed, together with the corresponding evolutions as calculated from (3) (The time-scale parameter γ is numerically determined from a projection operator approach, see below). Obviously there is good agreement. In Fig. 3 the $\sigma(t)$'s are displayed, again together with the corresponding predictions from (3). Obviously there also is a less pronounced but still reasonable similarity.

Further numerical investigations (the display of which we omit here for clarity) show that the agreement of the FPE, (or (3)) with quantum dynamics becomes worse if X becomes larger (which is in accord with the findings in [24]). The agreement also becomes worse for smaller models of the same type, i.e., $N = 14, 12, ...$ This encourages the guess that the agreement may become better in the limit of $X/N \ll 1$ but $N \to \infty$

Now the question arises whether the agreement between the quantum evolution and the FPE dynamics is merely incidental. Although we are unable to rigorously specify the class of systems and observables to which a naive FPE description of the above type applies, we provide in the following a consideration which indicates that the above specific spin system is most likely not just a singular example. This consideration is based on the time-convolutionless (TCL) projection operator method [23].

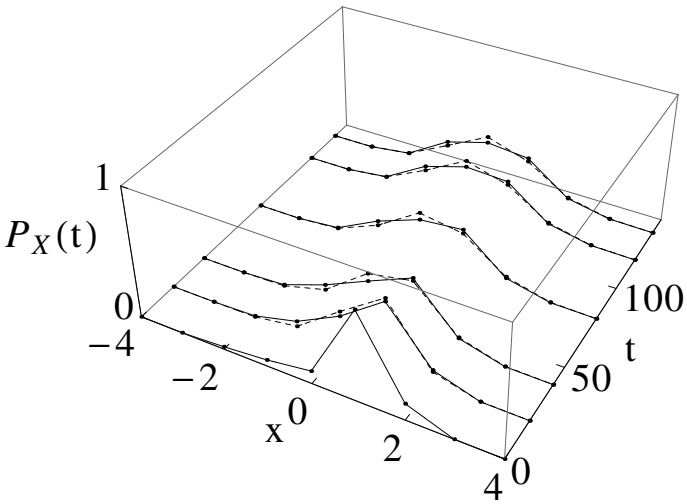

FIG. 1. Evolution of the probabilities of the magnetization differences X for initial state $\hat{\rho}_1(0)$ (see (5)) and coupling strength $\kappa = 0.2$. Solid lines correspond to the evolution as following from the Schroedinger equation, dashed lines to the evolution as following from the (discrete) Fokker-Planck equation (3)

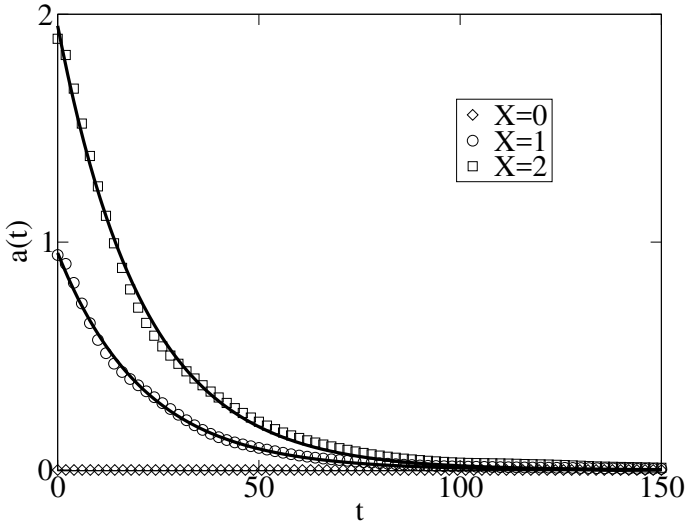

FIG. 2. Evolutions of the expectation values of the magnetization difference for initial states $\hat{\rho}_X(0)$ (see (5)) and coupling strength $\kappa = 0.2$. Symbols correspond to the quantum evolutions, solid lines to the evolutions as following from the Fokker-Planck equation.

We may define a projection superoperator $\mathcal{P}$ by:

$$\mathcal{P}\hat{\rho} = P_X \frac{\hat{P}_X}{d_X}, \quad P_X = \mathrm{Tr}\{\hat{P}_X\hat{\rho}\}, \quad d_X = \mathrm{Tr}\{\hat{P}_X\} \quad (6)$$

Following the TCL projection formalism yields an equation of motion for the P_X's which has the form of a master equation:

$$\dot{P}_Y = \sum_{X\neq Y} R^{TCL}_{Y,X}(t)P_X - \sum_{X\neq Y} R^{TCL}_{X,Y}P_Y \quad (7)$$

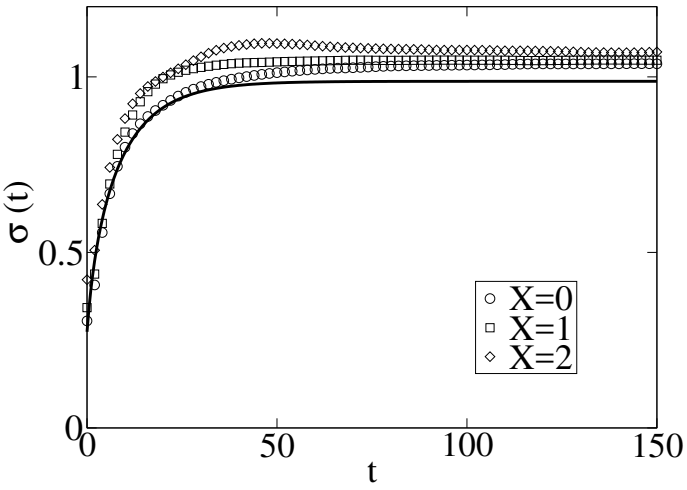

FIG. 3. Evolutions of the variances of the magnetization difference for initial states $\hat{\rho}_X(0)$ (see (5)) and coupling strength $\kappa = 0.2$. Symbols correspond to the quantum evolutions, solid lines to the evolutions as following from the Fokker-Planck equation.

(This equation technically applies only for initial states that fulfill $\mathcal{P}\hat{\rho}(0) = \hat{\rho}(0)$. However, more recent investigations imply that its applicability may be considerably wider [26]). The rates $R^{TCL}_{Y,X}(t)$ are given as expansions in the coupling strength κ. Readily assessable are the leading (second) order contributions which in many well-known cases suffice. They read

$$R^{TCL2}_{Y,X}(t) := \int_0^t C_{Y,X}(t')dt' \quad (8)$$

i.e., they are integrals over correlation functions which are given by

$$C_{Y,X}(t') = \frac{\kappa^2}{d_X}\mathrm{Tr}\{[V\hat{(}t'), \hat{P}_Y][V\hat{(}0), \hat{P}_X]\} \quad (9)$$

where $\hat{V}(t')$ denotes a time dependence w.r.t. the Dirac picture, i.e., unitary dynamics as generated only be $\hat{H}_0$. A straightforward but somewhat lengthy calculation yields

$$C_{Y,X}(0) = \delta_{Y,X\pm1}\frac{R_{X\to X\pm1}}{4\gamma} \quad (10)$$

This result is rigorous and implies that the correlation functions, from which the TCL-rates are calculated by temporal integration, feature initial values that are directly proportional to the rates as obtained from the naive stochastic description (3). This finding is furthermore independent of the details of the model, i.e., the "left" and "right" part of the system could be any Hamiltonian structure, of course the full system must preserves the z-component of the magnetization. For (10) to hold the system neither has to be a spin system, it could also be a fermionic (tight-binding) system that preserves the

overall particle number. In this case the observable would be the particle number difference between a left and right part of the system. However (10) does not necessarily render a naive description valid. Such a validity only results if i.) the true Schroedinger evolution is well approximated by a leading order TCL approach based on the projector (6) and ii.) all the correlation functions $C_{X\pm1,X}(t')$ as given in (9) decay in a similar fashion and on a similar time scale independent of X. Otherwise the initial proportionality of the correlation functions to the naive rates (10) does not carry over to a proportionality of the TCL-rates to the naive rates that can be made into an equality by appropriately choosing γ. Concerning ii.) one finds numerically that for the above specific spin model the correlation functions indeed decay in similar fashion on a similar time scale of $\tau \approx 3$ for $|X| \leq 2$. From numerical integration of the correlation functions for those small $|X|$ we find that in order to obtain $R^{TCL2}_{X\pm1,X}(t > \tau) \approx R_{X\pm1,X}$ one has to choose $\gamma = 0.528$. For larger $|X|$ the dynamics of the correlation functions becomes more and more irregular (longer relaxation times, persisting oscillations) accordingly the full Schroedinger dynamics are numerically found to be no longer in agreement with the FPE. Concerning i.), it has been reported that the matrix that represents $\hat{V}$ w.r.t. to the basis formed by the eigenstates of $\hat{H}_0$ must feature a certain structure in order for a leading order TCL approach to yield valid results (This being true regardless of the existence of so-called time scale separation, see below). The features of this structure are somewhat complex when stated formally [4, 27], however they are surely met for matrices the elements of which are chosen independently at random according to some distribution with mean zero. Although the Hamiltonian at hand does not contain any random numbers, $\hat{V}$ shows features of a random matrix, and thus give rise to the applicability of a leading order TCL approach. To illustrate this we display Figs. 4,5. Both are meant to give an impression of the structure of the matrix block that corresponds to the $X = 0 \to X = 1$ transition. Fig. 4 shows the individual elements of a 50 $\times$ 50 sector of the above block taken from the center w.r.t. energy. The elements are real, zero on average and show no apparent structure, i.e. appear random. To visualize the coarse structure we average the absolute squares of the matrix elements over small sectors of size 0.12×0.12 w.r.t. energy (each of these sectors still contains $\approx 1.4 \cdot 10^4$ individual elements). Obviously these weights are smoothly distributed on the coarse scale with a moderate concentration towards transitions between similar energies. In this sense the matrix is similar to a matrix the elements of which are drawn independently at random according to a distribution that only depends smoothly on the distance to the diagonal elements.

Regardless of the structure of the coupling matrix the coupling strength is of course crucial for the applicability of a leading order TCL projection approach. Generally projective approaches are considered "weak interaction limit approaches". And indeed in order to get essentially time-independent rates a separation of correlation and relaxation time scales is imperative. This separation grows when interactions become weaker. In our specific model for coupling strength $\kappa = 0.2$ those time scales differ be a factor of ≈ 10, i.e., time scale separation is barely implemented. This suggests even better results of a projective approach at weaker couplings. However, other than in the context of infinite systems, for finite systems there

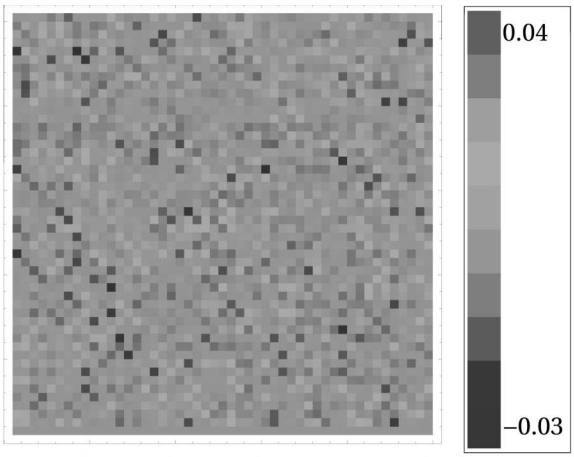

FIG. 4. Visualization of the fine structure of the matrix block corresponding to the $X = 0 \to X = 1$ transition. Displayed are the values of 50×50 matrix elements from the center of the above block w.r.t. energy. Obviously there is no apparent systematic pattern, the entries appear random

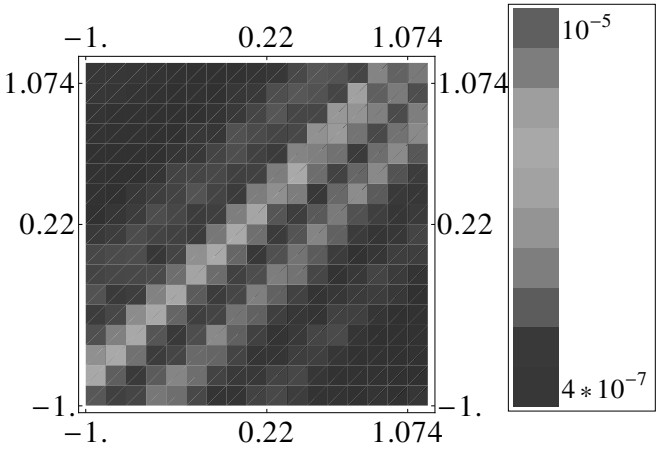

FIG. 5. Visualization of the coarse structure of the matrix block corresponding to the $X = 0 \to X = 1$ transition. Displayed are the averages over the absolute squares of the matrix elements over sectors of size 0.12×0.12 w.r.t energy. Both axis correspond to energy. Obviously there is a smooth coarse structure with a concentration of weight towards transitions between states of similar energy.

is also a limit in the direction of weaker couplings below which results become worse [27, 28]. Numerics indicate that this limit is already reached at $\kappa \approx 0.15$ for the model at hand as illustrated by Figs. 6, 7 Apparently

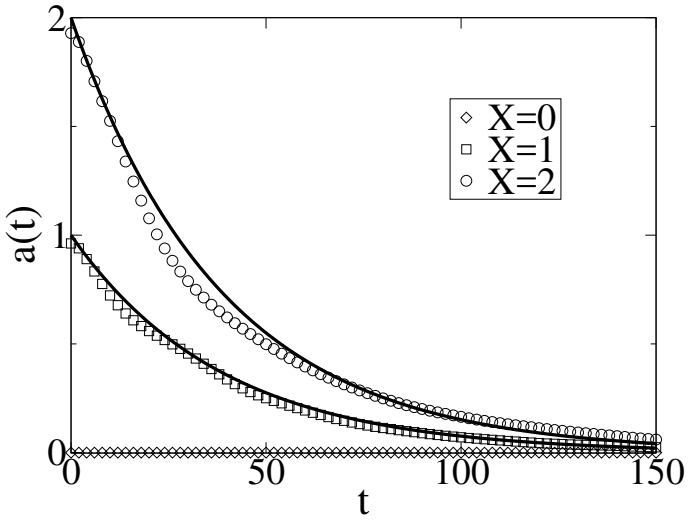

FIG. 6. Evolutions of the expectation values of the magnetization difference for initial states $\hat{\rho}_X(0)$ (see (5)) and coupling strength $\kappa = 0.15$. Symbols correspond to the quantum evolutions, solid lines to the evolutions as following from the Fokker-Planck equation.

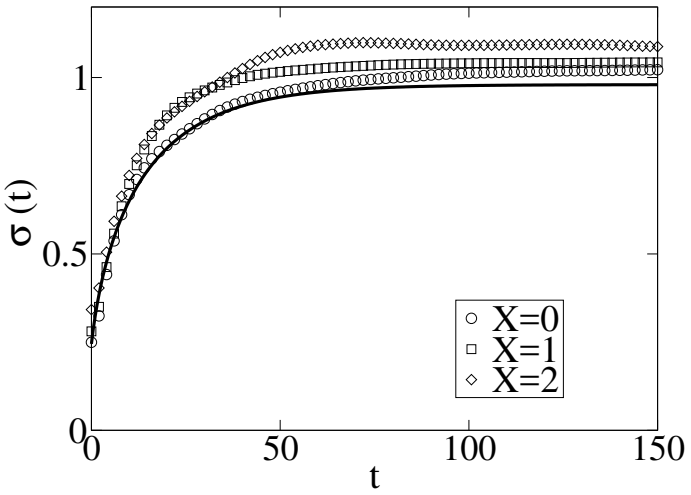

FIG. 7. Evolutions of the variances of the magnetization difference for initial states $\hat{\rho}_X(0)$ (see (5)) and coupling strength $\kappa = 0.15$. Symbols correspond to the quantum evolutions, solid lines to the evolutions as following from the Fokker-Planck equation.

the deviations of the true dynamics from the naive description already become more pronounced than for the case of $\kappa = 0.2$. Thus for the model at hand the range of possible coupling strengths seems to be quite narrow (κ roughly between 0.15 and 0.2). However, the lower limit of the coupling strengths is expected to approach zero very quickly if the system size approaches infinity. Thus the possible range of coupling strengths is expected to increase substantially for "longer spin ladders". Investigations in that direction are currently under way.

Concerning the applicability of the above naive stochastic description to generic systems it should be stated that it is a priori not clear whether or not the coupling $\hat{V}$ assumes the above "quasi-random" form when represented w.r.t. the energy eigenbasis of the decoupled parts $\hat{H}_0$. And it is relatively simple to name examples for which this quasi-random structure does not emerge, like, e.g., any two coupled regular lattices filled with non-interacting fermions, etc. Nevertheless the quasi-random structure of $\hat{V}$ is in a mathematical sense typical, furthermore the emergence of quasi-random matrices from non-random Hamiltonians has been found in other models, e.g., [29, 30]. Thus it appears reasonable to expect that naive descriptions will apply to a much wider range of models then just the specific spin model discussed in the paper at hand. Investigations in that direction are currently under way.

An apparent feature that cannot be in accord with any TCL approach of the above type (6) (that features a unique fixed point) is the fact that the final variances in Figs. 3, 7 appear to depend (weakly) on the initial state. This feature is absent for the expectation values in Figs. 2, 6 These findings may be viewed as a direct consequence of the fact that the ETH does not perfectly apply to the observable $\hat{x}^2$: For any observable $\hat{A}$ one expects in the long run $\langle\psi|\hat{A}(t)|\psi\rangle \to \sum_n \langle n|\hat{A}|n\rangle|\langle n|\psi(0)\rangle|^2$ ($|n\rangle$ being energy eigenstates) if sufficiently many incommensurate energies are involved [31]. This constant value can, however, only be fully independent of the initial state if the $\langle n|\hat{A}|n\rangle$'s are independent of n as the ETH claims and as is to good accuracy the case for, e.g., certain Hamiltonians comprising random numbers.[13, 16, 32]. In the case at hand that would require $\langle n|\hat{x}|n\rangle = 0$ and $\langle n|\hat{x}^2|n\rangle = 1.1$ for all eigenstates n from the relevant regime. While the former holds exactly true due to symmetry, the latter is only approximately fulfilled. As a consequence the mean values truly approach the same equilibrium value regardless of the initial state while this is only approximately correct for variances. This resembles the results in [33, 34], which also find the possibility of some memory effects even in non-integrable systems.
An issue that has received considerable attention in the context of open quantum systems and irreversibility is the role of the initial state. Projection operator methods, refer routinely to specific initial states (such as factorizing, thermal, etc.) and it is not obvious within the framework of projection operator methods what kind of dynamics will result from different initial states [23]. The initial states we have analyzed so far are factorizing and high entropy. Now we turn towards pure, i.e., zero entropy initial states. We investigate two types, factorizing and correlated, the latter here implies entangled. To evaluate the deviation from the expected relaxation behavior we calculate $\delta = \int_0^{150} |a_Q(t) - a_{FPE}(t)|dt/150$. Here

$a_Q(t)$ is the mean magnetization difference as resulting from the respective initial quantum state, $a_{FPE}(t)$ is the value as calculated from (3). For the factorizing initial states we draw pure states at random (uniformly w.r.t. the unitary invariant measure) but from the "5 spins-up" subspace on the left and the "3 -up" subspace on the right beam and compute the corresponding product states. For the entangled initial states we draw states from the full $X = 1$ subspace at random (which are certainly entangled [8]) For the product and entangled states we draw five initial states for each class and average the δ's. We find: $\delta = 0.0154$ for the mixed initial state as given in (5) with $X = 1$, $\overline{\delta} = 0.0161$ for the pure product states and $\overline{\delta} = 0.0162$ for the pure entangled states. Obviously all those dynamics follow the FPE evolution quite closely. This supports the concept of an equilibration that proceeds almost independently of the details of the initial quantum state as presented in [26].

We investigated the dynamics of the magnetization difference between the two beams of a specific 16 spin, ladder-type Heisenberg model. This dynamics is found to be to some extent in accord with a Fokker-Planck equation for an over-damped particle in a quadratic potential, thus making the model an example for the emergence of standard equilibration within finite closed quantum systems. An analysis which indicates that this behavior may be generic for a wider range of quantum systems is presented. Furthermore the equilibration appears to be in reasonable accord with the eigenstate thermalization hypothesis. Standard equilibration is found for mixed but also pure, (to some extent random) factorizing and entangled initial states which agrees with the concept of dynamical typicality.

We thank R. Tumulka, S. Goldstein, J. Lebowitz and J. Ummethum for fruitful discussions on this subject.

[1] W. Pauli, *Festschrift zum 60. Geburtstage A. Sommerfelds* (Hirzel, 1928) p. 30
[2] S. Goldstein, J. L. Lebowitz, R. Tumulka, and N. Zanghi, Eur. Phys. J. H **35**, 173 (NOV 2010)
[3] E. Schroedinger, *Statistical Thermodynamics*, A Course of Seminar Lectures (Cambridge University Press, 1948)
[4] L. VanHove, Physica **21**, 517 (1955)
[5] H. Tasaki, Phys. Rev. Lett. **80**, 1373 (1998)
[6] I. Bloch, J. Dalibard, and W. Zwerger, Rev. Mod. Phys. **80**, 885 (2008)
[7] S. Trotzky, Y. Chen, A. Flesch, I. McCulloch, U. Schollwock, J. Eisert, and I. Bloch, Nature Phys. **8**, 325 (2012)
[8] D. Page, Phys. Rev. Lett. **71**, 1291 (1993)
[9] S. Goldstein, J. Lebowitz, R. Tumulka, and N. Zanghi, Phys. Rev. Lett. **96**, 050403 (2006)
[10] S. Popescu, A. Short, and A. Winter, Nature Physics **2** (2006)
[11] J. Gemmer and G. Mahler, Eur. Phys. J. B **31**, 249 (2003)
[12] P. Reimann, Phys. Rev. Lett. **99**, 160404 (2007)
[13] J. M. Deutsch, Phys. Rev. A **43**, 2046 (1991)
[14] M. Srednicki, Phys. Rev. E **50**, 888 (1994)
[15] M. Rigol, V. Dunjiko, and M. Olshanii, Nature **452**, 854 (2008)
[16] S. Dubey, L. Silvestri, J. Finn, S. Vinjanampathy, and K. Jacobs, Phys. Rev. E **85**, 011141 (2012)
[17] M. Eckstein and M. Kollar, Phys. Rev. Lett. **100**, 120404 (2008)
[18] S. Genway, A. F. Ho, and D. K. Lee, Phys. Rev. Lett. **105**, 260402 (2010)
[19] A. V. Ponomarev, S. Denisov, and P. Haenggi, Phys. Rev. Lett. **106**, 010405 (2011)
[20] M. C. Banuls, J. I. Chirac, and M. B. Hastings, Phys. Rev. Lett. **106**, 050405 (2011)
[21] J. Zhang, C. Shen, and W. Liu, Phys. Rev. A **85**, 013637 (2012)
[22] L. Santos, A. Polkovnikov, and M. Rigol, Phys. Rev. E **86**, 010102R (2012)
[23] H.-P. Breuer and F. Petruccione, *The Theory of open quantum systems* (Oxford University Press, 2003)
[24] C. Ates, J. P. Garrahan, and I. Lesanovsky, Phys. Rev. Lett. **108**, 110603 (2012)
[25] J. Ummethum, Master's thesis, University of Osnabrueck (2008)
[26] C. Bartsch and J. Gemmer, Phys. Rev. Lett. **102**, 110403 (2009)
[27] C. Bartsch, R. Steinigeweg, and J. Gemmer, Phys. Rev. E **77**, 011119 (2008)
[28] J. Gemmer, M. Michel, and G. Mahler, *Quantum Thermodynamics* (Springer, 2009)
[29] S. Mukerjee, V. Oganesyan, and D. Huse, Phys. Rev. B **73**, 035113 (2006)
[30] A. Kolovsky and A. Buchleitner, Eur. Phys. Lett. **68**, 15 (2004)
[31] P. Reimann, Phys. Rev. Lett. **101**, 190403 (2008)
[32] J. Cho, , and M. Kim, Phys. Rev. Lett. **104**, 170402 (2010)
[33] G. Biroli, C. Kollath, and A. Lauchli, Phys. Rev. Lett. **105**, 250401 (2010)
[34] C. Gogolin, M. Muller, and J. Eisert, Phys. Rev. Lett. **106**, 040401 (2011)

Preprint version

Original publication: PRE, 90, 032127 (2014)
doi: 10.1103/PhysRevE.90.032127

Transport in tight-binding bond percolation models

Daniel Schmidtke,[1,*] Abdellah Khodja,[1,†] and Jochen Gemmer[1,‡]

[1] *Fachbereich Physik, Universität Osnabrück, Barbarastrasse 7, D-49069 Osnabrück, Germany*

Most of the investigations to date on tight-binding, quantum percolation models focused on the quantum percolation threshold, i.e., the analogue to the Anderson transition. It appears to occur if roughly 30% of the hopping terms are actually present. Thus, models in the delocalized regime may still be substantially disordered, hence analyzing their transport properties is a nontrivial task which we pursue in the paper at hand. Using a method based on quantum typicality to numerically perform linear response theory we find that conductivity and mean free paths are in good accord with results from very simple heuristic considerations. Furthermore we find that depending on the percentage of actually present hopping terms, the transport properties may or may not be described by a Drude model. An investigation of the Einstein relation is also presented.

PACS numbers: 05.60.Gg, 72.80.Ng, 66.30.Ma,

I. INTRODUCTION

Percolation theory is a well known method to describe transport properties of crystals or other systems which feature regular lattices with substantial amounts of defects, impurities etc. It has been vastly studied from a classical point of view [1, 2]. Here usually bonds (or sites) are filled at random on the above lattice with a probability p. It turns out that, depending on the type of lattice, there exists some p at which the probability of getting a connected cluster of bonds (sites) which extends through the whole lattice changes abruptly from approximately zero to approximately one. This p is called the critical probability p_c.

Due to increasing interest in microscopic structures, which may be significantly affected by quantum effects, percolation models based on quantum mechanics, have also received considerable attention. Also genuinely quantum phenomena like, e.g., quantum hall effect [3], Fermi-Bose mixtures [4] or general (anti)ferromagnetic systems [5], have been addressed by means of percolation theory.

The main focus of the literature on quantum percolation appears to be on the transition from the "non-transport" to the transport regime which is essentially of the same type as the the well-known Anderson transition [6, 7]. Much effort is dedicated to the determination of the quantum percolation threshold p_q. It is found that the quantum percolation threshold is greater than the classical one [6, 8, 9]. For example the classical threshold for bond percolation in three dimensions on a simple cubic lattice is determined to be $p_c^b \approx 0.25$ [2, 10] whereas the threshold for quantum percolation has been determined to lie at $p_q \approx 0.31$ [8, 11]. However, quantitative investigations of transport in the delocalized regime appear to be restricted to preliminary studies close to the quantum percolation threshold [6, 8, 11]. With the work at hand we aim in contrast at a more detailed understanding of transport in systems whose structures are on one hand far away from clean crystals but on the other also far from being collections of disconnected clusters. More specifically, we quantitatively address transport properties at bond probabilites p at which almost all energy eigenstates are delocalized. Generally we expect (and find) diffusive behavior. Unlike the diffusive behavior in periodic systems which is restricted to finite time (and length) scales [12–14] the diffusive behavior here persists due to broken translational symmetry.

The primary motivation for the work at hand is of principal and theoretical nature. Just like it has been recently done for the Anderson model [15], we intend to demonstrate that also in percolation models regular diffusive behavior must not necessarily be induced by decoherence sources like phonon-coupling, etc., but may emerge in a fully coherent set up from the electronic model itself. Furthermore, even in the absence of decoherence this transport behavior will be demonstrated to be in good accord with simple statistical descriptions like the Drude-model. However the considerations are not entirely detached from concrete experimental research. In the context of research based on ultra-cold atoms the dynamics of a moderate number of atoms (playing the role of electrons) subject to a trap and an underlying optical lattice (but completely isolated from any environment otherwise) is observed. Among the central questions

* danischm@uos.de
† akhodja@uos.de
‡ jgemmer@uos.de

are the transport properties of such coherent systems. [16, 17] The percolation models we address below may also possibly be implemented within such an an experimental framework through a modification of the optical lattice. In this context bond percolation may be more convenient to implement then site percolation. Furthermore, in the context of real materials, percolation models may be very rough descriptions of binary mixed crystal alloys in which the on-site potential of one species exceeds the band with of a regular crystal formed by the other species. In this case the lattice would separate in two sub-lattices, each formed by sites occupied by the the same species only. This would correspond to site percolation rather than bond percolation, however transport properties may be expected to behave similarly. Recent investigations on magnesium alloys indicate an massive increase of resistivity caused by the substitution of only a few percent of the sites by another species, this being in accord with the findings in the paper at hand [18]. This is discussed in more detail in Sec. VI

The paper at hand is organized as follows. In Sec. II we introduce our one-particle, tight-binding percolation model and comment rather briefly on localization using the density of states and the inverse participation number in Sec. III. Thereafter (Sec. IV) we specify the quantities of interest, namely the dc-conductivity and current auto-correlation function as connected by linear response theory. We address those quantities numerically and employ a method based on "quantum typicality" whenever samples are required that are too large to be assessed by means of exact diagonalization. We find hints of a transition from "non- Boltzmann" to Boltzmann-type transport with increasing p. Section V establishes the validity of the Einstein relation and, based on the latter introduces a mean free path. A numerical investigation of this mean free path confirms the above "non- Boltzmann" to Boltzmann-transport transition. Section VI is dedicated to a comparison of our results to experimental data on binary magnesium alloys. The paper closes with summary and conclusions in Sec. VII.

II. TIGHT-BINDING BOND PERCOLATION MODEL

The field of percolation models includes a vast number of various approaches to describe processes in semiconductors or other disordered materials. A general division is given by the description of defects, or whatever is causing the disorder, either by loss of particles (site percolation) or loss of bonds between sites (bond percolation), whereby instead of loss one can observe various bond-strength or energies at the sites as well [6, 8].
In the paper at hand we investigate transport in bond percolation models. The intention here is not the detailed description of any specific material but rather the overall description of transport in quantum models of the percolation type. Therefore we consider in the following

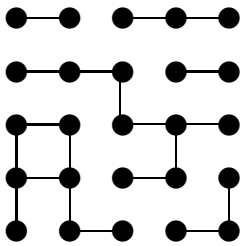

Figure 1. Two dimensional model of classical bond percolation with $p = 0.5$. In classical considerations this describes the situation right at the percolation threshold, whereas from a quantum point of view this model would be below the quantum percolation threshold, even in a three dimensional version. This is due to an effect comparable to Anderson localization.

a three dimensional cubic lattice with edge length L, i.e., the total number of sites (or quantum-dimension of the Hamiltonian) is $dim\left\{\hat{H}\right\} = \left(\frac{L}{a}\right)^3 = N$, where a denotes the lattice constant, i.e., the distance between neighbouring sites.
Generally (quantum) one-particle, tight-binding bond percolation may be described by

$$\hat{H} = \sum_{<ij>} t_{ij}\hat{a}_i^\dagger \hat{a}_j \quad , \tag{1}$$

where $< ij >$ denotes the summation over next neighbors and t_{ij} is known as transfer amplitude. This amplitude may given by

$$t_{ij} = \begin{cases} t\exp(-2\pi i\phi_{ij}) & \text{for connected bond} \\ 0 & \text{for disconnected bond} \end{cases} . \tag{2}$$

Here, t denotes a parameter which quantifies the hoping strength and ϕ_{ij} denotes a parameter which may describe interactions with an external field, e.g., magnetic fields; then ϕ_{ij} is the Peierls phase [6]. However, for simplicity and in order to guarantee time reversibility we set $\phi_{ij} = 0$. Moreover the on-site potential is set to zero for all sites, i.e. $t_{ii} = 0$. Note that we also set in all calculations $k_B = 1$ and $\hbar = 1$.
The distribution of the bond "strenghts" (one for connected, zero for disconnected) is given by

$$P(t_{ij}) = p\ \delta(t_{ij} = t) + (1-p)\ \delta(t_{ij} = 0) \quad . \tag{3}$$

Fig. (1) shows an two dimensional sketch of bond percolation $p = 0.5$. In the classical case one would certainly say that the percolation threshold is just reached, but as found in in [8, 9, 19] the quantum threshold is (possibly against a naive guess) higher than the classical threshold, i.e., quantum transport would be not possible in the above model, even if it was three-dimensional.

III. PRELIMINARY INVESTIGATION OF LOCALIZATION

Below (Sec. IV) we compute conductivities in the high temperature limit, i.e., all energy regimes contribute to transport. In such a setting an decrease of the conductivity with decreasing p may indicate both, either an increase of resistivity in the delocalized energy regime, or simply an increase of the fraction of localized energy eigenstates. Since we are primarily interested in the former we perform in the following a rough analysis of the fraction of delocalized states for different p's. Then we concentrate on the regime in which the vast majority of the energy eigenstates is delocalized. Generally the precise calculation of mobility edges is a challenge that is dealt with using sophisticated methods. [20–22]. For the purposes at hand, however a rather rough determination of the mobility edge suffices. To this end we follow the general approach presented in [23].
The investigation at hand is based on the inverse participation number (IPN)

$$I(E_n) = \sum_i |\psi_i(E_n)|^4 \quad , \tag{4}$$

where $\psi_i(E_n)$ denotes the the i-th component of the energy eigenstate corresponding to E_n. As described in [23] a convenient way to find the mobility edge is to plot the IPN at a given energy against the system size L on a doubly-logarithmic scale. In this representation graphs corresponding to localized states are expected to "bend upwards" while graphs corresponding to extended states are expected to "bend downwards". Only the logarithmic IPN's at the mobility edge are supposed to form a straight line, i.e., the inverse participation number is expected to scale as

$$I(E_c) \propto L^{-d_2} \quad , \tag{5}$$

where E_c denotes the critical energy (mobility edge) and d_2 is referred to as the fractal dimension. Though the exact determination of fractal dimensions is beyond the scope of this paper, we note that at $p = 0.38$ the fractal dimension in our model is approximately given by $d_2 \approx 1.6$ (cf. Fig (2)). This value stands in accord with results of a recent work [24] where the critical exponent for the localization length is $d = 1.627 \pm 0.055$.

Fig. (2) shows some of the described scaling graphs for various energies for $p = 0.38$, all calculated by means of direct numerical diagonalization. This Fig. suggests that the mobility edge is around $E \approx 1$ (since $E = 1$ appears to correspond to the straightest line). In accord with an overall symmetry of the spectrum w.r.t. energy (see Fig. (3)) we find the second mobility edge at $E = -1$. For later purpose it is useful to calculate the density of states (DOS) since it will allow us to estimate the energy range in which most energy eigenstates are delocalized. To that end we define the portion of delocalized eigenstates w.r.t. all eigenstates between the above calculated mobility edges which we denote by $\Phi(p)$.

$$\Phi(p) = \int_{\Delta E} \rho(E) dE \quad . \tag{6}$$

Before we proceed and introduce the main purpose of this work, we would like to have a closer look at the density of states for consistency of the given results.
One finds that for few impurities, i.e. $p > 0.65$, the density of states is smooth and the graph is well described by a Gaussian function, regardless some peaks which correspond to special cluster configurations within the system, cf. [9, 24].
At one hand one finds for low p's that the peaks become more visible, at the other hand one notices a dip around the energy $E \approx 0$, which becomes more significant for decreasing p's. For visualization of that fact we calculated the density of states for $p = 0.45$. The results are presented in Fig. (3).

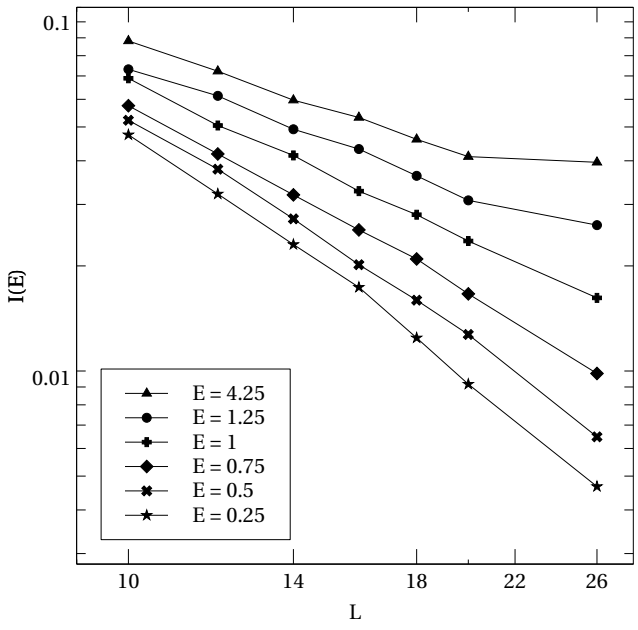

Figure 2. Scaling of the IPN with system size L at several energies and percolation ratio p=0.38. Since only at the mobility edge the scaling is allover linear we locate the mobility edges roughly at $E = -1$ and $E = 1$. Only the last one $E = 1$ is actually displayed above.

The results are displayed in Fig. 4. From the latter it is obvious that the regime in which the vast majority of eigenstates are delocalized is bound from below by $p \approx 0.5$. Furthermore the data appear to be in accord with the value of $p_c \approx 0.31$ from the literature for the Anderson transition.

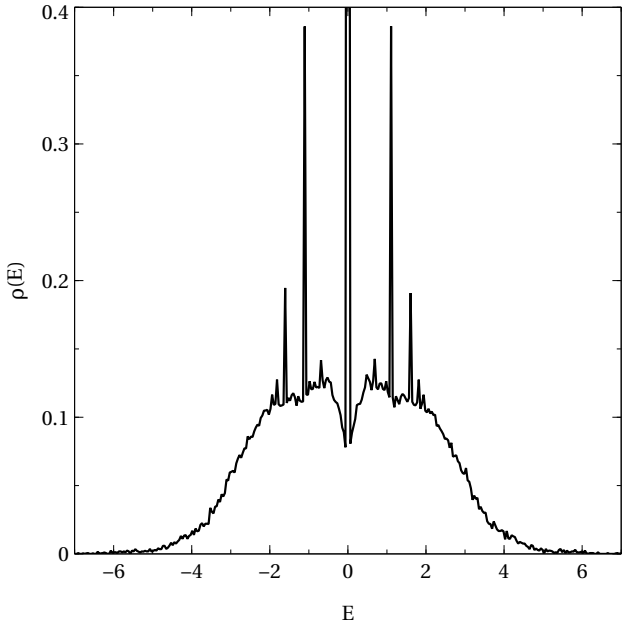

Figure 3. The density of states, here for $p = 0.45$, is symmetrical w.r.t. the energy $E = 0$. There are several distinct peaks, namely at $E = 0$, which correspond to special cluster configurations, cf. [9]. Also notable is the *dip* around $E = 0$, that only occurs at low p.

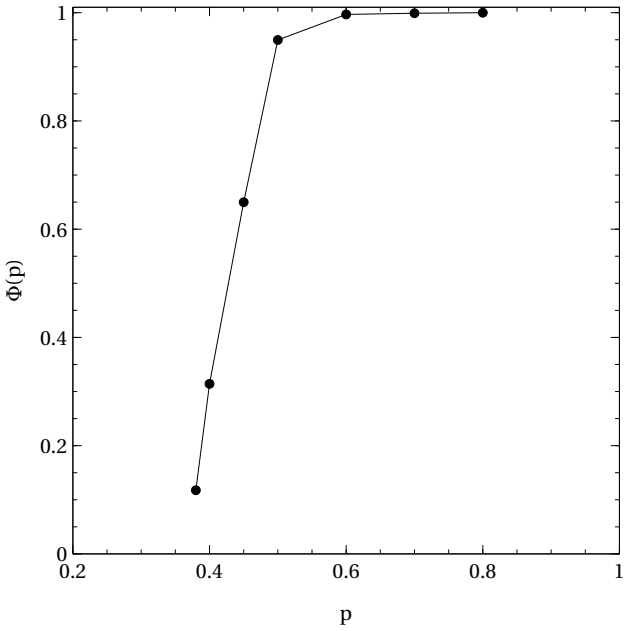

Figure 4. Ratio of delocalized eigenstates w.r.t. all energy eigenstates $\Phi(p)$ as calculated by counting the states between the mobility edges.

IV. CURRENT DYNAMICS AND CONDUCTIVITY

As already stated our primary interest in the paper at hand is (other than in many works in the respective literature) not the determination of the quantum percolation threshold, rather it is quantitative description of transport behavior well above that threshold, i.e., in a regime where the vast majority of states are extended. We aim at finding the dc-conductivity σ_{dc} from linear response theory (Kubo formula) which amounts to the calculation of the particle-current autocorrelation function.
We restrict ourselves here to the limit of high temperatures and low fillings. Therefore the framework of the grand canonical ensemble is used [25–28] which results in

$$\sigma_{dc} = \sigma(t \to \infty), \quad \sigma(t) = \frac{f}{k_B T} \int_0^t \frac{1}{V} \mathrm{Tr} \left\{ \hat{J}(t') \hat{J}(0) \right\} dt' \tag{7}$$

Here f denotes the filling factor, i.e. the number of particles per site at equilibrium, and $\hat{J}(t)$ denotes the current operator in the Heisenberg picture. Furthermore T is the temperature and k_B is the Boltzmann constant. The volume of the system is denoted by $V = a^3 N$.
In order to employ (7) we need to specify an adequate current operator. In the context of periodic systems this is often done using a continuity equation for the site-probabilities [29–31]. Since we do not have fully evolved periodicity here we follow [32] in starting from a velocity operator instead. The velocity operator (corresponding to motion in x-direction) reads:

$$\hat{v} = \frac{i}{\hbar} [\hat{H}, \hat{x}] \qquad , \tag{8}$$

where $\hat{x}$ denotes the x-position operator (x_i denotes the x-coordinate of the i-th site)

$$\hat{x} = \sum_{i=1}^{N} x_i \hat{n}_i \quad \hat{n}_i := \hat{a}_i^\dagger \hat{a}_i \quad x_i = ia. \tag{9}$$

Thus, the velocity operator $\hat{v}$ reads

$$\hat{v} = \frac{i}{\hbar} \sum_{ij}^{N} (i-j)\ a\ t_{ji} \hat{a}_j^\dagger \hat{a}_i \tag{10}$$

Note that this expression is at odds with periodic boundaries, i.e., a (short) transition from one edge of the sample through the the "periodic boundary closure" is, give (10), equivalent to a (long) transition through the whole sample in the opposite direction. Therefore we modify the expression to ensure that only the "shortest" transitions are taken into account. This is achieved by the following definition of the current operator:

$$\hat{J} = \sum_{ij}^{N} J_{ji} \hat{a}_j^\dagger \hat{a}_i \tag{11}$$

$$J_{ji} = \frac{q}{\hbar} \begin{cases} (j-i)\ a\ t_{ij} \quad , & |i-j|a < \frac{L}{2} \\ \mathrm{sign}(j-i)([L-(j-i)]\ a\ t_{ij}) \quad , & |i-j|a > \frac{L}{2} \end{cases}$$

Here q denotes the electric charge per particle, e.g., elementary charge of a single electron. In addition to the current operator we introduce one more quantity, namely the normalized current auto-correlation function $j'(t)$, which is better suited for the investigation of finite-size effects and convergence behavior than the actual current auto-correlation. It is given by

$$j'(t) = \frac{\mathrm{Tr}\left\{\hat{J}(t)\hat{J}(0)\right\}}{\mathrm{Tr}\left\{\hat{J}^2(0)\right\}} \quad . \tag{12}$$

Numerical results for (12) are displayed in Fig. (5) for various system sizes. (Each curve is the average over 15 runs for different models featuring the same p. However variations with different individual implementations turn out to be small.) Since the graphs coincide for times where they are significant different from zero for, say, $L \geq 18$, it is justified to assume that at $L = 28$ the system is no longer affected by finite-size effects. This conclusion is supported by the observation, that the calculation of (7) reveals a deviation of the results for a system with $L = 26$ compared to one with $L = 28$ of approximate 0.9%, and continuous decrease of the deviation for larger systems.

At this point a comment on numerical techniques is appropriate. Results up to $L = 24$ in this paper are always obtained by numerical matrix diagonalization, whereas all results for sizes above this limitation are calculated by means of a algorithm based on "typicality" that allows for the determination of correlation functions on the basis of propagation of single pure states. In the work at hand the pure state propagation is performed using a standard Runge-Kutta algorithm. For a full account of this typicality technique and its theoretical background, see Refs. [33–35]. We were able to treat systems up to $L = 34$ ($N \approx 39000$) with this algorithm on standard computing equipment, however as pointed out above, but $L = 28$ appears to be sufficient for a reasonable extraction of quantitative results. Nevertheless based on data only from exact diagonalization the whole investigation presented here would have been far less conclusive.

The results on conductivity are shown in Fig. (6) where σ' relates to the σ_{dc} from (7) as

$$\sigma_{dc} = \frac{fq^2t^2}{k_BTa\hbar[E]}\sigma', \tag{13}$$

thus σ' is a dimensionless integrated current autocorrelation function, i.e, $q, \hbar$ are set to unity and $[E]$ is the unity according to which energy is measured. Each conductivity represents the average over 15 different percolation models featuring the same p. The error bars indicate the mean square deviation corresponding to the respective 15 conductivities. As expected, the conductivity increases with increasing p. A systematic interpretation of this result appears challenging. Nevertheless we want to point out the reasonable agreement of the results displayed in

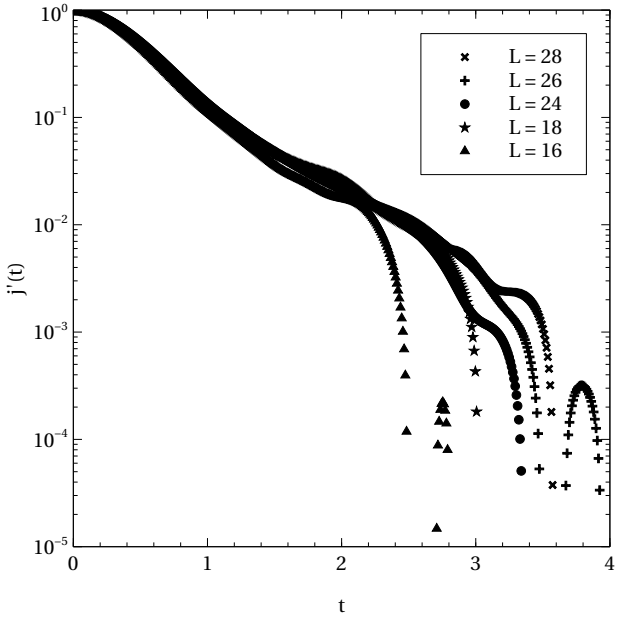

Figure 5. Normalized current auto-correlation functions $j'(t)$ for various system sizes L. The graphs coincide regardless of size in regions where they are substantially different from zero, for, say $L \geq 18$. Hence data can reliably be expected to contain negligible finite-size effects at $L = 28$.

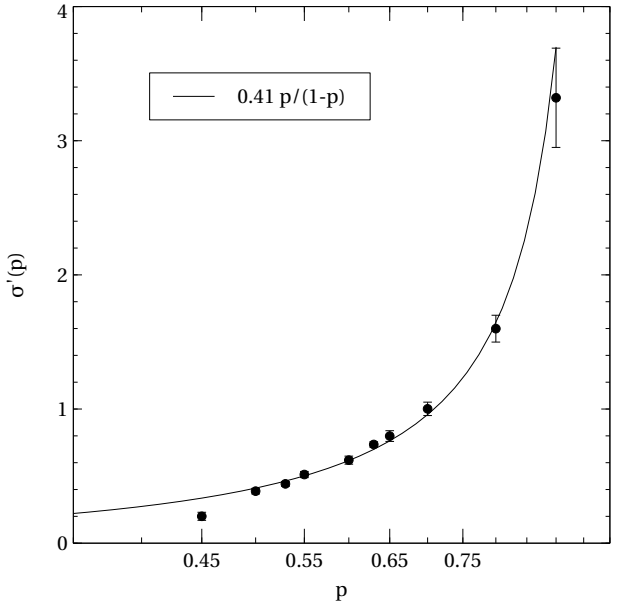

Figure 6. Numerically calculated scaled dc-conductivity $\sigma' := Tf^{-1}\sigma_{dc}$ compared to the result of a simple heuristic theory given in the text. The agreement is good, deviations appear at and below $p \approx 0.45$. This is due to non-negligible localization. Note that all data points carry error bars, however for small p they are barely visible.

(6) with results from a simple heuristic reasoning. From simple Drude type arguments one expects the conductivity to be proportional to the square of the mean particle velocity v^2 and the mean collision-free or relaxation time τ, i.e. [36],

$$\sigma \propto v^2 \tau. \tag{14}$$

For the square of the mean particle velocity one may simply take $v^2 := \mathrm{Tr}\left\{\hat{J}^2(0)\right\}/N$. From the current operator as given in (11) it is straightforward to see that his quantity must scale as p, i.e., e $v^2 \propto p$. The relaxation time τ is (by definition) inversely proportional to a scattering rate R. In the percolation model at hand scattering (and thus relaxation of the current) is caused by the "missing connections". The number of the latter is proportional to $1-p$, hence one obtains for the rate $R \propto 1/(1-p)$. Plugging those results into (14) yields

$$\sigma \propto \frac{p}{1-p} \tag{15}$$

The solid line in Fig. 6 shows a fit based on (15) yielding $\sigma' = 0.41p/(1-p)$. Obviously the agreement is rather good for $p \geq 0.45$. Apparently in this regime the above simple heuristic argument captures the relevant physics, even though below say $p \approx 0.9$ this regime can certainly not be classified as a weak scattering regime. Below $p \approx 0.45$ the fit appears to deviate, however, as may be inferred from Fig. 4, this is the point at which localization massively sets in. We thus conclude that the simple theory given in (15) holds for p down to the quantum percolation threshold. Furthermore it is clearly noticeable that the statistical splay of the results increases with increasing p. This however may be readily interpreted as a consequence of the law of large numbers: the fewer scattering centers there are the larger is the statistical variation of all quantities that depend on scattering.

Next we consider the specific kind of decay of the current auto-correlation function. As shown in Fig. (7) a transition of transport types appears to occur between $p = 0.9$ and $p = 0.6$. Decay at $p = 0.9$ is compared to a mono-exponential decay, as to be expected from a simple Drude model or a linear Boltzmann equation in relaxation time approximation [25, 36, 37], the agreement is reasonable. At $p = 0.65$, however, the decay behavior is much closer to a Gaussian as illustrated in Fig. (7). This transition from exponential to Gaussian decay behavior on the way from weak to strong scattering has been observed in various other, similar models before. There it has been explained within the framework of a time-convolutionless projection operator investigation [15, 38]. If one projects onto the current and performs a perturbative, leading order treatment, then exponential decay of the current auto-correlation function results at weak, and Gaussian decay at intermediate strength perturbations. From the results displayed in Fig. (7) it appears evident that the same applies to the model at hand as well.

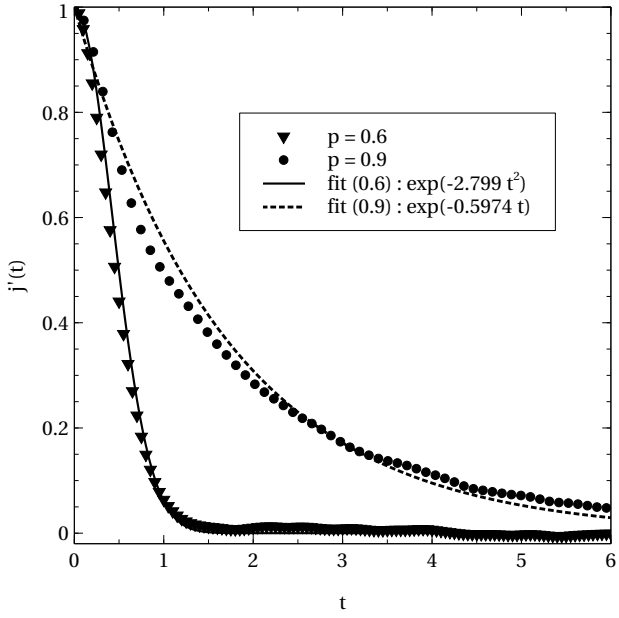

Figure 7. Normalized current auto-correlation functions $j'(t)$ at $L = 28$ for $p = 0.9$ (few defects) and $p = 0.6$ (medium defects). At $p = 0.6$ the decay appears to be Gaussian, whereas at $p = 0.9$ one finds rough agreement with an exponential decay. The latter hints in the direction of Drude-type transport.

V. EINSTEIN RELATION AND MEAN FREE PATH

The diffusion constant of a system is certainly interesting in its own right. However the main purpose of this section is to establish the validity of an Einstein relation in oder to arrive at a reasonable definition of a mean free path. The validity of the Einstein relation in quantum systems is frequently discussed [39, 40]. Here we examine it in its most elementary form, namely as the claim of a proportional relation between conductivity and diffusion constant

$$D(t) = \frac{T}{\epsilon^2}\sigma(t) \quad , \tag{16}$$

where $D(t)$ denotes the (time dependent) diffusion constant, ϵ^2 denotes the uncertainty (variance) of the transported quantity per site at equilibrium. Since the uncertainty for the dc-current equals at low densities the filling factor f, cf. [12], we find from linear response theory (7)

$$D_K(t) = \int_0^t \frac{1}{N}\mathrm{Tr}\left\{\hat{J}(t')\hat{J}(0)\right\}dt' \quad . \tag{17}$$

$D_{\mathrm{K}}(t)$ is to be compared to a direct computation of the diffusion constant in order to check (16). If a diffusion equation holds, the derivation w.r.t. time of the spatial variance of the diffusing quantity equals twice the diffusion constant [41].
To directly observe this spatial variance we define an ini-

tial density operator

$$\hat{\rho}(0) = \frac{1}{Z}\exp(-\frac{\left(\hat{x}-\frac{L}{2}\right)^2}{2d}), \quad Z = \mathrm{Tr}\{\exp(-\frac{\left(\hat{x}-\frac{L}{2}\right)^2}{2d})\}\ , \tag{18}$$

where d denotes an initial variance, which is here chosen as $d = 0.95$.
This implies that the initial site occupation probability is concentrated in a thin slab of a thickness on the order of one perpendicular to the x-axis.
Based on this $\hat{\rho}(0)$ we calculate the time-depended variance and take the derivative w.r.t. time to obtain a diffusion constant; here named $D_{\mathrm{D}}(t)$.

$$D_D(t) = \frac{1}{2}\frac{d}{dt}\mathrm{Tr}\left\{\hat{x}^2(t)\rho(0)\right\} \tag{19}$$

Note that, since the mean particle position does not drift $\frac{d}{dt}\mathrm{Tr}\left\{\hat{x}(t)\rho(0)\right\}$ remains without influence.

If the Einstein relation holds, $D_{\mathrm{K}}(t)$ and $D_{\mathrm{D}}(t)$ should coincide. Fig. (8) shows the comparison of both diffusion constants and reveals that the Einstein relation is apparently fulfilled. Moreover it is obvious that the calculation of the diffusion constant in the sense of (19) is strongly influenced by finite-size effects.

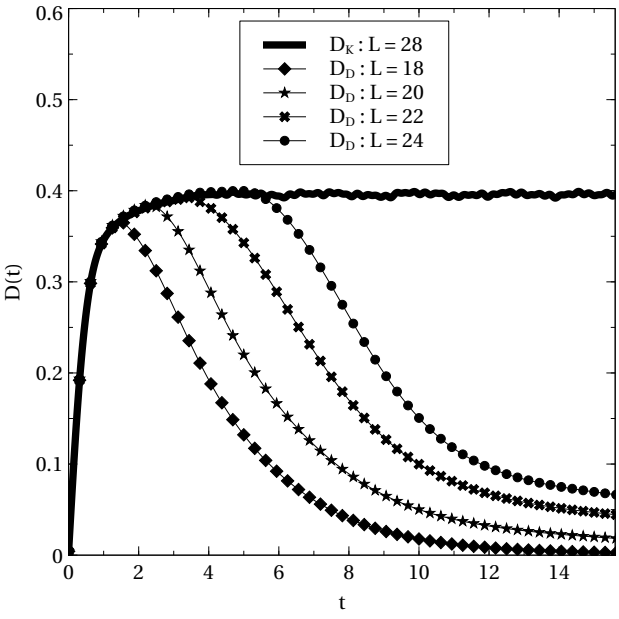

Figure 8. Comparison of time-dependent diffusion constants either calculated by (17) or (19) at $p = 0.5$. The calculation according to (19) obviously suffers from strong finite-size effects, however, agreement in the limit of large sizes is evident. This indicates the validity of the Einstein relation.

However, the validity of the Einstein relation allows for a reasonable definition of a mean free path λ which may be calculated based on (17).

Ballistic transport behavior, as exhibited by initially concentrated, free, non-scattering particles is characterized by a quadratic increase of the spatial variance w.r.t. time, i.e., $\langle\hat{x}^2\rangle \propto t^2$ or $D \propto t$, Since the increase of the diffusion constant is linear in the beginning, cf. Fig. (8), we define the increase of standard deviation $\sqrt{\langle\hat{x}^2\rangle}$ during this ballistic initial period as the mean free path λ. We define the ballistic initial period as the period before $D(t)$ has reached 90% of its final value. Of course this choice is not imperative, however from looking at Fig. (8) it appears reasonable. Fig. (9) shows the results for the mean free path λ

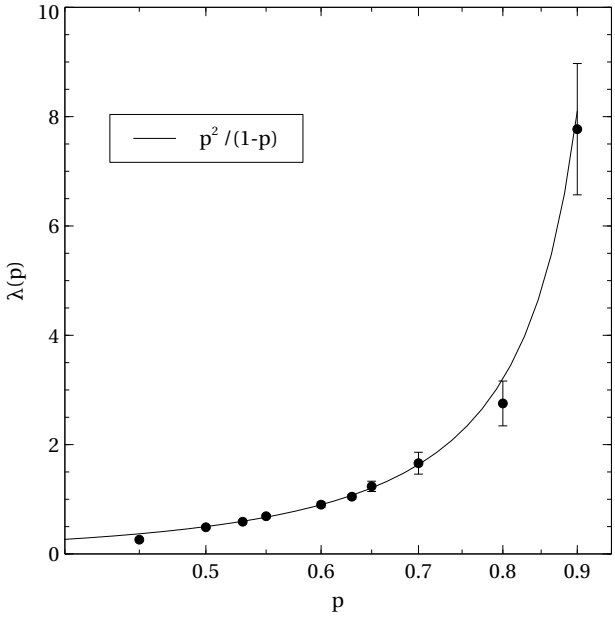

Figure 9. Numerically calculated mean free path λ compared to the result of a simple heuristic theory given in the text. The agreement is good, deviations appear below $p \approx 0.5$. This is due to non-negligible localization. Note that all data points carry error bars, however for small p they are barely visible.

Much like the consideration on conductivity in Sec. IV we discuss the agreement of a simple, heuristically derived form of λ with the computed data in Fig. (9) in the following. Consider some "chain" of either connections or voids along some crystal-axis. Assume, for simplicity that this chain was ordered (which it is in fact not). Assume furthermore that a longer sequence of connections alternates with just one void. Call the length of the sequence of connections l. Then the total ratio p of connections per total number of sites is $p = l/l + 1$. Or the length of the uninterrupted sequence of connections depends on the connection probability as:

$$l(p) = \frac{p}{1-p} \tag{20}$$

We may associate l with a free path. I order to find the mean free path we multiply l by p since this is the probability (relative frequency) of a "site" to sit on a

sequence of connections. We thus get:

$$\lambda(p) = \frac{p^2}{1-p} \tag{21}$$

This expression for the mean free path is represented in Fig. (9) by the solid line. Given the simplicity of the argument the agreement with the computed data is good. Of course such an expression can only be expected to yield reasonable results down to $p = 0.5$. However from Fig. (8) we now that below that localization effects set in anyway. Thus for the fully delocalized regime (21) appears to capture the relevant physics.

VI. SEMI-QUANTITATIVE COMPARISON OF THE RESULTS TO MEASURED CONDUCTION DATA ON BINARY ALLOYS

As already pointed out in the Introduction the primary intentions of the paper at hand are of principal nature. However a short comment on the relation of the results to conductivities of binary alloys should be in order. The electronic system of a binary alloy in a mixed crystal phase may be viewed as an implementation of a percolation model. If the valency of the solute element is very different from that of the host metal, the on-site potentials at the solute sites may be so low (high) that, as a rough approximation, the solute sites may be regarded as being "frozen out", i.e., not contributing to the conduction process. Such a picture suggests a site percolation rather than a bond percolation model, but since bond and site percolation are expected to behave more or less comparably we simply ignore this difference in this consideration. The conductivity of weakly or non-interacting fermions at rather low temperatures (k_BT small compared to the bandwidth) is roughly given by

$$\sigma_f \approx \frac{n(E_f)}{N} \int_0^t \frac{1}{\mathrm{Tr}\left\{\hat{P}_f\right\}} \mathrm{Tr}\left\{\hat{J}(t')\hat{J}(0)\hat{P}_f\right\} dt' \tag{22}$$

[25] where $n(E_f)$ is the density of states at the Fermi energy, N is the total number of states in the conduction band of the one-particle model and $\hat{P}_f$ is a projector which projects onto an energy shell (Hilbert space spanned by energy eigenstates) of width k_BT around the Fermi energy. Separating dimensionless quantities from quantities carrying dimensions yields

$$\sigma_f \approx \frac{n(E_f)q^2t^2}{Na\hbar[E]}\sigma'_f \tag{23}$$

where σ'_f is the corresponding dimensionless current auto-correlation function, just like σ' in (7). Since we are only doing an estimate we replace σ'_f by σ' as given in Fig. 6, i.e., $\sigma'_f \approx 0.41p/1-p$. If the percentage of solute atoms $c[\%] := 100(1-p)$ is low we may approximate $\sigma'_f \approx 41/c$. We intend to compare our results to recently measured data on magnesium alloys, specifically a magnesium-zirconium alloy [18]. In order to do so we use the following values in (23): The bandwidth of metallic magnesium is ca. $14eV$ [42], our simple cubic basis model yields a bandwidth of ca. $14eV$ if the hopping terms are chosen as $t = 1.2eV$. (Obviously we use eV as an energy unit). According to [42] we furthermore set the relative density of states to $n(E_f)/N \approx 0.16/eV$. Since our model does not account for any lattice distortions, the lattice constant is set to $a = 3\mathring{A}$ which is about the mean lattice constant of metallic magnesium. And, naturally, the transported charge per particle is the electron charge, i.e., $q = e$. Plugging in all these numbers and calculating the specific electrical resistivity $\rho = 1/\sigma_f$ rather than the conductivity itself, we get

$$\rho \approx c \cdot 1.3 \cdot 10^{-7}(\Omega m) \tag{24}$$

Of course this cannot be taken as an absolute result since even pure magnesium ($c = 0$) has a non-zero resistivity due to phonons, impurities, etc. But if one, as suggested by Matthiessen's rule, regards (24) as an expression for the increase of the resistivity due to the gradual addition of a a solute, (24) may be compared to experimental data. Pan et al. report in Ref. [18] for a magnesium-zirconium alloy a value of

$$\rho_{measured} = c \cdot 9.311 \cdot 10^{-8}(\Omega m) \tag{25}$$

The atomic volume difference between magnesium and zirconium is rather low, such that few lattice distortions can be expected. Furthermore the valency of zirconium (+4) is rather high. However, note that our model has simple cubic rather than hexagonal symmetry, we consider bond rather than site percolation, the concept of zirconium sites being frozen out is surely not completely correct, we neglect lattice distortions entirely, etc. Regarding all these limitations the agreement of (24) with (25) within about 30% appears reasonable.

VII. SUMMARY AND CONCLUSION

We investigated a simple quantum bond percolation model on the basis of an one-particle, tight-binding Hamiltonian. We focus on investigation of transport properties in the fully delocalized regime, i.e., a regime in which only a negligible fraction of all energy eigenstates is localized. This turns out to be the case at bond probabilities of $p \geq 0.5$. The conductivity in this regime has been calculated using linear reponse theory (Kubo-formula) and a numerical algorithm based on quantum typicality for the evaluation of the current autocorrelation function. As expected the conductivity increases rapidly with increasing p and is found to be in accord with the result of a simple heuristic reasoning involving mean collision free times and mean particle velocities. The latter may be defined even though at $p \geq 0.5$ no true dispersion relations exist. Furthermore a gradual transition from a

current decay that is not in accord with a Drude model to a current decay that is, is observed between $p \approx 0.6$ and $p \approx 0.9$. The proportionality of the conductivity and the diffusion constant, i.e., the Einstein relation is analyzed numerically and found to hold. This finding allows for a definition of a mean free path. Numerical calculations of this mean free path coincide well with results from yet another heuristic consideration based on counting the mean length of uninterrupted sequences of connections in the lattice. Thus, to conclude, in the regime above $p = 0.5$, although being fully quantum and strongly disordered, the dynamics of the model appear to be remarkably well described by by purely probabilistic, classical reasoning. Furthermore the result based on the percolation model are in reasonable agreement with measured data on binary magnesium alloys.

[1] B. Shapiro, *Percolation Structures and Processes*, vol. 5 (Annals of the Israel Physics Society, 1983).
[2] S. Kirkpatrick, Rev. Mod. Phys. **45**, 574–588 (1973).
[3] D. H. Lee, Phys. Rev. B **50**, 10788 (1994).
[4] A. Sanpera, A. Kantian, L. Sanchez-Palencia, J. Zakrzewski, and M. Lewenstein, Phys. Rev. Lett. **93**, 040401 (2004).
[5] R. Yu, T. Roscilde, and S. Haas, Phys. Rev. Lett. **94**, 197204 (2005).
[6] A. Kaneko and T. Ohtsuki, Journal of the Physical Society of Japan **68**, 1488 (1999).
[7] P. W. Anderson, Phys. Rev. **109**, 1492–1505 (1957).
[8] C. M. Soukoulis, Q. Li, and G. S. Grest, Phys. Rev. B **45**, 7724 (1992).
[9] G. Schubert, A. Weisse, and H. Fehske, Phys. Rev. B **71**, 045126 (2005).
[10] C. D. Lorenz and R. M. Ziff, Phys. Rev. E **57**, 230 (1998).
[11] R. Berkovits and Y. Avishai, Phys. Rev. B **53**, 16125 (1996).
[12] N. Hashitsume, M. Toda, R. Kubo, and N. Saito, *Statistical physics II: nonequilibrium statistical mechanics* (Springer, 1992).
[13] P. Gaspard, Phys. Rev. E **53**, 4379 (1996).
[14] R. Steinigeweg, J. Gemmer, H.-P. Breuer, and H.-J. Schmidt, Eur. Phys. J. B **69**, 275 (2009).
[15] R. Steinigeweg, H. Niemeyer, and J. Gemmer, New J. Phys **12**, 113001 (2010).
[16] U. Schneider and L. Hackmüller, Nature Physics **8**, 213 (2012).
[17] L. Hackmüller and U. Schneider, Science **327**, 1621 (2010).
[18] H. Pan and F. Pan, Journal of material science **49**, 3107 (2014).
[19] C. M. Soukoulis and G. S. Grest, Phys. Rev. B **44**, 4685 (1991).
[20] E. Abrahams, *50 Years of Anderson Localization* (World Scientific Publishing Company, 2010).
[21] D. J. Priour, Phys. Rev. B **85**, 014209 (2012).
[22] I. Mertig, E. Mrosan, and P. Ziesche, *Multiple Scattering Theory of Point Defects in Metals: Electronic Properties* (Teubner-Texte zur Physik, 1987), 11th ed.
[23] J. Brndiar and P. Markos, Phys. Rev. B **74**, 153103 (2006).
[24] L. Ujfalusi and I. Varga, *Quantum percolation transition in 3d* (2014), URL `http://arxiv.org/pdf/1405.1985`.
[25] J. Jaeckle, *Einführung in die Transporttheorie* (Vieweg, 1978).
[26] R. Kubo, J. Phys. Soc. Jpn. **12**, 570 (1957).
[27] R. Zwanzig, Annual Review of Physical Chemistry **19**, 67 (1965).
[28] R. Kubo, Rep. Prog. Phys. **29**, 255 (1966).
[29] F. Heidrich-Meisner, A. Honecker, D. C. Cabra, and W. Brenig, Phys. Rev. B **68**, 134436 (2003).
[30] J. Gemmer, R. Steinigeweg, and M. Michel, Phys. Rev. B **73**, 104302 (2006).
[31] J. Benz, T. Fukui, A. Klümper, and C. Scheeren, J. Phys. Soc. Jpn. **74**, 181 (2005).
[32] A. Khodja, H. Niemeyer, and J. Gemmer, Phys. Rev. E **87**, 052133 (2013).
[33] T. A. Elsayed and B. V. Fine, Phys. Rev. Lett. **110**, 070404 (2013).
[34] R. Steinigeweg, A. Khodja, H. Niemeyer, C. Gogolin, and J. Gemmer, Phys. Rev. Lett. **112**, 130403 (2014).
[35] R. Steinigeweg, J. Gemmer, and W. Brenig, Phys. Rev. Lett. **112**, 120601 (2014).
[36] N. W. Ashcroft and N. D. Mermin, *Solid State Physics* (Saunders College Publishing, New York, 1976).
[37] G. D. Mahan, *Many-Particle Physics* (Springer, 2000), 3rd ed.
[38] R. Steinigeweg and R. Schnalle, Phys. Rev. E **82**, 040103 (2010).
[39] R. Steinigeweg, H. Wichterich, and J. Gemmer, Europhys. Lett. **88**, 10004 (2009).
[40] Y. Roichman and N. Tessler, Appl. Phys. Lett. **80**, 1948 (2002).
[41] A. Einstein, Annalen d. Physik p. 549 (1905).
[42] S. Chatterjee and P. Sinha, J. Phys. F: Met. Phys. **5**, 2089 (1975).

Preprint version

Original publication: PRE, 93, 012125 (2016)
doi: 10.1103/PhysRevE.93.012125

Numerical Evidence for Approximate Consistency and Markovianity of some Quantum Histories in a Class of Finite Closed Spin Systems

Daniel Schmidtke[1,*] and Jochen Gemmer[1,†]

[1] *Fachbereich Physik, Universität Osnabrück, Barbarastrasse 7, D-49069 Osnabrück, Germany*

Closed quantum systems obey the Schrödinger equation whereas nonequilibrium behavior of many systems is routinely described in terms of classical, Markovian stochastic processes. Evidently, there are fundamental differences between those two types of behavior. We discuss the conditions under which the unitary dynamics may be mapped onto pertinent classical stochastic processes. This is first principally addressed based on the notions of "consistency" and "Markovianity." Numerical data are presented that show that the above conditions are to good approximation fulfilled for Heisenberg-type spin models comprising 12-20 spins. The accuracy to which these conditions are met increases with system size.

PACS numbers: 05.60.Gg, 72.80.Ng, 66.30.Ma,

I. INTRODUCTION

May quantum dynamics be mapped onto standard stochastic processes, especially in closed quantum systems? It is widely agreed that the general answer to this question is no (even though there have been investigations in this direction [36, 37]). Since the mid-2000s there has been increasing research activities in the field of "equilibration" and "thermalization" with respect to closed quantum systems, although the latter mechanisms are traditionally associated with stochastic processes. Most of these research activities have focused on the remarkable fact that after some, possibly very long, time [38–40], the behavior of many observables is very well be practically indistinguishable from standard phenomenological equilibrium behavior, despite the fact that the Schrödinger equation does not feature any attractive fixed point. Some of these attempts follow concepts of pure state quantum statistical mechanics [41, 42], typicality [43–45], or eigenstate thermalization hypothesis [44, 46]. However, according to textbook-level physics, a multitude of systems not only reach equilibrium after an extremely long time but also evolve towards it in a (quick) way that conforms with some master or Fokker-Planck equations. Moreover, there have recently been attempts to find and explain the emergence of Fokker-Planck-type dynamics in closed quantum systems [47–50]. Here we go a step further in that direction and investigate to what extent the quantum dynamics of certain observables in a specific system can be seen as being in accord not only with a Fokker-Planck equation, but also with the underlying stochastic process. The latter allows for producing individual stochastic trajectories.
The approach presented here is based on two central notions: "Markovianity" and "consistency".
Despite Markovianity already being a somewhat ambiguous term with differing definitions in the context of open quantum systems, cf. Refs. [51–53], we add below another definition which is furthermore applicable to closed quantum systems. The definition is based on mathematical constructions which have already been used by Wigner [54] to quantify probabilities for the occurrence of subsequent events. Our notion of consistency is the same as the one used in the context "consistent histories" which also deals with these mathematical constructions. Very loosely speaking, it quantifies the absence of coherence between different events. If the dynamics of some system with respect to some set of projectors is consistent, then the evolution of the expectation values of those projectors is independent of whether those projectors are repeatedly measured in time.

To avoid confusion it is important to note that (although measurements are mentioned) we neither address an open system scenario nor do we use open system analysis techniques [53]. This is to be contrasted with literature showing that in open systems, like the Caldeira-Leggett model, histories of, e.g., position measurements become consistent in the Markovian limit [55–57]. While the Caldeira-Leggett model is accessible by a Feynman-Vernon path integral approach that also allows for the formulation of consistency [55, 57], our models are not coupled to any baths, nor are their classical analogs integrable, thus rendering a path integral approach futile. A crucial point of our investigation is precisely the fact

* danischm@uos.de
† jgemmer@uos.de

that consistency and Markovianity may occur even without any kind of "environment-induced superselection."

The present paper is organized as follows: in Secs. II and IV the "consistency concept" is reviewed and our notion Markovianity is specified. Furthermore, we use the general point of view that unitary dynamics may be mapped onto classical stochastic processes, if the unitary dynamics are consistent and Markovian, onto a more formal basis. We also argue qualitatively that typical Hamiltonians yield consistent and Markovian unitary dynamics for typical observables in Sec. III.
Section V contains our main result. It is a specific numerical example supporting the correctness of the qualitative argument given in the previous Sec. III. We numerically investigate some generic sequences of transitions (or "quantum histories") in a generic spin system. We repeat the investigation for the same type of spin system but for sizes of 12-20 spins. This finite-size scaling suggests that the addressed quantum histories become indeed consistent and Markovian in the limit of large systems. Some comments on many-step Markovianity are given in Sec. VI where special attention is laid on comparison of sequences of identical events to random event sequences. Conclusions are drawn and possible further investigations are outlined in Sec. VII.

II. CONSISTENCY AND MARKOVIANITY CONDITIONS

Consistency is obviously a central concept in consistent history approaches [58], which is sometimes also called decoherent histories [55, 59]. In the context of the current paper we only need to introduce what is sometimes called the "decoherence functional" or "consistency condition" and its properties. The more philosophic aspects of the consistent history approach, concerning the interpretation of quantum mechanics are of no relevance here (for critical reviews see, e.g., Refs. [60, 61]). However, we will recapitulate the basic notions of the consistent history approach, in order to enable the reader unacquainted with the latter to develop a full understanding of the analysis within this paper.
Broadly speaking, one may describe quantum histories as a method to deal with the occurrence probabilities of certain event sequences. An event sequence consists of the alternating mathematical actions of measuring a certain property, encoded in some set of projection operators π_n, according to the von Neumann measurement scheme, and time-propagating the resulting state according to the Schroedigner equation. Note that the measured properties need not to be identical each time.
The term "consistent" expresses the accordance of history probabilities with the Kolmogorov axioms, and the degree of accordance is quantified by the previously mentioned consistency condition, which is one of the central notions of the paper. With these preliminary remarks we embark on a somewhat more formal presentation of the consistent history approach.

To begin with, we introduce a complete set of projectors, i.e.,

$$\sum_i \pi_i \;=\; \mathbb{1} \quad , \tag{1}$$

where $\mathbb{1}$ denotes the unity operator and each projector corresponds to a possible event or measurement result. The set of projectors corresponds to some property.

We denote by $\rho(t)$ the density operator describing the system at time t and obtain the occurrence probability of event i at time point t as

$$P(x_i(t)) = \mathrm{tr}\{\pi_i \rho(t)\} \quad . \tag{2}$$

To shorten the following expressions, we define two abbreviations, i.e., (i) $\Pi_i\,\rho \;=\; \pi_i\,\rho\,\pi_i$ and (ii) $\mathcal{U}(\tau)\,\rho \;=\; U(\tau)\,\rho\,U(\tau)^\dagger$, where U denotes the time-translation operator which propagates the system states in amounts of τ.
A history is now created by performing a time translation after each measurement. To each of these histories one now assigns an occurrence probability, e.g. the event sequence $x_1(0) \to x_2(\tau_1) \to x_3(\tau_1+\tau_2)$ occurs with the probability

$$\begin{aligned} P(x_1(0), x_2(\tau_1), x_3(\tau_1+\tau_2); \rho) = \\ \mathrm{tr}\{\Pi_3\,\mathcal{U}(\tau_2)\,\Pi_1\,\mathcal{U}(\tau_1)\,\Pi_1\,\rho\} \; . \end{aligned} \tag{3}$$

(This assignment was formally suggested in Ref. [54], i.e., before the consistent history concept was introduced.)

For simplicity, we will consider hereafter only equal time steps, i.e., $\tau = \tau_1 = \tau_2 = \cdots$, and therefore omit the time parameter.

A special situation in the context of consistent histories arises if the observation is not continuous, e.g., if one actually measures only in the beginning and the end and leaves the property at an intermediate time unmeasured. In this case (3) becomes

$$P(x_1, --, x_3; \rho) = \mathrm{tr}\{\Pi_k\,\mathcal{U}^2\,\Pi_i\,\rho\} \tag{4}$$

$$= \sum_{x_2} P(x_1, x_2, x_3; \rho) \tag{5}$$

$$+ \sum_{i \neq j} \mathrm{tr}\{\Pi_3\,\mathcal{U}(\,\pi_i(\,\mathcal{U}\,\Pi_1\,\rho)\,\pi_j)\} \tag{6}$$

where $--$ indicates that at this intermediate time-point no measurement is performed.

The crucial expression here is Eq. (6), since this is the above mentioned decoherence functional. Only if the latter vanishes (which is called the consistency condition) does perfect accordance with the third Kolmogorov axiom (KA 3) result. Put another way: If some main event may be obtained as the result of many different, independent "subevents," then the probability for the main event to occur is given by the sum of the probabilities of

the "subevents."
Since we will specifically calculate the value of decoherence functional numerically for some concrete examples, we rewrite the consistency condition here in an more explicit style,

$$\sum_{i\neq j} \mathrm{tr}\{\pi_3\, U\, \pi_i\, U\, \pi_1\, \rho\, \pi_1\, U^\dagger\, \pi_j\, U^\dagger\} \approx 0 \quad . \tag{7}$$

It is not to be expected that this expression ever vanishes precisely in a generic situation based on a finite quantum system, but it may possibly approach zero in the limit of infinitely large systems. It is this latter statement which is one of the main targets of this paper. At this point we would like to emphasize some consequence of (7) for later reference: If (7) applies, then, by virtue of (1), summing the probability of some quantum history over all possible events at specific times produces the probability of a quantum history in which there are no measurements at the corresponding times, e.g.:

$$\sum_{x_1,x_2} P(x_1, x_2, x_3; \rho) = P(x_3; \rho) \tag{8}$$

Here we close our outline of basic concepts in consistent histories and refer the interested reader to the pertinent literature, e.g., Refs. [58, 62], and turn towards Markovianity.

In the context of (open) quantum dynamics the term "Markovian" has been used for a variety of features [53]. However, for the remainder of this work, "Markovianity" will be used to describe a property of quantum histories. The rationale behind this concept is that histories will be called Markovian, if a few past measurement outcomes suffice to fix the probabilities for the next future measurement outcomes. Our definition employs the notion of conditional probabilities as inferred from quantum histories. The construction of such conditional probabilities is straightforward, and we simply define them as the ratio of the occurrence probability of the event sequence $x_k \to \cdots \to x_{n+1}$ to that of $x_k \to \cdots \to x_n$, i.e.,

$$\omega(x_{n+1}|x_k, x_{k+1}, \cdots, x_n; \rho) = \frac{P(x_k, \cdots, x_n, x_{n+1}; \rho)}{P(x_k, \cdots, x_n; \rho)} \quad . \tag{9}$$

We call such a conditional probability one-step Markovian if

$$\omega(x_{n+1}|x_n; \rho) = \omega(x_{n+1}|x_k, \cdots, x_n; \rho) \tag{10}$$

holds true, two-step Markovian if only

$$\omega(x_{n+1}|x_{n-1}, x_n; \rho) = \omega(x_{n+1}|x_k, \cdots, x_n; \rho) \tag{11}$$

holds, and so on. Obviously, conditional probabilities ω themselves as well as the validity of the above equations (10 and 11) depend on the initial state ρ. Below, in (21) we will focus on a specific class of initial states in order to get rid of this dependence.

III. QUALITATIVE CONSIDERATION ON THE TYPICALITY OF CONSISTENCY AND MARKOVIANITY

In the previous section consistency and Markovianity have been defined as properties of dynamics depending on both the Hamiltonian $\hat{H}$ of the system and the observable that is actually being watched, the latter being formalized by the set of projectors $\{\hat{\pi}_i\}$. Having a feasible scheme which allows us to decide whether, for given $\hat{H}, \{\hat{\pi}_i\}$, consistency and Markovianity are present would be very instructive and generally most desirable. Unfortunately, such a scheme is yet unknown (however, we consider its development as an ambitious and promising line of future research). Thus we primarily resort to numerics and give in Sec. V a concrete example for a system and an observable which is consistent and Markovian.

Numerics, however, cannot answer the principal and important question if consistency and Markovianity may, in some sense, be generally expected. While we are far from being able to answer the question conclusively, we outline in the following a qualitative argument pointing in the direction of consistency and Markovianity being indeed natural for systems and observables featuring large Hilbert spaces and few symmetries. The argument is along the lines of the more general concept of "typicality" [43, 63, 64].

Consider an addend of the sum which serves to specify consistency (7). Denote the eigenstates of the projectors by π_i, π_j by $\{|n_i\rangle\}, \{|n_j\rangle\}$, respectively. Then a single addend for specific i, j reads

$$\sum_{n_i,n_j} \langle n_j|U^\dagger \pi_3\, U\, |n_i\rangle\langle n_i|\, U\, \pi_1\, \rho\, \pi_1\, U^\dagger\, |n_j\rangle \tag{12}$$

For $i \neq j$ the above sum (12) comprises products of two factors, both of which are complex numbers. The phases of those numbers are neither related to each other by any general principle nor restricted to a certain interval within the full range of $]0, 2\pi]$. Thus the terms in the sum may " average out" to zero. Indeed, if U's are drawn at random, (such that the mapping of any pure state onto any other pure state is equally probable, cf. e.g., Ref. [64]), then the averages over the individual factors vanish, as long as $\langle n_j|n_i\rangle = 0$ [65]. Furthermore, fluctuations around this average vanish as $\propto 1/d$, where d is the dimension of the respective Hilbert space [65]. Thus for the (overwhelming) majority of U's (12) is expected to result into a very small number, which then implies consistency. This is to be contrasted with the situation $i = j$. In this case both factors of the addends of (12) are real, positive numbers. Hence summing many of them will typically yield a considerably larger positive number.

A similar argument can be formulated which indicates that Markovianity is typical in the same sense. Consider the probability to get measurement outcome x_3 after x_1 and x_2 have occurred. According to (9) the correspond-

ing conditional probability reads

$$\omega(x_3|x_1,x_2;\rho) = \frac{\sum_{n_2,m_2}\langle n_2|U^\dagger\pi_3\,U\,|m_2\rangle\langle m_2|\,U\,\pi_1\,\rho\,\pi_1\,U^\dagger\,|n_2\rangle}{\sum_{n_2}\langle n_2|\,U\,\pi_1\,\rho\,\pi_1\,U^\dagger\,|n_2\rangle} \tag{13}$$

where $|n_2\rangle, |m_2\rangle$ are eigenstates of π_2. If one, based on the same argument as given below (12), drops all terms that are not necessarily real and positive, this reduces to:

$$\omega(x_3|x_1,x_2;\rho) \approx \frac{\sum_{n_2}\langle n_2|U^\dagger\pi_3\,U\,|n_2\rangle\langle n_2|\,U\,\pi_1\,\rho\,\pi_1\,U^\dagger\,|n_2\rangle}{\sum_{n_2}\langle n_2|\,U\,\pi_1\,\rho\,\pi_1\,U^\dagger\,|n_2\rangle} \tag{14}$$

Again following the concepts of typicality one finds $\langle n_2|\,U\,\pi_1\,\rho\,\pi_1\,U^\dagger\,|n_2\rangle \approx 1/(\mathrm{tr}\{\pi_2\}\mathrm{tr}\{\pi_1\,\rho\,\pi_1\})$ for the overwhelming majority of all randomly distributed) U. Inserting this into (14) yields:

$$\omega(x_3|x_1,x_2;\rho) \approx \frac{\sum_{n_2}\langle n_2|U^\dagger\pi_3\,U\,|n_2\rangle}{\mathrm{tr}\{\pi_2\}} \tag{15}$$

$$= \omega(x_3|x_2;\pi_2) \tag{16}$$

Thus, for the majority of all U, neither the concrete initial state ρ nor the next-to-last observed value x_1 are relevant for the occurrence probability of x_3; it is only the very last observed value x_2 that matters. This is what has been defined as one-step Markovianity in (10). Hence, in this sense one-step Markovianity is typical.

It should be emphasized here, that all the above reasoning is based on "typical unitaries" U. While such a consideration is mathematically legitimate (and can be made rigorous [43, 45]), it does not imply that counterexamples do not exist. It does not even necessarily imply that counterexamples are rare in nature. Random U's are generated by Hamiltonians H that are essentially random, Hermitian matrices. However, most quantum many-particle models are characterized by Hamiltonians that differ significantly from random matrices: They are often sparse with respect to the site-occupation-number basis, they usually have only real entries, etc. Hence the considerations presented in the current section by no means replace the concrete numerical computations in Sect. V.

IV. FROM UNITARY DYNAMICS TO ONE-STEP STOCHASTIC PROCESSES

In this section, we establish that the dynamics of the above event probabilities, as following from the Schrödinger equation for non measured closed systems, may be rewritten as Markovian stochastic processes, provided that Eq. (7) and Eq. (10) hold. To this end we start by writing out the probability of some event x_{n+1} at the corresponding time in a seemingly complicated way, relying on (8):

$$P(x_{n+1}) = \sum_{x_1,\cdots,x_n} P(x_1,\cdots,x_n,x_{n+1};\rho) \tag{17}$$

This shall be rewritten in an even more complicated fashion as:

$$P(x_{n+1}) = \sum_{x_1,\cdots,x_n} \frac{P(x_1,\cdots,x_n,x_{n+1};\rho)}{P(x_1,\cdots,x_n;\rho)} P(x_1,\cdots,x_n;\rho). \tag{18}$$

However, if one-step Markovianity holds, i.e., if Eq. (10) applies, the above fraction may be replaced by the simpler one-step conditional probability,

$$P(x_{n+1}) = \sum_{x_n}\omega(x_{n+1}|x_n;\rho) \sum_{x_1,\cdots,x_{n-1}} P(x_1,\cdots,x_n;\rho). \tag{19}$$

Exploiting (8) again, this can be written as

$$P(x_{n+1}) = \sum_{x_n}\omega(x_{n+1}|x_n;\rho)P(x_n). \tag{20}$$

Except for the dependence of the transition probabilities ω on the very initial state, this equation is equivalent to a standard definition of a Markov chain on the sample space containing all x. For the remainder of this paper we specialize in certain initial states ρ of the form

$$\rho = \sum_i c_i\pi_i \quad c_i \geq 0 \quad . \tag{21}$$

The motivation for this choice is twofold. First, it may be viewed as a state in accord with Jayne's principle: If nothing is known about a quantum state except for the probabilities P_i of finding the outcome x_i, a state ρ of the form given in (21) with $c_i = P_i/\mathrm{tr}\{\pi_i\}$ maximizes the von Neumann entropy subject to the information given. Second, (16) suggests that a state ρ of the form of (21) produces transition probabilities in accord with the Markovian transition probabilities which are expected for typical unitaries U: It is simply a projector (in the specific example π_2) that takes the role of the initial state in (16).

From Eq. (9) it may also be inferred that for this class of initial states the transition probabilities ω are actually independent of the actual c_i, i.e., the transition probabilities ω are all the same for the entire class of initial states. Due to this, we omit, for brevity, ρ in the argument of ω, thus obtaining

$$P(x_{n+1}) = \sum_{x_n}\omega(x_{n+1}|x_n)P(x_n). \tag{22}$$

which defines a standard Markovian stochastic process.

To recapitulate the analysis so far, it can be stated that, if consistency and one-step Markovianity hold, it is straightforward to demonstrate that the unitary time propagation according to Schrödinger equation can also be expressed by a time-discrete stochastic process. Obviously the fact that we used one-step Markovianity is not necessary, i.e., also for more-step Markovianity stochastic processes may be formulated in an analogous way. However, since the models we investigate below

appear to exhibit one-step Markovianity to sufficient accuracy, we will restrict ourselves to this case in the present section.

For convenience, at this point we do not (re-)define the features consistency and Markovianity directly but rather quantify their complements "nonconsistency" $\bar{C}$ and "non-Markovianity" $\bar{M}$. Both are below defined to be real numbers with $0 \leq \bar{C}(\bar{M})$ in such a way that 0 indicates perfect consistency (Markovianity) and any larger value expresses a (gradual) violation of the respective feature. The definition of nonconsistency reads:

$$\bar{C}(x_k, \cdots, --, \cdots, x_n) = \left| 1 - \frac{P(x_k, \cdots, --, \cdots, x_n)}{\sum_\gamma P(x_k, \cdots, x_n)} \right| \quad , \tag{23}$$

where summation over all possible intermediate outcome sequences γ is denoted here as $\sum_\gamma$. In a similar fashion non-Markovianity is defined by:

$$\bar{M}(x_k, \cdots, x_n) = \left| 1 - \frac{\omega(x_{n+1}|x_{k-1}, \cdots, x_n)}{\omega(x_{n+1}|x_k, \cdots, x_n)} \right| \quad , \tag{24}$$

It may be worth noting here that this is not the only possible sensible definition of non-Markovianity even within this framework. It obviously refers only to some specific conditional probability and takes only one prior measurement into account. In the remainder of this paper we will mainly focus on the exemplary investigation of some specific measurement outcome sequences, and return to more general questions in Sec. VI.

V. NUMERICAL INVESTIGATIONS

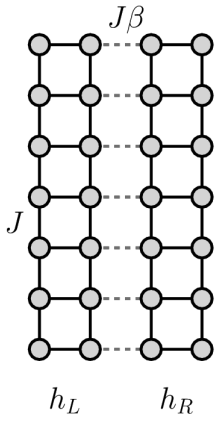

Figure 1. (Color online) Schematic visualization of a spin lattice consisting of two separable spin ladders. Each spin ladder has an assigned Hamiltonian h_L (h_R) where the spins are coupled by a strength J (solid lines). Both ladders are in turn coupled by a strength of order $J\,\beta$ (dashed lines).

The spin lattice that we are going to investigate basically consists of two spin ladders, with total number of spins $N = 4n$, which are brought into contact along opposing spines, cf. model in Fig. 1. Hence the Hamiltonian consists of three parts:

$$H = h_L \otimes h_R + V \quad , \tag{25}$$

where h_L (h_R) denotes the local Hamiltonian of the left (right) subsystem. V comprises the interaction between the subsystems. The left local Hamiltonian is defined by

$$\begin{aligned} h_L = & J \sum_{i=1}^{n} s_i^x s_{i+1}^x + s_i^y s_{i+1}^y + \Delta s_i^z s_{i+1}^z \\ & + J \sum_{i=1}^{n} s_i^x s_{i+n}^x + s_i^y s_{i+n}^y + \Delta s_i^z s_{i+n}^z \\ & + \text{ h.c.} \end{aligned} \tag{26}$$

where the $s_{\cdots}^{\cdots}$ denote the pertinent operators of components of $s = 1/2$ spins sitting at the respective positions. The Hamiltonian of the right subsystem, h_R, is obtained through shifting the indices in (26) by $2n$, i.e., $s_i \to s_{i+2n}$. The overall energy scale is set by J.
The interaction of the both subsystems takes place only between the two "central" chains of the lattice, namely in this model between the second and third chain. Thus the interaction term reads

$$V = J\beta \sum_{i=n+1}^{2n} s_i^x s_{i+n}^x + s_i^y s_{i+n}^y + \Delta s_i^z s_{i+n}^z + \text{ h.c.} \tag{27}$$

The observable (or property) we are going to analyze in detail is the magnetization difference between both subsystems, i.e.,

$$X = \sum s_{i,L}^z - \sum s_{i,R}^z \quad , \tag{28}$$

where each sum represents the present total magnetization in the z direction within the left (right) spin ladder. Furthermore we restrict our analysis to the subspace of vanishing total magnetization, i.e., $\sum s_{i,L}^z + \sum s_{i,R}^z = 0$. Note that the latter is a constant of motion in this model. This subspace was essentially chosen since it is the largest one with respect to the dimension of the corresponding Hilbert space. Furthermore, we choose our event-operators corresponding to the property x concretely as the following projectors:

$$\pi_{x,E} = \pi_E \, \pi_x \, \pi_E \quad , \tag{29}$$

where π_x is the projector spanned by all eigenstates of X featuring the same eigenvalue x, i.e., $X = \sum_x x\pi_x$. The projector π_E restricts the dynamics to a more or less narrow region in energy space: It is spanned by all energy eigenstates of the uncoupled system, (i.e., without taking V into account) that feature eigenvalues with $E_i \in [-1.2J\,, +0.6J]$. To put this another way: The full energetic width of the system is on the order of the number of of spins, i.e., NJ. Moreover the chosen interval contains the highest densities of states with respect to

energy.
Note that since $[\pi_E, \pi_x] = 0$ the $\pi_{x,E}$ are in fact orthogonal projectors. Obviously, the $\pi_{x,E}$ are not complete in the sense of (1). However, a formally complete set may always be introduced by adding the complement $\bar{\pi} = \mathbb{1} - \sum_x \pi_{x,E}$ to the $\pi_{x,E}$'s themselves. Practically, this hardly makes any difference since our numerics confirm that for our below choices of the model parameters almost no probability ever goes to $\bar{\pi}$, i.e., $P(\bar{\pi}, t) < 10^{-4}$.

Before we turn towards numerical results on consistency and Markovianity, we should point out that the whole setup, i.e., the Hamiltonian, the observable, the energy shell, etc., have been chosen in the specific way described above in order to find a nonrandom, finite system, in which consistency and Markovianity emerge already for rather small systems.
There are results in the literature that suggest to those ends a set-up like the one defined above: In Refs. [47–50] Fokker-Planck-type dynamics have been reported for more or less similar spin systems. Furthermore, results in Ref. [66] indicate that the so-called eigenstate thermalization hypotheses (ETH) may be best fulfilled for bipartite systems in which the local subsystems are not merely spin chains. (Since the ETH guarantees a single, attractive, long-time probability distribution of the events its applicability is necessary for the emergence of effective stationary stochastic process dynamics.) For a first rough and of course non-sufficient check of whether the dynamics of our model may be in accord with a stochastic description, we compute the dynamics of the $P[x(t)]$, starting from $P(x = 0) = 1$ at $t = 0$. The result is displayed in Fig. 2. The solid lines are obtained by solving simple transition-rate-based master equations. The agreement indicates that a fully stochastic description may be possible. Of course, since the model is finite, there will be (quasi-) recurrences. However, these are expected at times that are by magnitudes larger than any timescale considered here and thus excluded from our analysis. We fix the principal time scale of interest by means of Fig. 2. Although the true dynamics are strictly unitary, the $P[x(t)]$ appear to relax to towards constant values. Thus we call the the time scale at which this relaxation happens the "relaxation time" τ_R. Specifically, we infer $\tau_R = 20J$.

We now investigate nonconsistency and non-Markovianity as defined by (23) and (24), in more detail. As already pointed out before (29), nonconsistency and non-Markovianity here refer to sequences of transitions between certain magnetization differences. More precisely: the projectors which enter the definition of $\bar{C}, \bar{M}$ through (3) are the projectors $\pi_{x,E}$ as appearing in (29). Hence, below x continues to indicate the magnetization difference. To begin with we kept the number of spins fixed at $N = 12$ and calculated $\bar{C}, \bar{M}$ as functions of τ (the time elapsed between measurements) for various coupling strengths β. The paths chosen for this example are $x = 2 \to -- \to 0$ (nonconsistency) and $x = 2 \to 0 \to 0$ (non-Markovianity). The results are displayed in Fig. 3.

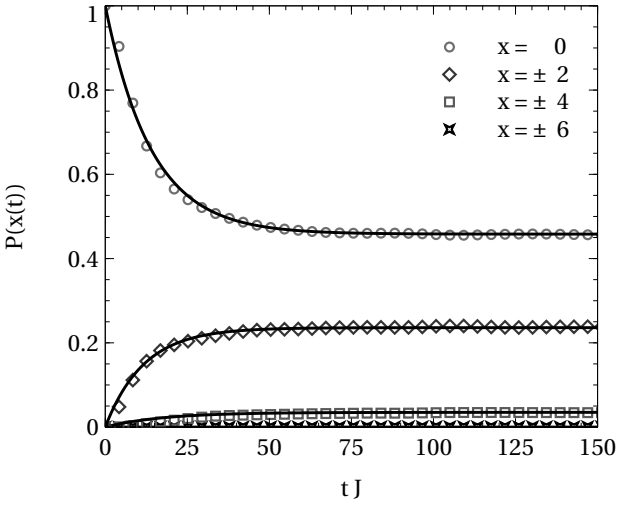

Figure 2. (Color online) Displayed are the dynamics of $P[x(t)]$ starting from $P(x = 0) = 1$ at $t = 0$ for all occurring values of x within a system of size $N = 12$, i.e., $x \in \{0, \pm 2, \pm 4, \pm 6\}$. These dynamics are compared to results from simple transition-rate-based master equations (solid lines). Agreement indicates that a fully stochastic description may be possible.

Though the graphs exhibit rather large values for small portions of relaxation time, they decrease significantly at times on the order of a tenth of the total relaxation time, i.e., $\tau \approx 0.1\,\tau_R$. Qualitatively, this behavior is the same for all investigated interaction strengths. This indicates that there is a lower limit on the time step τ, below which neither consistency nor Markovianity may be expected. This limit may, however, depending on the size and the structure of the system, only be a small fraction of the total relaxation time. Precisely finding the minimum time step which allows for consistency and Markovianity is left for further research. In the this paper we focus on a relatively large time step, i.e., $\tau = 0.5\tau_R$, and primarily investigate the effect of increasing system sizes. Furthermore, we restrict our further analysis to interaction strength $\beta = 0.5$. The result (which is our main numerical result) is displayed in Fig. 4. It shows nonconsistency and non-Markovianity for various system sizes N. Up to $N = 16$ the results have been computed by means of direct numerical diagonalization. Due to limitations in computing power, we computed the result for $N = 20$ using a numerical method based on dynamical typicality. This method has been used and described e.g., in Refs. [67–69]. Based on this method we are able to address $N = 20$ within reasonable computing time; however, the method involves random numbers and is thus subject to statistical errors. The magnitude of the latter is indicated by the corresponding error bars. Obviously nonconsistency and non-Markovianity are already small for moderate system sizes. Furthermore, both decrease monotonically with increasing system sizes. Figure 4 suggests that

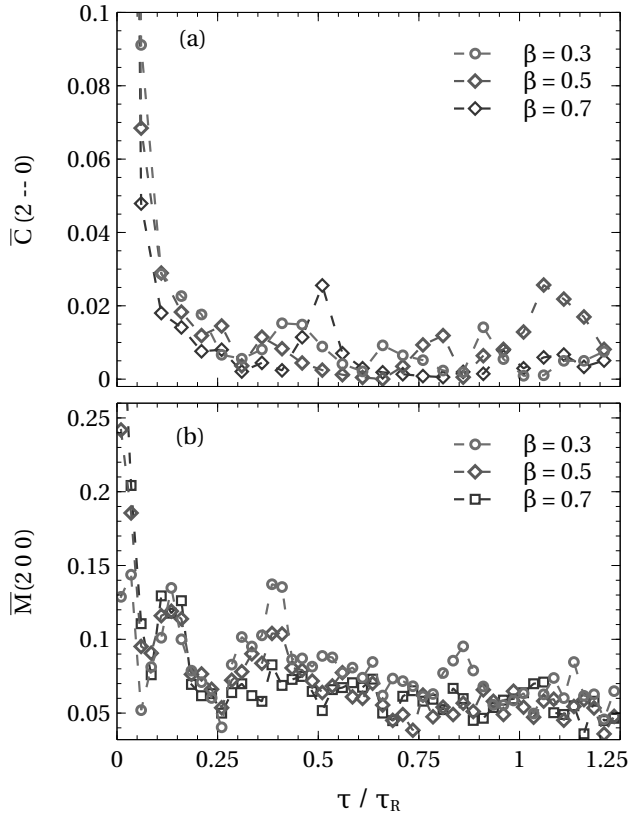

Figure 3. (Color online) Specific non-consistencies (a) and (one-step) non-Markovianities (b) are displayed for three different interaction strengths, depending on the "waiting time" τ between measurements. The latter are given in units of the respective relaxation time τ_R. The system size is fix at $N = 12$. For waiting times τ larger than, say, $\tau_R/10$ both nonconsistency and non-Markovianity, remain, while fluctuating, low compared to unity at all interaction strengths. For our further exemplary investigations we thus choose $\beta = 0.5$ and $\tau = 0.5\tau_R$.

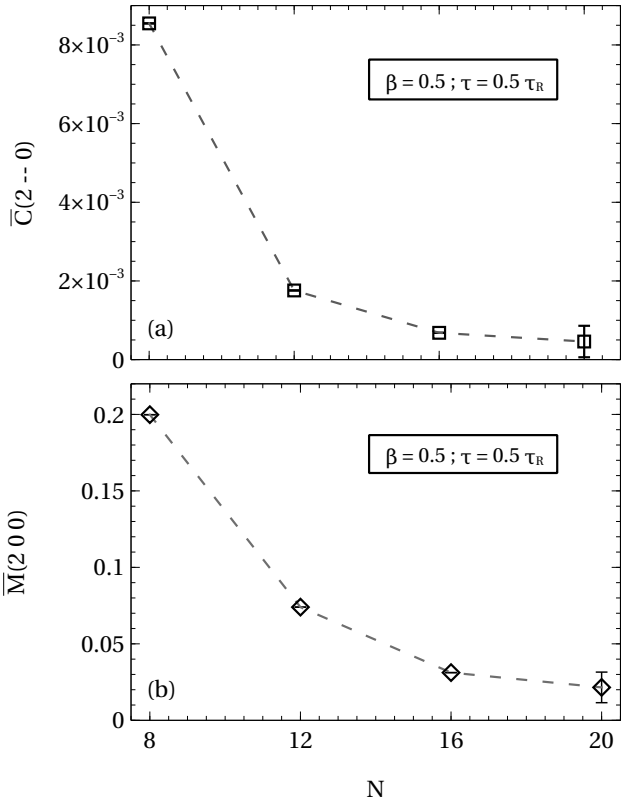

Figure 4. (Color online) Specific non-consistencies (a) and (one-step) non-Markovianities (b) are displayed for increasing system sizes N. Obviously both decrease with increasing system size. Although the data are not conclusive, it suggests that both may vanish in the limit of $N \to \infty$.

the dynamics become consistent and one-step Markovian in the limit of infinitely large systems. Whether this is indeed the case is not to be answered conclusively from our finite-size scaling. It is possible to perform the same numerical calculations for system sizes up to, say, $N = 36$ [69], but this requires high performance computing clusters. The present analysis, however, has been done using standard desktop computing equipment.

VI. "MORE-THAN-ONE"-STEP MARKOVIANITY

So far we primarily focused on one-step Markovianity throughout this paper. Furthermore, the numerical analysis in the previous section was based on a specific definition of one-step Markovianity (24) that takes only one prior outcome into account. Such an analysis is necessarily insufficient for the rigorous mapping of unitary dynamics onto a stochastic process. This may be seen most easily from considering two aspects: (i) If a stochastic process is not fully Markovian with respect to one-step Markovianity, it may nevertheless be possibly fully Markovian with respect to, e.g., two-step Markovianity. Thus some finite one-step non-Markovianity does not rule out a process from being Markovian altogether. (ii) Even if it is found that the conditional probability to get some event at time $(n+1)\tau$ does not change much if one takes the measurement outcome not only at time $n\tau$ but also at time $(n-1)\tau$ into account, this does not *a priori* mean that the conditional probability does not change much if, e.g., the outcome at time $(n-2)\tau$ is additionally taken into account. However, as explained below (24) only the former feature is captured by the definition of non-Markovianity and numerically analyzed in Sec. V. We emphasize again that the concept of "repeated measurements" employed here does not evolve any outside measurement apparatus or any external environment. It exclusively refers to histories as formulated in (3) and is thus well defined also for closed systems. Hence, the present consideration is not to be confounded with the Zeno effect where quickly

repeated external measurements "freeze" the dynamics [70]. While being always well defined our concept primarily addresses repeated measurements with time steps larger than the time at which consistency vanishes in the short time limit, cf. Fig. 3.

A full-fledged numerical analysis taking all possible histories and all above aspects of many-step-Markovianity exhaustively into account is beyond our possibilities, given the limit of reasonable computing time. However, in the following we focus on the many-step Markovianity of some special histories.

The first history we address is the one that is generated by getting, upon repeated measuring, always the same outcome. A history like this may be relevant in situations in which some measurement outcome corresponds to the equilibrium state of the system. As will be explained below, it turns out that such a history is necessarily λ-step Markovian, in the limit of large λ, irrespective of the concretely considered system.

Considering the occurrence probabilities for this type of history with initial states of the class introduced in (21) yields $P(x_i(0), x_i(\tau), \cdots, x_i(\lambda\tau)) := \mathrm{tr}\{\pi_i U \pi_i U \cdots U^\dagger \pi_i U^\dagger \pi_i\}$, where x_i characterizes the measured property and the second index λ labels the number of performed measurements. For brevity the index i will be omitted hereafter. Let us denote the eigensystem of the (non-Hermitian) matrix $U^\dagger\pi$ by $U^\dagger\pi|\varphi_n >= \phi_n|\varphi_n >$, and the occurrence probability of λ identical measurements by $P(\{x\}_\lambda)$. Then this occurrence-probability is given by

$$P(\{x\}_\lambda) = \sum_{ijk} c^*_{ik} c_{jk} \{\phi^*_i\}^\lambda \{\phi_j\}^\lambda \quad , \tag{30}$$

where the c_{ij} denote the complex matrix element of the transformation that maps the nonorthogonal eigenvectors $|\varphi_n >$ onto an orthonormal basis, i.e., $\sum_{ij} < \varphi_i|\varphi_j > c^*_{ik} c_{jl} = \delta_{kl}$.

All eigenvalues of $U^\dagger\pi$ are upper bounded by 1, hence $|\phi_i| \leq 1$ holds, and thus $\{\phi_i^\lambda\}$ describes a convex sequence with respect to λ. Consequently, $P(\{x\}_\lambda)$, consisting only of sums of convex functions, is also convex. Convexity implies

$$\frac{P(\{x\}_{\lambda+1})}{P(\{x\}_\lambda)} \leq \frac{P(\{x\}_{\lambda+2})}{P(\{x\}_{\lambda+1})} \;\forall\; \lambda \tag{31}$$

hence ω_λ, defined as

$$\omega_\lambda = \frac{P(\{x\}_{\lambda+1})}{P(\{x\}_\lambda)} \tag{32}$$

is a monotonously increasing sequence. From the definition of the history probability we immediately find $P(\{x\}_{\lambda+1}) \leq P(\{x\}_\lambda) \;\; \forall\lambda$. Thus ω_λ is upper bounded by one. Since ω_λ is monotonously increasing but upper bounded it must converge against some finite value $d \leq 1$:

$$\lim_{\lambda\to\infty} \omega_\lambda = d \;\in\; \mathbb{R}^+. \tag{33}$$

Plugging this result into the definition of non-Markovianity (24) yields

$$\lim_{\lambda\to\infty} \bar{M}_\lambda = \left|1 - \lim_{\lambda\to\infty} \frac{\omega_{\lambda+1}}{\omega_\lambda}\right| = \left|1 - \frac{d}{d}\right| \equiv 0 \quad . \tag{34}$$

Hence, in case of repeatedly measuring some property and consequently obtaining identical events as measurement outcomes, perfect Markovianity always results for sufficiently many steps. Although the implications of this result are limited (it only applies to a single type of history and takes consistency for granted) we consider it a valuable point of reference.

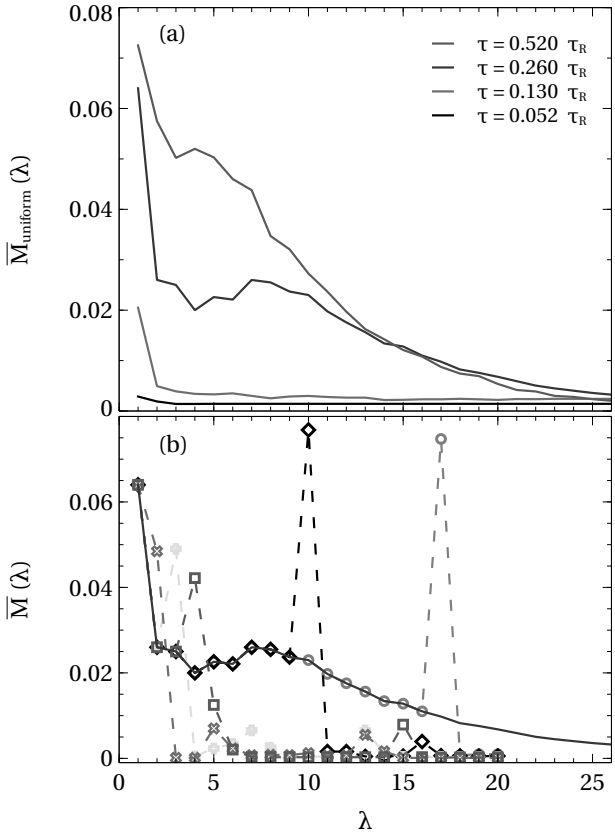

Figure 5. (Color online) Non-Markovianity for sequences comprising λ measurements which yield all $x = 0$ (a) or generated from drawing random numbers according to the one-step transition probabilities ω (b). Data in (a) confirm that λ-step transition probabilities always become perfectly Markovian in the limit of $\lambda \to \infty$ as claimed in the text. This result is independent of the waiting time τ. Data in (b) suggest that λ-step transition probabilities may become perfectly Markovian in the limit of $\lambda \to \infty$ also in the case of "generic stochastic trajectories." However, at the first deviation of the measurement sequence from a uniform sequence, somewhat larger non-Markovianities occur; for more comments see text.

The data displayed in Fig. 5 address λ-step non-Markovianity for both histories of the previously discussed type featuring identical outcomes, $x = 0$, in Fig. 5(a) and for some random event sequences of the typical

type which would occur if one simply took $\omega(x_{n+1}|x_n)$ as a fully one-step Markovian transition probability in Fig. 5(b). Since jump probabilities away from $x = 0$ are low but towards $x = 0$ are high, the latter typical random sequences are, similarly to the former, characterized by measuring $x = 0$ most of the times, but exhibit occasional "excursions" towards $x \neq 0$. We display data for $N = 12$ and various τ in Fig. 5(a) and $\tau = 0.26\tau_R$ in (b).

The graphs in (a) are obviously in accord with (34): Regardless of the "waiting-time" τ, histories become Markovian in the limit of large λ. Furthermore, non-Markovianity is not strictly monotonously decreasing with λ, but in the addressed data sample $\bar{M}_{\lambda>1} < \bar{M}_{\lambda=1}$ appears to be strictly obeyed. Furthermore sequences appear to be more Markovian for shorter waiting times. Altogether one may conclude that for the uniform histories Markovianity appears to improve if more steps are taken into account but a restriction to the "one-step-level" may nevertheless be a very reasonable approximation.

Considering the random histories in (b) it should first be noted that, while $\bar{M}_{\lambda>1} < \bar{M}_{\lambda=1}$ no longer strictly holds, non-Markovianities nevertheless remain very moderate also on the many-step level. Thus, also in these cases a restriction to the one-step level appears to be a very reasonable approximation. However, the peaks towards relatively higher non-Markovianities always occur at the most recent deviation from measuring identical outcomes. For example, in the history represented by the magenta circles, the first (past) 16 outcomes are $x = 0$, but the 17'th outcome is $x = 2$. Nevertheless, in all our examples, while Markovianity becomes worse for this most recent deviation, it becomes better again with taking even longer histories into account. Thus, considering Fig. 5(b) one may guess that a statement like (34) also holds for arbitrary histories, and whether or not this holds true remains a subject of future research.

VII. SUMMARY AND CONCLUSION

The possibility of describing the unitary dynamics as generated by the Schrödinger equation quantitatively in terms of pertinent stochastic processes is addressed. We discuss this possibility based on the notions of "consistency" and "Markovianity." While the former refers to the concept of consistent histories, the latter denotes the independence of probabilities for future measurement outcomes from measurement outcomes in the distant past. We outline how a mapping mapping of quantum onto stochastic dynamics can be performed if, indeed, the quantum dynamics is both consistent and Markovian. This obviously leads directly to the question whether closed system dynamics are approximately Markovian and consistent for specific, finite closed systems. This question is exemplarily discussed in the remainder of the paper. The degree to which the quantum dynamics are indeed consistent and Markovian is specified by introducing corresponding quantifiers. These quantifiers are numerically evaluated for a specific type of spin system. By means of finite-size scaling we give (strong) evidence that the dynamics of this closed spin system can indeed be considered consistent and Markovian. A somewhat more detailed analysis shows that one may rely on a description based on stochastic processes that take only the most recent past event into account. While an exhaustive numerical check of "consistency" and "Markovianity," covering all aspects of "stochasticity," is far beyond of what can be done in finite computing time, our results indicate that a dynamical stochastic description of closed quantum systems may be justified, even for rather small systems.

VIII. ACKNOWLEDGEMENTS

J. Gemmer acknowledges valuable input received at meetings of the European network COST Action MP1209 "Thermodynamics in the Quantum Regime".

[36] E. Nelson, Phys. Rev. **150**, 1079 (1966).
[37] W. J. Lehr and J. L. Park, J. Math. Phys. **18**, 1235 (1977).
[38] A. S. L. Malabarba, L. P. Garcia-Pintos, N. Linden, T. C. Farrelly, and A. J. Short, Phys. Rev. E **90**, 012121 (2014).
[39] F. G. S. L. Brandao, P. Cwiklinski, M. Horodecki, P.Horodecki, J. K. Korbicz, and M. Mozrzymas, Phys. Rev. E **86**, 031101 (2012).
[40] S. Goldstein, T. Hara, and H. Tasaki, Phys. Rev. Lett. **111**, 140401 (2013).
[41] A. Bendersky, F. Pastawski, and J. P. Paz, Phys. Rev. Lett. **100**, 190403 (2008).
[42] N. Linden, S. Popescu, A. J. Short, and A. Winter, Phys. Rev. E **79**, 061103 (2009).
[43] S. Goldstein, J. L. Lebowitz, R. Tumulka, and N. Zanghi, Phys. Rev. Lett. **96**, 050403 (2006).
[44] S. Goldstein, J. L. Lebowitz, R. Tumulka, and N. Zanghi, Eur. Phys. Jour. H **35**, 173 (2010).
[45] P. Reimann, Phys. Rev. Lett. **99**, 160404 (2007).
[46] M. Rigol, V. Dunjko, and M. Olshanii, Nature **452**, 854 (2008).
[47] H. Niemeyer, D. Schmidtke, and J. Gemmer, Europhysics Letters **101**, 1 (2013).
[48] C. Ates, J. P. Garrahan, and I. Lesanovsky, Phys. Rev. Lett. **108**, 110603 (2012).
[49] S. Ji, C. Ates, J. P. Garrahan, and I. Lesanovsky, J. Stat. Mech. p. P02005 (2013).

[50] I. Tikhonenkov, A. Vardi, J. R. Anglin, and D. Cohen, Phys. Rev. Lett. **110**, 050401 (2013).
[51] Ángel Rivas, S. F. Huelga, and M. B. Plenio, Reports on Progress in Physics **77**, 094001 (2014).
[52] B. Vacchini, A. Smirne, E.-M. Laine, J. Piilo, and H.-P. Breuer, New Journal of Physics **13**, 093004 (2011).
[53] H. P. Breuer and F. Petruccione, *The Theory of Open Quantum Systems* (Oxford University Press, 2010).
[54] E. P. Wigner, Am. J. Phys. **31**, 6 (1963).
[55] M. Gell-Mann and J. J. B. Hartle, *Complexity, Entropy and the Physics of Information* (Addison-Wesley, 1990).
[56] J. P. Paz and W. H. Zurek, Phys. Rev. D **48**, 2728 (1993).
[57] H. F. Dowker and J. J. Halliwell, Phys. Rev. D **46**, 1580 (1992).
[58] R. B. Grifiths, J. Stat. Phys. **36**, 219 (1984).
[59] J. J. Halliwell, Phys. Rev. D **80**, 124032 (2009).
[60] A. E. Allahverdyan, R. Balian, and T. M. Nieuwenhuizen, Phys. Rep. (2013).
[61] E. Okon and D. Sudarsky, Found. Phys. **44**, 19 (2014).
[62] R. Omnès, Phys. Lett. A **125**, 169 (1987).
[63] J. Cho and M. S. Kim, Phys. Rev. Lett. **104**, 170402 (2010).
[64] S. Goldstein, J. L. Lebowitz, C. Mastrodonato, R. Tumulka, and N. Zanghi, Phys. Rev. E **81**, 011109 (2010).
[65] J. Gemmer, M. Michel, and G. Mahler, *Quantum Thermodynamics: Emergence of Thermodynamic Behavior Within Composite Quantum Systems* (Springer, 2009), 2nd ed.
[66] R. Steinigeweg, A. Khodja, H. Niemeyer, C. Gogolin, and J. Gemmer, Phys. Rev. Lett. **112**, 130403 (2014).
[67] R. Steinigeweg, F. Heidrich-Meisner, J. Gemmer, K. Michielsen, and H. DeRaedt, Phys. Rev. B **90**, 094417 (2014).
[68] C. Bartsch and J. Gemmer, Phys. Rev. Lett. **102**, 110403 (2009).
[69] H. Niemeyer, K. Michielsen, H. DeRaedt, and J. Gemmer, Phys.Rev. E **89**, 012131 (2014).
[70] E. Joos, H. D. Zeh, C. Kiefer, D. Giulini, J. Kupsch, and I.-O. Stamatescu, *Decoherence and the Appearance of a Classical World in Quantum Theory* (Springer, 2002), 2nd ed.
[36] E. Nelson, Phys. Rev. **150**, 1079 (1966).
[37] W. J. Lehr and J. L. Park, J. Math. Phys. **18**, 1235 (1977).
[38] A. S. L. Malabarba, L. P. Garcia-Pintos, N. Linden, T. C. Farrelly, and A. J. Short, Phys. Rev. E **90**, 012121 (2014).
[39] F. G. S. L. Brandao, P. Cwiklinski, M. Horodecki, P.Horodecki, J. K. Korbicz, and M. Mozrzymas, Phys. Rev. E **86**, 031101 (2012).
[40] S. Goldstein, T. Hara, and H. Tasaki, Phys. Rev. Lett. **111**, 140401 (2013).
[41] A. Bendersky, F. Pastawski, and J. P. Paz, Phys. Rev. Lett. **100**, 190403 (2008).
[42] N. Linden, S. Popescu, A. J. Short, and A. Winter, Phys. Rev. E **79**, 061103 (2009).
[43] S. Goldstein, J. L. Lebowitz, R. Tumulka, and N. Zanghi, Phys. Rev. Lett. **96**, 050403 (2006).
[44] S. Goldstein, J. L. Lebowitz, R. Tumulka, and N. Zanghi, Eur. Phys. Jour. H **35**, 173 (2010).
[45] P. Reimann, Phys. Rev. Lett. **99**, 160404 (2007).
[46] M. Rigol, V. Dunjko, and M. Olshanii, Nature **452**, 854 (2008).
[47] H. Niemeyer, D. Schmidtke, and J. Gemmer, Europhysics Letters **101**, 1 (2013).
[48] C. Ates, J. P. Garrahan, and I. Lesanovsky, Phys. Rev. Lett. **108**, 110603 (2012).
[49] S. Ji, C. Ates, J. P. Garrahan, and I. Lesanovsky, J. Stat. Mech. p. P02005 (2013).
[50] I. Tikhonenkov, A. Vardi, J. R. Anglin, and D. Cohen, Phys. Rev. Lett. **110**, 050401 (2013).
[51] Ángel Rivas, S. F. Huelga, and M. B. Plenio, Reports on Progress in Physics **77**, 094001 (2014).
[52] B. Vacchini, A. Smirne, E.-M. Laine, J. Piilo, and H.-P. Breuer, New Journal of Physics **13**, 093004 (2011).
[53] H. P. Breuer and F. Petruccione, *The Theory of Open Quantum Systems* (Oxford University Press, 2010).
[54] E. P. Wigner, Am. J. Phys. **31**, 6 (1963).
[55] M. Gell-Mann and J. J. B. Hartle, *Complexity, Entropy and the Physics of Information* (Addison-Wesley, 1990).
[56] J. P. Paz and W. H. Zurek, Phys. Rev. D **48**, 2728 (1993).
[57] H. F. Dowker and J. J. Halliwell, Phys. Rev. D **46**, 1580 (1992).
[58] R. B. Grifiths, J. Stat. Phys. **36**, 219 (1984).
[59] J. J. Halliwell, Phys. Rev. D **80**, 124032 (2009).
[60] A. E. Allahverdyan, R. Balian, and T. M. Nieuwenhuizen, Phys. Rep. (2013).
[61] E. Okon and D. Sudarsky, Found. Phys. **44**, 19 (2014).
[62] R. Omnès, Phys. Lett. A **125**, 169 (1987).
[63] J. Cho and M. S. Kim, Phys. Rev. Lett. **104**, 170402 (2010).
[64] S. Goldstein, J. L. Lebowitz, C. Mastrodonato, R. Tumulka, and N. Zanghi, Phys. Rev. E **81**, 011109 (2010).
[65] J. Gemmer, M. Michel, and G. Mahler, *Quantum Thermodynamics: Emergence of Thermodynamic Behavior Within Composite Quantum Systems* (Springer, 2009), 2nd ed.
[66] R. Steinigeweg, A. Khodja, H. Niemeyer, C. Gogolin, and J. Gemmer, Phys. Rev. Lett. **112**, 130403 (2014).
[67] R. Steinigeweg, F. Heidrich-Meisner, J. Gemmer, K. Michielsen, and H. DeRaedt, Phys. Rev. B **90**, 094417 (2014).
[68] C. Bartsch and J. Gemmer, Phys. Rev. Lett. **102**, 110403 (2009).
[69] H. Niemeyer, K. Michielsen, H. DeRaedt, and J. Gemmer, Phys.Rev. E **89**, 012131 (2014).
[70] E. Joos, H. D. Zeh, C. Kiefer, D. Giulini, J. Kupsch, and I.-O. Stamatescu, *Decoherence and the Appearance of a Classical World in Quantum Theory* (Springer, 2002), 2nd ed.

Preprint version

Original publication: PRE, 93, 042101 (2016)
doi: 10.1103/PhysRevE.93.042101

Initial State Independent Equilibration at the Breakdown of the Eigenstate Thermalization Hypothesis

Abdellah Khodja,[1,*] Daniel Schmidtke,[1,1,†] and Jochen Gemmer[1,‡]

[1] *Fachbereich Physik, Universität Osnabrück, Barbarastrasse 7, D-49069 Osnabrück, Germany*

This work aims at understanding the interplay between the Eigenstate Thermalization Hypothesis (ETH), initial state independent equilibration and quantum chaos in systems that do not have a direct classical counterpart. It is based on numerical investigations of asymmetric Heisenberg spin ladders with varied interaction strengths between the legs, i.e., along the rungs. The relaxation of the energy difference between the legs is investigated. Two different parameters, both intended to quantify the degree of accordance with the ETH, are computed. Both indicate violation of the ETH at large interaction strengths but at different thresholds. Indeed the energy difference is found not to relax independently of its initial value above some critical interaction strength which coincides with one of the thresholds. At the same point the level statistics shift from Poisson-type to Wigner-type. Hence the system may be considered to become integrable again in the strong interaction limit.

PACS numbers: 03.65.Yz, 75.10.Jm,

I. INTRODUCTION

Even in closed quantum systems one may observe relaxation, in spite of time evolution being generated by unitary operations. This statement has many aspects, it may imply that a reduced density matrix of a part of some system approaches a thermal state [1–4], it may imply that expectation values of specific observables evolve more or less against constant values [5, 6], or it may additionally even imply that these constant values do not depend on the initial state [6–8]. It is this latter initial state independence (ISI) which is in the focus of the paper at hand. Among the concepts addressing this issue is the so called eigenstate thermalization hypothesis (ETH) [9, 10]. According to the ETH, the expectation values of a typical observable $\hat{D}$ as computed from energy eigenstates $|n\rangle$ should be a smooth function of energy E_n, i.e., $\langle n|\hat{D}|n\rangle \approx \langle n'|\hat{D}|n'\rangle = \bar{D}_{eq}(E)$ if $E_n \approx E_{n'} \approx E$. As is well known, if the ETH applies, the long time averages of all expectation value $\mathrm{Tr}\{\hat{\rho}\,\hat{D}(t)\}$ corresponding to any initial state $\hat{\rho}$ that lives inside some energy shell, are equal [11]. Furthermore, if the spectrum of the Hamiltonian $\hat{H}$ is "non-resonant" (roughly speaking: any energy difference occurs only once) and the ρ_{nn} are fairly spread over the energy shell, then the actual $\mathrm{Tr}\{\hat{\rho}\,\hat{D}(t)\}$ deviates from its long time average very rarely [12]. Hence, the three features, i. ETH agreement, ii. non-resonant spectrum and iii. dilute eigenstate occupation, guarantee the initial state independent (ISI) relaxation of the expectation value towards a specific "equilibrium" value. Since this behavior is observed and expected for practically all physical relaxation phenomena, the question arises whether the above three features apply to all those situations. This question has been approached from the perspective of quantum chaos, and various rigorous results exist that suggest i. and ii. apply to systems which have a direct classical counterpart which is chaotic [7]. Much less is known for systems that do not have a direct classical counterpart [10]. However, while the three features are sufficient for ISI, they are not necessary in a mathematical sense: classes of initial states exist that exhibit ISI even though the ETH may not apply. Some papers put much more emphasis on the extremely high relative frequency with which ISI may be expected if initial state are drawn essentially at random from some prescribed sets, rather than on the ETH [3, 5, 13, 46]. However, it may be the case that the relative frequency of initial states from the above sets, that exhibit a significant deviation of the respective expectation value from its equilibrium value at all, even at $t = 0$, is very low. In this case results of relative-frequency-type would imply the existence of a majority of states the expectation values of which start and remain in equilibrium. However, no conclusions on state, that actually do exhibit non-equilibrium expectation values in the beginning, could be drawn.

In view of this, a class of initial states that are specifically tailored to exhibit largely deviating expectation values, but live in narrow energy shells at the same time has

* akhodja@uos.de
† danischm@uos.de
‡ jgemmer@uos.de

recently been suggested [18]. These states (which will be explained in detail below) have been termed microcanonical observable displaced (MOD) states. MOD states are "natural" in the sense that they may be viewed as results of state determination according to Jayne's principle under the conditions of a given expectation value and the state living in an certain energy shell. For the remainder of this paper we focus on dynamics as resulting from such initial MOD states.

In order to set the content of the paper at hand in context to the state of research, we need to specify our notion of ETH in somewhat more detail. Consider

$$\bar{D} = \sum_{n=1}^{d} p_n D_{nn} , \quad \Sigma^2 = \sum_{n=1}^{d} p_n D_{nn}^2 - \bar{D}^2 , \qquad (1)$$

where D_{nn} are diagonal matrix elements with respect to the Hamiltonian eigenstates $|n\rangle$ with eigenvalues E_n, $p_n \propto e^{-(E_n-\bar{E})^2/2\sigma_E^2}$ is a probability distribution centered at $\bar{E}$, and d is the Hilbert-space dimension. The quantities $\bar{D}(\bar{E},\sigma_E)$ and $\Sigma(\bar{E},\sigma_E)$ are obviously functions of $\bar{E}$ and an energy width σ_E. Routinely, the ETH is said to be fulfilled if Σ is small for small σ_E. Technically, ISI equilibration is only guaranteed for all initial states from a given energy window σ_E at $\bar{E}$ iff $\Sigma = 0$, [14]. If instead a finte-size scaling scheme is employed, i.e., $\Sigma \to 0$ for $N \to \infty$ (N being the "system-size", e.g., the number of spins, etc.) not only the Hamiltonian, but also the observable $\hat{D}$ often scales with N in some fashion as well (cf. below). In this context it is relevant to note that ISI equilibration is only ensured if Σ itself approaches zero in the limit of large system sizes, the vanishing of, e.g., Σ^2/N, is not sufficient. However, in our analysis we do not intend to demonstrate ISI equilibration for all initial states of a given energy window but rather focus on the afore mentioned special class of states, i.e., MOD states. Below we will employ a quantifier which is closely related to Σ but independent of the scaling of the observable itself.

In order to put our work into perspective, we list some exemplary results from the literature on the generic scaling properties of Σ, and classify our results in relation to these. In the context of translational invariant, solid-state type observables and models, the observable is frequently defined to scale "extensively", like, e.g., a current, a total kinetic energy, etc. In this case, there is substantial numerical evidence that Σ scales more or less as $\Sigma \propto d_{eff}^{-\gamma}$, where d_{eff} is the effective dimension, i.e., the number of states within the respective energy shell and γ is some constant [27, 41, 45]. Note, however, that the scaling behavior of Σ generally depends strongly on whether the observable itself is defined to scale extensively, intensively or else. Since the effective dimension d_{eff} usually increases (exponentially) with system size, Σ tends to zero with increasing system size whenever $\gamma > 0$. The existing literature contains numerous examples exhibiting $0 \leq \gamma \leq 1/2$ for few body observables. $\gamma = 0$ appears to be related to integrable systems, $\gamma = 1/2$ for fully chaotic systems, where both definitions may vary depending on the respective authors [47].

In Ref. [41], however, also examples are discussed with $\gamma < 0$ for extensive observables, i.e., the unscaled Σ itself increases with system size. This occurs for spin and energy currents in the (integrable) Heisenberg chain at some parameter regime. In contrast to that, in Ref. [18] the same Heisenberg chain model is investigated while the considered observable is different, namely the energy difference between two parts of the chain. The latter observable is also extensive. Nonetheless, in this case $\Sigma = \text{const}$, i.e., $\gamma = 0$ is found. As already mentioned above, for $\gamma \leq 0$ ISI equilibration is not guaranteed, i.e., the construction of initial states for which the expectation value of $\hat{D}$ does not decay towards the corresponding equilibrium ensemble value is always possible. Thus we will primarily focus on the question whether such a "incomplete decaying" occurs for MOD states for models and observables exhibiting $\gamma \leq 0$.

For the remainder of this paper we follow [18] in investigating the (extensive) energy difference between certain system sections. We present a model that allows for a continuous tuning of the scaling parameter γ all the way from $\gamma > 0$ to $\gamma < 0$, i.e., depending on some system parameter, Σ either decreases, remains constant or increases under upscaling of the system-size. We also follow [18] in considering an alternative parameter v for the "prediction" of ISI for MOD states:

$$v = \left(\frac{\Sigma}{\delta_D}\right)^2 \qquad (2)$$

δ_D^2 denotes the spectral variance of the observable $\hat{D}$ in the respective energy shell, i.e., $\delta_D^2 = \Sigma_{n=1}^{d} p_n (\hat{D}^2)_{nn} - (\bar{D})^2$ (the bars over D symbolize the averaging as defined in Eq. (1)). Note that v is, other than Σ, dimensionless. Thus for the scaling behavior of v, the scaling behavior of the observable itself (extensive, intensive or else) is irrelevant. It has been proposed that ISI for MOD states occurs, if and only if $v \to 0$ in the limit of large systems. Although closely related to the ETH, the v criterion is not quite the same, for it may possibly approach zero even if Σ increases, if δ_D^2 increases more quickly.

The present paper is organized as follow: In section II, we shortly introduce the investigated models and the addressed observable, i.e., the energy difference. In section III, we present the results on Σ, v in dependence of the tuning parameter κ and show the existence of two different regimes based on the scaling behavior of the former. The computations in Sec. IV clarify whether MOD states give rise to ISI relaxation of the energy difference and how this relates to the results of Sec.III. We discuss the integrability of the model at hand in Sec. V using the generalized Brody parameter, whose behavior turns to be correlated to the ETH parameter v. Finally, we close with summary and conclusion.

II. MODELS AND OBSERVABLES

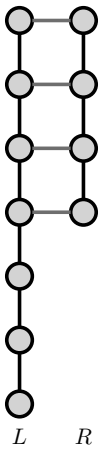

Figure 1. Schematic visualization of the investigated spin-ladder. To suppress symmetry, the number of spin in the right chain is taken to be different than the left chain in the following systematic fashion $N_L = 2N_R - 1$. Note that both chains only interact by vertically opposing sites (here indicated by red rungs).

The model we address in this work is an asymmetrical Heisenberg-ladder which consists of two XXZ spin-1/2 chains of different length, coupled along some "rungs" with interaction strength κ, cf. Fig. 1. The total Hamilton operator is given as follow

$$\hat{H} = \hat{H}_L + \hat{H}_R + \kappa \hat{H}_I \tag{3}$$

where

$$\hat{H}_{L,R} = \sum_{i=1}^{N_L,N_R} [(\hat{S}_i^x \hat{S}_{i+1}^x + \hat{S}_i^y \hat{S}_{i+1}^y) + \Delta \hat{S}_i^z \hat{S}_{i+1}^z] \tag{4}$$

describes the two side-chains. Δ denotes the anisotropy parameter, which is kept at $\Delta = 0.1$ throughout the entire investigation. N_L, N_R are the numbers of spins with respect to left and right spin chain respectively, thus the total number of spins is $N = N_L + N_R$. We choose $N_L = 2N_R - 1$ in order to suppress symmetry, since for the symmetrical case the ETH is trivially fulfilled. The two subsystems are allowed to exchange energy through the interaction Hamiltonian, which reads

$$\hat{H}_I = \sum_{i=1}^{N_L} [(\hat{S}_i^{x,L} \hat{S}_i^{x,R} + \hat{S}_i^{y.L} \hat{S}_i^{y,R}) + \Delta \hat{S}_i^{z,L} \hat{S}_i^{z,R}]$$

Obviously, at any non-zero κ, this model is not accessible by a Bethe ansatz. Thus, in this sense it is always non-integrable. For a more detailed discussion of integrability, see Sec. V

The observable we are going to investigate is the energy difference operator $\hat{D} = \hat{H}_L - \hat{H}_R$. Our motivation for this particular choice stems form the intuitive example of two the cups of coffee brought into contact with each other, where one anticipate more or less an uniform energy density throughout the system. The model (3) has been numerically studied in detail for weak interactions, where the ETH turned out to be valid [18],

III. COMPUTATION OF ETH-QUANTIFYING PARAMETERS

Numerical computation of ETH related data like Σ, $\bar{D}$, etc. for large systems is not a trivial task. Usually, it requires exact diagonalization [17, 18, 41] that is limited to rather small system sizes. Thus, we apply a recently suggested method [23] that is based on dynamical typicality and allows for the extraction of information about ETH from the temporal propagation of pure states. This propagation can be performed by iterative algorithms such as Runge-Kutta [23, 25, 26], Chebyshev [28, 29] etc. and is feasible for larger system sizes. We use a Chebyshev iterator with reasonably small time step in order to improve the computation accuracy. Due to typicality-related reasons, the so-computed quantities $\bar{D}$ and Σ are subjected to statistical errors. These errors, however, turn out to be small. Apart from the model size $N = 14$, which is treated by exact diagonalization (LAPACK-routine), all data in this section has been computed using the above technique. This way we are able to address systems up to $N = 26$.

We focus on a narrow energy shell around $E = 0$ which is the energy regime with the highest density of states. More precisely we choose $\bar{E} = 0$ and $\sigma_E = 0.6$. To set this into perspective, the total energy range of this type of model is on the order of N. The results for the ETH-fluctuations Σ are depicted in figure 2(a).

Figure 2(a) indicates that there are two clearly distinct regimes: Above $\kappa = 3.7$ a convergence of the ETH parameter Σ to zero appears unlikely, even though the presented data may not allow for the precise determination of Σ in the large system limit. At $\kappa = 3.7$ a simple linear scaling also indicates a non-zero Σ in the large system limit, even though the presented data may no be entirely conclusive. However, below $\kappa = 3.5$ Fig. 2(a) clearly indicates $\Sigma \to 0$ for $N \to \infty$. Thus for $\kappa \geq 3.7$ the considered model potentially shows no ISI relaxation of the energy differences between the two chains. This is to be contrasted with the overall concept of heat conduction or the second law of thermodynamics, which demands that energy eventually distributes evenly over all parts of a system, regardless of how uneven it was distributed in the beginning.

Figure 2(b) displays the ETH parameter v which has been suggested as a "detector" of ISI relaxation [18]. While the behavior of Σ and v may appear similar at first sight, there are relevant differences: for all $\kappa \leq 3.7$ v clearly vanishes in the limit of large systems, whereas at $\kappa = 4.0$ a more or less constant scaling occurs for $N \geq 20$. Thus the "switching" from vanishing to non-

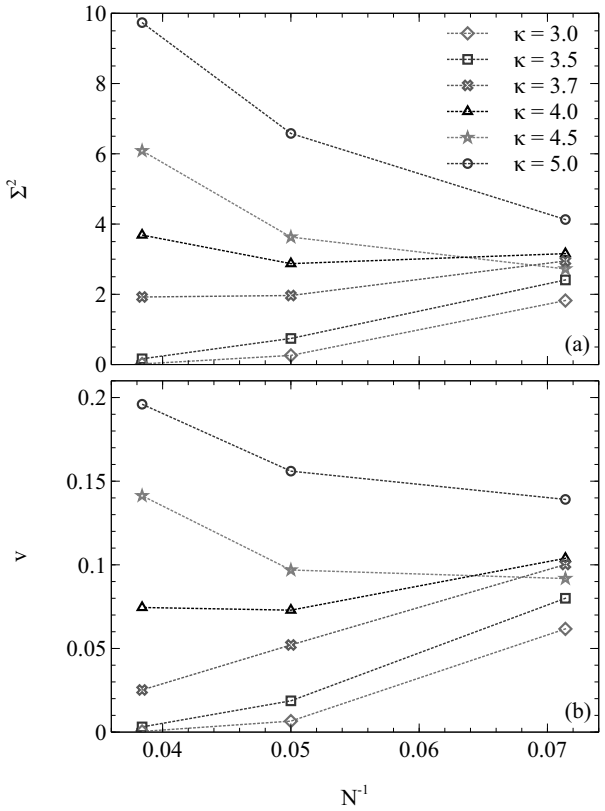

Figure 2. Comparison of the finite size scalings of the "bare" ETH-fluctuation Σ (a) and the scaled ETH parameter v (b) in dependence of the interaction strength κ. Both quantifiers vanish in the large system limit for small κ while they reach constant values (or possibly even diverge) for large κ. For Σ the transition between the two different regimes appears to occur at $\kappa \approx 3.7$. Whereas for v the transition appears to occur at $\kappa \approx 4.0$.

vanishing values in the large system limit appears to occur at $\kappa \approx 3.7$ for Σ, whereas it occurs at $\kappa \approx 4.0$ for v.

IV. INVESTIGATION OF ISI-RELAXATION OF ENERGY DIFFERENCES FROM INITIAL MOD-STATES

In this section we are going to discuss the long time behavior of $\langle D(t)\rangle$ as resulting from initial states from the class of MOD states. The latter are defined as follows:

$$\rho_{\mathrm{MOD}} :\propto e^{(-(\hat{H}-H_0\hat{1})^2-\beta^2(\hat{D}-D_0\hat{1})^2)/2\sigma^2}\,. \qquad (5)$$

These states may be viewed as being based on Jayne's principle: They represents the maximum-entropy states under given means and variances for the energy and the observable. Since $\hat{H}$ and $\hat{D}$ do not commute with each other, it is not possible to generate states with arbitrary values of total energy energy $\langle\hat{H}\rangle_{MOD}$, energy difference $\langle\hat{D}\rangle_{MOD}$ and the respective variances. However, by tuning the parameters H_0, D_0, β, σ, carefully, we are able to prepare initial states having a well-defined energy width $\sigma_E \approx 0.6$ around $E = 0$ and exhibiting initial expectation values for the observable $D(0) = \langle\hat{D}\rangle_{MOD}$, which deviate strongly from their corresponding equilibrium values D_{eq}; more quantitatively, $\langle D\rangle_{MOD}$ reaches about 50% of the difference between its highest possible value and its long-time average. To enable such strong deviations we choose $D_0 = \pm(N_L - 2)$ throughout all investigations. This is to be contrasted with various quench scenarios [30, 31], where the initial deviations from the equilibrium value are rather small. Note also that such MOD states do not necessarily feature a smooth probability distribution with respect to the corresponding energy eigenbasis, as required by Ref. [21] in order to establish ISI.

Neither constructing states of the MOD-type (5) nor propagating such states according to the Schroedinger equation is numerically simple for larger systems. Thus, we instead prepare and evolve a corresponding pure state $|\phi_{\mathrm{MOD}}\rangle$, which exhibits, up to very small statistical errors the same $\langle D(t)\rangle$ as ρ_{MOD}:

$$|\phi_{\mathrm{MOD}}\rangle = \langle\varphi|\rho_{\mathrm{MOD}}|\varphi\rangle^{-1/2}\,\rho_{\mathrm{MOD}}^{1/2}\,|\varphi\rangle\,, \qquad (6)$$

where $|\varphi\rangle$ is a random state drawn according to the unitary invariant (Haar-) measure. This concept relies on dynamical typicality and has been explained and applied in e.g, [18, 25, 39, 41].

As an example the time evolutions of $\langle D(t)\rangle$ for $D(0) = \pm 7, N = 26$ and two different interaction strengths, namely $\kappa = 3, 4.5$, are displayed in Fig. 3 First

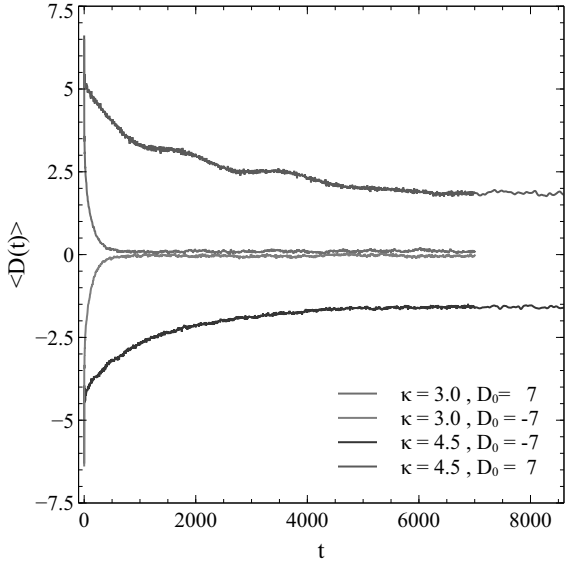

Figure 3. Time evolution of $\langle D(t)\rangle_{MOD}$ for various interaction strengths starting at $D_0 = \pm 7$ for systems of size $N = 26$. In case of $\kappa = 3.0$, ISI equilibration is obvious but for $\kappa = 4.5$ the expectation value converges against finite offsets indicating that some portion of the initial value persists (see text for details). Note that due to slightly different $|D(0)|$ occurring for $\kappa = 4.5$ the "equilibrium values" for corresponding curves also slightly differ.

of all one should note that the non resonance condition and the dilute eigenstate occupation principle obviously apply since in all instances $\langle D(t)\rangle$ converges against constant values with time. However, while the energy difference $\langle D(t)\rangle$ clearly vanishes quickly for $\kappa = 3.0$ (as required by the validity of the ETH) this is not the case at $\kappa = 4.5$. There it appears that a fixed portion of the initial value persists. Hence, this system indeed partially preserves an uneven distribution of local energy in the long time limit, which may be viewed to be at odds with the principle of heat conduction. This finding motivates the introduction of the "ISI quantifying" parameter Λ, which we define as the long time equilibrium value divided by the initial expectation value. Since the preserved portion seems to be more or less independent of actual D_0, we calculated only dynamics featuring $D_0 = N_L - 2$. Thus, the definition of the "ISI quantifying" parameter reads

$$\Lambda = \frac{\langle \phi_{\mathrm{MOD}}|D(t)|\phi_{\mathrm{MOD}}\rangle}{\langle \phi_{\mathrm{MOD}}|D(0)|\phi_{\mathrm{MOD}}\rangle} \quad \text{with} \quad t \gg \tau \ , \tag{7}$$

where τ is the relaxation time. Obviously $\Lambda = 0$ indicates ISI whereas larger Λ indicate a violation of ISI. Furthermore, note that Λ, like v, is insensible with respect to scaling of observables with system size and hence applies to any kind of observable. We computed Λ for three different interaction strengths κ for increasing system sizes. The result is displayed in Fig. 4 Clearly Λ vanishes in

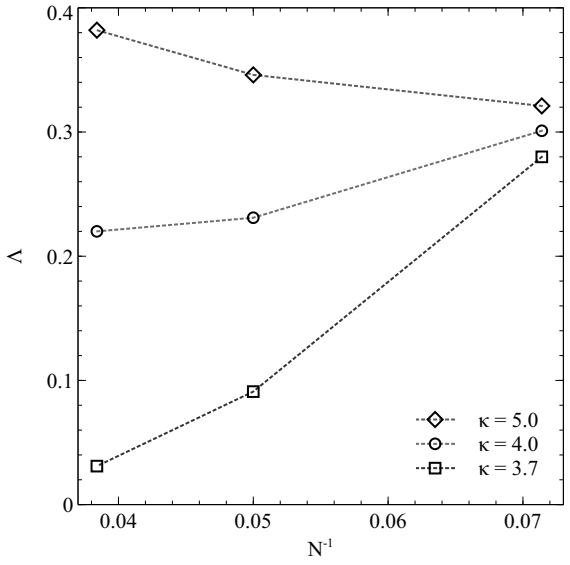

Figure 4. Scaling of Λ with various interaction strengths and system sizes. At $\kappa = 3.7$ the ISI-quantifying Λ tends to zero indicating ISI equilibration whereas for both larger interaction strengths Λ remains finite in the limit of large systems quantifying deviations from the equilibrium value D_{eq}. This behavior corresponds rather accurately to the finite size scaling behavior of v, cf. Fig. 1. Statistical errors are of order of symbol size.

the limit of large system for $\kappa = 3.7$, thus ISI relaxation holds at this interaction strength. At and above $\kappa = 4$, Λ appears to converge against non-zero values, hence no ISI relaxation exists at these interaction strengths, not even for $N \to \infty$. This result should be discussed in relation to the results of Sec. III. Obviously the transition form ISI to non-ISI with increasing interaction strength happens at the same point at which v starts to converge against non-zero values. Thus the behavior of v predicts ISI rather precisely. Σ, on the other hand, starts to converge against non-zero values at $\kappa > 3.5$, i.e., in a regime in which ISI is still present. Thus, in this sense, v appears to be a more reliable predictor of ISI than Σ. This is one of the main results of this paper.

V. INTEGRABILITY INVESTIGATIONS

So far, we focused on the issue of ISI equilibration of a specific observable and found the existence of two regimes, ISI and non-ISI, depending on the interaction strength. Next we address the existence of an integrable regime in the model at hand and study its relevance for the emergence of ISI for the MOD states. Again, similar to the discussion of ETH and ISI, a range of papers more or less explicitly states that non-integrability is imperative for ISI [20], whereas other works analyze ISI without even mentioning integrability. Also different features of "statistical relaxation" (other than ISI) are addressed; examples exist in which the occurrence of statistical relaxation does not depend on integrability [24]. However, this type of investigation generally suffers from a conceptual shortcoming: there is no unambiguous definition for integrability in quantum mechanics. Contrary to classical mechanics notions like phase space, Lyapunov exponents and ergodicity are not well defined. In the context of lattice particle systems, quantum integrability is sometimes associated with being accessible by the Bethe ansatz, i.e., the 1D quantum Heisenberg-chain with nearest neighbor interaction [34], the 1-D δ-function interacting Bose [35] and the Fermi [36] gases are considered as integrable. According to this later definition the model considered in this paper is integrable. Nevertheless, the break down of the ETH for large interaction strength may be viewed as being due to the proximity of the integrable (according to any standard definition) limit of non-interacting spin-dimers. In order to address and quantify this possible integrability, we resort to the well known approach which is based on the Nearest Neighbor Level Spacing Distribution (NNSD) denoted by $P(\Delta\epsilon)$ [42, 43]. The distinction between integrability and chaos is as follows: if the most frequent energy spacing is approaching zero $\Delta\epsilon = 0$ and the shape of the NNSD mimics a Poisson distribution, the system is considered to be integrable. Whereas, if the most frequent energy spacing takes some finite value (level repulsion) with an NNSD shape of Wigner-Dyson type, the system is considered to be non-integrable. This classification of

quantum systems using level statistics has been derived in the context of quantum models, whose corresponding classical counterparts are chaotic [37] and has been adopted even for quantum systems which do not have classical counterpart,.e.g., spin systems.

For most finite systems of condensed matter type the NNSD turns out not to correspond exactly neither to Poisson nor Wigner-Dyson like distributions. To deal with intermediate statistics, Brody proposed in Ref. [38] to compare each real NNSD to a one parameter ω-family of analytically given NNSD's, where $\omega = 0$ corresponds to pure Poisson and $\omega = 1$ to pure Wigner statistics. Matching a real NNSD to a pertinent Brody-NNSD thus yields a specific ω that may be used to quantify the closeness to either Poisson or Wigner, respectively. Following this scheme, we computed (by means of exact diagonalization) and normalized an NNSD for various interaction strengths and $N_R = 6$ in a narrow energy interval around $E = 0$. The results, for $\kappa = 0.3, 4.0$, together with the matching Brody NNSD's are displayed in Fig. 5. Obviously the agreement is rather good. This justifies the usage of the above described method to quantify the "degree of integrability" by means of the parameter ω. Finally, Fig. 6 displays ω as a function of κ together with the ETH parameter v. First one should note that for large interaction strengths the NNSD is much closer to Poisson than to Wigner. This indicates that this model class may indeed become integrable again for stronger interactions, say $\kappa \approx 3.7$, which are nonetheless far away from the integrable dimer limit at $\kappa \gg 1$. To repeat, this integrability is not induced by the possibility of applying a Bethe ansatz. We are furthermore unable to judge whether this integrability may be explained by stretching the quantum KAM theorem [48] all the way down from $\kappa \to \infty$ to $\kappa \approx 3.7$. However, it is striking that the transition from ISI to non-ISI (indicated by increasing v) happens at the very same point at which the NNSD changes from Wigner to Poisson (indicated by decreasing ω). While this finding is just based on numerics in suggests that "chaoticity" in the sense of a large Brody parameter may indeed be a sufficient criterion for the ISI relaxation of few-body observables for systems starting in MOD states. Investigations on different spin systems that point in a similar direction [41] also exist.

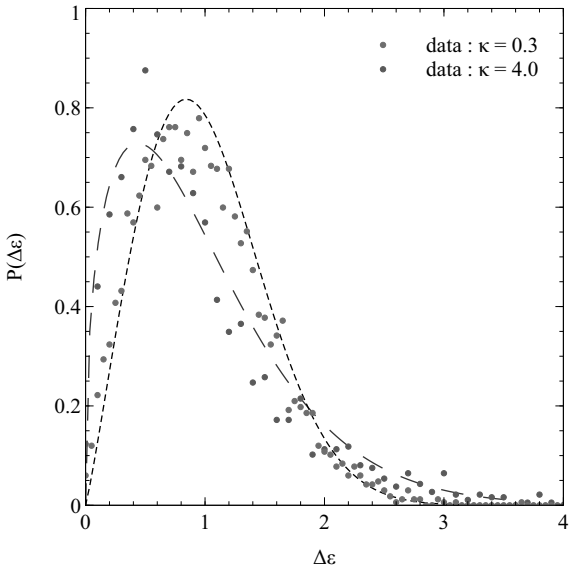

Figure 5. NNSD for $\kappa = 0.3$ and $\kappa = 4.0$ both for $N = 14$ where symbols display computed data and dashed lines corresponding Brody distributions. In case of $\kappa = 0.3$ the Brody parameter reads $\omega \approx 1.1$ (Wigner-Dyson type) and for $\kappa = 4.0$ the Brody parameter reads $\omega = 0.4$ (Poisson type).

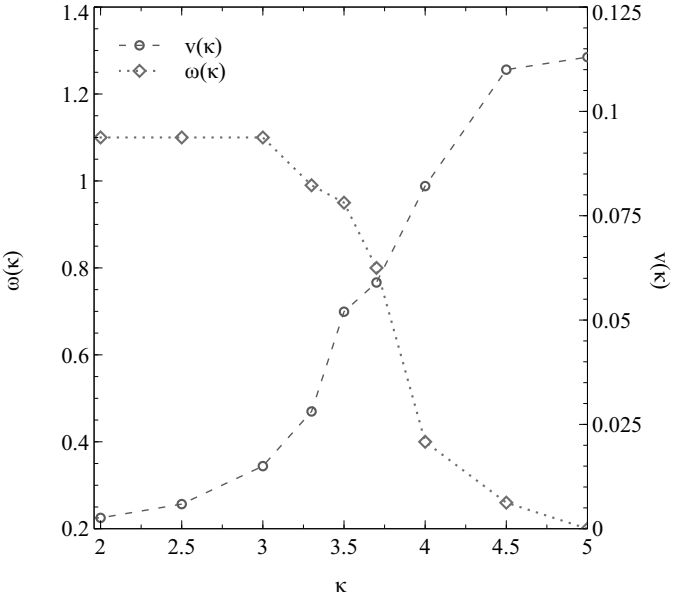

Figure 6. Comparison of Brody parameter ω and alternative ETH parameter v. The transition from integrable to non-integrable systems indicated by ω obviously coincides with the transition from the ISI to non-ISI regime, respectively. This links the equilibration dynamics to quantum chaos; see text for details. Note that that ω is gained from systems of $N = 14$ whereas v is gained from systems of size $N = 20$.

VI. TOWARDS THE PHYSICS BEHIND THE NUMERICAL FINDINGS

While the numerical results clearly indicate a breakdown of "chaoticity" as well as of full relaxation of differences of local energies at strong couplings, the physical reason for this behavior is yet unclear. In the following we shortly speculate about such physical reasons, thus arriving at at some suggestions for further research.
All our findings refer to exchange of local energy between two asymmetric legs of a ladder. It may, however, be elucidating to consider the exchange of local energy between the part of the system that is a regular ladder (upper part in Fig. 1) and the part that consists of the

"elongation" of one leg that really is just a chain (lower part in Fig. 1). If energy exchange between these two parts (ladder and chain) is suppressed, this will result in a suppression of energy exchange between the original asymmetric legs, since the two energy-differences surely have an overlap in the sense of a Mazur inequality [49]. Thus taking the "ladder and chain" point of view, two features are evident: In the limit of large κ the mean level spacing in the ladder will eventually become significantly larger than the mean level spacing in the chain. Furthermore, the chain is integrable in the sense of a Bethe-Ansatz, whereas the ladder is not. Regarding the increasing level spacing in the chain, it may be the case that transitions that amount to an exchange of local energy become more and more off-resonant. If the coupling strength (here: between ladder and chain, i.e., not κ) remains constant but the coupling becomes rather off-resonant, the relaxation of the respective observable may eventually not only be slowed down but inhibited completely [50]. Concerning the integrability, the eigenstates of the chain may in principle be described by a respective set of rapidities, whereas this is not applicable to the eigenstates of the ladder. This structural difference between the eigenstates may cause the eigenstates of the chain to scatter strongly at the interface, thus preventing them from penetrating deeply into the ladder. This could also lead to an effective suppression of the transitions that facilitate an exchange of local energy.
Deciding which of the two above schemes is (if at all) dominantly responsible for the inhibition of the exchange of local energy is beyond the scope of the present paper. Future research, however, could focus on the "ladder and chain partition" and take more variables, other than just local energy differences into account.

VII. SUMMARY AND CONCLUSION

The paper at hand aims at clarifying the interrelations between the eigenstate thermalization hypothesis (ETH), initial state independent relaxation and chaos in quantum systems. The investigations are of primarily numerical character and focus on a class of (asymmetric) ladder type spin systems with variable interaction strength between the legs. We investigated the energy difference between the legs of the spin system where we found that two ETH quantifying parameters, a standard one and an alternative, recently suggested one, indicate violation of the ETH, even in the limit of large systems above certain "threshold" interaction strengths. However, the thresholds differ for the standard and the alternative ETH parameter.
Furthermore, the relaxation behavior of the energy difference between the legs of the spin system is analyzed for a specific class of initials states. It is found that those energy differences no longer equilibrate to zero above a certain interaction strength. This interaction strength precisely coincides with the ETH violation threshold of the alternative ETH parameter but not with the threshold of the standard one.
Finally the level spacing statistics are considered. It turns out that they shift from Poisson-type to Wigner-Dyson type with increasing interaction strengths, again rather distinctly at the threshold of the alternative ETH parameter. To conclude: numerical evidence suggests that the alternative ETH parameter reliably signals the relaxation of an observable towards a common value that is independent of the initial, possibly largely off-equilibrium value of the respective observable. Moreover there appears to be a strong correlation of this alternative parameter with either chaotic or integrable type of level statistics.

[1] S. Popescu, A. J. Short, and A. Winter, Nature Physics **2**, 754 (2006)
[2] S. Goldstein, J.L. Lebowitz, R. Tumulka, and N. Zanghi, Phys. Rev. Lett **96**, 050403 (2006)
[3] O. Lychkovskiy, Phys. Rev. E **82**, 011123 (2010).
[4] J. Eisert, M. Friesdorf and C. Gogolin Nat. Phys. **11**, 124 (2015).
[5] P. Reimann Phys. Rev. Lett. **115**, 010403 (2015).
[6] J. von Neumann, *Beweis des Ergodensatzes und des H-theorems in der neuen Mechanik* Zeitschrift für Physik **57**, 30-70 (1929)
[7] Zelditch, Steve. "Quantum ergodicity and mixing of eigenfunctions." arXiv preprint math-ph/0503026 1 (2005): 183-196.
[8] A. I. Shnirelman Usp. Mat. Nauka **29**, 181 (1974).
[9] J. M. Deutsch, Phys. Rev. A **43**, 2046 (1991).
[10] M. Srednicki, Phys. Rev. E **50**, 888 (1994).
[11] M. Rigol, V. Dunjko, and M. Olshanii, Nature **452**, 854 (2008).
[12] P. Reimann, Phys. Rev. Lett. **101**, 190403 (2008).
[13] N. Linden, S. Popescu, A. J. Short, and A. Winter, Phys. Rev. E **79**, 061103 (2009).
[14] M. Rigol, Phys. Rev. Lett. **103**, 100403 (2009)
[15] J. Gemmer, M. Michel, and G. Mahler, *Quantum Thermodynamics: Emergence of Thermodynamic Behavior within Composite Quantum Systems*, Lect. Notes Phys. **657**, 2nd edition (Springer, Berlin, 2009)
[16] A. Riera, C. Gogolin, and J. Eisert, Phys. Rev. Lett. **108**, 080402 (2012).
[17] W. Beugeling, R. Moessner, and M. Haque, Phys. Rev. E **89**, 042112 (2014).
[18] A. Khodja, R. Steinigeweg, and J. Gemmer Phys. Rev. E **91**, 012120 (2015).
[19] C. Gogolin, Master thesis , The University Wurzburg, arXiv: 100.5058 (2010).
[20] K. R. Fratus and M. Srednicki, arXiv: 1505.04206 (2015).
[21] T. N. Ikeda, Y. Watanabe, and M. Ueda, Phys. Rev. E **87**, 012125 (2013).
[22] C. Gogolin, M. P. Muller, and J. Eisert Phys. Rev. Lett. **106**, 040401 (2011).

[23] R. Steinigeweg, A. Khodja, H. Niemeyer, C. Gogolin, and J. Gemmer, Phys. Rev. Lett. **112**, 130403 (2014).
[24] L. F. Santos, F. Borgonovi and F. M. Izrailev, Phys. Rev. Lett. **108**, 094102 (2012).
[25] T. A. Elsayed and B. V. Fine, Phys. Rev. Lett. **110**, 070404 (2013).
[26] R. Steinigeweg, J. Gemmer, and W. Brenig, Phys. Rev. Lett. **112**, 120601 (2014).
[27] W. Beugeling, R. Moessner and Masudul Haque, Phys. Rev. E **89** 042112 (2014).
[28] H. De Raedt and K. Michielsen, *Computational Methods for Simulating Quantum Computers* in *Handbook of Theoretical and Computational Nanotechnology* (American Scientific Publishers, Los Angeles, 2006).
[29] K. De Raedt, K. Michielsen, H. De Raedt, B. Trieu, G. Arnold, M. Richter, T. Lippert, H. Watanabe, and N. Ito, Comput. Phys. Commun. **176**, 121 (2007).
[30] D. Rossini, A. Silva, G. Mussardo, and G. E. Santoro, Phys. Rev. Lett. **102**, 127204 (2009).
[31] M. Rigol, M. Srednicki, Phys. Rev. Lett. **108**, 110601 (2012).
[32] M. Rigol, Phys. Rev. Lett. **103**, 100403 (2009).
[33] T. N. Ikeda, Y. Watanabe, and M. Ueda, Phys. Rev. E **84**, 021130 (2011).
[34] H. Bethe, Z. Phys. **71**, 205 (1931).
[35] E. H. Lieb and W. Liniger, Phys. Rev. B. **130**, 1605 (1963).
[36] M. Gaudin Phys. Lett. A. **24**, 55 (1967).
[37] M. C. Gutzwiller, *Chaos in Classical and Quantum Mechanics* (Springer-Verlag, New York, 1990).
[38] T. A. Brody Lett. nuovo cimento . **7**, 482 (1973).
[39] C. Bartsch, and J. Gemmer, Phys. Rev. Lett **102**, 110403 (2009)
[40] M. Olshanii, Phys. Rev. Lett. **81**, 938 (1998)
[41] R. Steinigeweg, J. Herbrych, and P. Prelovsek, Phys. Rev. E **87**, 012118 (2013)
[42] E. P. Wigner, Statistical distribution of the spacings of nuclear resonance levels, Camb. Phil. Soc: **47**, 790 (1951).
[43] F. J. Dyson, Statistical theory of the energy levels of complex systems, J. Math. Phys: **3**, 140 (1962).
[44] J. Gemmer, R. Steinigeweg and M. Michel Phys. Rev. B. **73**, 104302 (2006).
[45] S. Dubey, L. Silvestri, J. Finn, S. Vinjanampathy, and K. Jacobs Phys. Rev. E **85**, 011141 (2012).
[46] A. Hutter and S. Wehner Phys. Rev. A **87**, 012121 (2013).
[47] B. S. Shastry J. Phys. A **44**, 052001 (2011).
[48] K.-J. Shi, S.-J. Chang*The Physics of Phase Space Nonlinear Dynamics and Chaos Geometric Quantization, and Wigner Function*, Lect. Notes Phys. **278** (Springer, 130-132, 2005)
[49] P. Mazur Physica **43**, 533 (1969).
[50] C. Bartsch, R. Steinigeweg and J. Gemmer Phys. Rev. E **77**, 011119 (2008).

Preprint version

Original publication: PRB, 95, 134201 (2017)
doi: 10.1103/PhysRevB.95.134201

Interaction-Induced Weakening of Localization in Few-Particle Disordered Heisenberg Chains

Daniel Schmidtke,[1,*] Robin Steinigeweg,[1] Jacek Herbrych,[2,3,4] and Jochen Gemmer[1]

[1] *Department of Physics, University of Osnabrück, D-49069 Osnabrück, Germany*
[2] *Cretan Center for Quantum Complexity and Nanotechnology, Department of Physics, University of Crete, GR-71003 Heraklion, Greece*
[3] *Department of Physics and Astronomy, The University of Tennessee, Knoxville, Tennessee 37996, USA*
[4] *Materials Science and Technology Division, Oak Ridge National Laboratory, Oak Ridge, Tennessee 37831, USA*

We investigate real-space localization in the few-particle regime of the XXZ spin–1/2 chain with a random magnetic field. Our investigation focuses on the time evolution of the spatial variance of non-equilibrium densities, as resulting for a specific class of initial states, namely, pure product states of densely packed particles. Varying the strength of both particle-particle interactions and disorder, we numerically calculate the long-time evolution of the spatial variance $\sigma(t)$. For the two-particle case, the saturation of this variance yields an increased but finite localization length, with a parameter scaling different to known results for bosons. We find that this interaction-induced increase is the stronger the more particles are taken into account in the initial condition. We further find that our non-equilibrium dynamics are clearly inconsistent with normal diffusion and instead point to subdiffusive dynamics with $\sigma(t) \propto t^{1/4}$.

PACS numbers: 05.60.Gg, 71.27.+a, 75.10.Jm

I. INTRODUCTION

Non-interacting particles in a disordered potential are Anderson-localized in one dimension (1D), for any disorder strength and temperature[1–4]. Recently, it has become clear that Anderson localization is also stable against weak particle-particle interactions[5,6]. Moreover, numerous works suggest the existence of a many-body localized (MBL) phase beyond the weak-interaction limit and even at infinite temperature[7–9]. This MBL phase is a new state of matter with several fascinating properties, ranging from the breakdown of eigenstate thermalization[10–16] to the logarithmic growth of entanglement as a function of time after an initial quantum quench[17–19]. In particular the optical conductivity features a zero dc value[20–22] and a low-frequency behavior as described by Mott's law[20]. On the experimental side, an MBL phase was recently observed for interacting fermions in a quasi-random (bichromatic) optical lattice[23,24] as also delocalization by coupling identical 1D MBL systems[25]. Investigations of amorphous iridium-oxide indicate that MBL might play an important role for its insulating states[26].

The existence of a MBL phase at finite disorder and interaction strength implies that the decrease of disorder induces a transition from a localized phase (non-ergodic, non-thermal) to a delocalized phase (ergodic, thermal)[27]. This disorder-induced transition has been under active scrutiny and different probes have been suggested[28] such as subdiffusive power laws in the vicinity of the critical disorder[20] (which may or may not exist[21,29–35]). So far, a full understanding of the MBL transition is still lacking. This lack of knowledge is also related to restrictions of state-of-the-art numerical methods. On the one hand, full exact diagonalization is restricted to small systems with only a few lattice sites, where finite-size effects are strong in disorder-free cases[36–38]. On the other hand, much more sophisticated methods such as time-dependent density-matrix renormalization group are restricted to times scales with sufficiently low entanglement[35,39,40].

While the overwhelming majority of works has focused on the disorder-induced transition at half filling, much less is known on the transition induced by filling at fixed disorder strength[16,39]. Since a single particle is localized for any finite disorder, a transition from a localized phase to a delocalized phase has to occur, if the half-filling sector is delocalized. However, *when* and *how* such a transition happens exactly constitutes a non-trivial and challenging question. So far, this question has been investigated only partially, with a remarkable focus on the special case of two interacting bosons[41–44]. Though there are a few works containing results on two interacting fermions, see e.g. Refs. 45 and 46, there is, to the best of our knowledge, no detailed investigation for this case, especially in connection with increasing the particle number beyond two. The latter is the main focus of the work at hand.

Thus, we study this question for the XXZ spin-1/2 Heisenberg chain. To this end, we consider a non-equilibrium scenario. First, we prepare a pure initial state of densely packed particles (also known as bound states[47,48]), where all particles (↑-spins) are concentrated at adjacent sites and holes (↓-spins) are located on the other sites. Then, we calculate the evolution of the particle distribution in real time and real space, using a Runge-Kutta integration of the time-dependent Schrödinger equation[36,37,49,50]. While the time dependence of the distribution width allows us to study the type of dynamics in general, a convergence of this width to a constant value in the long-time limit (which may or may not exist) also allows us to extract a finite localization length. To eliminate that this length is a trivial boundary effect, we choose large system sizes. The latter are feasible for different particle numbers due to our integration scheme.

The paper is organized as follows: In Sec. II, we introduce the investigated model, namely a Heisenberg spin–1/2 chain subjected to random magnetic fields. Furthermore our main observable, i.e., the time-dependent particle density distribution arising from densely-packed initial states, comparable to so-called bound states, is discussed. Also its (dynamical) broadening in terms of standard statistical variances is presented. At the end of this section, we describe shortly our numerical methods. In Sec. III, the variance is investigated regarding the scaling behavior with particle number ranging from only one particle up to four. Sec. IV is dedicated to a thorough investigation of the scaling behavior of the saturation value of the aforementioned variance in the two-particle case. This scaling behavior is analyzed with respect to the particle-particle interaction and disorder strength within appropriate regimes, where we interpret finite saturation values of the variances as real-space localization lengths. In Sec. V, we provide evidence that the cases of non-interacting and interacting particles can be distinguished in terms of local density correlations where we again investigate exemplary only the two particle case. Finally we end with a short summary and conclusions in Sec. VI. In Appendix A we provide a thorough analysis regarding statistical error estimations for mean localization lengths and Appendix B presents a discussion of the behavior of two-particle localization lengths in the large interaction regime in comparison to results on bosons.

II. MODEL AND NON-EQUILIBRIUM DENSITIES

We study the XXZ spin-1/2 chain with a random magnetic field oriented in z direction. The Hamiltonian reads (with periodic boundary conditions)

$$H = \sum_{i=1}^{L} \left[J(S_i^x S_{i+1}^x + S_i^y S_{i+1}^y + \Delta S_i^z S_{i+1}^z) + h_i S_i^z \right] , \tag{1}$$

where $S_i^{x,y,z}$ are spin-1/2 operators at site i, L is the number of sites, $J > 0$ is the antiferromagnetic exchange coupling constant, and Δ is the exchange anisotropy. The local magnetic fields h_i are random numbers drawn from a uniform distribution in the interval $h_i \in [-W, W]$. We note that, via the Jordan-Wigner transformation[51], this model can be mapped onto a one–dimensional model of spinless fermions with particle-particle interactions of strength Δ and a random on-site potential of strength h_i. We are interested in the time evolution of the density distribution

$$\langle n_i(t) \rangle = \frac{1}{N} \operatorname{tr}[n_i \, \rho(t)] \, , \quad \sum_{i=1}^{L} \langle n_i(t) \rangle = 1 \, , \tag{2}$$

where N is the number of particles, $n_i = S_i^z + 1/2$ is the occupation-number operator at site i, and $\rho(t)$ is the density matrix at time t. In this way, we can investigate the time-dependent broadening of an initial state $\rho(0)$ in real space. In the few-particle regime, i.e., $N \ll L/2$, studied in this paper, due to short–range interactions, only initial states with a sharp concentration of particles at adjacent sites are appropriate. For such "narrow" initial states we can expect non-trivial dynamics, while "broad" initial states essentially correspond to the one-particle problem. Thus, our initial states $\rho(0) = |\psi(0)\rangle\langle\psi(0)|$ read (in the Ising basis)

$$|\psi(0)\rangle = \prod_{i=p}^{p+N-1} S_i^+ \, |\downarrow \ldots \downarrow\rangle = |\ldots \downarrow \underbrace{\uparrow \ldots \uparrow}_{N} \downarrow \ldots\rangle \, , \tag{3}$$

where S_i^+ is the creation operator at site i and p is chosen to concentrate particles (↑-spins) around $i = L/2$. These pure states of densely packed particles describe an alignment of N particles directly next to each other (known as bound states for $N \sim 2$ [47,48] and domain walls for $N \sim L/2$ [40,52]). Note that, due to periodic boundary conditions, the specific choice of p is irrelevant. However, to avoid boundary effects in the following definition it is convenient to choose $p \approx L/2$.

A central quantity of our paper is the spatial variance of the above introduced particle density distribution

$$\sigma^2(t) = \sum_{i=1}^{L} i^2 \, \langle n_i(t) \rangle - \left(\sum_{i=1}^{L} i \, \langle n_i(t) \rangle \right)^2 . \tag{4}$$

On the one hand, the time dependence of $\sigma(t)$ yields information on the type of dynamics such as power laws t^α [44,53] for sub- ($\alpha < 1/2$), normal ($\alpha = 1/2$), or super-diffusion ($\alpha > 1/2$). On the other hand, we can use the long-time value $l = \lim_{t\to\infty} \sigma(t)$ as a natural definition for the localization length. Since l, as well as all other quantities introduced, depend on the specific disorder realization considered, we average over a sufficiently large number of disorder realizations r, typically $r > 1000$, to determine the mean of l within negligible statistical errors, see Appendix A for details. To also ensure negligibly small finite-size effects, we set $L = 100$

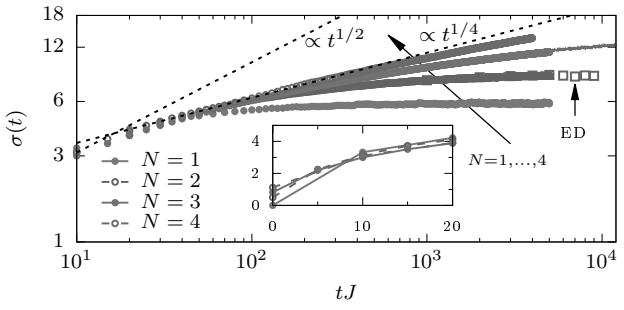

FIG. 1. (Color online) Log–log plot of the time evolution of the width $\sigma(t)$ for different particle numbers $N = 1, \ldots, 4$ for $\Delta = 1$, $W/J = 1$. For the $N = 2$ case, corresponding ED results are also shown. For the $N = 3$ case, long-time data for fewer $r \approx 100$ is further depicted. Power laws are indicated for comparison. Inset: Lin–lin plot for short times.

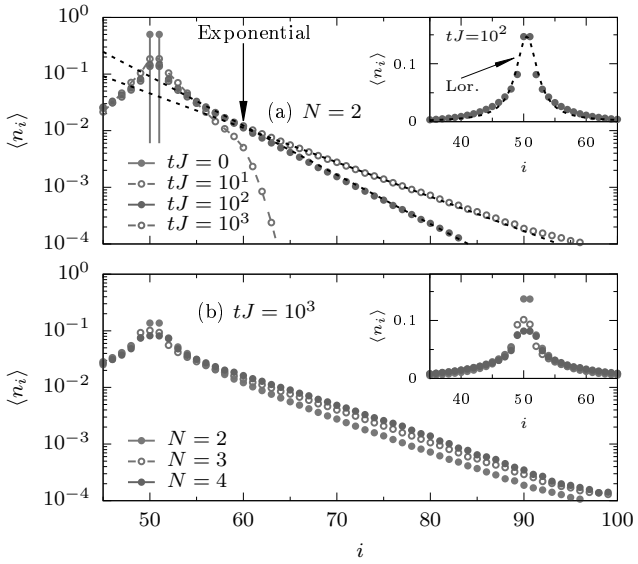

FIG. 2. (Color online) Site dependence of the density profile $\langle n_i(t) \rangle$ for $\Delta = 1$ and $W/J = 1$ at (a) times $tJ = 0, 10, 100$, and 1000 for $N = 2$ particles and (b) at fixed time $tJ = 1000$ for $N = 2, 3$ and 4 particles, both in a semi-log plot. In (a) exponential fits to the tails are indicated. Insets: Lin-lin plots with a Lorentzian fit indicated in (a).

throughout this paper. We checked that such L is sufficiently large for all quantities and time scales investigated here. Thus, for the two-particle case, i.e., $N = 2$, (with Hilbert-space dimension $\dim\mathcal{H} = 4950$), we use full exact diagonalization (ED). For larger N, e.g., $N = 3$ ($\dim\mathcal{H} = 161700$), we rely on a forward iteration of the pure state $|\psi(t)\rangle$ using fourth-order Runge-Kutta with a time step $t\,J = 0.01 \ll 1$[54], feasible for $L = 100$ due to sparse-matrix representations of operators, see Refs. 36, 37, and 50 for details. As demonstrated below, the results obtained from this iterative method coincide for $N = 2$ with the ED results.

III. SCALING OF THE VARIANCE

Now, we present our results, starting with the time evolution of the width $\sigma(t)$ and focusing on the isotropic point $\Delta = 1$ and intermediate disorder $W/J = 1$. Fig. 1 summarizes $\sigma(t)$ for different particle numbers $N = 1$, 2, 3, and 4 in a log-log plot, with statistical errors smaller than the symbol size used (see Appendix A).

Several comments are in order. First, in the long-time limit, $\sigma(t)$ increases monotonously as N increases from 1 to 4. Second, for $N = 1$ and 2, $\sigma(t)$ is approximately time-independent for $t\,J > 1000$ and takes on a constant value $\sigma < 10$, much smaller than the size of the lattice $L = 100$. On the one hand, the saturation for $N = 1$ is expected since in this case the actual value of Δ is irrelevant and single-particle Anderson localization persists[1,55]. On the other hand, the saturation for $N = 2$ is in qualitative accord with corresponding results on bosons[41–44,56]. Third, for $N > 2$ such conclusions are less obvious. The long time scale relevant for our dynamics, as typical for disordered problems[15,16,44,57], systematically increases with N and we do not observe a saturation of $\sigma(t)$ at the time scales depicted in Fig. 1. Note that we have also calculated $\sigma(t)$, for $N = 3$ and $r \approx 100$, up to very long $t\,J = 12000$, where it still increases significantly, see Fig. 1. This ongoing increase could be a signature of a diverging localization length and would be consistent with the delocalized phase at $N = L/2$ for this choice of Δ and W. Finally, the time dependence of $\sigma(t)$ is for all cases inconsistent with normal diffusion, where $\sigma(t) \propto t^{1/2}$, which has been found so far only in few disorder-free cases[58,59]. In fact, we find $\sigma(t) \propto t^{1/4}$ on intermediate time-intervals. The latter becomes more pronounced for larger N. This scaling is also expected for the chaotic spreading of nonlinear wave packets in disordered potentials[44,53]. Nevertheless, our data is not sufficient to state conclusively whether the observed agreement indeed indicates subdiffusion or whether it is essentially cross-over effect.

In clear contrast, for short times, $\sigma(t)$ in the inset of Fig. 1 is larger for smaller N, inverse to the long-time behavior discussed so far. This short-time behavior simply reflects that fewer particles expand in a more empty lattice. Here, disorder is not relevant yet.

To gain insight into the origin of the slow dynamics of $\sigma(t)$, we depict in Fig. 2 time snapshots of the site dependence of the underlying density profile $\langle n_i(t) \rangle$ for $N = 2$ in a semi-log plot. For simplicity, we focus only on the right part of the symmetric function. While the profiles are well approximated by Lorentzians around their center, see inset of Fig. 2 (a), the tails show a different behavior. Remarkably, they are well described by exponentials over orders of magnitude, as expected for Anderson-localized states[1,55], but here for interacting particles; see Ref. 60 for a similar decay behavior. We have found similar behavior for $N = 3$ and 4. In fact, as shown in

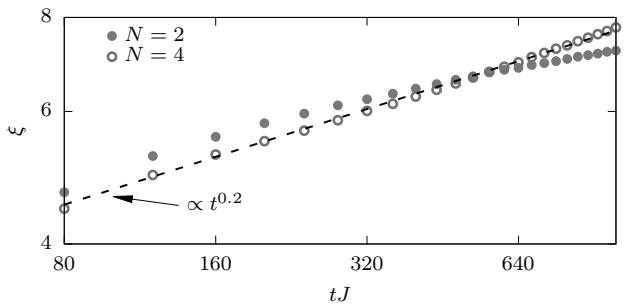

FIG. 3. (Color online) Log-log plot of the time-dependence of the inverse decay constant ξ for $\Delta = 1$ and $W/J = 1$. The crossover behavior is similar to the one found for the variance $\sigma(t)$; see inset of Fig. 1. Dashed line indicates power-law fit with $\xi \propto t^{0.21}$ for $N = 4$ supports sub-diffusive expansion of $\sigma(t)$ as discussed above.

Fig. 2 (b), the spatial decay appears to be very similar for different N at fixed t.

In the following, we are going to quantify this by extracting localization lengths from in Fig. 2 shown exponential tails according $\langle n_i \rangle \propto \exp(-i/\xi)$. As usual localization lengths are then denoted as the inverse decay constant, i.e., $l := \xi$. Fig. 3 shows the time-evolution of ξ for $N = 2$ and 4 in the time-interval $80 \leq tJ \leq 1000$. Note that for $t < 80$ exponential tails do not yet exist properly and density profiles are governed by the Lorentzian-type expansion at the center. Moreover since this Lorentzian-type behavior persists for all times and deviation from exponential decay may occur at the *edges* of the chain, we fit the tails only for $60 \leq i \leq 90$. Remarkably, the time evolutions show a similar behavior with respect to different particle numbers as the variance σ discussed above, i.e., at the beginning of the aforementioned time-interval the localization length is the larger the less particles are taken into account but it also increases the slower. Thus, subsequently at large times the localization length is the larger the more particles are taken into account. However, here the crossover occurs at much larger times than above. A power-law fit (see dashed lines in Fig. 3) suggests that for $N = 4$ it scales as $\xi \propto t^{0.21}$ for the entire interval shown. This is rather close to a sub-diffusive expansion with $\sigma(t) \propto t^{1/4}$ and thus supports the idea that the slow growth of the tails yields sub-diffusive expansion (at least in a certain interval for the particles numbers considered here).

IV. LOCALIZATION LENGTH

Next, we turn to the localization length l which is here only analysed for $N \leq 2$ since for more particles saturation is not observed on time-scales investigated here. In Fig. 4 we summarize our results for the Δ and W dependence of l for the two-particle case. There, we observe a clear saturation of $\sigma(t)$ at times $t\,J = 5000$ for all Δ and W considered, cf. Fig. 1. Thus, $l \approx \sigma(t\,J = 5000)$. In order to check saturation we also calculated $\sigma(t = 10^7)$ and found $\sigma(t = 10^7) \approx \sigma(5000)$; data not shown for clarity.

According to Fig. 4, the localization length l is finite for all parameters depicted. Clearly, at fixed interaction strength Δ, l increases as disorder W is decreased. At fixed W, l increases with interaction strength for $\Delta \leq \Delta_{\max} \approx 0.75$. The decrease of l for $\Delta > 0.75$ occurs since our initial state is an eigenstate of the Ising limit $\Delta \to \infty$. This might be seen as running into localized states comparable to Mott states[2]. In Appendix B, we provide results for $W/J = 0.7, 1$ for large interaction strengths, i.e., up to $\Delta \leq 14$, that visualize this behavior. Note that for $\Delta \to \infty$, bosons *act* like free fermions, i.e., there is no Mott insulting phase. Moreover, we find that the two-particle localization length $l_2 := l(\Delta \neq 0)$ scales approximately linear with the one-particle localization length $l_1 := l(\Delta = 0)$, at least in the disorder regime $0.7 \leq W \leq 1.25$. This becomes apparent from the enhancement factor $\lambda = l_2/l_1$ in Fig. 4 (inset). λ appears to be almost independently of W, and hence of l_1, and is largest in the region $\Delta \approx \Delta_{\max}$ where $\lambda \approx 1.4$. This is significantly different from the enhancement factor for bosons with, e.g., contact interaction where λ increases monotonously with l_1 at least in the regime of intermediate disorder, see e.g. Refs. 41–46. The dependence of λ on the interaction strength for bosonic models appears to be under dispute. E.g. in Refs. 41–44 the authors find also a monotonous increase of λ with interaction strength, whereas in Refs. 45 and 46 the authors find a similar behavior as the one at hand with a distinct interaction strength for which the enhancement is strongest (see Appendix B). Nevertheless in comparison to our results, there are still significant differences e.g. regarding the maximum enhancement and its distinct interaction strength; see Refs. 45 and 46 for details.

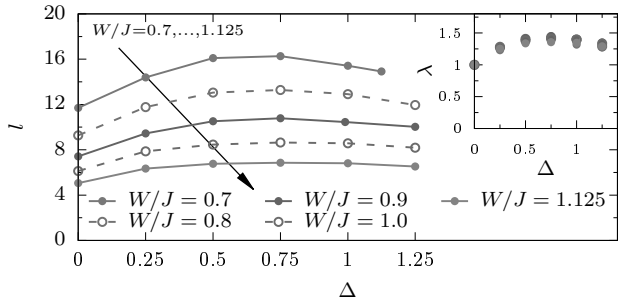

FIG. 4. (Color online) Dependence of the $N = 2$ localization length l on the interaction strength Δ for various disorders W, as obtained from $\sigma(t)$ at times $t\,J = 5000$. Inset: The same data as in main panel but for the relative localization length $\lambda = l(\Delta)/l(\Delta = 0)$.

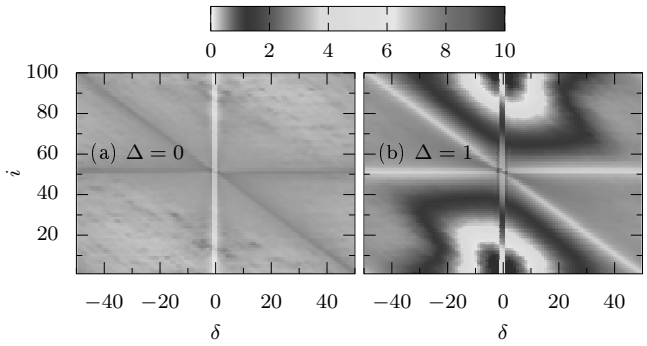

FIG. 5. (Color online) Local density correlator $C_{i,\delta}(t)$ vs. site i and distance δ for $N = 2$ particles, $W/J = 1$, and fixed time $tJ = 3500$. (a) shows results for the noninteracting case $\Delta = 0$ and (b) for the interacting case $\Delta = 1$.

V. LOCAL DENSITY CORRELATIONS

Finally, we intend to shed light on the nature of the transport process and on the differences between noninteracting and interacting cases, i.e., $\Delta = 0$ and $\Delta \neq 0$, respectively. To this end, we consider the local density correlator

$$C_{i,\delta}(t) = \frac{\langle n_i(t) n_{i+\delta}(t)\rangle}{\langle n_i(t)\rangle \langle n_{i+\delta}(t)\rangle} \tag{5}$$

of site i and another site in distance δ, both at a given time t. This correlation function can be interpreted as the probability to find simultaneously site i and $i + \delta$ occupied, weighted by their individual occupation probability. Thus, compared to similar correlator definitions, see e.g. Refs. 43, 47, and 48, ours is apt to display correlations even if $\langle n_i(t) n_{i+\delta}(t)\rangle$ is very small; here especially in the outer tails, see Fig. 2. Note that, uncorrelated sites have $C_{i,\delta}(t) \approx 1/2$.

In Fig. 5 we show our $N = 2$ results for $C_{i,\delta}(t)$ in a color map vs. site i and distance δ for interactions turned off ($\Delta = 0$) and interaction turned on ($\Delta = 1$), focusing on long times $t\,J = 3500$ and intermediate disorder $W/J = 1$. For the $\Delta = 0$ case in Fig. 5(a), there generally is no strong enhancement of correlations. The horizontal line visible, corresponding to site $i \approx L/2$ and arbitrary δ, has the slightly enhanced value ≈ 0.6. Note that the diagonal line is equivalent to the horizontal one. Thus these lines suggest that one particle moves freely while the other remains at the initial site. For the $\Delta = 1$ case in Fig. 5(b), correlations are much more enhanced. A striking feature are strong correlations at $i \ll L/2$ and $i \gg L/2$ but with a small δ. These correlations suggest that the two particles do not move independently and stay close to each other during the time evolution, in clear contrast to the noninteracting case $\Delta = 0$; cf. Refs. 47, 48, and 61 for results on the disorder-free case and Refs. 41 and 43 for bosons.

VI. SUMMARY AND CONCLUSIONS

In summary, we investigated real-space localization in the few-particle regime of the XXZ spin-1/2 chain with a random magnetic field. Our investigation focused on the time evolution of the spatial variance of non-equilibrium densities, as resulting for a specific class of initial states, namely, pure states of densely packed particles. We showed that our non-equilibrium dynamics are clearly inconsistent with normal diffusion and instead point to subdiffusive dynamics. For the two-particle case, our numerical results indicated that interactions lead to an increased but still finite localization length for all parameters considered, whereas for three and four particles saturation of the variance is not observed on time-scales manageable numerically here. We also found that this interaction-induced broadening of the non-equilibrium densities is the stronger the more particles are taken into account in the initial condition. We also performed an investigation of the scaling behavior of the localization length with particle-particle interaction strength and strength of the magnetic fields where our results differ significantly from those known for bosons. Finally, we also provided evidence that the cases of non-interacting and interacting particles can be distinguished in terms of local density correlations. Our corresponding results further suggested that two interacting particles cannot move independently and stay close to each other during the time evolution in accordance with other works.

ACKNOWLEDGMENTS

We thank F. Heidrich-Meisner and T. Prosen and for fruitful discussions. J. Herbrych acknowledges support by the U.S. Department of Energy, Office of Basic Energy Sciences, Materials Science and Engineering Division, the EU program FP7-REGPOT-2012-2013-1 under Grant No. 316165 and thanks the University of Osnabrück for kind hospitality.

Appendix A: Statistical Errors

As the local magnetic fields h_i are drawn at random, $\sigma_i(t)$ is randomly distributed around its mean $\langle\sigma(t)\rangle$ and it is necessary to estimate statistical errors. In Fig. 6 histograms for the individual deviations $\epsilon_i(t) = \sigma_i(t) - \langle\sigma(t)\rangle$ at fixed time $t\,J = 5000$, interaction $\Delta = 1$, and disorder $W/J = 1$ are shown. Note that we also computed the errors for all the other parameter choices in the same way as described below. For $N = 2$ and 3 the distributions are of Gaussian type while for $N = 1$ the distribution is slightly asymmetric. Interestingly, the distributions become broader as the particle number is increased.

In the inset of Fig. 6 we show the time evolution of

$$\langle \epsilon^2(t) \rangle = \frac{1}{r} \sum_{i=1}^{r} \epsilon_i(t)^2, \tag{A1}$$

for the same set of parameters. The time dependence of $\langle \epsilon^2(t) \rangle$ is similar to the one of $\langle \sigma(t) \rangle$ itself; however, $\langle \epsilon^2(t) \rangle < \langle \sigma(t) \rangle$. Furthermore, for $N = 1$ and 2, the time scale where $\langle \epsilon^2(t) \rangle$ saturates at its maximum is also comparable. For $N = 3$, $\langle \epsilon^2(t) \rangle$ still increases in the long-time limit, just as $\langle \sigma(t) \rangle$.

Given the Gaussian form in Fig. 6, we can estimate the error of determining $\langle \sigma(t) \rangle$ by r realizations from

$$\sqrt{\frac{\langle \epsilon^2(t) \rangle}{r}}. \tag{A2}$$

We choose r such large that this error is smaller than the symbol sizes used in the corresponding figures, i.e., typically $r > 1000$.

Appendix B: Two-particle localization length for large interaction strengths

As pointed out in the main text, the two-particle localization length l decreases if the interaction strength increases beyond a certain threshold. This fact is visualized for $W/J = 0.7, 1$ and $\Delta \leq 14$ in Fig. 7. Indeed the localization lengths decreases rather strong for increasing interaction strength. For comparison, the smallest localization length, i.e., when both particles are localization on adjacent sites with $l = 1/\sqrt{2}$, is displayed (dashed line). Note that our initial states are constructed to feature this value in the beginning. Clearly, for both disorder strengths the localization length tends toward this value in the large interaction regime. This also means that (detectable) dynamics of the system are not present anymore. For bosons such behavior in the high interaction regime is, as pointed out in the main text, a disputed topic. Some works propose a constant increase of the localization length with interaction strengths while others find also decreasing localization lengths as presented here. However, the differences between such results on bosons and our results remain quantitatively significant see e.g. Ref. 46 for results on the same interaction strength regime. Ref. 45 even shows that in the large interaction regime the enhancement vanishes, i.e., $l_2 \approx l_1$.

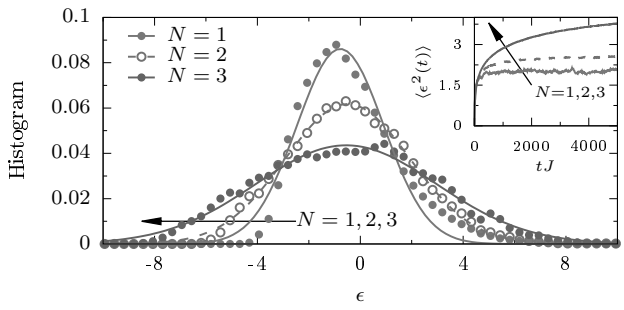

FIG. 6. (Color online) Histogram of $\epsilon_i(t) = \sigma_i(t) - \langle \sigma(t) \rangle$ for $N = 1$, 2, and 3 at fixed $tJ = 5000$ ($\Delta = 1$, $W/J = 1$, and $L = 100$). Clearly, the overall shape is Gaussian (solid lines) and the width grows with N. Inset: Time evolution of $\langle \epsilon^2(t) \rangle$ for the same parameters.

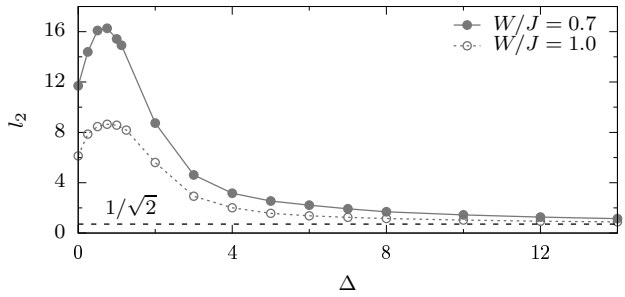

FIG. 7. (Color online) Two-particle localization length for $W/J = 0.7, 1$ and strong interaction, i.e., $\Delta \leq 14$. For comparison the smallest localization length $l = 1/\sqrt{2}$ (which is also the initial localization of our initial states) is displayed (dashed line). Obviously, l_2 tends to this value in the large interaction regime, i.e., there are no significant dynamics present anymore. Statistical errors are smaller than symbol size.

* danischm@uos.de

[1] P. W. Anderson, Phys. Rev. **109**, 1492 (1958).
[2] N. F. Mott, Phil. Mag. **17**, 1259 (1968).
[3] B. Kramer and A. MacKinnon, Rep. Prog. Phys. **56**, 1469 (1993).
[4] F. Evers and A. D. Mirlin, Rev. Mod. Phys. **80**, 1355 (2008).
[5] D. M. Basko, I. L. Aleiner, and B. L. Altshuler, Ann. Phys. **321**, 1126 (2006).
[6] L. Fleishman and P. W. Anderson, Phys. Rev. B **21**, 2366 (1980).
[7] A. Pal and D. A. Huse, Phys. Rev. B **82**, 174411 (2010).
[8] V. Oganesyan and D. A. Huse, Phys. Rev. B **75**, 155111 (2007).
[9] D. J. Luitz, N. Laflorencie, and F. Alet, Phys. Rev. B **91**, 081103 (2015).
[10] M. Serbyn, Z. Papic, and D. A. Abanin, Phys. Rev. Lett. **111**, 127201 (2013).
[11] D. A. Huse, R. Nandkishore, and V. Oganesyan, Phys. Rev. B **90**, 174202 (2014).
[12] D. A. Huse, R. Nandkishore, V. Oganesyan, A. Pal, and S. L. Sondhi, Phys. Rev. B **88**, 014206 (2013).

[13] R. Nandkishore and D. A. Huse, Annu. Rev. Condens. Mat. Phys. **6**, 15 (2015).
[14] D. J. Luitz, Phys. Rev. B **93**, 134201 (2016).
[15] E. Khatami, M. Rigol, A. Relaño, and A. M. García-García, Phys. Rev. E **85**, 050102 (2012).
[16] R. Mondaini and M. Rigol, Phys. Rev. A **92**, 041601 (2015).
[17] M. Žnidarič, T. Prosen, and P. Prelovšek, Phys. Rev. B **77**, 064426 (2008).
[18] J. H. Bardarson, F. Pollmann, and J. E. Moore, Phys. Rev. Lett. **109**, 017202 (2012).
[19] R. Vosk and E. Altman, Phys. Rev. Lett. **110**, 067204 (2013).
[20] S. Gopalakrishnan, M. Müller, V. Khemani, M. Knap, E. Demler, and D. A. Huse, Phys. Rev. B **92**, 104202 (2015).
[21] R. Steinigeweg, J. Herbrych, F. Pollmann, and W. Brenig, Phys. Rev. B **94**, 180401 (2016).
[22] T. C. Berkelbach and D. R. Reichman, Phys. Rev. B **81**, 224429 (2010).
[23] M. Schreiber, S. S. Hodgman, P. Bordia, H. P. Lüschen, M. H. Fischer, R. Vosk, E. Altman, U. Schneider, and I. Bloch, Science **349**, 842 (2015).
[24] S. S. Kondov, W. R. McGehee, W. Xu, and B. DeMarco, Phys. Rev. Lett. **114**, 083002 (2015).
[25] P. Bordia, H. P. Lüschen, S. S. Hodgman, M. Schreiber, I. Bloch, and U. Schneider, Phys. Rev. Lett. **116**, 140401 (2016).
[26] M. Ovadia, D. Kalok, I. Tamir, S. Mitra, B. Sacépé, and D. Shahar, Sci. Rep. **5**, 13503 (2015).
[27] J. A. Kjäll, J. H. Bardarson, and F. Pollmann, Phys. Rev. Lett. **113**, 107204 (2014).
[28] M. Filippone, P. W. Brouwer, J. Eisert, and F. von Oppen, Phys. Rev. B **94**, 201112 (2016).
[29] V. K. Varma, A. Lerose, F. Pietracaprina, J. Goold, and A. Scardicchio, arXiv:1511.09144.
[30] A. Karahalios, A. Metavitsiadis, X. Zotos, A. Gorczyca, and P. Prelovšek, Phys. Rev. B **79**, 024425 (2009).
[31] M. Žnidarič, A. Scardicchio, and V. K. Varma, Phys. Rev. Lett. **117**, 040601 (2016).
[32] I. Khait, S. Gazit, N. Y. Yao, and A. Auerbach, Phys. Rev. B **93**, 224205 (2016).
[33] O. S. Barišić, J. Kokalj, I. Balog, and P. Prelovšek, Phys. Rev. B **94**, 045126 (2016).
[34] K. Agarwal, S. Gopalakrishnan, M. Knap, M. Müller, and E. Demler, Phys. Rev. Lett. **114**, 160401 (2015).
[35] Y. Bar Lev, G. Cohen, and D. R. Reichman, Phys. Rev. Lett. **114**, 100601 (2015).
[36] R. Steinigeweg, J. Gemmer, and W. Brenig, Phys. Rev. Lett. **112**, 120601 (2014).
[37] R. Steinigeweg, J. Gemmer, and W. Brenig, Phys. Rev. B **91**, 104404 (2015).
[38] P. Prelovšek, S. El Shawish, X. Zotos, and M. Long, Phys. Rev. B **70**, 205129 (2004).
[39] G. Roux, T. Barthel, I. P. McCulloch, C. Kollath, U. Schollwöck, and T. Giamarchi, Phys. Rev. A **78**, 023628 (2008).
[40] J. Hauschild, F. Heidrich-Meisner, and F. Pollmann, Phys. Rev. B **94**, 161109 (2016).
[41] D. L. Shepelyansky, Phys. Rev. Lett. **73**, 2607 (1994).
[42] K. Frahm, EPJ B **10**, 371 (1999).
[43] D. O. Krimer, R. Khomeriki, and S. Flach, JETP Letters **94**, 406 (2011).
[44] M. V. Ivanchenko, T. V. Laptyeva, and S. Flach, Phys. Rev. B **89**, 060301 (2014).
[45] I. V. Ponomarev and P. G. Silvestrov, Phys. Rev. B **56**, 3742 (1997).
[46] K. M. Frahm, EPJ B **89**, 115 (2016).
[47] M. Ganahl, E. Rabel, F. H. L. Essler, and H. G. Evertz, Phys. Rev. Lett. **108**, 077206 (2012).
[48] T. Fukuhara, P. Schauß, M. Endres, S. Hild, M. Cheneau, I. Bloch, and C. Gross, Nature **502**, 76 (2013).
[49] R. Steinigeweg, J. Herbrych, X. Zotos, and W. Brenig, Phys. Rev. Lett. **116**, 017202 (2016).
[50] T. A. Elsayed and B. V. Fine, Phys. Rev. Lett. **110**, 070404 (2013).
[51] P. Jordan and E. Wigner, Z. Phys. **47**, 631 (1928).
[52] R. Steinigeweg, J. Gemmer, and M. Michel, Europhys. Lett. **75**, 406 (2006).
[53] T. V. Laptyeva, J. D. Bodyfelt, D. O. Krimer, C. Skokos, and S. Flach, EPL (Europhysics Letters) **91**, 30001 (2010).
[54] The build-up errors ϵ arising from the Runge-Kutta algorithm remain much smaller, due to the very small iteration step, than the symbol sizes we use. In fact $\epsilon \sim O(Ndt^4)$ where N denotes the number of iteration steps. See, e.g., Ref. 62 for details.
[55] E. Abrahams, P. W. Anderson, D. C. Licciardello, and T. V. Ramakrishnan, Phys. Rev. Lett. **42**, 673 (1979).
[56] M. Aizenman and S. Warzel, Commun. Math. Phys. **290**, 903 (2009).
[57] D. J. Luitz, N. Laflorencie, and F. Alet, Phys. Rev. B **93**, 060201 (2016).
[58] R. Steinigeweg, EPL **97**, 67001 (2012).
[59] R. Steinigeweg, J. Herbrych, P. Prelovšek, and M. Mierzejewski, Phys. Rev. B **85**, 214409 (2012).
[60] G. Dufour and G. Orso, Phys. Rev. Lett. **109**, 155306 (2012).
[61] R. Vlijm, M. Ganahl, D. Fioretto, M. Brockmann, M. Haque, H. G. Evertz, and J.-S. Caux, Phys. Rev. B **92**, 214427 (2015).
[62] A. E. Feiguin and S. R. White, Phys. Rev. B **72**, 020404 (2005).

Preprint version

Original publication: PRB, 95, 035155 (2017)
doi: 10.1103/PhysRevB.95.035155

Real-time broadening of non-equilibrium density profiles and the role of the specific initial-state realization

R. Steinigeweg,[1,*] F. Jin,[2] D. Schmidtke,[1] H. De Raedt,[3] K. Michielsen,[2,4] and J. Gemmer[1,†]

[1] *Department of Physics, University of Osnabrück, D-49069 Osnabrück, Germany*
[2] *Institute for Advanced Simulation, Jülich Supercomputing Centre, Forschungszentrum Jülich, D-52425 Jülich, Germany*
[3] *Zernike Institute for Advanced Materials, University of Groningen, NL-9747AG Groningen, The Netherlands*
[4] *RWTH Aachen University, D-52056 Aachen, Germany*

The real-time broadening of density profiles starting from non-equilibrium states is at the center of transport in condensed-matter systems and dynamics in ultracold atomic gases. Initial profiles close to equilibrium are expected to evolve according to linear response, e.g., as given by the current correlator evaluated exactly at equilibrium. Significantly off equilibrium, linear response is expected to break down and even a description in terms of canonical ensembles is questionable. We unveil that single pure states with density profiles of maximum amplitude yield a broadening in perfect agreement with linear response, if the structure of these states involves randomness in terms of decoherent off-diagonal density-matrix elements. While these states allow for spin diffusion in the XXZ spin-1/2 chain at large exchange anisotropies, coherences yield entirely different behavior.

PACS numbers: 05.60.Gg, 71.27.+a, 75.10.Jm

I. INTRODUCTION

The mere existence of equilibration and thermalization is a key issue in many areas of modern many-body physics. While this question has a long and fertile history, it has experienced an upsurge of interest in recent years [1] due to the advent of cold atomic gases [2] as well as due to the discovery of new states of matter such as many-body localized phases [3]. In particular, the theoretical understanding has seen substantial progress by the fascinating concepts of eigenstate thermalization [4–6] and typicality of pure quantum states [7–14] as well as by the invention of powerful numerical methods such as density-matrix renormalization group [15]. Much less is known on the route to equilibrium as such [16] and still the derivation of the conventional laws of (exponential) relaxation and (diffusive) transport on the basis of truly microscopic principles is a challenge to theory [17].

In strictly isolated systems any coupling to heat baths or particle reservoirs and any driving by external forces is absent. In such systems, the only possibility to induce a non-equilibrium process is the preparation of a proper initial state. While different ways of preparation can be chosen, a sudden quench of the Hamiltonian is a common preparation scheme [18]. However, once a specific state is selected, a crucial question is: To what extent is this state a non-equilibrium state? To answer this question, it is natural to measure the observable one is interested in. If the expectation value is far from equilibrium, the state should be also. If this value is close to equilibrium, the state should be correspondingly. Moreover, only in the latter case, the resulting dynamics of the expectation value and linear response theory are expected to agree with each other. While this line of reasoning is certainly intuitive, it neglects internal degrees of freedom of the initial state. In particular, the measurement of a single observable cannot detect if the underlying state is pure or mixed, entangled or non-entangled, etc. Therefore, an intriguing question is: Do such internal details play any role for the dynamics of an expectation value?

In this paper, we investigate exactly this question for the anisotropic spin-1/2 Heisenberg chain. Dynamics in this integrable many-body model has been under active scrutiny in various theoretical works and, in particular, spin dynamics constitutes a demanding problem resolved only partially despite much effort [19–40], even within the linear response regime and at high temperatures. While it has become clear that quasi-local conservation laws [25, 26] necessarily lead to ballistic behavior below the isotropic point, numerical studies [36–39] have reported signatures of diffusion above this point, in agreement with perturbation theory [39] and classical simulations [40].

To investigate spin transport, we first introduce a class of pure initial states. These initial states feature identical

* rsteinig@uos.de
† jgemmer@uos.de

density profiles, where a maximum δ peak is located in the middle of the chain and lies on top of a homogeneous background, similar to [38]. For a subclass with internal randomness we then show analytically that the resulting non-equilibrium dynamics can be related to equilibrium correlation functions via the concept of typicality. This relation is verified in addition by large-scale numerical simulations. These numerical simulations also unveil the existence of remarkably clean diffusion for large exchange anisotropies, as one of our central findings. Eventually, we demonstrate that entirely different behavior emerges without any randomness in the initial state.

II. MODEL AND OBSERVABLES

The Hamiltonian of the XXZ spin-1/2 chain with periodic boundary conditions reads

$$H = J\sum_{r=1}^{L}(S_r^x S_{r+1}^x + S_r^y S_{r+1}^y + \Delta S_r^z S_{r+1}^z)\,, \qquad (1)$$

where $S_r^{x,y,z}$ are spin-1/2 operators at site r, L is the number of sites, $J > 0$ is the antiferromagnetic exchange coupling constant, and $(\Delta - 1)$ is the anisotropy. For all parameters, this model is integrable in terms of the Bethe Ansatz and the total magnetization $S^z = \sum_r S_r^z$ is a strictly conserved quantity. We take into account all subsectors of S^z, i.e., we consider the case $\langle S^z\rangle = 0$. We note that, via the Jordan-Wigner transformation, this model can be mapped onto a chain of spinless fermions with particle interactions of strength Δ and total particle number $N = S^z + L/2$, i.e., $\langle N\rangle = L/2$ (see Appendix A for the half-filling case $N = L/2$).

We are interested in the non-equilibrium dynamics of the local occupation numbers $n_r = S_r^z + 1/2$. Specifically, we consider the expectation values $p_r(t) = \mathrm{tr}[n_r\,\rho(t)]$ for the density matrix $\rho(t)$ at time t. In this way, we study the time-dependent broadening of density profiles for a given initial state $\rho(0)$. In this paper, we focus on pure states $\rho(0) = |\psi(0)\rangle\langle\psi(0)|$.

III. INITIAL STATES

Obviously, it is possible to choose many different initial states $|\psi(0)\rangle$ and the resulting dynamics can depend on details of the specific choice. A frequently used preparation scheme is a quantum quench, i.e., $|\psi(0)\rangle$ is the eigenstate of another Hamiltonian. In this paper, however, we proceed in a different way.

To introduce our class of initial states, let $|\varphi_k\rangle$ be the common eigenbasis of all n_r, i.e., the Ising basis. Then, this class reads

$$|\psi(0)\rangle \propto n_{L/2}\,|\Phi\rangle\,, \quad |\Phi\rangle = \sum_{k=1}^{2^L} c_k\,|\varphi_k\rangle\,, \qquad (2)$$

where c_k are complex coefficients and $n_{L/2}$ projects onto Ising states with a particle in the middle of the chain. By construction, $p_{L/2}(0) = 1$ is maximum.

In the above class, a particular state is the one where all c_k are the same. It yields $p_{r\neq L/2}(0) = p_{\mathrm{eq.}} = 1/2$ and still $p_{L/2}(0) = 1$. Hence, its density profile has a δ peak on top of a homogeneous background. However, exactly this density profile also results when the c_k are drawn at random according to the unitary invariant Haar measure [11] (where real and imaginary part of the c_k are drawn from a Gaussian distribution with zero mean, as done in our numerical simulations perfomed below). In other words, it is impossible to distinguish the two states with equal and random coefficients by a measurement of their initial density profiles $p_r(0)$ [41]. Only at times $t > 0$, their density profiles $p_r(t)$ can be different, if these density profiles differ at all. Note that similar $p_r(0)$ have been studied in Ref. [38].

Because our initial states are pure and have maximum $p_{L/2}(0) = 1$ as well, these states have to be considered as far-from-equilibrium states. Thus, it is natural to expect that the resulting dynamics of $p_r(t)$ cannot be described by linear response theory. However, such a expectation turns out to be wrong for the case of random c_k. In this case, $|\Phi\rangle$ is a typical state [7–14], i.e., a trace $\mathrm{tr}[\bullet]$ can be approximated by the expectation value $\langle\Phi|\,\bullet\,|\Phi\rangle$ with high accuracy in large Hilbert spaces. Using this fact and exact math (see Appendix B for more details), we find the relation

$$p_r(t) - p_{\mathrm{eq.}} = 2\,\langle(n_{L/2} - p_{\mathrm{eq.}})(n_r(t) - p_{\mathrm{eq.}})\rangle\,, \qquad (3)$$

where $\langle\bullet\rangle = \mathrm{tr}[\bullet]/2^L$. This relation is a first main result of our paper. It unveils that the expectation value $p_r(t)$ of a far-from-equilibrium state is directly connected to a equilibrium correlation function. It is important to note that such a relation cannot be derived for the other case of equal c_k (see also Appendix C for the specific type of randomness).

Due to the above relation, it is also possible to connect our non-equilibrium dynamics to the Kubo formula. To this end, one has to define the spatial variance

$$\sigma(t)^2 = \sum_{r=1}^{L} r^2\,\delta p_r(t) - \Big[\sum_{r=1}^{L} r\,\delta p_r(t)\Big]^2 \qquad (4)$$

with $\delta p_r(t) = 2(p_r(t) - p_{\mathrm{eq.}})$ and $\sum_{r=1}^{L}\delta p_r(t) = 1$. Then, following Ref. [42], it is straightforward to show that the time derivative of this variance

$$\frac{\mathrm{d}}{\mathrm{d}t}\sigma(t)^2 = 2\,D(t) \qquad (5)$$

is given by the time-dependent diffusion coefficient

$$D(t) = \frac{4}{L}\int_0^t \mathrm{d}t'\,\langle j(t')j\rangle\,, \qquad (6)$$

where $j = \sum_{r=1}^{L} S_r^x S_{r+1}^y - S_r^y S_{r+1}^x$ is the well-known spin current. For $\Delta = 0$, $[j, H] = 0$ leads to $\mathcal{D}(t) \propto t$ such that

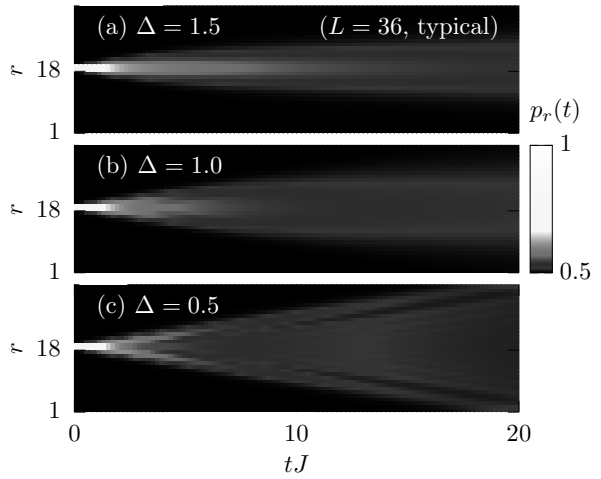

FIG. 1. (Color online) Time-space density plot of occupation numbers $p_r(t)$ for a *typical* initial state $|\psi(0)\rangle$ in the XXZ spin-1/2 chain with $L = 36$ sites and different anisotropies: (a) $\Delta = 1.5$, (b) $\Delta = 1.0$, (c) $\Delta = 0.5$. The broadening in (a) is consistent with a diffusive process while the broadening in (c) is ballistic.

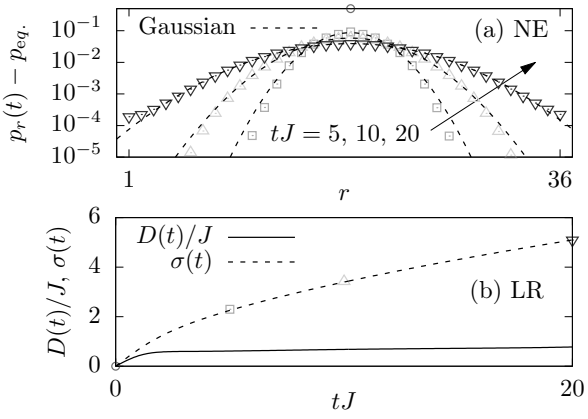

FIG. 2. (Color online) (a) Density profile $p_r(t)$ with respect to site r at fixed times $tJ = 0$, 5, 10, 20 for a single anisotropy $\Delta = 1.5$ (and the parameters in Fig. 1), shown in a semi-log plot (symbols). The Gaussian fits indicated describe the data very well over several orders of magnitude (curves). (b) Time dependence of diffusion coefficient $D(t)$ and profile width $\sigma(t)$ according to linear response theory, calculated in Ref. [31] for the same anisotropy $\Delta = 1.5$ and $L = 34$ sites (curves). For comparison, the standard deviation $\sigma(t)$ of the Gaussian fits in (a) is depicted (symbols).

$\sigma(t) \propto t^2$ scales ballistically. The partial conservation of j for $\Delta < 1$ [19–31] also excludes diffusive scaling $\sigma(t)^2 \propto t$ in this Δ regime. In fact, signatures of diffusion at high temperatures have been found only in the regime of large anisotropies $\Delta > 1$ [36–39]. Note that $\sigma(t)^2 \propto t$ is merely a necessary and no sufficient criterion for diffusion since, by definition, the variance yields no information beyond the width of the distribution $\delta p_r(t)$. This is why we study the full space dependence. For a recent numerical survey of Eq. (5), see [45].

IV. NUMERICAL METHOD AND RESULTS

Numerically, the time evolution of a pure state $|\psi(t)\rangle$ can be calculated by the method of full exact diagonalization. But this method is restricted to $L \sim 20$ sites, even if symmetries such as the translation invariance of H are taken into account. Thus, we proceed differently and rely on a forward propagation of $|\psi(t)\rangle$ in real time. Such a propagation can be done by the use of fourth-order Runge-Kutta [14, 30, 31] or more sophisticated schemes such as Trotter decompositions or Chebyshev polynomials [43, 44]. Here, we use a massively parallelized implementation of a Chebyshev-polynomial algorithm. In this way, we can treat system sizes as large as $L = 36$. For such L, we can guarantee that the initial δ peak is located sufficiently far from the boundary of the chain. Otherwise, we would have to deal with trivial finite-size effects and also Eq. (5) would not hold [42].

Next, we turn to our numerical results, starting with a typical initial state $|\psi(0)\rangle$, i.e., the case of random c_k. For a single realization of this state, we summarize in Fig. 1 the resulting expectation value $p_r(t)$ in a 2D time-space density plot for different anisotropies $\Delta = 1.5$, 1.0, 0.5 and a large system with $L = 36$ sites. Several comments are in order. First, for all values of Δ shown, the initial δ peak monotonously broadens as a function of time and the non-equilibrium density profiles have the irreversible tendency to equilibrate. Such equilibration is non-trivial in view of our isolated and integrable model. Second, for times below the maximum $tJ = 20$ depicted, the spatial extension of the density profiles is still smaller than the length of the chain. Thus, unwanted boundary effects do not emerge for such times. Third, the broadening of the density profiles is faster for smaller values of Δ because the scattering due to particle interactions decreases as Δ decreases. Moreover, for the small $\Delta = 0.5$ in Fig. 1 (c), the width of the density profile clearly increases linearly as a function of time. This linear increase is the expected ballistic dynamics arising from partial conservation of the spin current. In contrast, for the larger $\Delta = 1.5$ and 1.0 in Figs. 1 (a) and (b), the width of the density profiles does not increase linearly and is rather reminiscent of a square-root behavior. However, such a conclusion is not possible on the basis of a density plot.

To gain insight into the dynamics at $\Delta = 1.5$, we depict in Fig. 2 (a) the site dependence of the expectation values $p_r(t)$ at fixed times $tJ = 0$, 5, 10 and 20. Conveniently, we subtract the equilibrium value $p_{\text{eq.}}$ and use a semi-log plot to visualize also the tails of the density profiles. As illustrated by fits, the site dependence can be described by Gaussians (with $\sigma_{\text{f}}(t)$ as the only fit parameter)

$$p_r(t) - p_{\text{eq.}} = \frac{1}{2}\,\frac{1}{\sqrt{2\pi}\,\sigma_{\text{f}}(t)}\,\exp\left[-\frac{(r - L/2)^2}{2\,\sigma_{\text{f}}(t)^2}\right] \qquad (7)$$

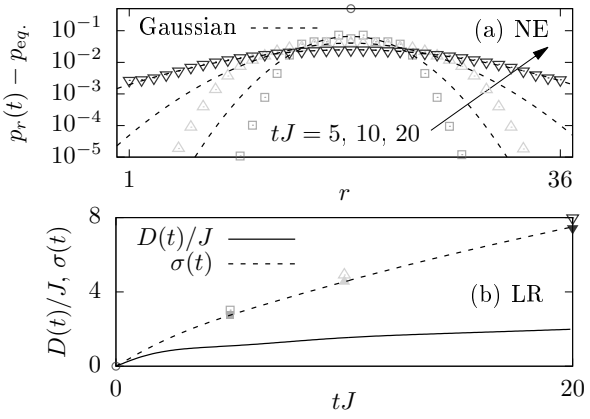

FIG. 3. (Color online) The same data as depicted in Fig. 1 but now for the anisotropy $\Delta = 1.0$. In (a) the Gaussian fits cannot describe the tails of the density profiles accurately. In (b) the standard deviation of these fits (open symbols) and according to Eq. (4) (closed symbols) still agrees with linear response; however, the time dependence is clearly inconsistent with diffusion. Note that finite-size effects are negligibly small, see Appendix D.

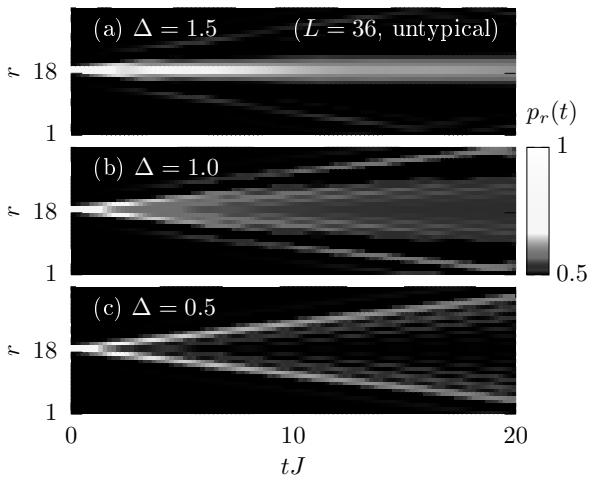

FIG. 4. (Color online) Time-space density plot of occupation numbers $p_r(t)$ for another and *untypical* initial state $|\psi(0)\rangle$ in the XXZ spin-1/2 chain with $L = 36$ sites and different anisotropies: $\Delta = 1.5$, (b) $\Delta = 1.0$, (c) $\Delta = 0.5$. Compared to Fig. 1, the dynamics is frozen in (a), similar to [33], and features pronounced jets in (c).

and, remarkably, over several orders of magnitude. Such a pronounced Gaussian form of the density profiles is a second main result of our paper and has, to best of our knowledge, not been reported in the literature yet. This result unveils that the standard deviation $\sigma_{\rm f}(t)$ is not just a width but also the only parameter required to describe the full site dependence. Furthermore, the Gaussian form is one of the clearest signatures of diffusion so far. Still, diffusion requires that $\sigma_{\rm f}(t)$ scales as $\sigma_{\rm f}(t) \propto \sqrt{t}$.

To further judge on diffusion, we show in Fig. 2 (b) the standard deviation $\sigma_{\rm f}(t)$, as resulting from the Gaussian fits in Fig. 2 (a). We further depict linear-response results for $\sigma(t)$ in Eq. (5) and the underlying $D(t)$ in Eq. (6), as calculated in Ref. [31] for $L = 34 \sim 36$. On the one hand, the excellent agreement shows the very high accuracy of the typicality relation in Eq. (3). On the other hand, this agreement demonstrates that the known linear-response result $\sigma(t) \propto \sqrt{t}$, resulting from $D(t) \approx$ const. at such t [31, 38, 39], also holds for our non-equilibrium density dynamics. Hence, together with the Gaussian form, we can conclude that diffusion exists.

An analogous analysis for the isotropic point $\Delta = 1.0$ in Fig. 3 (a) shows that simple Gaussians are not able to describe the tails of the density profiles accurately. This is why the standard deviation $\sigma_{\rm f}(t)$ of corresponding fits slightly deviates from the linear-response result in Fig. 3 (b). But these deviations disappear if $\sigma(t)$ is calculated exactly according to Eq. (4). Most notably, however, the time dependence of $\sigma(t)$ is inconsistent with diffusion, as can be seen easiest from the non-constant $D(t)$. In fact, $\sigma(t)$ points to superdiffusion [37, 40], contrary to [46].

Now, we turn to the untypical initial state $|\psi(0)\rangle$, i.e., the case of equal c_k. Recall that for this state we obtain the same initial density profile but the relations in Eqs. (3) and (5) do not need to hold. In Fig. 4 we summarize the resulting expectation values $p_r(t)$ in a 2D time-space density plot again. Compared to Fig. 1, the broadening turns out to be clearly different. The dynamics is frozen for $\Delta = 1.5$ in Fig. 4 (a) and features pronounced jets for $\Delta = 0.5$ in Fig. 4 (c). In particular, we do not find obvious indications of equilibration, at least for all times considered. These observations constitute a third main result of our paper. This result suggests that the lack of internal randomness in the initial condition is essential for the observation of non-equilibrium dynamics beyond linear response theory.

Finally, let us briefly mention another property of the untypical initial state $|\psi(0)\rangle$, which could be responsible for the special dynamics found. This property is the lack of entanglement. In fact, it is easy to see that $|\psi(0)\rangle$ can be written as the product state

$$|\psi(0)\rangle \propto \ldots (|\uparrow\rangle + |\downarrow\rangle) \otimes |\uparrow\rangle \otimes (|\uparrow\rangle + |\downarrow\rangle) \ldots \qquad (8)$$

with a spin-up state $|\uparrow\rangle$ in the middle of the chain and a spin-up/spin-down superposition $|\uparrow\rangle + |\downarrow\rangle$ at all other sites. By definition, such a product state is not entangled at all. In clear contrast, the typical initial state cannot be written as a product state.

V. CONCLUSIONS

In this paper, we have investigated the real-time broadening of non-equilibrium density profiles in the spin-1/2 XXZ chain. First, we have introduced a class of pure initial states with identical density profiles where a maximum δ peak is located in the middle of the chain. Then,

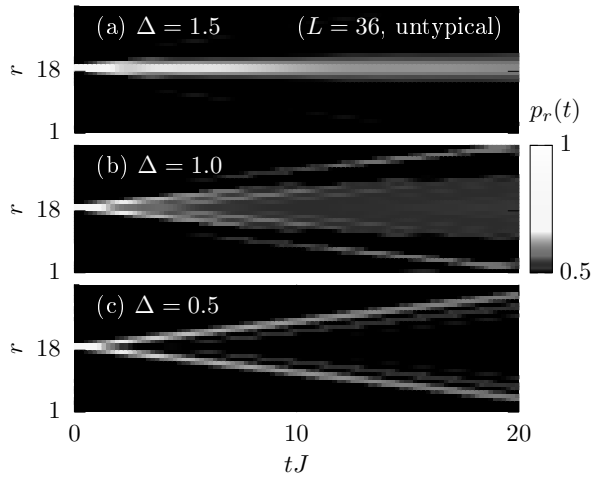

FIG. 5. (Color online) The same data as shown in Fig. 4 but now for the half-filling sector $S^z = 0$.

we have shown for a subclass with internal randomness that the resulting non-equilibrium dynamics can be connected to equilibrium correlation functions via the concept of typicality. This analytical result has been also verified by large-scale numerical simulations. These numerical simulations have further unveiled the existence of diffusion for large exchange anisotropies, as one of our key results. Finally, we have demonstrated that entirely different behavior emerges without any randomness in the initial state. Promising future directions of research include the identification of typical and untypical initial states in non-integrable models, in many-body localized phases, and at low temperatures as well as a systematic analysis of the role of entanglement.

ACKNOWLEDGMENTS

We sincerely thank T. Prosen and F. Heidrich-Meisner for fruitful discussions. In addition, we gratefully acknowledge the computing time, granted by the "JARA-HPC Vergabegremium" and provided on the "JARA-HPC Partition" part of the supercomputer "JUQUEEN" [47] at Forschungszentrum Jülich.

Appendix A: Half-Filling Sector

To demonstrate that our results do not depend on our specific choice of $\langle S^z \rangle = 0$, we do the calculation in, e.g., Fig. 4 again for the half-filling sector $S^z = 0$. We depict the corresponding results in Fig. 5. It is clearly visible that the real-time broadening of the expectation values $p_r(t)$ is practically the same, apart from minor details related to $p_{\text{eq.}} \approx 1/2$ in the half-filling case.

Appendix B: Typicality Approximation

Here, we provide details on the calculation leading to the relation in Eq. (3) of the main text. By carrying out the multiplication of the two brackets in the correlation function

$$C(t) = 2\,\langle (n_{L/2} - p_{\text{eq.}})(n_r(t) - p_{\text{eq.}})\rangle + p_{\text{eq.}} \tag{B1}$$

and applying $\langle n_r(t)\rangle = p_{\text{eq.}}$, we obtain

$$C(t) = 2\,\langle n_{L/2}\, n_r(t)\rangle = 2\,\frac{\text{tr}[n_{L/2}\, n_r(t)]}{2^L}\,. \tag{B2}$$

Using $n_{L/2}^2 = n_{L/2}$ and a cyclic permutation in the trace, we get

$$C(t) = 2\,\frac{\text{tr}[n_{L/2}\, n_r(t)\, n_{L/2}]}{2^L}\,. \tag{B3}$$

Exploiting typicality of the pure state $|\Phi\rangle$, the correlation function can be rewritten as

$$C(t) = 2\,\frac{\langle\Phi|\, n_{L/2}\, n_r(t)\, n_{L/2}\,|\Phi\rangle}{\langle\Phi|\Phi\rangle} + \epsilon \tag{B4}$$

with the small error $\epsilon \propto 2^{-L/2}$. Due to $n_{L/2}^\dagger = n_{L/2}$, this expression becomes

$$C(t) = 2\,\frac{\langle n_{L/2}\,\Phi|\, n_r(t)\,|n_{L/2}\,\Phi\rangle}{\langle\Phi|\Phi\rangle} + \epsilon \tag{B5}$$

and, due to $n_r(t) = e^{\imath Ht}\, n_r\, e^{-\imath Ht}$, it reads

$$C(t) = \frac{\langle e^{-\imath Ht}\, n_{L/2}\,\Phi|\, n_r\,|e^{-\imath Ht}\, n_{L/2}\,\Phi\rangle}{\langle\Phi|\Phi\rangle/2} + \epsilon\,, \tag{B6}$$

where we have moved in addition the factor 2 from the front to the denominator. Finally, due to the definition of $|\psi(0)\rangle$, we can write

$$C(t) = \langle\psi(t)|\, n_r\,|\psi(t)\rangle + \epsilon = p_r(t) + \epsilon\,. \tag{B7}$$

Therefore, comparing Eqs. (B1) and (B7) and skipping the small error ϵ for clarity yields

$$p_r(t) - p_{\text{eq.}} = 2\,\langle (n_{L/2} - p_{\text{eq.}})(n_r(t) - p_{\text{eq.}})\rangle\,. \tag{B8}$$

Appendix C: Specific Type of Randomness

As stated in the main text, the relations in Eqs. (3) and (5) have to be understood for typical states $|\Phi\rangle$ drawn at random according to the unitary invariant Haar measure (where real and imaginary part of the c_k are drawn from a Gaussian distribution with zero mean). However, it is instructive to consider other types of randomness. Thus, we choose

$$c_k \propto e^{\imath\,\alpha_k} \tag{C1}$$

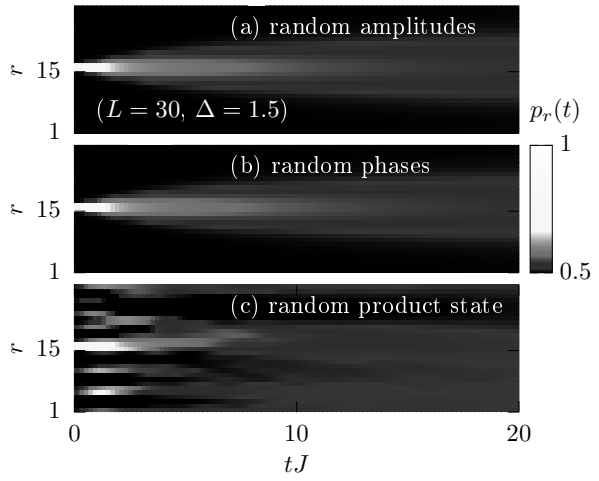

FIG. 6. (Color online) Time-space density plot of occupation numbers $p_r(t)$ in the spin-1/2 XXZ chain with $L = 30$ sites and a single anisotropy $\Delta = 1.5$ for three different types of randomness in the pure initial state: (a) random amplitudes, (b) random phases, (c) random product state; see text for the detailed definitions.

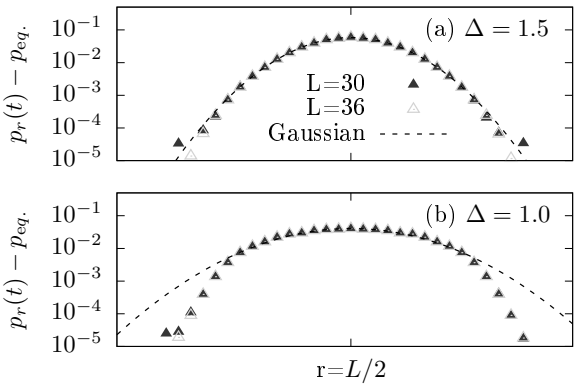

FIG. 7. (Color online) Density profile $p_r(t)$ with respect to site r at a single time $tJ = 10$ for the two system sizes $L = 30$ and $L = 36$ and for the two anisotropies (a) $\Delta = 1.5$ and (b) $\Delta = 1.0$ (symbols). Gaussian fits are indicated for comparison (curves).

with constant amplitudes $|c_k|^2$ and random phases α_k drawn from a uniform distribution $[0, 2\pi]$. In Fig. 6 (a) and (b) we compare the resulting real-time broadening of the expectation values $p_r(t)$ for this and the previous choice of the c_k, where we focus on a single anisotropy $\Delta = 1.5$ and restrict ourselves to a chain length $L = 30$ to reduce computational effort. The excellent agreement demonstrates that the specific type of randomness does not matter. Moreover, constant amplitudes $|c_k|^2$ as such are not responsible for the untypical dynamics observed in Fig. 4.

Note that not any kind of randomness can yield the same dynamical behavior. To illustrate this fact, let us randomize the product state in Eq. (8) of the main text in the following way: At all sites $r \neq L/2$ we replace the spin-up/spin-down superposition $|\uparrow\rangle + |\downarrow\rangle$ by

$$e^{\imath\,\alpha_r}\,|\uparrow\rangle + e^{\imath\,\beta_r}\,|\downarrow\rangle \tag{C2}$$

with site-dependent phases α_r, β_r drawn from a uniform distribution $[0, 2\pi]$. This randomized product state has still $p_{r\neq L/2}(0) = 1/2$ and $p_{L/2}(0) = 1$. It involves only $2(L-1)$ random numbers, in contrast to the state from the Haar measure with 2^L random numbers. In Fig. 6 (c) we depict the resulting dynamics of the expectation values $p_r(t)$. Compared to the two other random cases in Figs. 6 (a) and (b), the dynamical behavior turns out to be very different. This difference suggests again that the lack of entanglement could be the source of untypical dynamics.

Appendix D: Finite-Size Effects

Eventually, we show that our numerical results for the real-time broadening of the expectation values $p_r(t)$ are free of significant finite-size effects. To this end, we redo the $tJ = 10$ calculations in Figs. 2 (a) and 3 (a) for a smaller but still large system size $L = 30$. In Fig. 7 we depict the results of these calculations, together with the previous $L = 36$ data. It is clearly visible that finite-size effects are negligibly small and are not responsible for the non-Gaussian tails at the isotropic point $\Delta = 1.0$.

[1] J. Eisert, M. Friesdorf, and C. Gogolin, Nature Phys. **11**, 124 (2015).
[2] T. Langen, R. Geiger, and J. Schmiedmayer, Annu. Rev. Condens. Matter Phys. **6**, 201 (2015).
[3] R. Nandkishore and D. A. Huse, Annu. Rev. Condens. Matter Phys. **6**, 15 (2015).
[4] J. M. Deutsch, Phys. Rev. A **43**, 2046 (1991).
[5] M. Srednicki, Phys. Rev. E **50**, 888 (1994).
[6] M. Rigol, V. Dunjko, and M. Olshanii, Nature **452**, 854 (2008).
[7] J. Gemmer and G. Mahler, Eur. Phys. J. B **31**, 249 (2003).
[8] S. Goldstein, J. L. Lebowitz, R. Tumulka, and N. Zanghì, Phys. Rev. Lett. **96**, 050403 (2006).
[9] S. Popescu, A. J. Short, and A. Winter, Nature Phys. **2**, 754 (2006).
[10] P. Reimann, Phys. Rev. Lett. **99**, 160404 (2007).
[11] C. Bartsch and J. Gemmer, Phys. Rev. Lett. **102**, 110403 (2009); EPL (Europhys. Lett.) **96**, 60008 (2011).
[12] S. Sugiura and A. Shimizu, Phys. Rev. Lett. **108**, 240401 (2012).
[13] S. Sugiura and A. Shimizu, Phys. Rev. Lett. **111**, 010401 (2013).

[14] T. A. Elsayed and B. V. Fine, Phys. Rev. Lett. **110**, 070404 (2013).
[15] U. Schollwöck, Rev. Mod. Phys. **77**, 259 (2005); Ann. Phys. **326**, 96 (2011).
[16] P. Reimann, Nature Commun. **7**, 10821 (2016).
[17] M. Buchanan, Nature Phys. **1**, 71 (2005).
[18] F. H. L. Essler and M. Fagotti, J. Stat. Mech. Theor. Exp., 064002 (2016).
[19] B. S. Shastry and B. Sutherland, Phys. Rev. Lett. **65**, 243 (1990).
[20] B. N. Narozhny, A. J. Millis, and N. Andrei, Phys. Rev. B **58**, 2921R (1998).
[21] X. Zotos, Phys. Rev. Lett. **82**, 1764 (1999).
[22] J. Benz, T. Fukui, A. Klümper, and C. Scheeren, J. Phys. Soc. Jpn. **74**, 181 (2005).
[23] F. Heidrich-Meisner, A. Honecker, D. C. Cabra, and W. Brenig, Phys. Rev. B **68**, 134436 (2003).
[24] S. Fujimoto and N. Kawakami, Phys. Rev. Lett. **90**, 197202 (2003).
[25] T. Prosen, Phys. Rev. Lett. **106**, 217206 (2011).
[26] T. Prosen and E. Ilievski, Phys. Rev. Lett. **111**, 057203 (2013).
[27] J. Herbrych, P. Prelovšek, and X. Zotos, Phys. Rev. B **84**, 155125 (2011).
[28] C. Karrasch, J. H. Bardarson, and J. E. Moore, Phys. Rev. Lett. **108**, 227206 (2012).
[29] C. Karrasch, J. Hauschild, S. Langer, and F. Heidrich-Meisner, Phys. Rev. B **87**, 245128 (2013).
[30] R. Steinigeweg, J. Gemmer, and W. Brenig, Phys. Rev. Lett. **112**, 120601 (2014).
[31] R. Steinigeweg, J. Gemmer, and W. Brenig, Phys. Rev. B **91**, 104404 (2015).
[32] J. M. P. Carmelo, T. Prosen, and D. K. Campbell, Phys. Rev. B **92**, 165133 (2015).
[33] D. Gobert, C. Kollath, U. Schollwöck, and G. Schütz, Phys. Rev. E **71**, 036102 (2005).
[34] J. Sirker, R. G. Pereira, and I. Affleck, Phys. Rev. Lett. **103**, 216602 (2009); Phys. Rev. B **83**, 035115 (2011).
[35] S. Grossjohann and W. Brenig, Phys. Rev. B **81**, 012404 (2010).
[36] P. Prelovšek, S. El Shawish, X. Zotos, and M. Long, Phys. Rev. B **70**, 205129 (2004).
[37] M. Žnidarič, Phys. Rev. Lett. **106**, 220601 (2011).
[38] C. Karrasch, J. E. Moore, and F. Heidrich-Meisner, Phys. Rev. B **89**, 075139 (2014).
[39] R. Steinigeweg and W. Brenig, Phys. Rev. Lett. **107**, 250602 (2011).
[40] R. Steinigeweg, EPL (Europhys. Lett.) **97**, 67001 (2012).
[41] Strictly speaking, by drawing c_k at random, it is possible to get the outcome $c_k = \text{const.}$ for all $k = 1, \ldots, 2^L$.
[42] R. Steinigeweg, H. Wichterich, and J. Gemmer, EPL (Europhys. Lett.) **88**, 10004 (2009).
[43] R. Steinigeweg, F. Heidrich-Meisner, J. Gemmer, K. Michielsen, and H. De Raedt, Phys. Rev. B **90**, 094417 (2014).
[44] F. Jin, R. Steinigeweg, F. Heidrich-Meisner, K. Michielsen, and H. De Raedt, Phys. Rev. B **92**, 205103 (2015).
[45] C. Karrasch, T. Prosen, and F. Heidrich-Meisner, arXiv:1611.04832 (2016).
[46] I. Khait, S. Gazit, N. Y. Yao, and A. Auerbach, Phys. Rev. B **93**, 224205 (2016).
[47] M. Stephan and J. Docter, J. Large-Scale Res. Facil. A1, 1 (2015).

Preprint version

Pre-print server: arXiv:1710.10871 (2017)
submitted to PRE

Stiffness of Probability Distributions of Work and Jarzynski Relation for Non-Gibbsian Initial States

Daniel Schmidtke,[1,*] Lars Knipschild,[1,†] Michele Campisi,[2] Robin Steinigeweg,[1] and Jochen Gemmer[1,‡]

[1] *Department of Physics, University of Osnabrück, D-49069 Osnabrück, Germany*
[2] *Dipartimento di Fisica e Astronomia, Università di Firenze and INFN Sezione di Firenze, via G. Sansone 1, I-50019 Sesto Fiorentino, Italy*

We consider closed quantum systems (into which baths may be integrated) that are driven, i.e., subject to time-dependent Hamiltonians. Our point of departure is the assumption that, if systems start in non-Gibbsian states at some initial energies, the resulting probability distributions of work may be largely independent of the specific initial energies. It is demonstrated that this assumption has some far-reaching consequences, e.g., it implies the validity of the Jarzynski relation for a large class of non-Gibbsian initial states. By performing numerical analysis on integrable and non-integrable spin systems, we find the above assumption fulfilled for all considered examples. Through an analysis based on Fermi's Golden Rule, we partially relate these findings to the applicability of the eigenstate thermalization ansatz to the respective driving operators.

I. INTRODUCTION

The long-standing question regarding whether, and in which way, closed finite quantum systems approach thermal equilibrium has recently gathered renewed attention. On the theoretical side thermalization and equilibration have been investigated e.g. for rather abstract settings [1–6] and also for more specific condensed-matter type systems [7–10]. In these works major concepts are the eigenstate thermalization hypothesis (ETH) and typicality, both of which will also play certain roles in the paper at hand. The developments of experiments on ultra-cold atoms now allow for testing what have been merely theoretical results before; see e.g. Ref. [11–13].
Rather than just the existence of equilibration within closed quantum systems, lately the very peculiarities of the dynamical approach to equilibrium have moved to the center of interest [11, 14]. Questions addressed in this context include limits on relaxation time scales and agreement of unitary quantum dynamics of closed quantum systems with standard statistical relaxation principles, such as Fokker-Planck equations [15–18], or more general, standard stochastic processes [19, 20]. But also the emergence of universal non-equilibrium behavior involving work and driven systems is under discussion at present [21].

To a large extent universal non-equilibrium behavior may be captured by fluctuation theorems, see e.g. Ref. [22] and references therein. The Jarzynski relation (JR), a general statement on work that has to be invested to drive processes also and especially far from equilibrium, is a prime example of such a fluctuation theorem. Many derivations of the JR from various starting grounds have been presented. These include classical Hamiltonian dynamics, stochastic dynamics such as Langevin or master equations, as well as quantum mechanical starting points [22–27]. However, almost all these derivations assume that the system, that is acted on with some kind of "force", is strictly in a Gibbsian equilibrium state before the process starts. (The notion of "the system" here routinely includes the bath.) Thus, this starting point differs significantly from the progresses in the field of thermalization: There, the general features of thermodynamic relaxation are found to emerge entirely from the system itself without any necessity of evoking external baths or specifying initial states in detail. Clearly, the preparation of a strictly Gibbsian initial state requires the coupling to a bath prior to starting the process.

This situation renders the question whether or not the JR is valid for systems starting in other states than Gibbsian states rather exigent. Clarifying this question is the main purpose of the paper at hand. Since counterexamples may be constructed, there cannot be any affirmative answer without restrictions on the quantum system and the process protocol. However, previous works [28–31] have shown that, when the initial state is microcanonical, the JR does not follow, but a related entropy-from-work relation emerges instead. The question remains, however, if and under what conditions the JR holds approximately for non-canonical initial states. Thus, the emphasis in the search for the origins of the JR's validity

* danischm@uos.de
† lknipschild@uos.de
‡ jgemmer@uos.de

is shifted from specifying the initial state to specifying the nature of the system.

An intimately related question has lately also been addressed in Ref. [32]. There the validity of fluctuation theorems for typical pure initial states is traced back to certain features of the bath, including the existence of a "quantum speed limit" (Lieb-Robinson bound) within the bath. While this argument is certainly valid, it requires rather large baths to apply for enduring processes. In the examples discussed below, processes are too long and systems are too small to employ the argument given in Ref. [32] to explain the validity of the JR. Indeed the paper at hand offers a largely unrelated, alternative approach.

The paper at hand is organized as follows: Sect. II starts with the introduction of our basic hypothesis of probability distribution functions of work (work pdf's) being largely independent of the respective initial energy for microcanonical initial states. The validity of the JR is shown to follow from this assumption. In order to quantify this independence ("stiffness"), we discuss an appropriate measure which is one main target of the later numerical investigations. In Sect. III we describe our spin models as well as the specific microcanonical initial states and the general form of the work-inducing protocols. After these introductive sections we finally present in Sect. IV and V the numerical results on the stiffness of the work pdf's and verify the asymptotic validity of the JR directly. In order to provide indications that our results may be understood by more fundamental concepts, i.e., Fermi's Golden Rule (FGR) and eigenstate thermalization hypothesis, we also present matrix representations of the driving operators and discuss them in Sect. VI. At last we briefly summarize in Sect. VII and draw conclusions.

II. STIFFNESS OF WORK PDF'S AND JARZYNSKI RELATION FOR NON-GIBBSIAN INITIAL STATES

The analysis at hand focuses exclusively on closed systems. While it is physically appropriate to interpret the examples in Sect. III in terms of "considered system" and "environment" or "bath", we technically treat the system+environment compound regardless of the coupling strength as one closed system. Thus, since there is no external source or sink of heat, any energy change of the full system is to be counted as work W (for an overview over different perspectives, see e.g. Ref. [33].) In this respect we choose the same starting point as employed in derivations of the JR as described, e.g., in Ref. [31] and references therein. However, while in Ref. [31] the assumption of a canonical, Gibbsian initial state is of vital importance, we base our consideration on much larger classes of initial states of the full system. The central role which the assumption of a strictly Gibbsian state plays in the aforementioned works is replaced by the assumption of "stiffness" of the work pdf's [as introduced in detail below in Eq. (5)].

A. Stiffness of Work pdf's and Jarzynski Relation for Microcanonical Initial States

We now embark on the detailed presentation of our approach to a derivation of the JR for microcanonical initial states. Our initial states are given in terms of projection operators $\pi^{\alpha}_{E,\sigma}$. These $\pi^{\alpha}_{E,\sigma}$ are spanned by the energy eigenstates of some Hamilton operator H_α, featuring eigenvalues from the interval $[E-\sigma/2, E+\sigma/2]$. The "shell width" σ is supposed to be small compared to any physical energy scale in the scenario described below [34]. The parameter α may take on the values i, f, indicating "initial" and "final", respectively. The microcanonical initial states $\rho_i(E)$ may then be simply written as:

$$\rho_i(E) := \pi^{i}_{E,\sigma}/\mathrm{Tr}\{\pi^{i}_{E,\sigma}\} \quad . \tag{1}$$

The considered process is driven by a time-dependent Hamiltonian $H(t)$. We denote the duration of the driving by T such that $H_i = H(0)$ and $H_f = H(T)$. For later reference we also introduce the Hamiltonian $\tilde{H}(t)$ which implements the "backward protocol" as $\tilde{H}(t) := H(T-t)$. The forward protocol induces a unitary time-propagation operator $\mathbf{U}(t)$ defined by:

$$\mathbf{U}(t) := \mathcal{T} \exp\left(-i \int_0^t H(t')dt'\right) \quad , \tag{2}$$

where $\mathcal{T}$ is the time-ordering operator and we tacitly set $\hbar = 1$. The time propagation for the backward protocol $\tilde{\mathbf{U}}(t)$ is defined by an completely analogous expression based on $\tilde{H}(t)$. Now we are set to define the work pdf for the forward protocol $p_E(W)$, namely the probability density with which the process consumes an amount of work W if the system was initialized at energy E and driven according to $H(t)$:

$$p_E(W) := \frac{1}{\delta}\mathrm{Tr}\{\pi^{f}_{E+W,\delta}\, \mathbf{U}(T)\, \rho_i(E)\, \mathbf{U}^{\dagger}(T)\} \tag{3}$$

Here, δ is the energy resolution of the work pdf. For reasonable results it is chosen large compared to the level spacing of the full system, but small compared to the involved energy scales of E, W. We assume that a range of such δ exists for which $p_E(W)$ indeed becomes approximately independent of δ. (All our numerical investigations at hand agree with this assumption, see Appendix A). Obviously, $p_E(W)$ may equally well be simply perceived as the transition probability density with which the full system ends up at energy $E + W$ if it started at E under the forward driving. By $\tilde{p}_{E'}(W')$ we denote the corresponding work pdf for the backward protocol. Its definition is completely analogous to Eq. (3), but with the replacements $E \to E', W \to W', \mathbf{U}(T) \to \tilde{\mathbf{U}}(T), i \leftrightarrow f$.

We remark that below in Eq. (5) we will assume a certain property of the work pdf's $p_E(W)$, $\tilde{p}_{E'}(W')$. While this assumption appears physically plausible, we want to emphasize that acquiring any information on the work pdf's requires the solution of the time-dependent Schrödinger equation for the full system, since Eq. (3) comprises the time propagation operator $\mathbf{U}(t)$. Computing the latter is in general accompanied by great numerical efforts, especially when the Hamiltonian is explicitly time-dependent and the underlying Hilbert space is high-dimensional, as is usually the case for relevant setups in this context; see e.g. Refs. [35, 36] and Appendix B. We further remark that a classical version of the approach at hand has already been mentioned and numerically addressed in [37].

Irrespective of the concrete forms of the work pdf's, microcanonical fluctuation theorems [28, 38] offer a connection between the work pdf's and the densities of states (DOS) Ω_α of the corresponding Hamiltonians H_α:

$$\frac{p_E(W)}{\tilde{p}_{E+W}(-W)} = \frac{\Omega_f(E+W)}{\Omega_i(E)} \quad . \tag{4}$$

This microcanonical fluctuation theorem is expected to hold for dynamics as generated by microreversible Hamiltonians $H(t)$ [30]. We note that the models analyzed below are not microreversible in the standard sense [30, 39], since they involve magnetic fields. However, due to a property which is somewhat similar to microreversibility, Eq. (4) applies to these models as well; for details see Appendix C.

Next we define a property of the work pdf's which we call "stiffness". We call a forward work pdf $p_E(W)$ stiff if does not depend on the initial energy E. Likewise we call a backward work pdf $\tilde{p}_{E+W}(-W)$ stiff if it does not depend on its initial energy $E+W$. To be more explicit, stiffness implies

$$p_E(W) = p_{E_0}(W) \quad , \quad \tilde{p}_{E+W}(-W) = \tilde{p}_{E_0}(-W) \quad , \tag{5}$$

where E_0 is some fixed, constant energy. Note that Eq. (5) is the central assumption from which the validity of the JR for microcanonical initial states will eventually be inferred. Of course, Eq. (5) is not expected to hold for all energies E. Here we only require that the relations in Eq. (5) hold for energies E from an energy interval $[E_0 - \Delta/2, E_0 + \Delta/2]$ such that

$$\int_{E_0-\Delta/2}^{E_0+\Delta/2} p_{E_0}(W)\, dW \approx 1 \; . \tag{6}$$

This means, the stiffness Eq. (5) must hold at least for an energy interval which is large enough to comprise almost the entire work pdf $p_{E_0}(W)$.

If the work pdf's are indeed stiff, Eq. (4) may be rewritten as

$$\frac{p_{E_0}(W)}{\tilde{p}_{E_0}(-W)} = \frac{\Omega_f(E+W)}{\Omega_i(E)} \quad . \tag{7}$$

Obviously, the l.h.s. of Eq. (7) no longer depends on energy E. This, however, restricts the possible functional forms of Ω_i, Ω_f to the following:

$$\Omega_i(U) \stackrel{!}{=} Z_i e^{\beta U}, \quad \Omega_f(U) \stackrel{!}{=} Z_f e^{\beta U} \quad , \tag{8}$$

where U parametrizes the inner energy and should not be confused with the previously introduced time propagation operator. (So far, Z_i, Z_f, β are just constants. Later on they will take the roles of partition functions and inverse temperature, respectively.) This implies that stiff work pdf's can only occur if the DOS's of the initial and the final Hamiltonian are both exponential in energy at least on the energy interval where the pdf's are non-negligible, with the same energy prefactor β. Note, however, that the converse does not hold, i.e., DOS's in agreement with Eq. (8) do by themselves neither imply stiffness of the work pdf's, nor the validity of the JR for microcanonical initial states.

Note furthermore that the form of the DOS in Eq. (8) implies that the respective systems are actually thermal reservoirs in the following sense: According to a standard definition of (inverse) temperature [cf. below Eq. (15)] the temperatures of H_i, H_f are constant over the energy regime set by the possible amounts of work, W. This also elucidates for what general type of physical scenario the validity of Eq. (8) may be reasonably be expected.

Plugging Eq. (8) back into Eq. (4) and rearranging a little yields:

$$\tilde{p}_{E+W}(-W) = p_E(W)\frac{Z_i}{Z_f}e^{-\beta W} \quad . \tag{9}$$

In general, the backward work pdf's do not necessarily sum up to unity in the following sense [29]: $\int \tilde{p}_{E+W}(W)dW \neq 1$. However, under the assumption of stiffness of the backward work pdf's in Eq. (5), they do, i.e.,

$$\int \tilde{p}_{E+W}(-W)dW = \int \tilde{p}_{E_0}(-W)dW = 1 \quad . \tag{10}$$

Upon inserting Eq. (9) into Eq. (10) and rearranging one obtains

$$\int p_E(W)e^{-\beta W}dW = \frac{Z_f}{Z_i} \quad , \tag{11}$$

which formally is a JR for the work pdf's obtained by starting from microcanonical initial states, with the temperature replaced by a parameter describing the exponential growth of the DOS of the full system. As such Eq. (11) already represents the main result of the present section. Note that Eq. (11) holds for arbitrary processes and its r.h.s. only contains static, process-independent model parameters. However, in order to demonstrate even closer analogy with the standard JR, it remains to be explained in which sense the r.h.s of Eq. (11) may be considered as the familiar r.h.s of the standard JR,

$e^{-\beta\Delta F}$, where F is the free energy. Such an identification would hold if

$$-\frac{\ln Z_\alpha}{\beta} \stackrel{?}{=} F_\alpha \quad . \tag{12}$$

In order to judge whether or not Eq. (12) is justified, consider the logarithm of Eq. (8),

$$\ln \Omega_\alpha = \ln Z_\alpha + \beta U \quad . \tag{13}$$

If one identifies, along the lines of Boltzmann's original approach, the entropy S_α as

$$\ln \Omega_\alpha := S_\alpha \tag{14}$$

(where we tacitly set $k_B = 1$), one may convert Eq. (13) into

$$-\frac{\ln Z_\alpha}{\beta} = U - \frac{S_\alpha}{\beta}. \tag{15}$$

Note that, in accordance with Eq. (8), $\partial_U S_\alpha = \beta$, hence β has the meaning of inverse temperature, and the r.h.s. of Eq. (15) is accordingly the free energy F as introduced in standard textbooks on phenomenological thermodynamics. In this sense Eq. (12) indeed holds, which entails the rewriting of Eq. (11) in a form closer to the familiar one:

$$\langle e^{-\beta W} \rangle_E = e^{-\beta \Delta F} \quad , \tag{16}$$

where $\langle \cdots \rangle_E$ denotes the microcanonical expectation value corresponding to energy E. This concludes our consideration on the validity of a JR for microcanonical initial states under the assumption of stiff work pdfs.

While we argue below that the JR holds for an even larger class of initial states, the following sections may be skipped and reading may be continued in Sect. II D for a first overview.

B. Typical Validity of Jarzynski Relation for Random Pure States from an Energy Shell

So far, only microcanonical initial states that are diagonal in the energy eigenbasis of the initial Hamiltonian have been considered. However, some arguments related to "typicality" suffice to establish that, given the validity of Eq. (5), the validity of a JR will hold, even for a very large majority of pure states. Consider to this end pure states $|\psi_{E,\sigma}\rangle$ which are drawn at random according to the unitary invariant Haar measure from the Hilbert space spanned by the projector $\pi^i_{E,\sigma}$. The corresponding work pdf is then given by

$$p_E(W) := \frac{1}{\delta} \langle \psi_{E,\sigma} | \mathbf{U}^\dagger(T) \pi^f_{E+W,\delta} \, \mathbf{U}(T) | \psi_{E,\sigma} \rangle \, . \tag{17}$$

Of course, here $p_E(W)$ technically depends on the specific $|\psi_{E,\sigma}\rangle$. However, employing the methods and results of "typicality" [40, 41] one finds for the "Hilbert-space average" (HA[...]) of $p_E(W)$ over the above $|\psi_{E,\sigma}\rangle$

$$\mathrm{HA}[p_E(W)] = \frac{1}{\delta} \mathrm{Tr}\{\pi^f_{E+W,\delta} \, \mathbf{U}(T) \, \rho_i(E) \, \mathbf{U}^\dagger(T)\} \, , \tag{18}$$

which equals the corresponding result for the mixed, microcanonical initial state $\rho_i(E)$, cf. Eq. (3). While this finding points in the direction of the JR being fulfilled for the vast majority of the $|\psi_{E,\sigma}\rangle$, it is, by itself, not sufficient to conclude for the latter. In order to do so, it remains to be shown that the corresponding "Hilbert-space variances" (HV[...]) is small. Expressions for such Hilbert space variances may also be found in the literature [40, 41]. Prior to computing these expressions for the current case, we introduce some convenient notation. Let $\Sigma^2(A)$ denote the variance of the spectrum of some operator A, with A being Hermitian, i.e., featuring real eigenvalues. Then the Hilbert-space variance for the work pdf is given by [40, 41]:

$$\mathrm{HV}[p_E(W)] = \frac{\Sigma^2(\pi^i_{E,\sigma} \mathbf{U}^\dagger(T) \pi^f_{E+W,\delta} \, \mathbf{U}(T) \pi^i_{E,\sigma})}{\mathrm{Tr}\{\pi^i_{E,\sigma}\} + 1} \tag{19}$$

Since the operator for which the spectral variance has to be determined contains only projectors and unitaries, i.e., has only eigenvalues between zero and one, an upper bound on the spectral variance is readily found:

$$\sigma^2(\pi^i_{E,\sigma} \mathbf{U}^\dagger(T) \pi^f_{E+W,\delta} \, \mathbf{U}(T) \pi^i_{E,\sigma}) < 1 \tag{20}$$

(This bound may easily be tightened, but this is of no further relevance here). This yields an upper bound for the Hilbert-space variance

$$\mathrm{HV}[p_E(W)] < \frac{1}{\mathrm{Tr}\{\pi^i_{E,\sigma}\} + 1} \, . \tag{21}$$

The crucial quantity here is obviously $\mathrm{Tr}\{\pi^i_{E,\sigma}\}$ which is just the number of eigenstates of the initial Hamiltonian H_i within the energy interval of size σ around E. For any finite σ it is to be expected that this number of eigenstates increases quickly (exponentially) with increasing bath size. Hence, for large baths $\mathrm{HV}[p_E(W)]$ becomes very small, thus rendering the outcome for $p_E(W)$ for the overwhelming majority of individual $|\psi_{E,\sigma}\rangle$'s indeed very close to the outcome one obtains from the microcanonical initial state $\rho_i(E)$. Or, to rephrase, all above findings on microcanonical initial states $\rho_i(E)$ transfer to pure initial states $|\psi_{E,\sigma}\rangle$for all practical purposes. In this sense the JR also applies to very many pure states. Moreover, this principle underlies all numerical calculations of work pdf's for large systems presented in the paper at hand. Time evolutions of a mixed states $\rho_i(E)$ are simply replaced by the time evolution of a randomly drawn, pure $|\psi_{E,\sigma}\rangle$, since the latter are numerically much less costly, cf. Appendix B.

C. Energetically Broader Initial States

Next we discuss the generalization of the validity of the JR for initial states which live within the region to which the stiffness assumption Eq. (5) applies. For conciseness we only discuss generalized diagonal (w.r.t. H_i) initial states. However, the generalization to corresponding typical pure states analogous to the considerations in Sect. II B is straightforward. Such a more general initial state R_i may be written as

$$R_i := \sum_n K(E_n)\rho_i(E_n), \quad \sum_n K(E_n) = 1 \quad , \tag{22}$$

where the $K(E_n)$ are the probabilities to find the system initially in the energy interval around E_n. As mentioned above, the work pdf's $p_E(W)$ may be viewed as conditional probability densities. Thus, the total probability density $p(W)$ to invest the work W is given by

$$p(W) = \sum_n K(E_n) p_{E_n}(W) \quad . \tag{23}$$

Computing the average exponential of work thus yields

$$\begin{aligned} \int p(W) e^{-\beta W} dW &= \sum_n K(E_n) \int p_{E_n}(W) e^{-\beta W} dW \\ &= \sum_n K(E_n) \frac{Z_f}{Z_i} = \frac{Z_f}{Z_i} \quad , \end{aligned} \tag{24}$$

where we used Eqs. (23), (22) and (11). This concludes the reasoning for the validity of the JR for more general, diagonal initial states.

D. Quantifying Stiffness

Prior to investigating specific models and protocols in Sect. III, we now introduce a measure that allows us to quantify the "quality" of stiffness for specific cases in Sect. IV and V. By making use of well-tailored numerical techniques we are able to compute the work pdf's $p_E(W), \tilde{p}_{E+W}(-W)$ at reasonable expense for system sizes that allow for significant results; see below for details. (For conciseness we formally introduce the "stiffness quantifier" $\bar{\chi}$ for the forward processes only.) The difference of two work pdf's $p_E(W)$, $p_{E'}(W)$ induced by the same protocol, but for two different microcanonical initial states may most simply be quantified as

$$\chi(E, E') := \int \left[p_{E'}(W) - p_E(W)\right]^2 dW \quad . \tag{25}$$

Evidently, the $\chi(E, E')$ are positive by construction. The mean difference of the work pdf's as resulting from microcanonical initial states from an energy region of size Δ around a central energy E_0 [cf. paragraph above Eq. (6)] from the work pdf corresponding to the initial state living at E_0 may be written as

$$\bar{\chi} := \frac{1}{\Delta} \int_{E_0 - \Delta/2}^{E_0 - \Delta/2} \chi(E_0, E') dE' \quad . \tag{26}$$

Since all $\chi(E, E')$ are positive, a small $\bar{\chi}$ not only implies a small average, but also that most of the respective $\chi(E, E')$ must be individually small. Or, to rephrase, if one had $\bar{\chi} = 0$, this would be sufficient to infer that $\chi(E_0, E') = 0$. Thus below we employ $\bar{\chi}$ as a reliable stiffness quantifier or, more specific, $\bar{\chi} \ll 1$ signals stiff work pdf's.

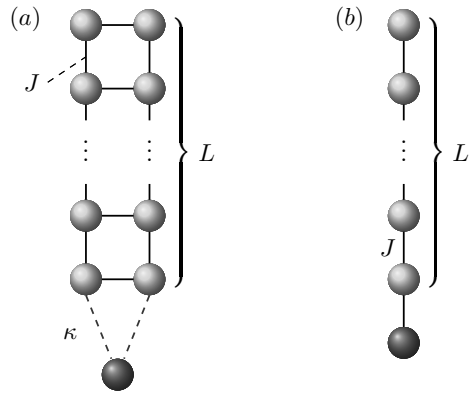

FIG. 1. Sketches of the spin models. (a) displays a spin ladder (green dots) acting as bath for an additional spin (red dot) which is coupled to the ladder with strength κ. Each leg of the ladder consists of L spins. (b) displays an isotropic spin chain (green dots) also consisting of L spins. Here the additional spin just enlarges the chain by one site.

III. MODELS, INITIAL STATES, AND DRIVING PROTOCOL

In the paper at hand, we focus our investigation on models that can be associated to actual spin resonance experiments (see e.g. [42, 43]). For this purpose we consider an isotropic Heisenberg spin–1/2 ladder (denoted as "bath") to which we attach an additional spin–1/2 as displayed in Fig. 1(a). Non-integrable spin ladders (in the sense of the Bethe ansatz) and derivates of it are already intensively studied regarding e.g. relaxation of magnetization [17, 18, 20] or energy imbalances [44, 45] and thus are ideal systems to start with. Note that, in order to allow for a non-trivial resonant driving protocol, we apply also a static magnetic field on the additional spin.

Furthermore, we investigate a second model, which stands in contrast to the first, where we drop (i) the non-integrability, (ii) the "distinction" between bath and system, and (iii) the resonant driving. This results here in a simple spin–1/2 chain as displayed in Fig. 1(b). In both cases we allow only for next neighbor interactions.

The bath Hamiltonian for the ladder model reads

$$H'_{\text{ladder}} = J\sum_{r=1}^{2}\sum_{i=1}^{L-1}\left(S^x_{i,r}S^x_{i+1,r} + S^y_{i,r}S^y_{i+1,r} + S^z_{i,r}S^z_{i+1,r}\right) + J\sum_{i=1}^{L}\left(S^x_{i,1}S^x_{i,2} + S^y_{i,1}S^y_{i,2} + S^z_{i,1}S^z_{i,2}\right) \quad , \tag{27}$$

where $S^{x,y,z}_{i,r}$ are spin–1/2 operators at site (i,r). Likewise, the bath Hamiltonian for the chain model reads

$$H'_{\text{chain}} = J\sum_{i=1}^{L-1}\left(S^x_i S^x_{i+1} + S^y_i S^y_{i+1} + S^z_i S^z_{i+1}\right) \quad . \tag{28}$$

In all cases, J denotes the exchange coupling constant which throughout this work is set to $J = 1$.
As seen in Fig. 1, for the ladder model we attach the additional spin in such a way that it only interacts with the last spin of each leg with coupling strength κ, whereas for the chain model the system spin simply enlarges the chain by one site. Thus, for the ladder model the bath-system interaction reads

$$H''_{\text{ladder}} = J\Big[(S^x_{L,1}+S^x_{L,2})S^x_{\text{sys}} + (S^y_{L,1}+S^y_{L,2})S^y_{\text{sys}} + (S^z_{L,1}+S^z_{L,2})S^z_{\text{sys}}\Big] \quad , \tag{29}$$

where $S^{x,y,z}_{\text{sys}}$ denote the respective spin–1/2 operators of the additional (system) spin. Furthermore, we apply a static magnetic field B in z direction onto the additional spin, i.e.,

$$H_{\text{mag}} = BS^z_{\text{sys}} \quad . \tag{30}$$

Finally, the whole time-independent Hamiltonian (at time $t = 0$) for the spin ladder model is given by

$$H^0_{\text{ladder}} := H'_{\text{ladder}} + \kappa H''_{\text{ladder}} + H_{\text{mag}} \quad . \tag{31}$$

In case of the chain model the bath-system interaction reads

$$H''_{\text{chain}} = J\left[S^x_L S^x_{\text{sys}} + S^y_L S^y_{\text{sys}} + S^z_L S^z_{\text{sys}}\right] \tag{32}$$

and hence the whole time-independent Hamiltonian for the chain model is

$$H^0_{\text{chain}} := H'_{\text{chain}} + H''_{\text{chain}} \quad . \tag{33}$$

In order to use hereafter a unified parameter denoting the corresponding system size of either model we introduce the total number of sites N. Thus, for the ladder model we have $N = 2L+1$ and for the chain model $N = L+1$.
Next we explain the driving protocol which is here a time-dependent magnetic field in x direction, applied onto the additional spin, similar to spin-resonance experiments; see e.g. [42, 43]. The time-dependent driving Hamiltonian reads

$$H_D(t,\nu) = \lambda\sin(\nu t)S^x_{\text{sys}} \quad , \tag{34}$$

where λ denotes the strength of the irradiation and ν its frequency. We remark here that for the ladder model we choose $\nu = B$ so that the driving is indeed resonant, whereas for the chain model where no static magnetic field is applied the protocol is inevitably non-resonant.

Finally we can state the time-dependent Hamiltonians describing the dynamics during the entire protocol as

$$H_{l/c}(t) = H^0_{l/c} + H_D(t,\nu) \quad , \tag{35}$$

where the subscript denotes either the ladder model (l) or the chain model (c).

Calculating work pdf's according to (3) for the above models and driving protocols is numerically rather costly. Thus we restrict the analysis to a few concrete implementations. This concerns concrete choices of the interaction strength κ and the magnetic field B for the ladder set-up, as well as the driving strength λ, the driving frequency ν, and the duration of the driving T for all set-ups. Choosing parameter sets which are, in the present context, most significant is rather subtle. For some "trivial" choices the JR may be fulfilled for reasons that are entirely unrelated to stiffness. E.g. one trivial limiting case features very strong driving λ together with very weak coupling κ. In this case the bath coupling may be neglected during the process. Hence, the JR is routinely fulfilled if the system spin is initially in a Gibbs state. The latter is to be expected for systems which fulfill the ETH and initial states which are (a mixture of) energy eigenstates of the full system. The other trivial limiting case features very weak driving togehter with very strong coupling. In this case the dynamics may remain in the adiabatical following regime. In order to simulate ladder-scenarios that are far away from these trivial cases we choose an approriate "weak" and a "strong" coupling strength, i.e., $\kappa_{\text{weak}}, \kappa_{\text{strong}}$ respectively. Furthermore, we choose two different driving strengths, i.e., λ_{weak} and λ_{strong}. (For details on the elaborate selection procedure of theese parameters see Appendix E). Though just the two combinations $(\kappa_{\text{weak}}, \lambda_{\text{weak}})$ and $(\kappa_{\text{strong}}, \lambda_{\text{strong}})$ are most far away from the trivial cases in this setup, we investigate all four possible combinations [46]. For the chain-scenario we also choose one specific "non-trivial" driving, cf. Appendix E. We apply the drivings for different durations T, but all T correspond to half-integer multiples of the respective driving periods. This way driving is cyclic and forward and backward protocols are actually the same. (For concrete parameter values, cf. captions of the respective figures below.)

At last we recall that our initial states are microcanoncical states as implemented by Eq. (1). Since generating such states requires exact diagonalization, which is only feasible for small systems, we employ for systems consisting of more than 15 spins an approximation scheme based on typicality that allows for computing energetically sharp states; cf. [36, 45, 47] and Appendix F. Likewise, work pdf's for large systems cannot be gained directly, i.e., we again need to employ an approximation

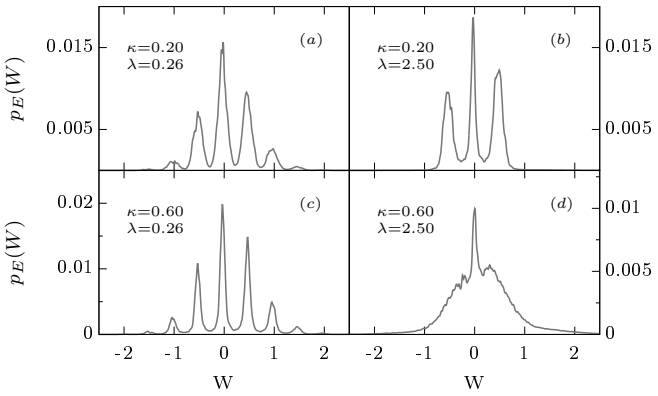

FIG. 2. Work pdf's for the ladder model for $N = 19$, $E \approx -3.2$ and all four combinations of $\kappa_{\text{weak}} = 0.2, \kappa_{\text{strong}} = 0.6$ and $\lambda_{\text{weak}} = 0.26, \lambda_{\text{strong}} = 2.5$. Note that for λ_{weak} the duration of the protocol is $T = 13\pi/\nu$ whereas for λ_{strong} it is only $T = \pi/\nu$. In all cases driving is resonant at $B = \nu = 0.5$.

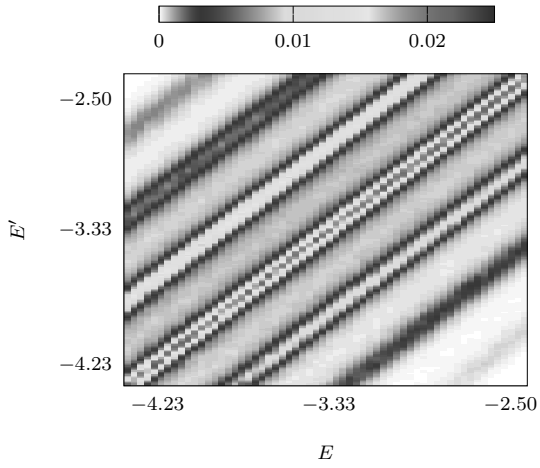

FIG. 3. Colormap of work pdf's ($N = 17$) corresponding to weak coupling and weak driving (for parameters, see Fig. 2). Displayed is the function $p_E(W = E' - E)$, cf. (3). The data indicate stiffness of the respective work pdf's.

scheme as discussed in Appendix D.

IV. PROBABILITY DISTRIBUTIONS OF WORK FOR THE SPIN-LADDER MODEL

With all parameters set, numerical simulations of the spin-resonance experiment as outlined in Sect. III can be performed and work pdf's according to Eq. (3) can be extracted. Some exemplary results are displayed in Fig. 2. The work pdf's for weak driving are qualitatively nicely interpretable in terms of time-dependent perturbation theory: Since the spin is resonantly exposed to radiation of frequency $\nu = 0.5$, energy may be absorbed or released in quanta of $\epsilon = 0.5$. This corresponds to the peaks appearing in distances of $\Delta W = 0.5$. If the irradiation endures, a second, third, etc. quantum of amount ϵ may be absorbed/released. Thus, more peaks appear at the sides, with decreasing intensity, though. The only work pdf that defies this interpretation is the one corresponding to strong interaction and strong driving [panel (d)]. Since the interpretation roots in time-dependent perturbation theory, this is hardly surprising. Note that the set-ups addressed in panels (a) and (d) are most far away from the two trivial limiting cases discussed in Appendix E, while the set-ups corresponding to panel (b) and (c) are much closer to them.

We now turn to the central question of the probability distributions being stiff. Fig. 3 shows a colormap of work pdf's corresponding to weak coupling and weak driving. Displayed is the function $p_E(W = E' - E)$, cf. (3). In this display style, a structure which is invariant w.r.t. translations along the diagonal of the graph indicates a stiff work pdf in the sense of Eq. (5). Thus qualitatively stiffness may already be inferred from Fig. 3. In order to investigate stiffness more thoroughly, we calculate the corresponding $\bar{\chi}$ according to Eq. (26) for different system sizes. The results are displayed in Fig. 4 for $E_0 \approx -0.2\,N$ and $\Delta = 2.5$. The data strongly indicate that in the limit of large systems the work pdf's indeed become strictly stiff, as $\bar{\chi}$ quickly tends to zero as $1/N \to 0$ ($N \to \infty$). This appears to be true for all cases considered, i.e., regardless of whether the coupling is weak or strong and regardless of whether the driving is weak or strong. This finding is a main result of the paper at hand.

As argued in Sect. II A, these results also render the JR valid for massively non-Gibbsian, e.g., microcanonical initial states. However, in order to demonstrate this directly, we display in Fig. 5 results for $\langle \exp(-\beta W) \rangle_E$. Since we consider cyclic processes, perfect agreement with the JR would yield $\langle \exp(-\beta W) \rangle_E = 1$. The data in Fig. 5 is obtained based on ≈ 50 (slightly differing with system size), energetically equidistant microcanonical initial states from the same energy regime which is also addressed in Fig. 4. As outlined in Sect. II A, we expect good agreement with the JR if β (inverse temperature) is chosen as the scaling exponent of the DOS, which is $\beta \approx 0.68$ for all considered system sizes here (see Appendix E). The symbols in Fig. 5 display the respective averages of the $\langle \exp(-\beta W) \rangle_E$ over the above microcanonical initial states, the "error bars" indicate the corresponding standard deviations. Clearly, the mean values tend towards 1 for large systems, in the same limit the standard deviations appear to vanish quickly, i.e., the data suggest agreement with the JR in the limit of infinitely long ladders.

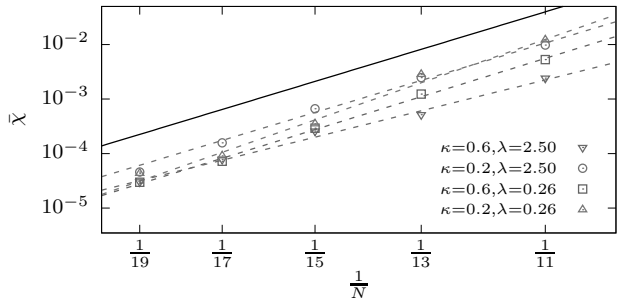

FIG. 4. Scaling of the stiffness of work pdf's with system size in a double logarithmic plot, system paremters as given in Fig. 2. Symbols correspond to $\bar{\chi}$. (Dashed lines indicate power-law fits and, as guide to the eye, the solid line indicates a power-law $\propto N^{-\alpha}$ with mean exponent w.r.t. these fits, i.e., $\alpha \approx 9.5$.) These data indicate stiffness in the limit of large system sizes for all considered system parameters.

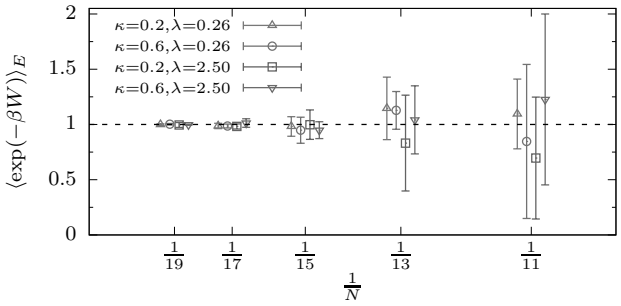

FIG. 5. Finite-size scaling of $\langle \exp(-\beta W) \rangle_E$ for microcanonical initial states and system parameters as given in Fig. 2. Displayed are averages (symbols) and standard deviations (bars) of $\langle \exp(-\beta W) \rangle_E$ for various microcanonical initial states from a certain energy regime, see text. As perfect agreement with the JR would result in $\langle \exp(-\beta W) \rangle_E = 1$, the data suggest increasing agreement with increasing system size.

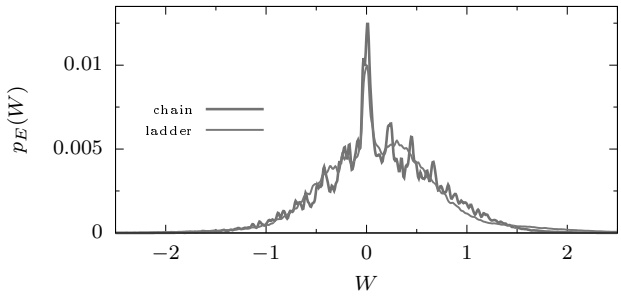

FIG. 6. Work pdf for the driven chain model for $N = 19$ and $E \approx -3.4$. The protocol parameters are $\lambda = 3.85, \nu = 0.75, T = \pi/\nu$. For comparison the work pdf for the strongly coupled, strongly driven ladder model is also re-displayed. Apart from minor peaks in the work pdf of the chain model the general shape of both distributions is very similar, although the chain model is integrable and the ladder model is non-integrable; see text for details.

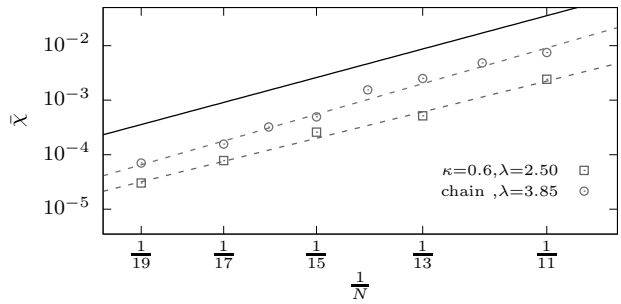

FIG. 7. Scaling of the stiffness of work pdf's with system size in a double logarithmic plot, system parameters as given in Fig. 6. Symbols correspond to $\bar{\chi}$. (Dashed lines indicate power-law fits and, as guide to the eye, the solid line indicates a power-law $\propto N^{-\alpha}$ with mean exponent w.r.t. these fits, i.e., $\alpha \approx 8.4$.) These data indicate stiffness in the limit of large system sizes for the chain model. For comparison the corresponding data for the strongly coupled, strongly driven ladder model is also re-displayed.

V. PROBABILITY DISTRIBUTIONS OF WORK FOR THE SPIN CHAIN MODEL

As in Sect. IV, we again calculate the work pdf's according to the prior identified parameters and display exemplarily in Fig. 6 for one fix initial energy a corresponding work pdf. For comparison, Fig. 6 also includes a work pdf for the strongly coupled and strongly driven ladder model ($\kappa_{\rm strong}, \lambda_{\rm strong}$). In order to analyze the stiffness of the work pdf's, we again compute $\bar{\chi}$ for increasing chain lengths and display the results in Fig. 7 (again along with the results for the strongly coupled, strongly driven ladder model). Here we used $E_0 \approx -0.18\,N$ and $\Delta = 2.5$. The behavior of stiffness of the work pdf's appears to be very similar to the one for the non-integrable ladder model. The data indicate that also for the integrable chain model the work pdf's become strictly stiff in the limit of large system sizes. This finding is another main result of the paper at hand. Just like in the case of the ladder model, it implies the validity of the JR also for massively non-Gibbsian, i.e., microcanonical initial states. Thus, evidently, this asymptotic validity is not restricted to chaotic models, otherwise it could not occur in a clean spin chain.

At last, similar to Sect. IV, we display in Fig. 8 data concerning $\langle \exp(-\beta W) \rangle_E$, in order to check the validity of the JR directly. Again we show averages (symbols) and standard deviations (vertical bars) of $\langle \exp(-\beta W) \rangle_E$ for a set of ≈ 50 (slightly differing with system size) microcanonical initial states from the energy regime which is also addressed in Fig. 7. Again, we expect good agreement with the JR if β is chosen as the scaling exponent of the DOS, cf. Sect. II A which is $\beta \approx 0.86$ for all considered chain model sizes here [see Appendix G]. (We

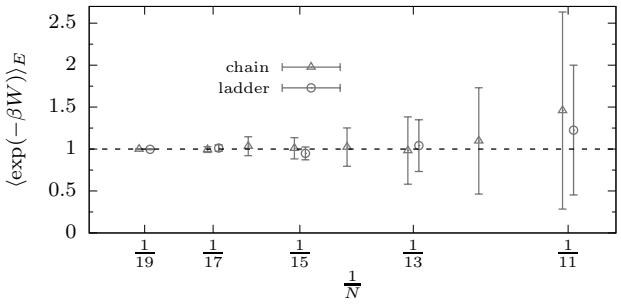

FIG. 8. Finite-size scaling of $\langle \exp(-\beta\, W) \rangle_E$ for microcanonical initial states and system parameters as given in Fig. 6. Displayed are averages (symbols) and standard deviations (bars) of $\langle \exp(-\beta\, W) \rangle_E$ for various microcanonical initial states from a certain energy regime, see text. As perfect agreement with the JR would result in $\langle \exp(-\beta\, W) \rangle_E = 1$, the data suggest increasing agreement with increasing system size.(The corresponding data for the strongly coupled, strongly driven ladder model are re-ploted for better comparability.)

also re-plot the results for the strongly coupled, strongly driven ladder model for comparison). The overall results for the chain set-up are very similar to those for the ladder set-up. However, in comparison to the ladder model the standard deviations for smaller system sizes are somewhat larger. Nevertheless, the data suggest validity of the microcanonical JR in the thermodynamic limit for the chain model also.

VI. STIFFNESS OF FERMI'S GOLDEN RULE RATES AND EIGENSTATE THERMALIZATION HYPOTHESIS

Since all the various examples addressed so far point to stiff work pdf's in the limit of large systems, the question arises whether this phenomenon can be made accessible by more general concepts. The present paragraph shows that this is indeed the case: If the driving operator agrees with the ETH-ansatz and the DOS is exponential, stiffness may indeed be expected, at least at weak driving. Recall that an exponential DOS in itself is not sufficient to justify this expectation.

As a first step in this direction we analyze the structure of the matrices that represent the driving operator $S^x_{\rm sys}$, displayed in the basis formed by the energy eigenstates of the non-driven system, i.e., $H^0_{\rm ladder}, H^0_{\rm chain}$. In the case of weak driving, a link between the work pdf's and the above driving matrices arises from Fermi's Golden Rule (FGR). As mentioned before, the work pdf's may simply be viewed as transition probabilities from energy E to energy $E+W$. In the weak-driving case, these transition rates may be well-described by rates as calculated from FGR which we denote by $\gamma_{E\to E'}$. The latter, however, have to be computed from the driving (perturbation) operator w.r.t. the above basis of energy eigenstates (for details, see below). Thus, if the actual dynamics are well captured by a FGR approach, the stiffness of the work pdf's implies a corresponding stiffness of the FGR rates, namely

$$\gamma_{E\to E'} \stackrel{!}{=} \gamma(E-E') \quad . \tag{36}$$

This can, however, only hold if the matrix representing the driving operator features a corresponding structure. (We investigate the structure of the corresponding matrix directly numerically in Appendix H.) In general, the FGR rate for the transition from an energy eigenstate $|i\rangle$ from a small interval around E into the set of eigenstates $\{|j\rangle\}$ that span the energy interval around E' under the influence of some (weak) driving of the form $H_D(t) = \sin(|E-E'|\,t)\,V$ (i.e. in our specific case $V = \lambda S^x_{\rm sys}$) is given by [39]

$$\gamma_{i\to E'} = \frac{2\pi}{\delta} \sum_{j\,\in\,E'} |V_{ij}|^2 \quad , \tag{37}$$

where $V_{ij} := \langle i|V|j\rangle$ and "$j \in E'$" is short for: "such that the energy eigenvalue of $|j\rangle$ lays in the interval of width δ around E'" (for the size of δ cf. Eq. (3) and below). In order to convert the transition probability from a single state to an energy interval, $\gamma_{i\to E'}$, to the transition probability from an energy interval to another energy interval, $\gamma_{E\to E'}$, one has to coarse grain, i.e., to average:

$$\gamma_{E\to E'} = \frac{1}{\delta\cdot\Omega(E)} \sum_{i\,\in\,E} \gamma_{i\to E'} \quad , \tag{38}$$

where the notation is completely analogous to that used in Eq. (37). Exploiting Eq. (37), a reformulation of Eq. (38) reads:

$$\gamma_{E\to E'} = \frac{2\pi}{\delta^2\cdot\Omega(E)} \sum_{\substack{i\,\in\,E\\ j\,\in\,E'}} |V_{ij}|^2 \tag{39}$$

Whether or not Eq. (36) applies obviously depends on the matrix elements V_{ij}. On one side, this can simply be checked for specific cases by computing the FGR rates according to Eq. (39) numerically. (Of course this requires the numerically exact diagonalization of the undriven Hamiltonians $H^0_{\rm ladder}, H^0_{\rm chain}$). On the other side, Eq. (39) can be used to show that the condition (36) is closely related to quantities occurring in the so-called ETH ansatz. The latter may be described as follows.

Within the framework of the ETH, it has been suggested that the matrix representation of a generic few-body operator V w.r.t the basis formed by the eigenstates $|n\rangle, |m\rangle$ of an Hamiltonian should be in accord with the following description [7, 48, 49]:

$$V_{mn} = \mathcal{V}(\bar{E})\,\delta_{mn} + \Omega\left(\bar{E}\right)^{-\frac{1}{2}}\, f\left(\bar{E},\omega\right)\, R_{mn} \quad , \tag{40}$$

where $\bar{E} = (E_m+E_n)/2$, $\omega = E_n - E_m$. Furthermore, both, $\mathcal{V}\left(\bar{E}\right)$ and $f\left(\bar{E},\omega\right)$, are assumed to be "smooth

functions of their arguments" [48] and R_{mn} may be "conveniently thought of as independent random variables with zero mean and unit variance" [48]. For a detailed discussion on the comparability of many-body Hamiltonians and random matrices see [50]. (To repeat: often and in all our examples, the R_{mn} are real.) For the purpose of the present investigation we interpret "smooth" in the sense of "approximately constant on the interval δ". Hence, we may equivalently define $\bar{E}, \omega$ on the basis of the interval labels rather than the individual energy eigenvalues as $\bar{E} := (E + E')/2, \omega = E - E'$. Plugging the ansatz in Eq. (40) into Eq. (39) yields

$$\gamma_{E\to E'} = \frac{2\pi}{\delta^2 \cdot \Omega(E)} \sum_{\substack{i \in E \\ j \in E'}} \frac{f^2\left(\bar{E},\omega\right) R_{ij}^2}{\Omega\left(\bar{E}\right)} \quad . \tag{41}$$

Since the summation runs over i, j, it essentially only concerns the R_{ij}^2 within the summand. The latter, however, are independent random numbers with variances normalized to unity. This implies that, to an accuracy set by the law of large numbers, the summation simply amounts to counting the number of terms whitin the sum, i.e.,

$$\sum_{\substack{i \in E \\ j \in E'}} R_{ij}^2 \approx \delta^2 \cdot \Omega(E) \cdot \Omega(E') \; . \tag{42}$$

Plugging (42) into (41) yields

$$\gamma_{E\to E'} \approx \frac{2\pi f^2\left(\bar{E},\omega\right) \Omega(E')}{\Omega\left(\bar{E}\right)} \quad . \tag{43}$$

In order to proceed further, we now specialize in exponential DOS's, i.e. , $\Omega(U) \propto e^{\beta U}$, as given in and argued for above Eq. (8). Doing so yields

$$\gamma_{E\to E'} \approx 2\pi f^2\left(\bar{E},\omega\right) e^{-\beta\omega}. \tag{44}$$

This unveils that the stiffness of the FGR rates (36) depends directly on $f^2\left(\bar{E},\omega\right)$. To be more specific: If $f^2\left(\bar{E},\omega\right)$ varies negligibly with $\bar{E}$ on an interval Δ as defined by Eq. (6), then the FGR rates are stiff, i.e., Eq. (36) applies, since then the r.h.s. of Eq. (44) only depends on ω. Hence, the approximate independence of $f^2\left(\bar{E},\omega\right)$ w.r.t. $\bar{E}$ is, together with an exponential DOS and the applicability of FGR, sufficient for the validity of the microcanonical JR at weak driving. This is a central result of the present section.

Motivated by the previous considerations, we proceed by numerically investigating the applicability of the ETH ansatz (40) to the driving operator S_{sys}^x for the ladder and the chain scenario. Particularly relevant is the function $f\left(\bar{E},\omega\right)$ and its dependence on $\bar{E}$. In order to visualize $f\left(\bar{E},\omega\right)$ from the respective matrix representation of S_{sys}^x, we use the construction

$$f(E',E) \propto \frac{\sum_{\substack{i \in E \\ j \in E'}} |V_{ij}| \sqrt{\Omega\left(\frac{E+E'}{2}\right)}}{\Omega(E')\Omega(E)} \quad . \tag{45}$$

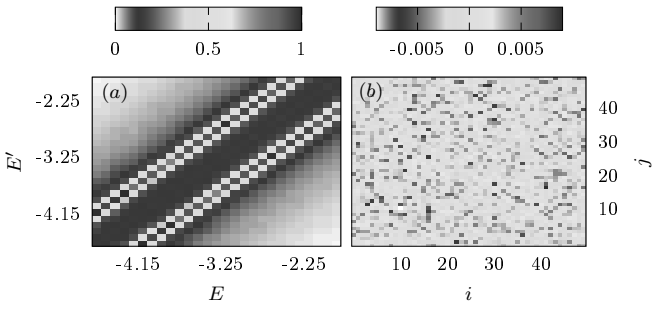

FIG. 9. (a) Vizualization of the ETH-related function $f(E', E)$ [according to Eq. (45)] corresponding to the S_{sys}^x operator for the ladder model ($N = 15, \kappa = 0.2$) for an exemplary energy section. (b) 50×50 matrix elements of the S_{sys}^x operator in energy basis of H_{ladder}^0 at $E \approx -3.1, E' \approx -3.3$.

In Fig. 9 (left panel) we display $f(E', E)$ for the weakly coupled ladder setup and $V \propto S_{\text{sys}}^x$. As varying $\bar{E}$ corresponds to moving parallel to the diagonal on the panel, it is obvious that $f(E', E)$ is indeed practically independent of $\bar{E}$. (Furthermore, Fig. 9(a) essentially reflects the weakly damped Larmor oscillations of the spin's x component). The right panel of Fig. 9 visualizes a small sector of the S_{sys}^x matrix on the level of individual matrix elements. Their values are plotted in false color against their indices. Without any further analysis it appears reasonable to interpret the individual matrix elements as independent random numbers in the sense of the R_{mn} from Eq. (40). Performing the same analysis for the integrable chain set-up produces data as displayed in Fig. 10. Again, the left panel visualizes $f(E', E)$ whereas the right panel shows individual matrix elements. Obviously, regardless of integrability, $f(E', E)$ appears to be independent of $\bar{E}$ to very good approximation, too. (Moreover, Fig. 10(a) essentially indicates the absence of any Larmor precession in this case and the comparatively quick decay of the S_{sys}^x autocorrelation function.) This, in the sense described above, explains the validity of the microcanonical JR in spite of integrability. On the level of individual matrix elements, however, the consequences of integrability are clearly visible: most matrix elements are strictly zero. Since the S_{sys}^x operator may only couple eigenstates from the same conserved subspaces, the many conservation laws of the spin chain render most matrix elements zero. However, if strictly ordered according to energy, as done here, the non-zero matrix elements appear at more or less random positions. Furthermore, their values appear to be random with zero mean. The results on the microcanonical JR suggest that these properties suffice for the applicability of FGR.

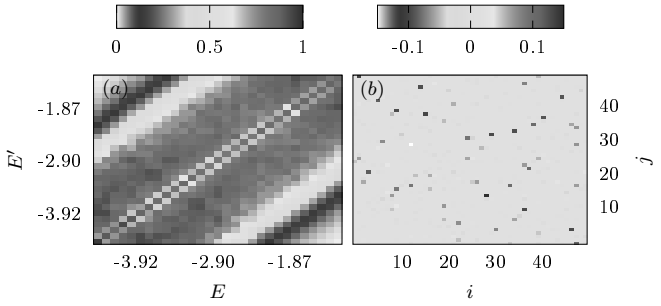

FIG. 10. (a) Vizualization of the ETH-related function $f(E', E)$ [according to Eq. (45)] corresponding to the $S^x_{\rm sys}$ operator for the chain model ($N = 15$) for an exemplary energy section. (b) 50×50 matrix elements of the $S^x_{\rm sys}$ operator in energy basis of $H^0_{\rm chain}$ at $E \approx -2.8, E' \approx -3$.

VII. SUMMARY AND CONCLUSION

In the paper at hand we investigated the question whether for closed systems (into which a bath may be included), that are driven and initially in a microcanonical state, the resulting work pdf's are independent of the actual initial energy. We find that this assumption, denoted as stiffness, can only hold if the DOS of the underlying system is strictly exponential w.r.t. energy. Furthermore, this assumption has far-reaching consequences, e.g., the validity of the Jarzynski relation for a large class of non-Gibbsian states. We studied the stiffness of work pdf's numerically for integrable and non-integrable spin models for various parameter sets. We found that (i) integrability seems to have no influence on the behavior of the stiffness of work pdf's and (ii) for all studied cases stiff work pdf's are expected in the thermodynamic limit. Eventually, we provided a study of the driving operator based on Fermi's Golden Rule which unveils a relation of our above findings to the applicability of the eigenstate thermalization hypothesis to the driving operator.

Lastly, we remark the connection of the present findings with the theory of ensemble equivalence in equilibrium statistical mechanics. It is known that for a very large system with an exponential DOS, equilibrium microcanonical and canonical expectations (with a corresponding temperature) of ordinary quantum observables coincide. Here we have been focussing rather on a non-ordinary two-point quantum observable (i.e. the work W), and on its statistics under a non-equilibrium setting. According, a non equilibrium object, namely the stiffness of the work pdf gives information about the DOS, and in turn about an equilibrium property, namely ensemble equivalence.

ACKNOWLEDGMENTS

This work has been funded by the Deutsche Forschungsgemeinschaft (DFG)-GE 1657/3-1; STE 2243/3-1. We sincerely thank the members of the DFG Research Unit FOR2692 for fruitful discussions.

Appendix A: Energy graining of final work pdf's

The exact work distribution $P_{E'}(W)$ after the driving protocol for an initial state starting at energy E' is given by

$$P_{E'}(W) = \sum_n |\langle E_n|\mathbf{U}(T)|E'\rangle|^2 \, \delta(W + E' - E_n) \quad . \tag{A1}$$

For any finite system the energy spectrum is discrete and thus initial states at different energies will in general yield different $P_{E'}(W)$. However, in the thermodynamic limit the energy spectra can be seen as quasi-continuous, i.e., Eq. (A1) may be replaced by

$$\begin{aligned} P_{E'}(W) &= \int dE'' \, |\langle E''|\mathbf{U}(T)|E'\rangle|^2 \, \delta(W + E' - E'') \\ &= |\langle E' + W|\mathbf{U}(T)|E'\rangle|^2 = c(E', W) \quad . \end{aligned} \tag{A2}$$

Since $c(E', W)$ is per definition continuous and normalized, we can interpret it as a work pdf, i.e., $p_{E'}(W) := c(E', W)$ as used in the main text. Note that in all cases studied, the energy spectra are far off from being (quasi-)continuous. Nevertheless, it is possible, by properly graining the resulting work distributions as calculated from Eq. (A1), to obtain distributions that behave like actual work pdf's, i.e., are independent of the graining parameter. To do so, we have to make sure that (i) the graining width δ (or energy resolution) is much smaller than the energy scale on which the details we are interested in appear and (ii) δ has to be larger than the individual level spacing of the energy spectrum. This gives us a lower and upper bound for δ where the lower bound decreases with increasing system size due to the exponential growth of the Hilbert space. As prior said, the main indication for a "good" graining parameter δ is given by the fact that the resulting work distribution will be mostly independent of the actual used δ. In order to demonstrate that this is indeed the case for the systems studied, we display for the ladder model ($N = 15$) in Fig. 11(a) the "ungrained" work distribution according to Eq. (A1) and in Fig. 11(b) exemplarily three grained work distributions for several distinct δ. The lower panel clearly suggests that the general shape of the work distribution is indeed independent of the actual choice of the graining parameter δ. Thus, we are able to interpret these distributions as accurate work pdf's. Note that fluctuation decrease as the system size increases as is the case in e.g. Fig. 2.

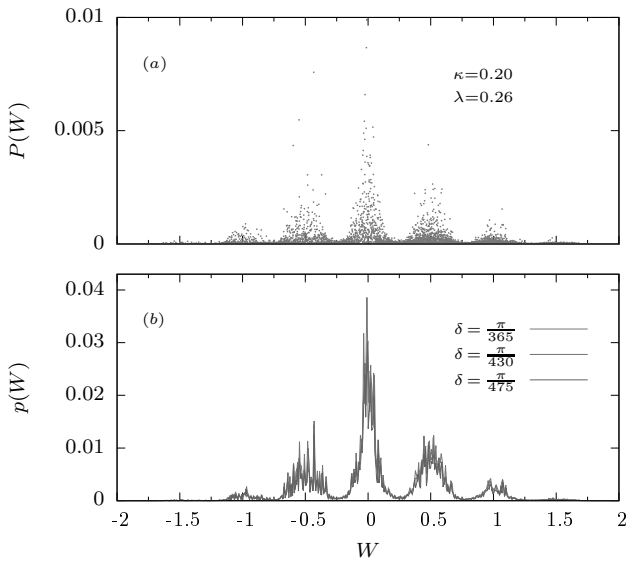

FIG. 11. (a) Discrete "ungrained" work distribution as calculated by Eq. (A1) and (b) "grained" work distributions for three distinct graining parameter δ for $N = 15$. All data for the ladder model. The grained versions suggest that the general behavior of the distribution becomes nearly independent of the actual choice of δ.

Appendix B: Solving the time-dependent Schrödinger equation (TDSE)

In the paper at hand we deal with time-dependent Hamiltonians, i.e., $H_{l/c}(t) = H^0_{l/c} + H_D(t,\nu)$ [cf. Eq. (35) in main text], where $H^0_{l/c}$ is the time-independent Hamiltonian that describes the whole system at $t = 0$, and $H_D(t,\nu)$ denotes the time-dependent driving operator [see main text Eq. (34)]. Since we do not need to distinguish between ladder and chain models as is necessary in the main text we omit hereafter the subscripts. Thus, the dynamics are governed by the TDSE

$$i\,\frac{\partial}{\partial t}|\psi(t)\rangle = H(t)\,|\psi(t)\rangle \quad , \tag{B1}$$

where $|\psi(t)$ denotes the wave function of the system and solutions may be written as

$$\begin{aligned} |\psi(t+\delta t)\rangle &= \mathbf{U}(t+\delta t,t)\,|\psi(t)\rangle \quad , \\ \mathbf{U}(t+\delta t,t) &= \mathcal{T}\exp\left(-i\int_t^{t+\delta t} H(t')dt'\right) \quad . \end{aligned} \tag{B2}$$

Note that we set $\hbar = 1$ here.
In general, getting these solutions is accompanied by extensive amounts of numerical efforts; see e.g. Refs. [35, 36]. Here we employ an iterative approximation scheme for small time steps δt.
To do so, we assume that for some sufficiently small δt the Hamiltonian can be considered as being constant during each time step, i.e., $H(t) \approx H(t+\delta t/2)$ on the interval $[t, t+\delta t]$. Then the iterative solutions for Eq. (B1) read

$$|\psi(t+\delta t)\rangle = \exp\left[-i\,H(t+\delta t/2)\,\delta t\right]\,|\psi(t)\rangle \quad . \tag{B3}$$

Hence, to solve the TDSE one can conveniently use any iteration scheme as long as the Hamiltonian fulfills the step-wise-constant condition.
Here we use a fourth-order Runge-Kutta iteration scheme [45, 47] where in each time step we recalculate the Hamiltonian, i.e., evaluate the present protocol terms $H_D(t+\delta t/2)$. In the following we sketch the general numerical process.

1. Calculate the initial Hamiltonian and the initial state, and store them into temporary objects, i.e., $H' = H(t=0)$ and $|\phi\rangle = |\psi(t=0)\rangle$
2. Evaluate the four temporary Runge-Kutta vectors

$$\begin{aligned} |\nu_1\rangle &= i\,\delta t\,H'\,|\phi\rangle \quad , \\ |\nu_2\rangle &= i\,\delta t/2\,H'\,|\nu_1\rangle \quad , \\ |\nu_3\rangle &= i\,\delta t/3\,H'\,|\nu_2\rangle \quad , \\ |\nu_4\rangle &= i\,\delta t/4\,H'\,|\nu_3\rangle \end{aligned} \tag{B4}$$

3. Collect all Runge-Kutta vectors to form the final state $|\psi(t+\delta t)\rangle = |\phi\rangle + |\nu_1\rangle + |\nu_2\rangle + |\nu_3\rangle + |\nu_4\rangle$
4. Recalculate H' and $|\phi\rangle$, i.e., $H' = H(t+\delta t)$ and $|\phi\rangle = |\psi(t+\delta t)\rangle$
5. Repeat 2-4 till the end of the protocol duration

For sufficiently small δt the accumulated error remains negligible; see e.g. [51].

Appendix C: Applicability of microreversibility to the models

As mentioned in the main text, Eq. (4) holds if the Hamiltonian of the system is microreversible. This requirement is sufficient, but not necessary. In this section we assume that $H(t)$ is a real, symmetric matrix for all times t regarding a basis $\mathfrak{B}$, which will be proven to be another sufficient condition in a way similar to microreversibility:

$$H(t) \equiv H(t)^* \tag{C1}$$

The matrices in this and in the subsequent equations, which depend on the concrete choice of a basis, are all meant regarding the basis $\mathfrak{B}$.
Before describing the details of the proof, we discuss briefly the ladder model again. This model is a spin system with a static magnetic field acting on a single spin of this system. This magnetic field breaks the microreversibility, cf. e.g. Ref. [39]. Nevertheless, the time-dependent Hamiltonian has a real, symmetric matrix representation with respect to the eigenbasis of the S^z_{sys}-operators of the spins (possible choice for $\mathfrak{B}$ in this case).

This can be easily seen by expressing the $S^x_{\rm sys}$ and $S^y_{\rm sys}$ by the respective creation and annihilation operators. Next we show that these conditions suffice to proof the validity of Eq. (4) even so the system is not microreversible. To this end we start from the left side of Eq. (4). By using Eq. (1) and (3) we find:

$$\begin{aligned}\frac{p_E(W)}{\tilde{p}_{E+W}(-W)} &= \frac{\mathrm{Tr}(\pi^f_{E+W,\delta})}{\mathrm{Tr}(\pi^i_{E,\delta})} Q \quad , \\ Q &= \frac{\mathrm{Tr}(\pi^f_{E+W,\delta} U \pi^i_{E,\delta} U^\dagger)}{\mathrm{Tr}(\pi^f_{E+W,\delta} \tilde{U}^\dagger \pi^i_{E,\delta} \tilde{U})}\end{aligned} \tag{C2}$$

In order to prove that Q is identical to 1 and thus Eq. (C2) becomes equivalent to Eq. (4), we complex-conjugate the numerator of Q, which does not affect its value:

$$Q = \frac{\mathrm{Tr}(\pi^f_{E+W,\delta} U^* \pi^i_{E,\delta} (U^\dagger)^*)}{\mathrm{Tr}(\pi^f_{E+W,\delta} \tilde{U}^\dagger \pi^i_{E,\delta} \tilde{U})} \tag{C3}$$

We used Eq. (C1), which implies that $\pi^f_{E+W,\delta}$ and $\pi^i_{E,\delta}$ have real representations regarding $\mathfrak{B}$ as well. In order to show that Q is identical to 1, we show that

$$U^* = \tilde{U}^\dagger \quad . \tag{C4}$$

We start from a more explicit form of the time-ordered exponential [52]:

$$\begin{aligned}\tilde{U}^\dagger &= \sum_{n=0}^{\infty} \frac{1}{n!} \tilde{W}^\dagger_n \quad , \\ \tilde{W}_n &= \int_{\mathfrak{X}^n} \mathrm{d}^n\tau \; \mathcal{T} \left[\prod_{j=1}^{n} (-i) \tilde{H}(\tau_j) \right] \quad , \\ \mathfrak{X}^n &= [0,t]^n\end{aligned} \tag{C5}$$

Firstly we calculate $\tilde{W}^\dagger_n$:

$$\tilde{W}^\dagger_n = \int_{\mathfrak{X}^n} \mathrm{d}^n\tau \; \tilde{\mathcal{T}} \left[\prod_{j=1}^{n} i \tilde{H}(\tau_j) \right] \tag{C6}$$

$\tilde{\mathcal{T}}$ is the inverse time-ordering operator. Next we replace $\tilde{H}$ with its definition and apply the following integral transformation:

$$\phi : \mathbb{R}^n \to \mathbb{R}^n, \tau_j \mapsto T - \tau_j \tag{C7}$$

Since $\phi^{-1}(\mathfrak{X}^n) = \mathfrak{X}^n$ and $|\det(\mathrm{d}\phi)| = 1$ the integral finally becomes:

$$\tilde{W}^\dagger_n = \int_{\mathfrak{X}^n} \mathrm{d}^n\tau \; \mathcal{T} \left[\prod_{j=1}^{n} i H(\tau_j) \right] = W^*_n \tag{C8}$$

W_n is defined in the same way as $\tilde{W}_n$, just for H instead of $\tilde{H}$. In the last step we used Eq. (C1) again. Thus, Eq. (C4) is valid where the necessity of microreversibility is replaced by the validity of Eq. (C1).

Generally, the fluctuation theorem holds whenever the Hamiltonian $H(t)$ is invariant under the action of an anti-unitary transformation K, at each time t. Combination of the property of invariance $[H(t), K] = 0$, and anti-unitarity of K (specifically the property $KuK^\dagger = u^*$ for any complex u [53]), imply that the instantaneous evolution be reversed by K, $Ke^{-iH(t)\delta}K^\dagger = e^{iH(t)\delta}$ with δ an arbitrary small real number. The latter, combined with the peculiar property $\mathrm{Tr}\, KAK^\dagger = \mathrm{Tr}\, A^\dagger$ of anti-unitary transformation (A being any trace class linear operator), is the crucial property that is employed in proving the fluctuation theorem, either in the microcanonical form of Eq. (4) or in the canonical form and as well in other forms [31, 54]. Thus invariance under time-reversal Θ (which is a anti-unitary operation) at each time t implies the validity of the fluctuation relation [31, 55]. In the case studies presented in the main text, even though a magnetic field is present, which breaks the time-reversal invariance, the Hamiltonian is invariant, at each time t, under the complex conjugation $K_{\mathfrak{B}}$ relative to the representation $\mathfrak{B}$ which is evidently an anti-unitary operator [53]. Accordingly the fluctuation theorem is obeyed. It is worth recalling, that generally, when a magnetic field B is present, $H = H(t, B)$, time reversibility breaks, but since $\Theta\; H(t, B) = H(t, -B)\; \Theta$ holds, the validity of the FT can be realised under the further provision that the magnetic field be reversed in the backward protocol [31, 55]. In the present cases, such reversal would be superfluos.

Appendix D: Density of states and energy distributions

The density of states (DOS) $\Omega(E)$ can be written as

$$\Omega(E) = d^{-1} \sum_n \delta(E - E_n) \quad , \tag{D1}$$

where n runs over all eigenvalues of $H = H^0(t = 0)$ and $d = \dim\{\mathcal{H}\}$ denotes the dimension of the Hilbert space of the respective system. Equivalently, we can express it in terms of time evolutions as

$$\Omega(E) = \frac{1}{2\pi} \int_{-\infty}^{+\infty} e^{i\,E\,t}\, \mathrm{Tr}\left\{ e^{-i\,H\,t} \right\}\, dt \quad . \tag{D2}$$

Note that the trace in the latter equation can be evaluated accurately by employing quantum typicality [47, 56], i.e.,

$$\frac{\mathrm{Tr}\left\{ e^{-i\,H\,t} \right\}}{d} \approx \langle \phi(0) | e^{-i\,H\,t} | \phi(0) \rangle = \langle \psi(0) | \phi(t) \rangle \quad , \tag{D3}$$

where d is again the dimension of the underlying Hilbert space and $|\phi(t)\rangle$ is a random state drawn according the Haar measure. The error scales with $1/\sqrt{d}$. As before,

$|\phi(t)\rangle$ can conveniently be calculated by a fourth-order Runge-Kutta scheme.
Now, the DOS can be approximated by

$$\Omega(E) \approx C \int_{-\Theta}^{+\Theta} e^{i\,E\,t}\,\langle\psi(0)|\phi(t)\rangle\,dt \quad , \tag{D4}$$

where C accounts for the normalization of the DOS and Θ denotes the time range required to obtain the energy resolution π/Θ. Note that the Nyquist sampling theorem presents a restriction according the time steps that can be used (see e.g. Ref. [56]). However, here we use such parameters that errors remain small.
At last we want to demonstrate that in a very similar way as just presented we can obtain energy distributions of any pure quantum state $|\Psi\rangle$. To do so, we consider the discrete energy distribution

$$p(E) = \sum_i |\langle E_i|\Psi\rangle|^2\,\delta(E-E_n) \tag{D5}$$

where $|E_n\rangle$ denotes the i-th eigenvector. In terms of time evolutions it reads

$$\begin{aligned} p(E) &= \frac{1}{2\pi}\int_{-\infty}^{+\infty} e^{i\,E\,t}\,\langle\Psi|e^{-i\,H\,t}|\Psi\rangle\,dt \\ &\approx C\int_{-\Theta}^{+\Theta} e^{i\,E\,t}\,\langle\Psi(0)|\Psi(t)\rangle\,dt \quad . \end{aligned} \tag{D6}$$

We want to emphasize that the concept of typicality does not enter the last derivation.

Appendix E: Appropriate Choice of Parameters for Spin-Ladder Setup: Density of States and Free Relaxation Dynamics

As argued in Sect. II, the stiffness of the work pdf's is conditioned on the DOS being exponential. Thus, prior to examining the work pdf's as resulting from an actual driving, we numerically analyze the DOS of the non-driven model in order to identify exponential regions. Later on we will choose our starting energies and driving protocols such that the work pdf's essentially remain within those exponential regions. In Fig. 12 we display semi-log plots of the DOS Ω for several system sizes, $N = 13-19$, and system-bath coupling strength $\kappa = 0.2$, within an intermediate energy regime. (The energy resolution (graining) is for all cases fix, ≈ 0.09.) Note that Ω becomes smoother with increasing system size. Within energy regimes $[E_0 - \Delta/2, E_0 + \Delta/2]$ (with $E_0 \approx -0.2\,N$ and $\Delta = 2.5$) we indeed find the DOS well described by $\Omega \propto \exp(\beta E)$ with $\beta = 0.68$, see fits in Fig. 12. Thus in the following we restrict our investigations to the above energy regimes. Computing concrete work pdf's based on specific system and driving parameters is numerically rather costly, especially for larger system sizes. Thus

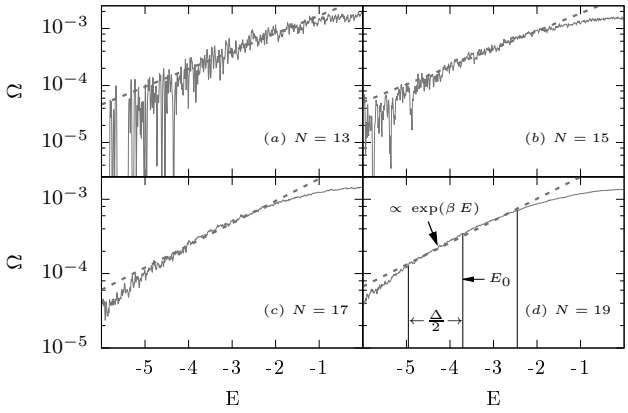

FIG. 12. Semi-log plots of the DOS (Ω) for the ladder model for $L = 6-9$ and $\kappa = 0.2$. Dashed lines indicate exponential fits within a specific energy regime (see text) of the displayed energy range. The fits correspond to $\beta \approx 0.68$. Ω becomes smoother with increasing system size. Note that for $\kappa = 0.6$ we find a very similar behavior.

we intend to restrict our analysis to a few carefully performed simulations. As argued in Sect. III, there are certain trivial limiting cases for which JR is fulfilled without invoking stiffness. Here we intend to give a reasoning for specific choice of parameters κ and λ that allow for scenarios most possible away from such trivial cases in the present set-up (see Sect. III).
In these limiting cases the time scale corresponding to the driving strength, i.e. $2\pi/\lambda$ [57], will either be much shorter or much larger than the relaxation dynamics of the system spin in the coupled but non-driven systen. Thus, to obtain meaningful, non-trivial examples, we want to choose the driving strength λ such that $2\pi/\lambda$ becomes comparable to the time scale of the "free relaxation" dynamics. To this end we first analyze the free relaxation dynamics of the magnetization of the system spin and its dependence on κ. In order to obtain relaxation dynamics, i.e. $\langle S^z_{\rm sys}(t)\rangle$, corresponding to the energy regime around E_0, we employ initial states of the form

$$\rho = \frac{\pi^{\rm bath}_{E_0,\sigma}\otimes\pi_m}{{\rm Tr}\left\{\pi^{\rm bath}_{E,\sigma}\otimes\pi_m\right\}} \quad , \tag{E1}$$

where $\pi^{\rm bath}_{E_0,\sigma}$ denotes an energy projector onto an energy shell of the isolated bath described by $H'_{\rm ladder}$, with mean energy E_0 and width σ, and π_m denotes a projector onto one of the eigenstates of $S^z_{\rm sys}$, i.e., $m = \pm 1/2$. (Note that, for simplicity of numerics, we restrict the initial state to the conserved magnetization subspace with $M_{\rm tot} = \sum_{i=1}^N S^z_i = (N-1)/2$). For these initial states ρ we compute $\langle S^z_{\rm sys}(t)\rangle$ based on $H^0_{\rm ladder}$ with $B = 0.5$. In Fig. 13 we summarize the results for two interaction

strength $\kappa = 0.2$ and $\kappa = 0.6$. As the relaxation dynamics are eihter clearly exponential ($\kappa = 0.2$) or clearly non-exponential ($\kappa = 0.6$) we classify them as examples of weak and strong coupling, respectively. (For details cf., e.g., [17, 58]). From Fig. 13 we infer relaxation time scales τ_R as $\tau_R \approx 24$ for weak coupling and $\tau_R \approx 2.5$ for strong coupling [59]. Accordingly we choose two corresponding driving strengths as $\lambda = 0.26(\approx 2\pi/24)$ and $\lambda = 2.5(\approx 2\pi/2.5)$. Eventually the duration of the driving must be fixed. In general a longer driving will result in a larger amounts of delivered work which is favorable. On the other hand we intend to induce work pdf's that essentially live in the above exponential region of the DOS. Given this condition, the weak driving may be applied longer than the strong driving. A duration of the driving of 6.5 periods in the case of weak driving and a duration of a half period in the case of strong driving are reasonable choices. While the parameter combinations ($\kappa = 0.2, \lambda = 0.26$) and ($\kappa = 0.6, \lambda = 2.5$) are most far away from both trivial limiting cases, below we also compute work pdf's for the "remaining" combinations ($\kappa = 0.2, \lambda = 2.5$) and ($\kappa = 0.6, \lambda = 0.26$), for completeness. The latter are much closer to either of the above trivial limiting cases. A side comment on the relaxation dynamics itself may be in order. Irrespective of the coupling strengths and the initial value, $\langle S^z_{\rm sys}(t)\rangle$ appears to converge against an "universal" expectation value. This value is in accord with the corresponding standard, canonical equilibrium value at inverse temperature $\beta \approx 0.68$, as suggested by Fig. 12. This example thus agrees with the principles of "canonical typicality" [2, 41] and the ETH in the sense discussed in Ref. [60].

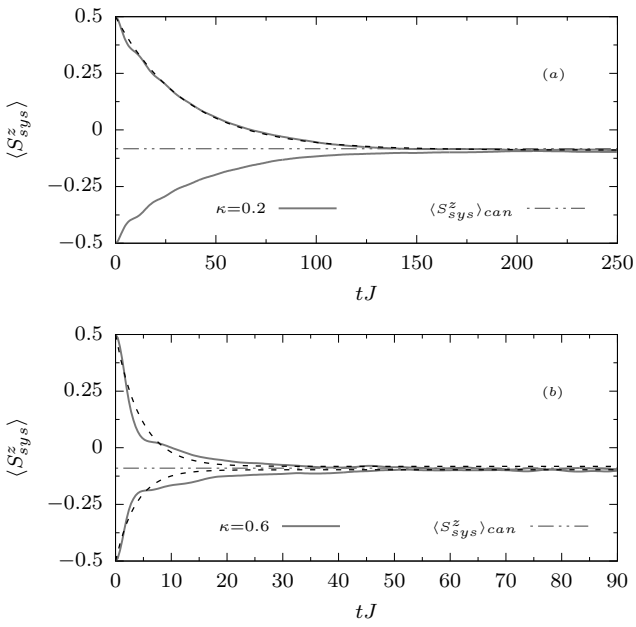

FIG. 13. Dynamics of the expectation $\langle S^z_{\rm sys}\rangle$, for weak ($\kappa = 0.2$, upper panel) and strong ($\kappa = 0.6$, lower panel) coupling between bath and system for $N = 19$. Dashed lines show exponential fits. While for the weak coupling we find exponential decay, we find for strong coupling a strong non-exponential behavior. However, both dynamics tend toward a "universal" expectation value corresponding to $\beta \approx 0.68$ (see text).

Appendix F: Generating initial states

Since for our models exact diagonalization is only feasible for system comprising maximal 15 spins ($\dim\{\mathcal{H}_{15}\} = 32768$), we employ for larger systems a typicality-based approximation scheme [10, 45, 47] to mimic the initial states as defined in the main text. To be precise, we generate Gaussian projections of random states $|\phi\rangle$, drawn according to the Haar measure, onto narrow energy shells of the total Hilbert space of the corresponding system, i.e.,

$$|\psi_E\rangle = C^{-1}\ \exp\left(-\frac{(H^0-E)^2}{4\,\sigma^2}\right)|\phi\rangle \quad , \qquad \text{(F1)}$$

where $C = \langle\phi|\exp\left(-\frac{(H^0-E)^2}{2\,\sigma^2}\right)|\phi\rangle$. This state mimics for small σ to good accuracy a sharp energy shell around energy E. In order to calculate the r.h.s. of Eq. (F1) we again employ a fourth-order Runge-Kutta scheme. However, here we replace $H' = (H^0 - E)^2$ and use imaginary time steps $\delta t = i\,\delta\tau$. The final "time" is correspondingly $T = 1/4\,\sigma^2$.
Comparison with exact-diagonalization data for $N = 15$ yields that $\sigma = 1/\sqrt{1000}$ is an appropriate choice to mimic the initial states defined in the main text. Again, we choose such time steps that errors remain negligible.

Appendix G: Appropriate Choice of Parameters for the Spin-Chain Setup: Density of States and Free Relaxation Dynamics

Since, as argued in Sect. II, stiff pdf's may only occur in regions featuring an exponential DOS, we start (just like in Appendix E) by identifying such exponential regions in the DOS of the spin chain (as defined in Sect. III) as displayed in Fig. 14. In accord with the literature [61], the calculations indicate that there are energy regimes in which the DOS is well described by an exponential growth, e.g. , at $E_0 \approx -0.18\,N$ and $\Delta = 2.5$. . There we find the DOS well described by $\Omega \propto \exp(\beta E)$ with $\beta \approx 0.86$. As for the ladder model, the agreement between Ω and the exponential fits increases as the system size becomes larger. Thus also for this model, regardless of its integrability, stiff work pdf's are possible. Again, in order to stay away from the trivial limiting cases (cf. Sect. E), we want to chosse the driving strength λ such that corresponding driving time scale is comparable to the time scale of the free relax-

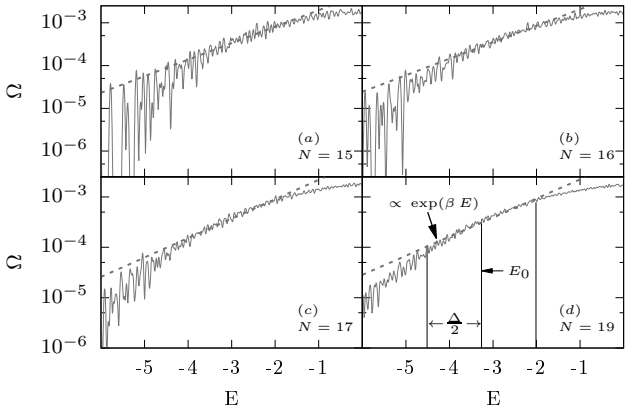

FIG. 14. Semi-log plots of the density of states for the chain model for $N = 15 - 19$. As in Fig. 12 dashed lines indicate exponential fits. The fits correspond to $\beta \approx 0.86$. Here, also, it seems that the energy range for which Ω agrees well with the fits increases as the system size rises.

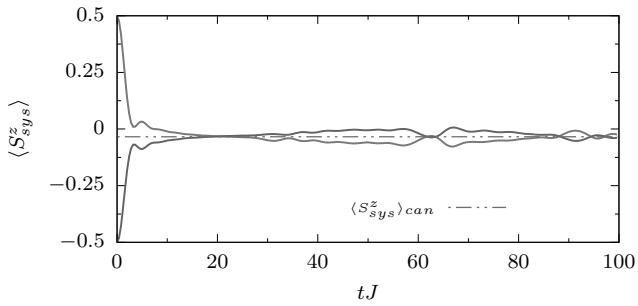

FIG. 15. Dynamics of the magnetization for the integrable chain model ($N = 19$). The relaxation behavior is strongly non-exponential and features fluctuations even for large times. Nevertheless, the dynamics fluctuate around an "universal" expectation value corresponding to $\beta \approx 0.86$. The relaxation time τ_R is similar to the one for the strongly coupled ladder system.

ation. To this end we compute the free relaxation dynamics based on an initial state according to Eq. (E1) with $\pi^{\rm bath}_{E,\sigma}$ based on $H'_{\rm chain}$. The relaxation behavior of $\langle S^z_{\rm sys}\rangle$ is displayed in Fig. 15. We infer a relaxation time of $\tau_R \approx 1.6$ and correspondingly choose a driving strength of $\lambda = 3.9(\approx 2\pi/1.6)$. We furthermore choose a (off-resonant) driving frequency of $\nu = 0.75$ and aply the driving for half a sine-period. (Note that because of the large λ and small detuning corrections [57, 62] for the Rabi frequency due to the off-resonant driving are negligible here.) A few side comments on the relaxation behavior itself may be in order. The relaxation behavior is reminiscent of that of the strongly coupled ladder model. However, $\langle S^z_{\rm sys}\rangle$ fluctuates around some long-time average. Up to the times shown here, apparently these fluctuations are no finite-size effect but persist in the limit of large systems. This principal difference reflects the integrability of the system. Nevertheless, irrespective of the initial value, $\langle S^z_{\rm sys}(t)\rangle$ appears to converge against, or fluctuate around, an "universal" expectation value. This value is also in accord with the corresponding standard, canonical equilibrium value at inverse temperature $\beta \approx 0.86$, as suggested by Fig. 14. Regardless of integrability this example thus also agrees with the principles of "canonical typicality" [2, 41] and the ETH in the sense discussed in Ref. [60]. For a more detailed discussion of thermalization in the presence of conservation laws, see e.g. [63].

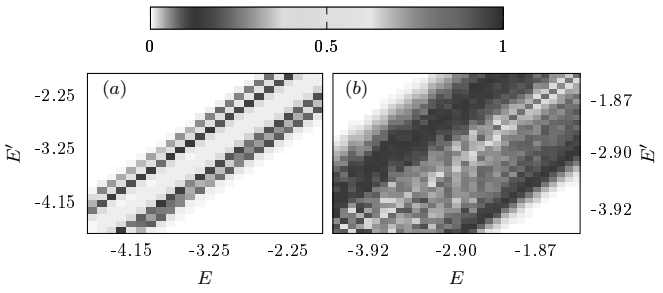

FIG. 16. Colormap of the energy dependencies of transition rates $\gamma_{E\to E'}$ vs. E, E' according to Fermi's Golden Rule for the (a) spin ladder and (b) spin chain [arbitrary units]. Both indicate that the transition rates do only depend on the energy difference $E - E'$, i.e., $\gamma_{E\to E'} = \gamma(E - E')$, in the energy regimes onto which we focused our investigations.

Appendix H: Investigation of the transition rates according Fermi's Golden Rule

As discussed in Sect. VI (main text) for weak driving, the internal transition rates from energy E to E' may be well-described by Fermi's Golden Rule. There, we denoted these transition rates as $\gamma_{E\to E'}$ and the underlying perturbation operator is identified as the $S^x_{\rm sys}$ operator. Here we will display our results on these $\gamma_{E\to E'}$ in a similar way as we have done for the ETH-related quantity $g(E', E)$. In fact, as pointed out in Sect. VI, both quantities may be related to each other. Moreover, if $\Omega(E) \propto e^{\beta E}$ holds true, one can calculate the one from the other. Fig. 16 shows the energy dependence of $\gamma_{E\to E'}$ for the ladder model (left panel) and the chain model (right panel) in the corresponding energy regimes as discussed in the main text. Both matrix presentations indicate that the transition rates do only depend on the energy difference $E - E'$, i.e., $\gamma_{E\to E'} = \gamma(E - E')$.

[1] S. Popescu, A. J. Short, and A. Winter, Nat. Phys. **2**, 754 (2006).
[2] S. Goldstein, J. L. Lebowitz, R. Tumulka, and N. Zanghì, Phys. Rev. Lett. **96**, 050403 (2006).
[3] P. Reimann, Phys. Rev. Lett. **101**, 190403 (2008).
[4] P. Reimann, Phys. Rev. Lett. **115**, 010403 (2015).
[5] J. Eisert, M. Friesdorf, and C. Gogolin, Nat. Phys. **11**, 124 (2015).
[6] C. Gogolin and J. Eisert, Rep. Prog. Phys. **79**, 056001 (2016).
[7] M. Rigol, V. Dunjko, and M. Olshanii, Nature **452**, 854 (2008).
[8] R. Steinigeweg, J. Herbrych, and P. Prelovšek, Phys. Rev. E **87**, 012118 (2013).
[9] W. Beugeling, R. Moessner, and M. Haque, Phys. Rev. E **89**, 042112 (2014).
[10] R. Steinigeweg, A. Khodja, H. Niemeyer, C. Gogolin, and J. Gemmer, Phys. Rev. Lett. **112**, 130403 (2014).
[11] P. Reimann, Nat. Comm. **7**, 10821 (2016).
[12] B. N. Balz and P. Reimann, Phys. Rev. Lett. **118**, 190601 (2017).
[13] J. Tomkovič, W. Muessel, H. Strobel, S. Löck, P. Schlagheck, R. Ketzmerick, and M. K. Oberthaler, Phys. Rev. A **95**, 011602 (2017).
[14] A. S. L. Malabarba, L. P. García-Pintos, N. Linden, T. C. Farrelly, and A. J. Short, Phys. Rev. E **90**, 012121 (2014).
[15] I. Tikhonenkov, A. Vardi, J. R. Anglin, and D. Cohen, Phys. Rev. Lett. **110**, 050401 (2013).
[16] C. Ates, J. P. Garrahan, and I. Lesanovsky, Phys. Rev. Lett. **108**, 110603 (2012).
[17] H. Niemeyer, D. Schmidtke, and J. Gemmer, EPL **101**, 10010 (2013).
[18] H. Niemeyer, K. Michielsen, H. De Raedt, and J. Gemmer, Phys. Rev. E **89**, 012131 (2014).
[19] J. Gemmer and R. Steinigeweg, Phys. Rev. E **89**, 042113 (2014).
[20] D. Schmidtke and J. Gemmer, Phys. Rev. E **93**, 012125 (2016).
[21] H. J. D. Miller and J. Anders, New J. Phys. **19**, 062001 (2017).
[22] U. Seifert, Eur. Phys. J. B **64**, 423 (2008).
[23] A. J. Roncaglia, F. Cerisola, and J. P. Paz, Phys. Rev. Lett. **113**, 250601 (2014).
[24] P. Hänggi and P. Talkner, Nat. Phys. **11**, 108 (2015).
[25] M. Esposito, U. Harbola, and S. Mukamel, Rev. Mod. Phys. **81**, 1665 (2009).
[26] C. Jarzynski, Annu. Rev. Condens. Matter Phys. **2**, 329 (2011).
[27] M. A. Cuendet, Phys. Rev. Lett. **96**, 120602 (2006).
[28] P. Talkner, P. Hänggi, and M. Morillo, Phys. Rev. E **77**, 051131 (2008).
[29] M. Campisi, Phys. Rev. E **78**, 051123 (2008).
[30] P. Talkner, M. Morillo, J. Yi, and P. Hänggi, New J. Phys. **15**, 095001 (2013).
[31] M. Campisi, P. Hänggi, and P. Talkner, Rev. Mod. Phys. **83**, 771 (2011).
[32] E. Iyoda, K. Kaneko, and T. Sagawa, Phys. Rev. Lett. **119**, 100601 (2017).
[33] S. Vinjanampathy and J. Anders, Contemp. Phys. **57**, 545 (2016).
[34] Note that a finite energy width σ is not mandatory. We introduced it here meanly due to numerical restriction; see Appendix F. In fact one may also choose initially a single energy eigenstates. In all cases one has to ensure that at least one eigenstate of the considered system contributes to the initial state.
[35] H. D. Raedt, Computer Physics Reports **7**, 1 (1987).
[36] F. Jin, R. Steinigeweg, H. De Raedt, K. Michielsen, M. Campisi, and J. Gemmer, Phys. Rev. E **94**, 012125 (2016).
[37] B. Cleuren, C. Van den Broeck, and R. Kawai, Phys. Rev. Lett. **96**, 050601 (2006).
[38] P. Talkner and P. Hänggi, J. Phys. A **40**, F569 (2007).
[39] J. J. Sakurai and J. J. Napolitano, *Modern quantum mechanics* (Pearson Higher Ed, 2014).
[40] G. Mahler, J. Gemmer, and M. Michel, Physica E: Low-dimensional Systems and Nanostructures **29**, 53 (2005).
[41] C. Bartsch and J. Gemmer, Phys. Rev. Lett. **102**, 110403 (2009).
[42] C. P. Poole, *Electron spin resonance* (Courier Corporation, 1996).
[43] A. C. Melissinos and J. Napolitano, *Experiments in modern physics* (Gulf Professional Publishing, 2003).
[44] A. Khodja, R. Steinigeweg, and J. Gemmer, Phys. Rev. E **91**, 012120 (2015).
[45] A. Khodja, D. Schmidtke, and J. Gemmer, Phys. Rev. E **93**, 042101 (2016).
[46] Note that even the combinations $(\kappa_{\text{weak}}, \lambda_{\text{strong}})$ and $(\kappa_{\text{strong}}, \lambda_{\text{weak}})$ still correspond to non-trivial cases for the concrete parameters here.
[47] T. A. Elsayed and B. V. Fine, Phys. Rev. Lett. **110**, 070404 (2013).
[48] M. Srednicki, J. Phys. A **32**, 1163 (1999).
[49] L. D'Alessio, Y. Kafri, A. Polkovnikov, and M. Rigol, Adv. Phys. **65**, 239 (2016).
[50] E. J. Torres-Herrera, J. Karp, M. Távora, and L. F. Santos, Entropy **18** (2016), 10.3390/e18100359.
[51] A. E. Feiguin and S. R. White, Phys. Rev. B **72**, 020404 (2005).
[52] A. M. Zagoskin, *Quantum theory of many-body systems* (Springer, 1998).
[53] A. Messiah, *Quantum Mechanics* (North Holland, Amsterdam, 1962).
[54] M. Campisi, J. Phys. A: Math. Theo. **47**, 245001 (2014).
[55] D. Andrieux and P. Gaspard, Phys. Rev. Lett. **100**, 230404 (2008).
[56] A. Hams and H. De Raedt, Phys. Rev. E **62**, 4365 (2000).
[57] P. W. Atkins and R. S. Friedman, *Molecular quantum mechanics* (Oxford University Press, 2011).
[58] C. Bartsch and P. Vidal, EPJ ST **151**, 29 (2007).
[59] The relaxation time τ_R is here defined as the full-width-half-maximum range.
[60] C. Bartsch and J. Gemmer, EPL **118**, 10006 (2017).
[61] D. Forster, *Hydrodynamic fluctuations, broken symmetry, and correlation functions* (Perseus Books, 1975).
[62] C. Cohen-Tannoudji, B. Diu, and F. Laloe, *Quantum Mechanics* (Wiley-Interscience, 2006).
[63] J. Sirker, N. P. Konstantinidis, F. Andraschko, and N. Sedlmayr, Phys. Rev. A **89**, 042104 (2014).

Eidesstattliche Erklärung

Hiermit erkläre ich an Eides Statt, dass ich die vorliegende Dissertation selbständig verfasst, keine anderen als die angegebenen Hilfsmittel verwendet und noch keinen Promotionsversuch unternommen habe.

Daniel Schmidtke
Oldenburg, 28. Mai 2018